Non-coding RNA and protein effectors of ciliary biology : identification of let-7b as a modulator of ciliogenesis and putative ciliary roles for Ataxin-7 in spinocerebellar ataxia 7

Lorraine Fievet

▶ **To cite this version:**

Lorraine Fievet. Non-coding RNA and protein effectors of ciliary biology : identification of let-7b as a modulator of ciliogenesis and putative ciliary roles for Ataxin-7 in spinocerebellar ataxia 7. Neurobiology. Université de Strasbourg, 2019. English. NNT : 2019STRAJ050 . tel-03510164

HAL Id: tel-03510164
https://theses.hal.science/tel-03510164v1

Submitted on 4 Jan 2022

HAL is a multi-disciplinary open access archive for the deposit and dissemination of scientific research documents, whether they are published or not. The documents may come from teaching and research institutions in France or abroad, or from public or private research centers.

L'archive ouverte pluridisciplinaire **HAL**, est destinée au dépôt et à la diffusion de documents scientifiques de niveau recherche, publiés ou non, émanant des établissements d'enseignement et de recherche français ou étrangers, des laboratoires publics ou privés.

Université de Strasbourg

UNIVERSITÉ DE STRASBOURG

École Doctorale des Sciences de la Vie et de la Santé STRASBOURG

ÉCOLE DOCTORALE DES SCIENCES DE LA VIE ET DE LA SANTÉ

IGBMC, CNRS UMR7104, Inserm U1258

THÈSE présentée par :

Lorraine FIEVET

soutenue le : **19 Septembre 2019**

pour obtenir le grade de : **Docteur de l'université de Strasbourg**

Discipline/ Spécialité : Aspects moléculaires et cellulaires de la biologie

ARN non-codants et protéines effecteurs de la biologie du cil

Identification du microARN *let-7b* comme modulateur de la ciliogenèse et rôle ciliaire putatif de l'Ataxine-7 dans l'ataxie spinocérébelleuse 7

THÈSE dirigée par :

Dr TROTTIER Yvon	Directeur de recherche, université de Strasbourg
Dr DAVIS Erica	Professeure des universités, université de Duke

RAPPORTEURS :

Dr BACHMANN-GAGESCU Ruxandra	Professeures des universités, université de Zurich
Dr ROEPMAN Ronald	Professeur des universités, université de Nimègue

AUTRES MEMBRES DU JURY :

Dr DOLLFUS Hélène	Professeure des universités, université de Strasbourg

Acknowledgements

I am grateful for the continuous guidance I received from my thesis co-supervisors Dr. Yvon Trottier and Dr. Erica Davis. Thank you for sharing your immense knowledge with me. Thank you Yvon for the freedom to experience and for your encouragements. Thank you Erica for your advices and enthusiasm.

I would like to thank my thesis committee: Dr. Ruxandra Bachmann-Gagescu, Dr. Ronald Roepman and Dr. Jamel Chelly for accepting to evaluate my work. And thank you to my mid-thesis committee: Dr. Christelle Golzio and Dr. Edor Kabashi who helped me transitioning from one project to another.

A special thanks to three wonderful scientists and friends who I have met during my studies. A thousand thanks to Samantha for teaching me all about zebrafish and for being an enthusiastic, generous and wonderful friend. Thank you Maria for your advices and support, both professional and personal. And special thanks to Ashot for committing to the success of my least favorite experiments and for the support during my frustrations.

I could not forget the Company with Francesca and Dami O. We were very involved into brainstorming to find ideas to become business partners and make a better world. I cannot remember laughing more than during those lunches.

I am grateful to the great minds and helpful colleagues with who I have shared stimulating scientific conversations: the polyQ and CHDM teams, and especially Fabrice, Julien, Wes, Julie, Dami A., Gary, and Marie. Thank you Chantal for the tips (solution 1, 2, 3!), support and friendship. I also acknowledge the zebrafish caretakers and especially Sandrine, Zak and Ed.

Also, to the Student and Post-doc Board of IGBMC and the Duke Zebrafish Community: it was great working with you and organizing events. Special thanks to Dr. John Rawls for coordinating the Zebrafish symposiums and to Jamie for her friendship.

And last but not least, I would like to thank my wonderful parents Bruno and Laure, my brilliant brother and sister Frédéric and Tiphaine for their continuous support.

Table of Contents

List of Tables – Introduction

List of Figures - Introduction

List of Tables

let-7b chapter

List of Figures

let-7b chapter

ATXN7 chapter

Abbreviations and Symbols

AcTub	Acetylated tubulin
ADAMTS9	A Disintegrin And Metalloproteinase with Thrombospondin type 1 motif 9
AGO	Argonaute
AHI1	Abelson Helper Integration site 1
AMPK	Adenosine MonoPhosphate-activated protein Kinase
APC	Adenomatous Polyposis Coli Protein
ARL13B	ADP Ribosylation Factor Like GTPase 13B
ARPE-19	Adult Retinal Pigment Epithelial cell line-19
ATAT1	Alpha Tubulin Acetyltransferase 1
ATP	Adenosine TriPhosphate
ATXN7	Human Ataxin-7; gene is italicized
AURKA	Aurora Kinase A
B9D1	B9 Domain containing 1
B9D2	B9 Domain containing 2
BB	Basal body
BBS	Bardet-Biedl Syndrome
BMPR	Bone Morphogenic Protein Receptor
CaMKII	Calcium/Calmodulin dependent protein Kinase II
cAMP	Cyclic Adenosine MonoPhosphate
CaN	Calcinurin
CAV1	Caveolin 1
CC2D2A	Coiled-Coil And C2 Domain Containing 2A
CED	Sensenbrenner Syndrome
CEP	Centrosomal Protein
cGMP	Cyclic Guanosine MonoPhosphate
CHDM	Center for Human Disease Modeling, Duke University Medical Center
CK1	Casein Kinase 1
CP110	Centrosomal protein
CRX	Cone-Rod homeobox
CSL	Also called RBPJ for Recombination signal Binding Protein for immunoglobulin kappa J region
CTEF	Corrected Total Embryo Fluorescence
DAAM1	Dishevelled Associated Activator of Morphogenesis 1
DAG1	Dystroglycan 1
DAV	Distal Appendage Vesicle
DGCR8	DiGeorge syndrome Critical Region 8
DIDO3	Death Inducer-Obliterator 3
DVL	Dishevelled
EDH1	EH Domain-containing protein 1
EvC	Ellis-Van Creveld syndrome protein

EZR	Ezrin
FBF1	Fas Binding Factor 1
FOXJ1	Forkhead Box J1
FZD	Frizzled
GLI	Glioma family zinc-finger
GO	Gene Ontology
GPCR	G-Protein Coupled Receptor
GPR161	G-Protein coupled Receptor 161
GRB2	Growth factor Receptor Bound protein 2
GSK	Glycogen Synthase Kinase
GTPase	Guanosine TriPhosphate hydrolase
H2B-GFP	Histone 2B-Green Fluorescent Protein
H9c2	Rat embryonic cardiomyocyte cell line
HDAC6	Histone Deacetylase 6
HEF1	also called NEDD9 for Neural precursor cell Expressed, Developmentally Down-Regulated 9
her12	Hairy related 12
HH	Hedgehog
Hpf/dpf	Hours- or days-post-fertilization
HTT	Huntingtin
IFT	Intraflagellar transport
IFT-A	Intraflagellar transport complex A
IFT-B	Intraflagellar transport complex B
IMCD3	Inner Medullary Collecting Duct 3 (mouse cell line)
INPP5E	Inositol Polyphosphate-5-Phosphatase E
ITGA or ITGB	Integrin Alpha or Integrin Beta
JATD	Jeune Asphyxiating Thoracic Dystrophy
JBTS	Joubert Syndrome
JNK	c-Jun N-terminal kinase
KAP	Kinesin associated protein
KIAA0586	also called Talpid3
KIF	Kinesin family
LATS	Large Tumor Suppressor
LCA	Leber congenital amaurosis
LEF	Lymphoid Enhancer Binding Factor
LIN28	Lineage 28
LKB1	also called STK11 for Serine/Threonine Kinase 11
LRP	Low density lipoprotein Receptor-related Protein
MAF	Minor Allele Frequency
MAPK/ERK	Mitogen-Activated Protein Kinase / Extracellular signal-Regulated Kinase
MARK4	Microtubule Affinity Regulating Kinase 4
mATXN7	mutant Ataxin-7
miRNA	micro-RNA

MKS	Meckel-Grüber Syndrome
mRNA	messenger RNA
MSN	Moesin
MST1/2	Myeloproliferative Syndrome, Transient
MTOC	Microtubule Organization Center
mTOR	mechanistic Target Of Rapamycin
mTORC1	mechanistic Target Of Rapamycin Complex 1
mTORC2	mechanistic Target Of Rapamycin Complex 2
NCID	Notch intracellular domain
NDE1	NudE Neurodevelopment Protein 1
NEK2	(Never In Mitosis Gene A)-Related Kinase 2
NES	Nuclear Exportation Signal
NF-κB	Nuclear Factor Kappa B
NFAT	Nuclear Factor Of Activated T Cells
NLS	Nuclear Localization Signal
NPHP	Nephronophthisis
NRK	Nik Related Kinase
OFD	Orofaciodigital Syndrome
OMIM	Online Mendelian Inheritance in Man
P85	Phosphoinositide-3-kinase regulatory subunit 1
PC1	Polycystin-1
PC2	Polycystin-2
PCP	Planar Cell Polarity
PDGF	Platelet-Derived Growth Factor
PDGFR	Platelet-Derived Growth Factor receptor
PI	Phosphoinositide
PI3K-AKT	Phosphatidylinositol-4,5-Bisphosphate 3-Kinase – protein kinase
PIFO	Primary Cilia Formation
PKA	Protein Kinase A
PKC	Protein Kinase C
PKD	Polycystic Kidney Disease
PLCγ	Phospholipase C Gamma
pLI	probability of being Loss-of-function Intolerant
PP1	Protein Phosphastase 1
PP2A	Protein Phosphatase 2 phosphastase Activator
polyQ	polyglutamine
PR	Photoreceptor
pre-miRNa	Precursor micro-RNA
pri-miRNA	Primary micro-RNA
PTCH	Patched
PVRL2	Also called NECTIN2, nectin cell adhesion molecule 2
RAB	Ras-Associated Protein

RAB3IP	RAB3A Interacting Protein
RAC	Rac GTPase
RDX	Radixin
RFX	Regulatory Factor X
RHEB	Ras Homolog Enriched In Brain
RHO	Ras Homolog
RISC	RNA-induced silencing complex
RNA-seq	RNA-sequencing
RPGR	Retinitis Pigmentosa GTPase Regulator
RPGRIP1L	Retinitis Pigmentosa GTPase Regulator Interacting Protein 1 Like
SAGA	Spt-Ada-Gcn5 Acetyltransferase
SAV1	Salvador Family WW Domain Containing Protein 1
SAV1	Salvador Family WW Domain Containing Protein 1
SCA7	Spinocerebellar ataxia 7
SCLT1	Sodium Channel And Clathrin Linker 1
siRNA	silencing RNA
SKP	S-phase Kinase associated Protein
SLC9A1	Solute Carrier family 9 member A1
SLS	Senior-Loken Syndrome
SMAD	Mother Against Decapentaplegic
SMO	Smoothened
SRP	Short rib polydactyly
ss	Somite-stage
SUFU	Suppressor of Fused
TCF	Transcription Factor
TCHP	Trichoplein
TCTN	Tectonic
TEAD1-4	TEA Domain transcription factor
TGF	Transforming Growth Factor
TMEM	Transmembrane protein
TPM1	Tropomyosin 1
TRAM-1a	Translocating chain Associated Membrane protein 1a
TRBP	Trans-activation responsive RNA-Binding Protein
TRPC1	Transient Receptor Potential Cation Channel Subfamily C Member 1
TRPV4	Transient Receptor Potential Cation Channel Subfamily V Member 4
TSC	Tuberin
TTBK2	Tau Tubulin Kinase 2
TULP3	Tubby Like Protein 3
TUT4	Terminal Uridylyl Transferase 4
TZ	Transition zone
UI	Uninjected control embryo
UTR	Untranslated Region

VANGL2	Van Gogh-Like protein 2
VCL	Vinculin
WDR35 or 44	WD Repeat Domain 35 or 44
WNT	Wingless-integrated
XPO5	Exportin 5
YAP/TAZ	Yes Associated Protein / Tafazzin
ZnF	Zinc-Finger
β-TrCP	beta-Transducin repeat Containing Protein

NON-CODING RNA AND PROTEIN EFFECTORS OF CILIARY BIOLOGY

Identification of *let-7b* as a modulator of ciliogenesis and putative ciliary roles for Ataxin-7 in spinocerebellar ataxia 7

INTRODUCTION

Introduction

*Cilia are conserved microtubule-based appendages residing at the apical surface of almost all terminally-differentiated cell types. Based predominantly on the past two decades of research, we now know that cilia function both during embryogenesis and also in differentiated tissues to regulate a multitude of cellular processes [1-3]. From a historical perspective, cilia are among the oldest observed organelles; they were discovered in the 17th century by van Leeuwenhoek and noted for their remarkable motile properties [4]. The appreciation for motile cilia intensified with the realization that multiciliated cells are present in diverse vertebrate tissue types and include cilia lining the respiratory tract, lungs, inner ear, and brain ventricles [5-7]. In 1998, a landmark study uncovered a link between a distinct form of motile cilia in the node and mammalian determination of left–right asymmetry during development [8]. While initial functional studies were focused on motile cilia because of their obvious functions in fluid or cell propulsion, the primary cilium was largely neglected and considered a vestigial structure, despite documentation in the 19th century [9]. Several key findings brought functional relevance to the primary cilium; these include but are not limited to: (1) the causal relationship between primary ciliary dysfunction and the cystic renal pathology in the Oak Ridge Polycystic Kidney mouse (*Tg737^{OPRK}*) [10,11]; (2) the discovery of a role for primary cilia in Hedgehog (HH) signal transduction in mice [12]; and (3) the observation that polycystin-1 and polycystin-2, both associated with renal disease, mediate calcium mechanosensation in a primary cilia-dependent manner [13]. Subsequent* in vitro *and* in vivo *work associated the primary cilium to additional morphogenetic pathways including Notch, Wnt, Hippo, mTOR, and PDGFR signaling, redefining the cilium as a cellular antenna critical for development, homeostasis and regenerative processes [14,15].* (Paragraph from [16])

This opening paragraph, extracted from a recent review on cilia written by CHDM investigators, summarizes how our appreciation of cilia grew over the years and how cilia progressively gained importance in the understanding of physiology and human disease.

Due to the extraordinary inter- and intra-species diversity of cilia (**Figures 1 and 4**), which range from the flagella of *Chlamydomonas reinhardtii* to the stereocilia in the human organ of sound perception cochlea, it is challenging to describe a typical ciliary organelle which could represent all. Therefore, I will focus on the vertebrate cilium which is more relevant to this work focusing on human pathology. However, it is important to note that work performed in *C. reinhardtii*, *Caenorhabditis elegans*, *Drosophila melanogaster* and other invertebrates have greatly contributed to the knowledge of cilia and often pioneered our understanding of cilia structures and functions which explain why some citations will refer to studies in those organisms.

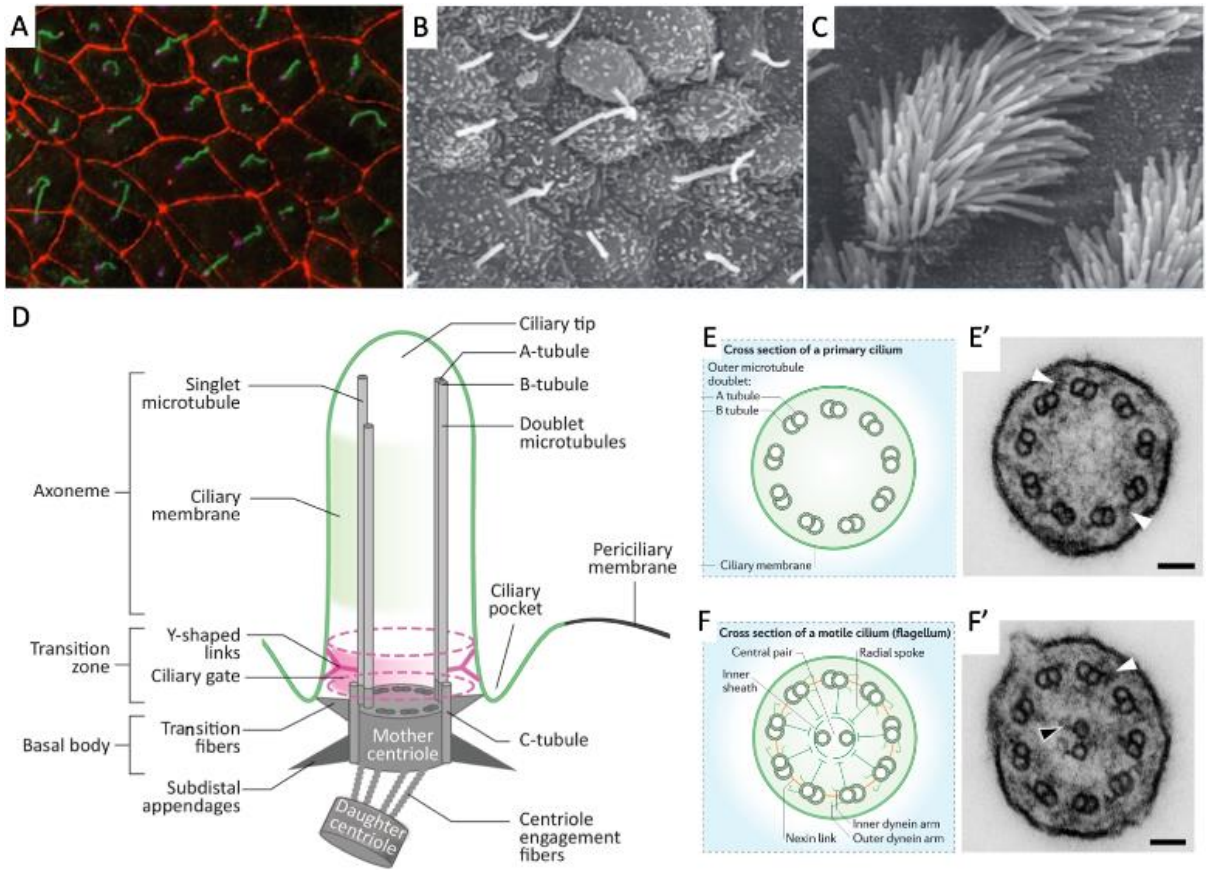

Figure 1: Structure of primary and motile cilia.

A. Primary cilia (green) from cultured inner medullary collecting duct (IMCD3) cells extend from the basal body (magenta). Cell–cell junctions are shown in red. **B, C.** Scanning electron micrographs of mouse nodal cilia (**B**) and mouse tracheal motile cilia (**C**). **D.** Simplified schematic of ciliary ultrastructure. **E, E'.** Cross-section diagrams of a non-motile primary cilium (**E**) and transmission electron microscopy of its structure (**E'**). **F, F'.** Cross-section diagrams of a motile cilium (**F**) and transmission electron microscopy of its structure. Scale bars = 50 nm. Figures A-C, E and F are from [17], D is from [18] and E' and F' are from [19].

I. Cilia structure

Cilia can be divided in 5 functional sub-domains which are: the basal body (BB), the transition zone (TZ), the ciliary membrane, the axoneme and the tip (**Figure 1**).

Whether they are present as a single primary cilium on a neuron or multiple motile cilia on an epithelial cell, each cilium is anchored to a BB (**Figure 1D**). The BB is derived from the mother centriole which docks to the cell membrane after exit from the cell cycle. This barrel-shaped structure is composed of a characteristic scaffold of 9 peripheral microtubule triplets, where a triplet is composed of 1 complete tubule A and 2 partial tubules B and C, and where a tubule is made of γ-tubulin dimers [20,21]. The BB is attached to the cell cortex under the plasma membrane via transition fibers and associated proteins CEP164, CEP83, CEP89, SCLT1 and FBF1 [22]. It also possesses basal feet which have been shown to play a role in stability and maintenance of the submerged portion of the cilium [23]. In the case of motile cilia, there is a unique basal foot per cilium which is aligned with the direction of the beating to allow coordinated movements [24]. The role of the BB is to serve as an anchor for the axoneme of the cilium and as a hub to import proteins into the ciliary compartment. Numerous proteins have been found to localize to the BB such as CEP170, OFD1, RPGRIP1L, MKS1 and the 8 components of the BBSome (a complex made of proteins which are mutated in Bardet-Biedl syndrome (BBS)), and most of them are involved in the formation of the BB or protein trafficking [20]. The end of the BB sub-domain is defined by the end of the C tubules (only tubules A and B elongate in the axoneme) and the transition fibers.

The TZ is composed of microtubule-to-membrane connectors called y-links and the ciliary necklace which together form a physical barrier to prevent cytoplasmic proteins to freely enter the ciliary compartment (**Figure 1D**). The ciliary necklace consists in defined wave-like rows of membrane particles that encircle the base of the cilium [25,26]. More than 20 soluble and membrane associated proteins are associated with the TZ and enable selective trafficking. There are three conserved modules of TZ proteins that have been described: the NPHP module (NPHP1 and NPHP4), the MKS module (MKS1, B9D1, B9D2, TCTN1, TCTN2,

TCTN3, CC2D2A, TMEM17, TMEM67, TMEM107, TMEM216, TMEM231, TMEM237) and the CEP290 module (CEP290 and NPHP5). These modules interact with each other and with additional proteins such as RPGRIP1L and TMEM138. Since some interactions between components of each module have been observed in both ciliated and non-ciliated cells, parts of the modules are thought to be assembled before reaching the TZ during ciliogenesis [27]. Mutations in any of the TZ proteins can lead to severe developmental defects as observed in Meckel-Grüber syndrome [28]. The TZ is often called a ciliary gate for its role in the selective trafficking of ciliary components in collaboration with the BBSome, intraflagellar transport (IFT) complexes and small-GTPases [29]. For instance, CEP290 prevents TRAM-1a from entering the ciliary compartment and ARL13B from leaking out [30]. The TZ also acts as a lipid gate to regulate the composition of the ciliary membrane and modulate signal pathways [31,32].

The invagination of the plasma membrane at the level of the transition zone is called the ciliary pocket (**Figure 1D**). It is shaped by an actin skeleton and is enriched in clathrin-coated pits to allow endocytosis [33]. Although it is continuous with the plasma membrane, the ciliary membrane has a distinct protein and lipid composition. The protein ARL13B is a small GTPase (can bind to GTP but is not able to hydrolyze it), which localizes exclusively to the ciliary membrane with cooperation from TULP3, and plays an important role in the assembly and stabilization of the axoneme [34,35]. The cilium is often referred as an antenna because of its role in sensing the extracellular environment and detecting signaling molecules and this is possible through the presence of receptors and channels concentrated in the ciliary membrane [36]. For instance, the mammalian HH signaling pathway is cilia-dependent and necessitates Smoothened (SMO) receptors to be targeted at the ciliary membrane by ARL13B to allow signal transduction [34,37]. Additionally, the distribution of proteins in the ciliary membrane is regulated by lipid composition. While both the plasma membrane and the ciliary membrane contain phosphoinositides (PI) PI(4)P and PI(4,5)P_2, the ratio is different: PI(4)P is more abundant in the ciliary membrane while PI(4,5)P_2 is rare [32]. This is due to the presence of the phosphatase INPP5E which is enriched in the ciliary membrane via targeting by ARL13B [38]. It has been shown that unbalanced lipid composition affects the Sonic HH

signaling pathway [31,32]. Although observed predominantly in *C. reinhardtii* and *C. elegans*, the ciliary membrane of vertebrates is also able to form extracellular vesicles as exemplified by the shedding of the photoreceptor outer segment [39], or as suggested by the presence of polycyctin-1 and -2 (PC1 and PC2) in extracellular vesicles found in urine [40,41]. More recent studies showed that cilia in cultured glioblastoma cells were capable of releasing vesicles to communicate with surrounding cells [42], and that cultured IMCD3 cells were producing exosomes to regulate the accumulation of receptors at the tips of their cilia [43].

The axoneme is anchored in the BB from which the microtubule skeleton elongates (**Figure 1D**). The microtubule skeleton is composed of two types of tubules which differ by their shape: microtubules A are complete and present a tubular shape, while microtubules B are incomplete with a half-tubular shape and are only found adjacent to microtubules A. (**Figure 1E, F**) [17]. Ciliary axonemes are typically composed of either the 9+0 conformation with nine peripheral microtubule doublets (**Figure 1E, E'**), or the 9+2 conformation which has 2 additional central microtubule singlets (**Figure 1F, F'**). Motile cilia usually have the 9+2 conformation while primary cilia have the 9+0 conformation. Known exceptions include nodal cilia which are motile but have a 9+0 conformation; and the olfactory nonmotile cilia with either 9+0 and 9+2 conformations depending on the distance from the basal body [44,45]. In addition to these examples of discordance between function (motile or nonmotile) and structure (9+2 or 9+0), studies have shown the presence of non-traditional conformations such as the 9+4 microtubule conformation in the rabbit node [19]. In the axoneme, microtubules are heterodimers of α- and β-tubulin and often carry post-translational marks such as the acetylation on lysine 40 of α-tubulin by ATAT1 which is thought to increase the microtubule flexibility and stability [46,47], or glutamylation by CEP41 required for proper axoneme formation [48]. To allow beating of motile cilia, additional structures articulate the axoneme. Peripheral microtubule doublets are connected to the central pair and depend upon the radial spokes, which are themselves connected to central pair projections. Additionally, peripheral doublets are linked to their neighbors via nexin. Outer and inner dynein arms are periodically distributed at 24 nm and 96 nm respectively along the microtubule A. [49,50]

(**Figure 1F**). Towards the distal part of the axoneme, the doublets usually become singlets (loss of B tubules) and decrease in number while preserving their radial organization [51]. The axoneme serves as a track for the members of the IFT complexes, associated with their molecular motor kinesin or dynein for anterograde or retrograde transport respectively, to transport the cargos essential for ciliary function and maintenance.

The tip is the most distal part of the cilium (**Figure 1D**), it is a dynamic turnover zone where microtubules polymerize or depolymerize during the elongation and maintenance of the axoneme. Several structures can be found at the tip of motile cilia including the central cap and the ciliary crown. The central cap links the central pair of microtubules of the axoneme to the ciliary membrane through distal filaments and has been observed at the tips of cilia on tracheal cells [52]. A possible role could be the strengthening of the ciliary skeleton to resist to forces generated by the beating [53]. Ciliary crowns are trans-membranous filaments anchored in the central cap that protrude from the ciliary tip. They have been observed in a number of mammalian epithelial cilia such as the murine oviduct epithelium [54] and the guinea pig tracheal epithelium [52]. The precise role(s) of the ciliary crown remains unclear but studies suggest that its negative charge might play a role in the adhesive property of cilia [55]. The axoneme of primary cilia usually ends with A tubules of unequal length, topped by an electron-dense area bound to the ciliary membrane which remains to be characterized [56]. In the kidney, the A tubules of the primary cilia bend progressively toward the center at the tip of the cilium to create a narrow end [57]. Finally, a fascinating example of a ciliary tip is exemplified by the outer segment of photoreceptors present in the retina. This highly specialized structure corresponds to an elongated ciliary tip shaped as a rod or a cone and packed with membrane discs containing Opsin. This sensory cilium can detect light and convert it to an electric signal transmitted by the retinal neurons to the brain [58].

II. Ciliogenesis and maintenance

Ciliogenesis is an intricate process which requires the proteasomal degradation of a pool of inhibitory proteins [59,60] and the coordination of vesicle and protein transport to the site of microtubule nucleation [61] (**Figure 2**).

Cilia are formed when cells are quiescent (G_0) or during the interphase (in G_1 particularly) for proliferating cells [62,63]. NDE1, a regulator of the mitotic spindle, is highly expressed during mitosis and is a known negative regulator of ciliogenesis. Its degradation through the proteasome is one of the first ciliogenesis-permissive steps [59]. Next, ciliogenesis requires the maturation of the mother centriole into a BB. Multiciliated cells have one BB per cilium and thus additional BB are generated through deuterosomes which first appear adjacent to the daughter centriole and then disperse [64]. The abundance of BB in this cell type is regulated by the availability of the cell surface area [65]. The mother centriole is located at the center of the cell and its structure is similar to that of the BB with an array of 9 peripheral microtubule triplets. It possesses a distal appendage which will give rise to the transition fibers, and a sub-distal appendage which will gives rise to the basal foot/feet. The mother centriole is connected to the daughter centriole via engagement fibers to form the centrosome, also called the Microtubule Organizing Center (MTOC), which is responsible for the mitotic spindle formation and chromosome segregation during the cell cycle [66].

CEP164 protein mediates the accumulation of RAB11-positive recycling endosomes at the distal appendage, called distal appendage vesicles (DAVs), when the mother centriole progresses slowly towards the apical cell plasma membrane [67,68] (**Figure 2A**). The mechanisms by which the mother centriole recognizes the apical pole of a cell remain unclear. The transition fibers anchor and stabilize the BB to the cell cortex [22]. DAVs contain EDH1 proteins which remove the capping protein CP110 from the mother centriole to allow maturation into the BB and elongation of the axoneme. ODF2, MARK4 and TTBK2 have also been associated with the removal of the CP110-CEP97 inhibitory complex [69,70]. Proteasomal degradation of the ciliogenesis inhibitor TCHP is also necessary for axoneme

growth [71]. EDH1 allows the DAVs to fuse into the ciliary vesicle which grows with the accumulation of RAB3IP and RAB8 (**Figure 2A**). Additional vesicles, derived from the Golgi apparatus and containing IFT20 and TZ proteins, are delivered to the ciliary vesicle [72]. The axoneme grows under the ciliary vesicle which differentiates into the ciliary membrane and the TZ is formed. BBSome proteins associated with RAB8 have been shown to participate in the extension of the ciliary membrane [73]. In sum, the initial steps of ciliogenesis require the degradation of the inhibitory proteins NDE1, CP110-CEP97, TCHP; and the growth of a ciliary vesicle which is formed through the fusion vesicles containing ciliary components.

Once the BB is correctly localized, the axoneme elongates and ciliary proteins need to be distributed along the ciliary membrane. Elongation of the microtubule skeleton through tubulin polymerization occurs at the distal part of the axoneme, at the plus (+) end of tubules A and B [74], but there is no protein synthesis in the ciliary compartment. Therefore, a constant importation of axonemal components is operated by the members of the intraflagellar transport complex B (IFT-B) and Kinesin-2, which are capable of anterograde transport (**Figure 2B**).

The IFT-B complex is composed of a core subcomplex with IFT22, IFT25/HSPB11, IFT27, IFT46, IFT52, IFT56/TTC56, IFT70, IFT74, IFT81 and IFT88, and a peripheral subcomplex with IFT20, IFT38/CLUAP1, IFT54/TRAF3IP1, IFT57, IFT80 and IFT172 [75]. Kinesin-2 motors are composed of KIF3A and KIF3B subunits with an accessory subunit KAP [76]. Tomographic electron microcopy has enabled the visualization of “long trains” of IFT-B/Kinesin-2 complexes bound to the B tubules of the axoneme [77]. Those “long trains” not only carry tubulin but also contain IFT complex A members (IFT-A) and Dynein-2 which are used for retrograde transport.Dynein-2 is loaded on anterograde trains away from the microtubules and in an autoinhibitory form [78]. Knockdown or knockout of IFT-B proteins or Kinesin-2 usually results in short cilia or complete absence of cilia [10,79-81]. BBSome proteins have also been observed travelling up and down the cilium to import proteins [73]. As

the microtubules grow, there is an accumulation of tubulin marks such as glycylation which participate in the increase of cilia length [82,83].

At the tip of the cilium, tubulin is continuously incorporated into the axoneme, whether it is growing or after the optimal length is reached. Thus, microtubule growth and cilia length are regulated by KIF7 [84], and tubulin can also be removed by the ciliary tip protein KIF19A [85].

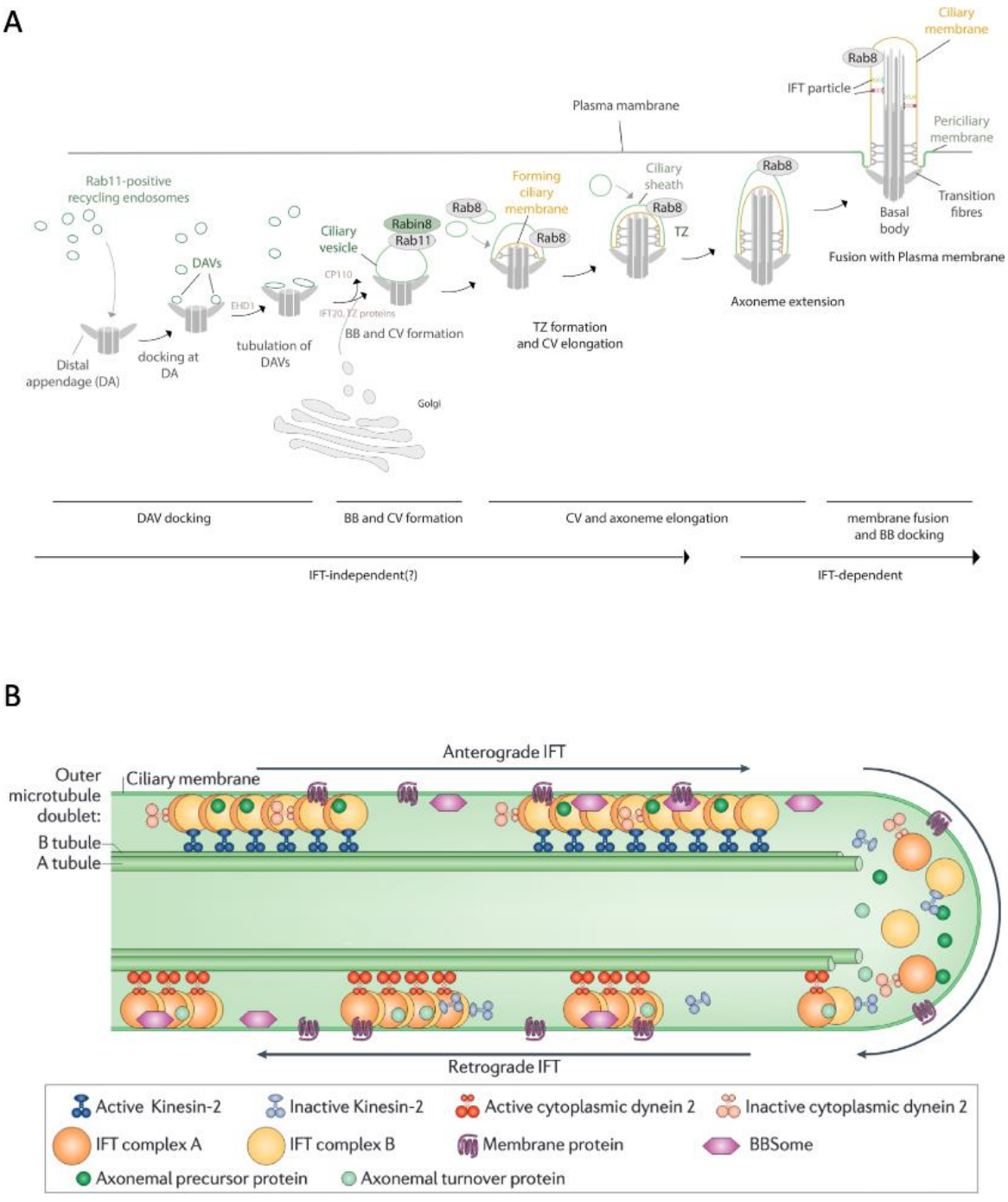

Figure 2: Ciliogenesis and cilia maintenance.

Figure 2: Ciliogenesis and cilia maintenance.

A. Model of early ciliogenesis. Rab11-positive recycling endosomes trafficked toward the mother centriole-associated distal appendages (DA). When the vesicles dock into the DA, they become distal appendage vesicles (DAVs). EHD1 included in the DAVs triggers SNARE-dependent membrane fusion to form the ciliary vesicle (CV). EHD1 also triggers transition of the mother centriole to the basal body (BB) by removing CP110 from the mother centriole. After the formation of CV and BB, small GTPase Rab8 is accumulated in the CV and is activated by Rabin8 from Rab11, facilitating elongation of the CV and axoneme. In addition, IFT20 and TZ proteins are delivered to the CV by Golgi-derived vesicles. During elongation of the CV and axoneme, the TZ is formed and the CV membranes are differentiated into the ciliary membrane (orange) and the ciliary sheath (green). Finally, the cilium is formed by the fusion of the ciliary sheath with the apical plasma membrane. The ciliary sheath becomes the periciliary membrane (green). **B.** Intraflagellar transport machinery. The canonical anterograde intraflagellar transport (IFT) motor, heterotrimeric Kinesin-2, transports IFT complexes A and B, axonemal proteins and cytoplasmic dynein 2 (previously known as cytoplasmic dynein 1b) to the tip of cilium. During this anterograde motion, Kinesin-2 is active and the retrograde motor, cytoplasmic dynein 2, is kept inactive to allow smooth processive anterograde movement. At the tip of cilium, anterograde IFT trains release axonemal proteins and rearrange their conformation for retrograde IFT. Cytoplasmic dynein 2 is activated and transports retrograde IFT trains to the cell body. Subsets of IFT trains are involved in transporting membrane proteins and the BBSome. Figure A and legend from [61], Figure B and legend from [17].

The switch from anterograde to retrograde transport also occurs at the tip of the cilium. IFT proteins, molecular motors and cargo dissociate and undergo a reorganization process to switch from anterograde to retrograde transport, now operated by IFT-A [86,87] (**Figure 2B**). IFT-A is composed of IFT43, IFT121, IFT122, IFT139, IFT140 and IFT144 and its associated molecular motor Dynein-2 is composed of DYNC2H1, WDR34, DYNC2L1 and DYNLL1. Together, they enable the repatriation of IFT-B particles to the BB for turnover by forming “short trains” associated to A tubules [77]. Retrograde transport is not required for ciliogenesis

but mutations in Dynein-2 components lead to stubby cilia in mice caused by protein accumulation [88]. Thus, cargo transport along the axoneme occurs at a steady state to enable the growth and maintenance of the axoneme [89]. Ciliary proteins first need to be brought to the ciliary compartment before they can circulate inside the cilium. Proteins involved in the importation of components from the *trans*-Golgi network to the TZ include the BBSome, IFT20 and small Rab GTPases [18]. The first transport mechanism is mediated by RAB11 and RAB8, similar to the formation of the ciliary vesicle. Vesicles coming from the *trans*-Golgi network and containing ciliary proteins, dock to the periciliary membrane with the cooperation of the exocyst complex, and deliver proteins to the TZ [90,91]. An important negative regulator of vesicle trafficking to the ciliary base is actin remodeling triggered by the Hippo pathway [92]. The second mechanism relies on IFT20 which is the only known IFT particle to localize to the Golgi apparatus [93]. IFT20 has been suggested to facilitate transport of ciliary integral membrane proteins from the *trans*-Golgi network to the BB [94]. Finally, the BBSome can recognize cilia-targeting sequences on transmembrane proteins and mediate vesicle transport to the BB. *Bbs2* and *Bbs4* knockout mice were shown to present structural and functional cilia defects. *Bbs2* knockout mice have fewer connecting cilia in their photoreceptors which results in the mis-localization of rhodopsin and cell death [95]. Additionally, *Bbs4* knockout mice have shorter and fewer cilia on olfactory sensory neurons [96], but longer cilia on renal tubule epithelial cells [97]. These examples illustrate a key role for the BBSome in the importation of proteins to the ciliary compartment. Proteins are then selectively allowed to cross the TZ. TULP3 has been shown to target ARL13B to the ciliary membrane but also works with IFT-A to assist the trafficking of G-protein-coupled receptors (GPCR) to the ciliary membrane [98]. The Hippo pathway complex MST1/2-SAV1 associates with the NPHP module and promotes ciliary localization of cargo during ciliogenesis [99]. The NPHP module also recruits KIF13B, of which localization in the ciliary compartment is necessary to maintain the restricted localization of CAV1 at the base of primary cilia membrane to promote Sonic HH signaling [100]. The TZ also regulates exportation of proteins

outside the ciliary compartment. Indeed, BBSome and IFT-B proteins facilitate the export of SMO and Patched (PTCH) receptors to allow transduction of the HH signaling pathway [101].

A feedback loop between autophagy, the proteasome, cilia and the mTOR pathway have been linked to ciliogenesis and cilia length regulation. Autophagy processes are required to provide amino acids for the building of cilia, and inhibition of autophagy typically impedes ciliogenesis [102]. Additionally, ciliogenesis prevents mTOR from inhibiting autophagy to allow ciliary elongation. On the other hand, short cilia activate the mTOR pathway which inhibits autophagy through HH signaling and subsequently increases the proteasome activity and thus decreases cilia length [103]. In sum, elongation of the axoneme and maintenance of the cilium is performed through the coordinated transport of proteins to the TZ mainly by the BBSome and the vesicular transport from the *trans*-Golgi network. Once, inside the ciliary compartment, transport along the axoneme is facilitated by IFT-B and IFT-A complexes.

Upon reentry in mitosis, a cell needs to disassemble and resorb its cilium to free the mother centriole, which is required for the formation of the MTOC. Several parallel signals can trigger this process. When activated, HDAC6 can destabilize microtubules by removing the acetylation marks on tubulin. This protein is usually spread in the cytoplasm but can be recruited to the ciliary compartment by the actin cytoskeleton and tumor-suppressor protein DIDO3 [104]. The cell reentry in mitosis corresponds to the inactivation of the Hippo pathway, and thus the activation of the downstream YAP/TAZ pathway and Aurora kinase A, which is encoded by *AURKA*. AURKA is a regulator of cell cycle progression and can associate with HEF1 and PIFO to phosphorylate and activate HDAC6 [92,105]. Depolymerization of microtubules is achieved by KIF24 when activated by the NEK2 kinase, which is highly expressed in S/G_2 phase [106].

III. Cilia function

1. Primary cilia facilitate transduction of signaling pathways

Non-motile primary cilia function as antennae which expose receptors to detect external cues and trigger an appropriate intracellular response (**Figure 3** and **Figure 4E**). Primary cilia can also modulate a number of signaling pathways not because of their shape but through the intervention of ciliary proteins. The well-studied signaling pathways associated with primary cilia are usually critical for organogenesis, cell homeostasis, and regeneration, including the HH pathway and the WNT pathway. Consequently, mutations in genes coding for ciliary components often result in defective signal transduction and thus severe developmental defects or cancer [107]. Here, I briefly describe some of the pathways known to signal through primary cilia in vertebrates to illustrate the complex role of what used to be called a vestigial organelle [9].

Hedgehog signaling. HH signaling plays a major role during embryonic development, where gradients of *HH* expression dictate patterns of cell fate for proper organogenesis. It was discovered in 1980 in *Drosophila* mutants with segmentation defects that were covered with denticles, hence the hedgehog analogy [108]. HH signaling is cilia-independent in *Drosophila*. In 2003, Huangfu *et al.* discovered the first clue associating the HH pathway and cilia in vertebrates when they identified two IFT-B mouse mutants (*Ift172* and *Ift88*) with phenotypes characteristics of Sonic HH signaling defects. They showed that IFT proteins regulate HH transduction and intervene downstream of the trans-membrane receptor PTCH and upstream of HH targets [12]. A few years later, different independent groups further characterized the link between HH signaling and cilia in vertebrates and showed that IFT proteins are responsible for trafficking HH effectors in and out of the cilia [37,88,109,110]. There are a variety of HH ligands produced across species, for instance mammals can produce three HH ligands: Sonic HH, Indian HH and Desert HH, and the zebrafish (*Danio rerio*) can produce six HH ligands: Sonic HHa, Tiggy-Winkle HH (or Sonic HHb), Indian HHa, Echidna HH (or Indian

HHb), Qiqihar HH and Desert HH. Despite being paralogs, they are all processed the same way and only differ by their expression patterns [111]. In the absence of HH ligand, PTCH receptors are localized to the ciliary membrane to prevent SMO from entering the ciliary compartment and GLI transcription factors are brought by IFT-B and sequestered at the tips of primary cilia by Suppressor of Fused (SUFU) (**Figure 3A**). Additionally, G-Protein coupled receptor 161 (GPR161) is targeted to the cilium by TULP3 and activates Protein kinase A (PKA), which in turn allows GLI3 repressor (GLI3R) to localize to the nucleus and prevent expression of target genes. Binding of HH ligand to PTCH receptors triggers PTCH and GPR161 to exit the ciliary compartment. PTCH exit from the ciliary compartment allows SMO to enter in the cilium where it is activated by EvC and can then inhibit SUFU to release GLI. Activated GLI2 then travels down the cilium via IFT-A and translocates to the nucleus where it can activate the transcription of target genes. GPR161 exit interrupts the production of GLI3R and activated GLI3 can trigger expression of target genes instead [112,113] (**Figure 3A**).

***Wingless-integrated* or WNT pathway.** Components of the WNT pathway were first described in the late 1970's-early 1980's. *wingless* was discovered in *Drosophila* and described as a key regulator of fly development [114], and its ortholog *Integrated1* was identified in mouse mammary tumor cells and described as an oncogenic factor [115]. The WNT pathway has three mechanisms of action which are β-catenin dependent (canonical WNT) or independent (Planar Cell Polarity or PCP, and calcium pathway). β-catenin is an integral E-cadherin involved in cell-cell adhesion and it also functions as a transcriptional co-regulator. The role of primary cilia in canonical WNT remains unclear [116]. Some evidence shows that canonical WNT is functional in the absence of cilia in mouse embryo [117] and developing zebrafish [118], but also that cilia can modulate the pathway, notably by restricting the activation of Dishevelled (DVL) [119] and sequestering AHI1 [120], which are two effectors of the WNT pathway.

Briefly, in unstimulated cells, the "destruction complex" (formed by Axin, APC and GSK-β) and CK1 phosphorylate β-catenin to trigger its ubiquitination by β-TrCP/SKP and thus

proteasomal degradation. In stimulated cells, WNT ligands bind to Frizzled (FZD) receptors which recruit the co-receptor LRP5/6 and activate DVL through phosphorylation. DVL destabilizes the “destruction complex” by removing GSK-β which then allows β-catenin to translocate to the nucleus where it associates with the transcription factors TCF and LEF to activate expression of target genes [121].

In contrast, the link between primary cilia and PCP has been well established because of the polarizing role of cilia on the epithelium. PCP corresponds to the homogenous orientation of cells within the plane of an epithelium and requires coordinated remodeling of the cytoskeleton and positioning of the centrosome/BB. To accomplish collective cell movements, cells secrete WNT ligands that will bind to FZD or VANGL2 trans-membrane receptors present on their neighboring cells, which in turn recruit the protein DVL. DVL can form a complex with intracellular DAAM1 to activate downstream effectors including the small GTPases RHO and RAC to initiate the c-Jun N-terminal kinase (JNK) pathway and trigger actin cytoskeleton remodeling [122] (**Figure 3B**). Actin cytoskeleton remodeling, as well as DVL and other BB proteins are then required for the proper migration of the BB to the apical pole of the cells and to allow PCP [123-125]. Alternatively, the binding of WNT-activated FZD to DVL can induce a calcium influx. Elevated intracellular calcium activates CaMKII, CaN and PKC which in turn activate the transcription factors NFAT and NF-κB to trigger the expression of target genes [122]. Not only do primary cilia enable non-canonical WNT signaling, but it has also been shown that WNT signaling can trigger cilia disassembly. CK1 can phosphorylate DVL2 to allow its interaction with the kinase PLK1, mostly known for its role at the kinetochores during the M phase of the cell cycle. The DVL2/PLK1 complex then stabilizes HEF1/AURKA complex to trigger cilia disassembly [126].

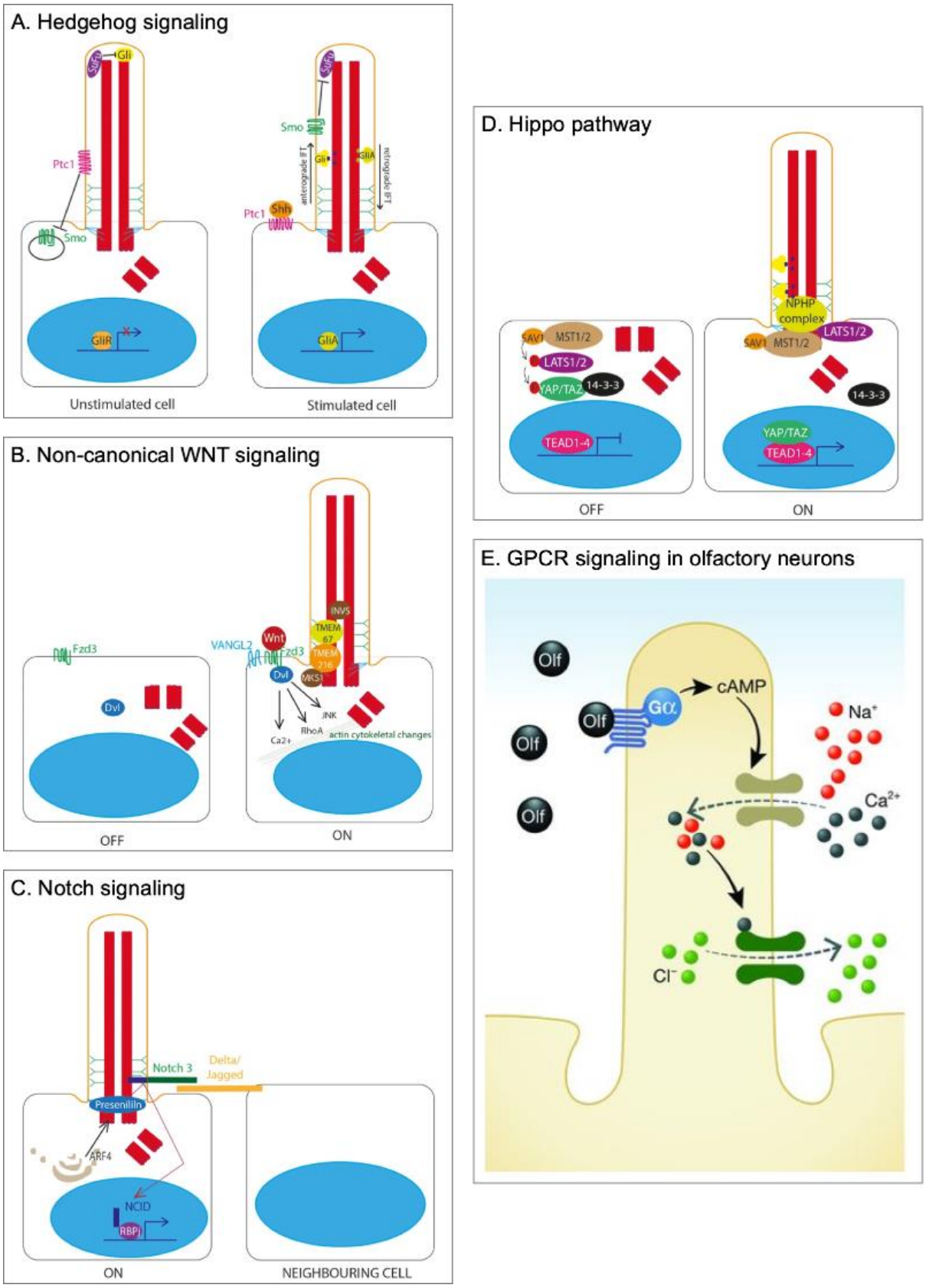

Figure 3: Signaling through the primary cilium.

Figure 3: Signaling through the primary cilium.

A. Unstimulated state: PTCH (here Ptc1) excludes SMO from the cilium. GLI are sequestered and inhibited by SUFU at the ciliary tip. Hedgehog signaling in stimulated state: HH binds to PTCH and relieves the repression of SMO. SMO represses SUFU and releases activated GLI (GLIA) which translocates to the nucleus and activates expression of downstream target genes. **B.** Non-canonical WNT ligand binds to FZD (here Fzd3) which can recruit DVL. Subsequent activation cascades result in changes in intracellular calcium and actin cytoskeleton remodeling. In PCP, the migration of the BB is regulated by DVL, TMEM67, TMEM216, INVS and MKS1. **C.** After contact between a Notch receptor and a membrane-bound Delta or Jagged ligand on an adjacent cell, Presenilin cleaves the NICD which can enter the nucleus and associate with RBPj to activate expression of target genes. **D.** Unstimulated state: a phosphorylation cascade inhibits YAP/TAZ. Phosphorylated YAP/TAZ is sequestered in the cytoplasm by 14-3-3. Hippo pathway activation: inhibitors of YAP/TAZ localize at the basal body through interactions with the NPHP complex, thus YAP/TAZ can enter the nucleus and complex with TEAD1-4 to activate transcription of target genes. **E.** GPCR signaling in olfactory cilia relies on the cAMP-dependent opening of ion channels, leading to an influx of Na+ and Ca2+ ions into the ciliary compartment, which in turn activates chloride channels, causing efflux of Cl^-, which results in a further depolarization of the cell. Olf: ligands for olfactory receptors. Figures A-D from [15] with adapted legends, E and its legend are from [127].

Notch signaling. Notch signaling is involved in cell fate and tissue homeostasis, and relies on the contact between the Notch receptor in the ciliary membrane and the transmembrane Delta or Jagged proteins from a neighboring cell. The γ-secretase Presenilin is located at the BB and cleaves the Notch intracellular domain (NICD) after the *trans* interaction occurred. The released NICD translocates to the nucleus and associates with the CSL transcription factor complex (composed of CBF1, Suppressor of Hairless, and Lag-1) to activate the expression of target genes [128] (**Figure 3C**). In zebrafish, Notch signaling leads to transcription of *her12* in the embryonic node which modulates the ratio of motile and immotile cilia required for proper establishment of the left-right axis [129].

Hippo pathway. This pathway obtained its name from the organ overgrowth phenotypes observed in *Drosophila* mutants for members of this pathway [130,131]. The Hippo pathway regulates cell fate during development and regeneration and is inhibited when cells are cycling, and thus do not possess primary cilia. In unstimulated cells, the transcription

co-activators and effectors of Hippo signaling YAP/TAZ are either degraded or retained in the cytoplasm by 14-3-3 because of their phosphorylated state (**Figure 3D**). In a stimulated cell starting to differentiate and grow a primary cilium, the Hippo pathway kinases MST1/2 and LATS1/2 localize at the BB through binding to the NPHP complex. MST1/2 forms a complex with SAV1 to phosphorylate and activate LATS1/2, which in turn phosphorylates YAP/TAZ [132]. MST1/2 can phosphorylate AURKA to prevent cilia disassembly and regulate cargo transport into the ciliary compartment to allow ciliogenesis [99], while non-phosphorylated YAP/TAZ can enter the nucleus and associate with TEAD1-4 to trigger transcription of target genes [132] (**Figure 3D**).

Platelet-Derived Growth Factor (PDGF) signaling. PDGF signaling is involved in cell migration and tissue homeostasis. PDGF receptors (PDGFR) are tyrosine-kinase receptors present in the ciliary membrane (PDGFRα) or cytoplasmic membrane (PDGFRβ), which need to dimerize upon ligand binding to initiate a response cascade. PDGF ligand binding to PDGFRα causes the dimer to auto-phosphorylate and thus be recognized by either P85 to initiate the PI3K-AKT cascade, or GRB2 to initiate the MEK-ERK cascade. Those signals function in parallel to allow activation and proper homogenous localization of the SLC9A1 Na^+/H^+ antiporter channels at the leading edge of migrating cells, as well as cytoskeleton reorganization [133]. Additionally, PDGFRβ initiates ciliary resorption by activating the PLCγ pathway and AURKA [134].

Transforming Growth Factor β (TGF-β) and Bone Morphogenic Protein (BMP) signaling. Receptors of TGF-β and BMP ligands, TGF-βR and BMPR respectively, are located at the tip of primary cilia and form homodimers upon activation. TGF-βR then travel to the ciliary pocket where they undergo clathrin-mediated endocytosis but can also activate ERK1/2 while still in the ciliary compartment [135]. The transcription factors SMAD2/3 are anchored in early endosomes at the base of the cilia and are activated by TGF-βR. Activated SMAD2/3 then associates with SMAD4 to translocate to the nucleus and initiate expression of target genes [136]. On the other hand, activated BMPR travels down the cilium and activates

SMAD1/5/8 directly, and also requires SMAD4 for entry into the nucleus. Proteins involved in the recycling of TGF-βR [137,138] and feedback inhibitors of TGF-β/BMP [135,139] signaling are localized at the base of the cilia to allow rapid turnover.

mechanistic Target Of Rapamycin (mTOR) signaling. mTOR signaling can be activated downstream of WNT signaling, pathways triggered by growth factors (such as PDGF) and hormones (such as insulin), and many others. mTOR is an atypical serine/threonine kinase which can assemble in two complexes: rapamycin-sensitive mTORC1 which modulates protein and lipid synthesis, autophagy and energy metabolism; and rapamycin-insensitive mTORC2 which regulates cell survival and metabolism as well as cytoskeletal organization [140]. In the context of primary cilia, mTOR has been studied predominantly in kidneys. Urine flow in renal tubules activates LKB1 located in cilia which then travels down to the BB to phosphorylate AMPK, which in turn phosphorylates Tuberin (TSC). TSC can increase GTP hydrolysis on the small GTPase RHEB to inactivate it. As a consequence, RHEB can no longer phosphorylate and activate mTORC1 [141]. Additionally, PC1, a protein mutated in polycystic kidney disease (PKD), also inhibits mTORC1 to prevent cell hypertrophy and proliferation. Rapamycin can thus be used as a treatment to reverse PKD caused by mutations in PC1 [142]. In zebrafish, stimulation of mTORC1 leads to longer cilia while rapamycin treatment leads to shorter cilia through a possible regulation of autophagy and thus protein availability for cilia growth [143].

2. Cell-type specific specialization of primary or motile cilia

Besides facilitating the transduction of critical signaling pathways involved in development and homeostasis, a subset of primary cilia is also specialized in the perception of the environment. One example is the previously mentioned connecting cilium in the photoreceptors, which uses a different signaling cascade involving the GPCRs to communicate with other retinal neurons. Furthermore, motile cilia present on epithelial cells, allow fluid flow in tubular organs.

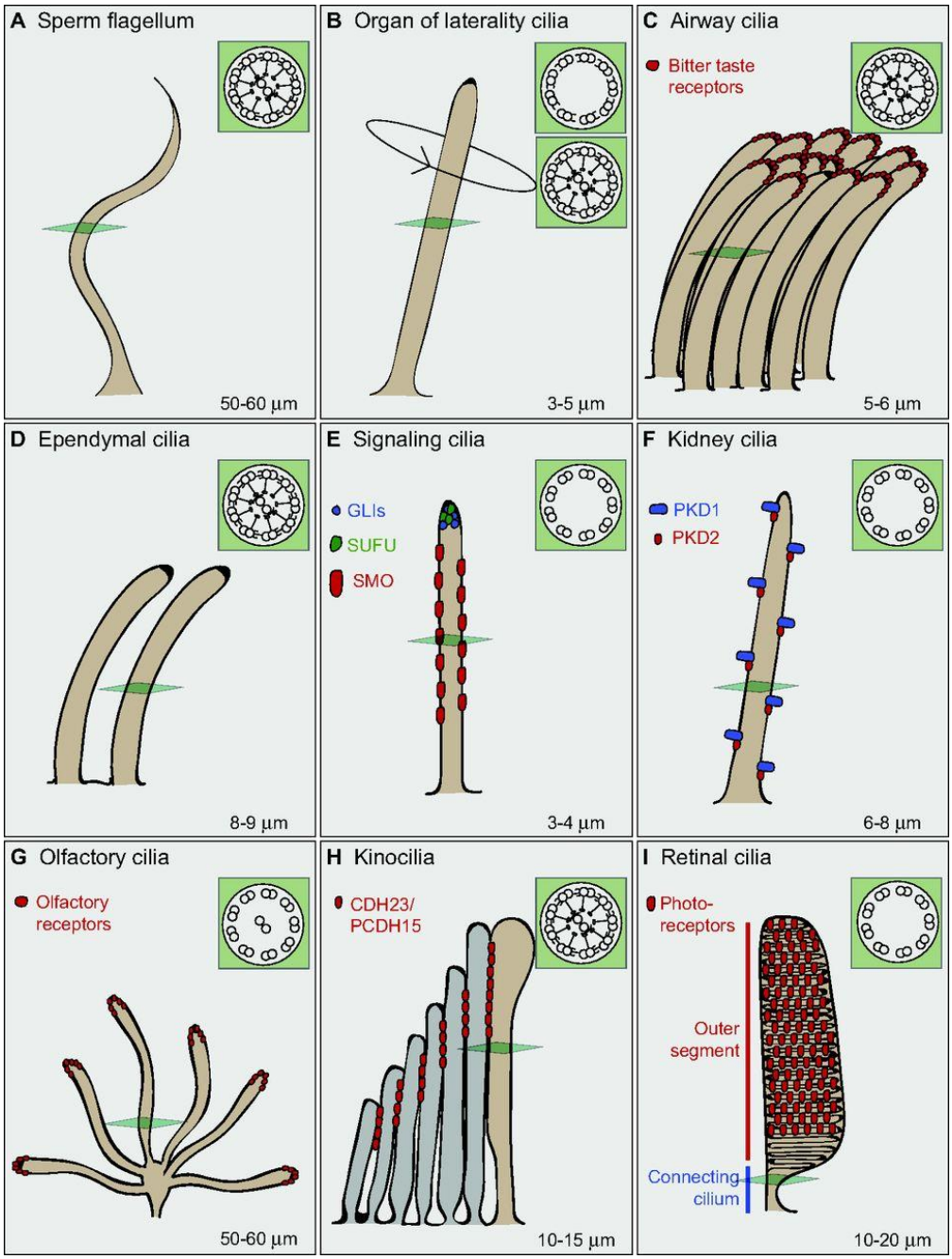

Figure 4: Specialized cilia in vertebrates.

The numbers of cilia drawn indicate how many cilia are present per cell (one or many), whereas the average lengths of the cilia found in humans, mice or rats is given in the bottom right of each panel. The insets depict the ultrastructure of a transverse section of the cilium (position of sections indicated in green). **A.** The sperm flagellum moves with a whip-like motion. **B.** Motile nodal cilia move in a vertical manner. **C.** Human airway cilia with bitter taste receptors. **D.** Biciliated ependymal cells. **E.** HH signaling pathway signals through the solitary signaling cilia. **F.** Mechanosensory proteins PKD1/2 localize to renal cilia to sense urine flow. **G.** Cilia on olfactory sensory neurons. **H.** The kinocilium serves to polarize the stereocilia (gray) during development of auditory hair cells. CDH23, cadherin 23; PCDH15, protocadherin 15. **I.** Retinal cells have a specialized connecting cilium that gives way to the outer segment. Figure and shortened legend from [144].

GPCRs. GPCRs can be found on the primary cilia of a variety of cells including neurons, cholangiocytes and renal epithelial cells. In the inactivated state, GPCRs are bound to an inactive heterotrimeric complex of α, β and γ G-proteins. Upon ligand binding to the GPCR, the G-protein α subunit exchanges its GDP for a GTP which triggers its dissociation from the two other subunits β and γ. G-protein α subunit and the complex formed by the β and γ subunits can then regulate their own effectors. In the meantime, the activated GPCR is phosphorylated by a G-protein-coupled-receptor kinase (GRK) which can then attract β-arrestins. β-arrestins promote the internalization of activated GPCR to regulate signaling [145]. GPCRs on neurons can be activated by neurotransmitters such as dopamine [146], photons [147] and odorant molecules [148]. The photoreceptors in the retina are specialized neurons capable of sensing light through their outer segment (**Figure 4I**). Opsins are GPCR chromophores with 11-cis-retinal which undergo a conformation change upon absorption of a photon. Downstream effectors cause a decrease in intracellular cGMP levels, the closing of cGMP-gated channels and thus a hyperpolarization of the photoreceptors. The electrical stimulus is then transmitted to the brain via the retinal neurons [145,147]. Olfactory sensory neurons are multiciliated cells and each ciliary tip is covered with odorant GPCRs. Their activation causes the following ordered response: an increase in the intra-cilium level of cAMP, an increase in calcium level, the activation of calcium-gated chloride channels and the depolarization of the olfactory sensory neuron [145,148] (**Figure 3E**). GPCRs on cholangiocytes are activated by bile acids and can trigger ERK1/2 signaling to regulate cell proliferation. Defective cilia on cholangiocytes can affect fluid secretion and lead to hepatic fibrosis [149,150]. The primary cilia on kidney epithelial cells have been associated with at least two types of GPCRs: vasopressin receptors [151] (**Figure 3E**) and the dopaminergic receptors. Vasopressin hormone plays a key role in maintaining the hydroelectrolytic homeostasis in mammals and dopamine has been associated with ciliary maintenance in the context of the kidney [152].

Mechanosensation. Specialized cilia can be stimulated physically by fluid flow or vibrations. In renal epithelial cells, PC1 and PC2 localize to primary cilia membranes and are

capable of sensing urine flow in the kidney tubules [13] (**Figure 4F**). The bending of cilia by fluid is detected by the large extracellular domain of PC1. PC1 then activates the non-selective cation channel PC2 which causes a calcium influx in the primary cilium which is propagated into the cytoplasm via activation of the ryanodine receptor [153,154]. PC2 is also able to complex with TRPC1 or TRPV4 in response to fluid flow to increase intracellular calcium and regulate MEK/ERK signaling [155,156]. Another example of mechanosensory cilia, stereocilia in the cochlea are arranged in small arrowhead-like groups composed of three rows of cilia sorted according to their size (**Figure 4H**). Sound waves trigger vibrations in the tectorial membrane in the organ of Corti which causes the stereocilia to bend. This change activates the mechanoelectrical transduction channels which allow calcium entry into the cells and subsequent electrical signal transmission to the brain [157]. Although most of the literature currently links mechanosensation to calcium signaling, recent findings questioned this hypothesis by showing that no calcium flux was detected in cultured stimulated kidney epithelial cells [158].

Cilia beating generates fluid flow and allows motility. Multiciliated epithelial cells (up to 300 motile cilia/cell) can be found lining the surface of the ependymal canal and brain ventricles to allow circulation of the cerebrospinal fluid and signaling molecules [159] (**Figure 4D**); the respiratory tracts to move mucus [160] (**Figure 4C**); and in the Fallopian tubes to transport eggs to the uterus [161]. Motile monocilia include nodal cilia and sperm flagella (**Figure 4A, B**). Early in development, nodal cilia generate a leftward fluid flow [8,129] which is detected by surrounding non-motile primary cilia bearing PC2 channels. The subsequent signaling cascade involving calcium influx and the TGF-β Nodal allow transcription of target genes to establish the left-right patterning [162]. However, recent findings argue that fluid sensing is not sufficient to trigger symmetry breakdown and that the fluid flow might also enable the transport of signaling molecules [163]. Sperm are propelled by flagella to travel to the oocyte for fertilization [164]. The length of the cilia and the beating speed vary across tissues and species: ependymal cilia have been reported to be longer (8.2 μm) and to beat faster (40.7 Hertz) than tracheal cilia (5.5 μm, 20.9 Hertz) in rats [165], and human sperm

flagella length can vary between 36.18 to 49.75 µm [166]. Beating of motile cilia is facilitated by the molecular motor dynein, which uses ATP to provoke sliding of the peripheral microtubule doublets and the bending of the axoneme [50]. The radial spokes and central microtubule doublet coordinate the sliding. Studies in *Chlamydomonas* showed that kinases (PKA and CK1) and phosphatases (PP1 and PP2A) localize to the radial spokes in flagella, and are involved in regulating cilia motility by controlling dynein activity [167-169].

3. Primary cilia in cancer

Primary cilia and cancer are inevitably linked because of the dual identity of the centrosome being the MTOC during mitosis or the BB in differentiated cells. Loss of primary cilia have been observed in several types of cancer including pancreatic, breast and ovarian cancers [170-172]. The presence of a cilium on a cell inhibits its proliferation until it is resorbed. As a result, any defect in ciliogenesis or cilia disassembly will have consequences on the cycling capacity of a cell. The ciliary disassembly proteins HEF1, NEK2 and KIF24 have been found to be overexpressed in breast cancer and to contribute to metastasis [173]. Additionally, the signaling pathways described above (HH, Hippo, etc) regulate cell fate, cell proliferation and cell homeostasis which can lead to cancer if mis-regulated [174]. Knockdown of IFT20 in mouse fibroblasts has been showed to inhibit ciliogenesis and to prevent the localization of PDGFRα at the ciliary membrane. Spread in the plasma membrane, PDGFRα were overactivated and triggered uncontrolled cell proliferation [175].

To conclude, cilia are involved in virtually every step of life: from embryonic development to later homeostasis and allow organisms to perceive and respond to their environment.

IV. Ciliopathies

Consistent with the near-ubiquitous presence of cilia across tissues, and their critical role in organogenesis and maintenance, it is not surprising that perturbation in cilia structure or function causes a host of human genetic disorders. Primary ciliary dyskinesia, characterized by situs inversus, hydrocephalus and chronic airway infections [176], garnered initial attention as a clinical entity caused by impaired motile ciliary beating capacity. In the early 2000s, defects in the primary cilium were implicated as the molecular cause of additional rare human genetic disorders, including isolated renal cystic disease (nephronophthisis [177,178]); and BBS, a genetically heterogeneous disorder characterized by retinitis pigmentosa, polydactyly, obesity, learning difficulties, and renal anomalies [179]. These studies established a role for cilia in human disease; defined the ciliopathies as a clinical collection of organellar disorders; and led to the identification of a multitude of additional phenotypically-overlapping pathologies [180]. Ciliopathies manifest in a spectrum of hallmark phenotypes with variable penetrance and expressivity [3,180,181]. Although individually rare, there are ~100 suspected or established cilia-related clinical synopses reported in the Online Mendelian Inheritance in Man database (https://omim.org/) with a collective incidence of ~1:1000, which is comparable to Down syndrome [182]. (Paragraph from [16]),

1. Clinical synopses and diagnosis

Hallmark ciliopathy phenotypes include: retinopathy, cysts (in kidneys, liver, pancreas), skeletal abnormalities (thoracic dystrophy, craniofacial anomalies and polydactyly), hydrocephaly, encephalocele, infertility, obesity, respiratory infections, cerebellar hypoplasia, intellectual disability and *situs inversus* [180,182] (**Figure 5**). Leber congenital amaurosis, a non-syndromic ciliopathy characterized primarily by retinitis pigmentosa, is incapacitating but not life-threatening and represents an example of the mild end of the ciliopathy severity spectrum [15,183].

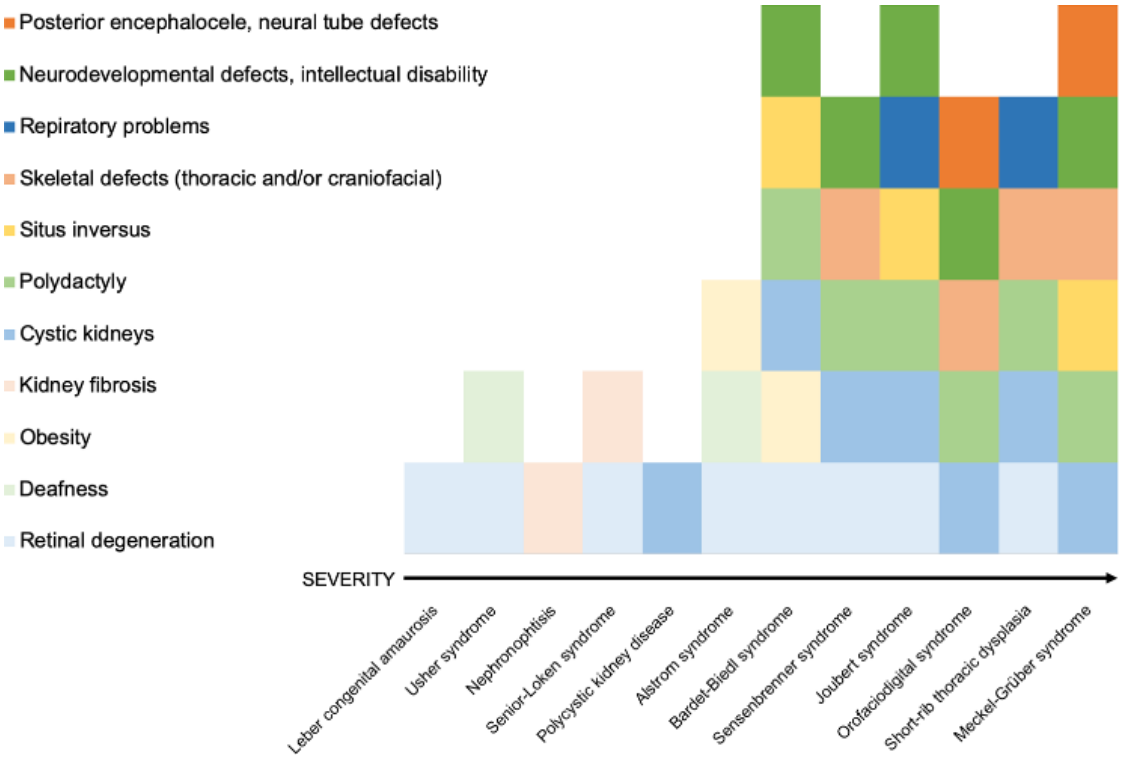

Figure 5: Spectrum and overlap of clinical manifestations in ciliopathies.

Non-exhaustive chart showing the different symptoms predominant in ciliopathies and how they overlap across syndromes. There is an intuitive correlation between the number of affected organs and the severity of a ciliopathy. Ciliopathies at the beginning of the spectrum (left) usually correspond to non-syndromic manifestations that do not impair reproductive fitness while syndromes at the end of the spectrum (right) can be lethal. Figure 5 produced with data from [184] and [182].

One approach for defining ciliopathy disease severity has been proposed based on the number of organ systems that are affected: Usher syndrome and Senior-Loken syndrome are both characterized by a retinopathy plus an additional affected organ (deafness and nephronophthisis, respectively), and Joubert syndrome is clinically characterized by a retinopathy, kidney defects, cerebellar hypoplasia and intellectual disability. Among the most severe ciliopathies, Meckel-Grüber syndrome is characterized by defects in all assessed organs, and the non-closure of the neural tube is embryonic lethal [185] (**Figure 5**).

Proposed classification of ciliopathies. Recently, Reiter & Leroux have proposed a classification for ciliopathies [3]. First, they proposed a distinction between first-order ciliopathies caused by mutations in genes coding for proteins directly involved in cilia biology, and second-order ciliopathies caused by mutations in genes coding for proteins which do not localize to cilia but indirectly regulate ciliogenesis and cilia maintenance. For instance, mutations in the IFT-A complex member IFT139/TTC21B, involved in retrograde transport in cilia, have been associated with the first-order ciliopathies nephronophthisis and short-rib thoracic dysplasia (also known as Jeune syndrome) (**Table 1**) [186]. Alternatively, mutations in the dynein assembly factors which localize to the cytoplasm are responsible for the second-order ciliopathy primary ciliary dyskinesia [187]. The RFX family of transcription factors and the FOXJ1 transcription factor have been associated with the expression of many genes coding for ciliary proteins [144]. Although no ciliopathies have been reported to be caused by mutations in either gene yet, they are predicted to result in second-order ciliopathies. Second, an intuitive separation between motile and sensory ciliopathies has been proposed [3]. Thus, primary ciliary dyskinesia can be considered a second-order motile ciliopathy and nephronophthisis is a first-order sensory ciliopathy. Finally, Reiter & Leroux suggested a third group of ciliopathies called extraciliary disorders to account for diseases caused by mutations in proteins having ciliary and non-ciliary functions. To date, no human disease has been firmly associated with this category. However, the craniofacial phenotype caused by impaired collagen secretion in mice with *Ift20* specifically knocked-out in neural crest cells could fall in this category [3,188].

From mutation to clinical manifestation. Due to the distinct functions of motile *versus* primary cilia, it is possible to predict, albeit with some exceptions, the symptoms that can result from defects in each ciliary subtype. Defects in proteins involved in ciliary motility likely cause chronic airway infections due to improper mucus clearance; infertility due to poor sperm motility or oocyte transport; and headaches or hydrocephalus due to dysregulated flow of the cerebrospinal fluid [176,189]. Establishing relationships between protein defects and symptoms in non-motile ciliopathies is more challenging because of the multiple roles of

primary cilia. Most skeletal anomalies have been attributed to ciliary defects affecting HH signaling [190,191] and retinopathies have been linked to degeneration of the photoreceptors caused by defects in the connecting cilia [192,193], however the tissue-specific manifestation of defective ubiquitous ciliary proteins remains to be elucidated. Symptoms can also be categorized in developmental or degenerative defects. If a signaling pathway essential for organogenesis or the establishment of the neuronal network connectivity is affected, symptoms will likely be detected prenatally or during early childhood. For instance, 61% of individuals with Bardet–Biedl syndrome have learning difficulties [194], likely due to impaired brain development [195]. However, the degeneration of photoreceptors, hair cells in the ear, or the formation of cysts, is progressive and symptoms might appear later in life [196]. Finally, the variable phenotypic severity observed within affected members of a family highlight the variable expressivity of ciliopathies. For example, in a case report describing a family with a deleterious mutation in *WDR35*, patients' symptoms range from fulfilling clinical diagnostic criteria for Sensenbrenner syndrome to an unclassified short rib-polydactyly condition [197]. Thus, improved mechanistic knowledge about ciliary proteins intersected with mutational data and longitudinal phenotype data from ciliopathy cases will improve our predictive capacity and clinical management of patients.

Treatments. To date, available treatments for ciliopathies are few and seek to alleviate symptoms. Even so, research in gene therapy, stem cell transplantation, and discovery of pharmacological molecules is still ongoing [198,199].The intranasal injection of a IFT88-GFP adenovirus in *Tg737*^{OPRK} mice successfully rescued ciliary defects and restored olfactory functions [200]. More recently, two novel approaches were developed to improve visual acuity of individuals with Leber congenital amaurosis caused by the intronic mutation c.2991+1655A>G, which leads to the aberrant inclusion of intronic sequence and a premature STOP codon in *CEP290*. The intravitreal injection of an antisense oligonucleotide was shown to efficiently restore the correct splicing of *CEP290* transcripts in patients [201], and Maeder *et al.* developed the EDIT-101 genome-editing therapeutic approach which uses the CRISPR/Cas9 technology to crop out a genomic region around the mutation in patients'

fibroblasts [202]. Human stem cell therapy also offers a therapeutic opportunity to treat retinopathies. However, only RPE cells have been successfully transplanted to date and further trials are required to allow photoreceptor transplants [203]. Read-though therapy can be used in the case of disorders caused by a premature STOP codon. It consists in transforming a premature STOP codon into a missense mutation by administrating drugs which destabilize proofreading mechanisms [204]. It has been proposed in the treatment of Usher syndrome through the PTC124 drug [205], retinitis pigmentosa via the G418 and PTC124 drugs [206], and primary ciliary dyskinesia through aminoglycosides [207]. In other cases, molecules are used to modulate specific biological pathways. The administration of valproic acid, guanabenz or a Caspase12 inhibitor can protect photoreceptors from cell death in *Bbs12* mutant mice [208] and cAMP signaling has been proposed as a target in the treatment of PKD [209]. More recently, the flavonoid compound eupatilin has been shown to restore the localization of Nphp5 at the ciliary base in *Cep290* mutant mice and to improve their retinopathy [210]. Finally, the pharmaceutical company Rhythm has an ongoing clinical trial to treat obesity in BBS patients. It consists in daily subcutaneous injections of setmelanotide, an agonist of the melanocortin-4 receptor, to reduce hunger in affected individuals [211]. Overall, the genetic heterogeneity of the ciliopathies has imposed major challenges for therapeutic development, but the greatest potential for drug advancement is currently in the readily accessible cell types of the eye.

2. Genetic architecture of ciliopathies

Ciliopathies are inherited in an autosomal recessive manner with few exceptions: autosomal dominant polycystic kidney disease [212], Von Hippel-Lindau syndrome (autosomal dominant) [213] and X-linked forms of primary ciliary dyskinesia [214] and retinitis pigmentosa [215]. Overlap across ciliopathies are seen not only at the clinical manifestation level but also at the genetic level (**Table 1)**, suggesting that the genetics underlying ciliopathies is more complex than a simple monogenic paradigm.

Linear relationships between allele and symptom. In some cases, there is a robust correlation between a mutation and its clinical manifestation. This can be specific to a particular gene, the allele strength (e.g. loss of function versus hypomorph), and the protein domain in which the mutation resides. For instance, BBS8 is enriched in mammalian photoreceptors and a case report of a consanguineous pedigree showed that a splice-site mutation in *BBS8* was sufficient to cause non-syndromic retinitis pigmentosa [216]. This type of relationship between tissue specificity and symptoms was also observed at the level of specific isoforms of *BBS8* [217] and *RPGR* [218]. Some genes do not show such a strong organ specificity but have a tendency to associate with defects in specific tissues. For instance, mutations in *IFT140* are associated with severe kidney defects [219], but an explanation for this organ sensitivity remains to be elucidated. In some instances, the severity of a syndrome could be linked to the disrupting level of an allele: in the same gene *MKS1*, a frameshift mutation and a substitution in a splice donor site result in Meckel-Grüber syndrome [220], while substitutions causing amino acid missense lead to the milder BBS [221]. Similarly, truncating mutations in *MKS3* cause Meckel-Grüber syndrome but missense mutations cause nephronophthisis [222]. Furthermore, it is hypothesized that the outcome of missense mutations in *IFT172* depends on which macromolecular complex association is disrupted by the mutation (IFT or BBSome) [3,223]. This illustrates how interdisciplinary studies merging genetics (nature of alleles), cell biology (role of proteins) and biochemistry (protein interactions) has contributed to refined explanations for a portion of the variability observed in ciliopathies. Finally, a global study on the morbid genome of ciliopathies based on the sequencing of 371 ciliopathy patients from 265 mostly consanguineous families concluded on a fully penetrant model for the 225 causal mutations identified (85% of the families), further supporting a monogenic model for ciliopathies [224].

Table 1: Genetic overlap and genes contributing to total mutational load in 10 ciliopathies.

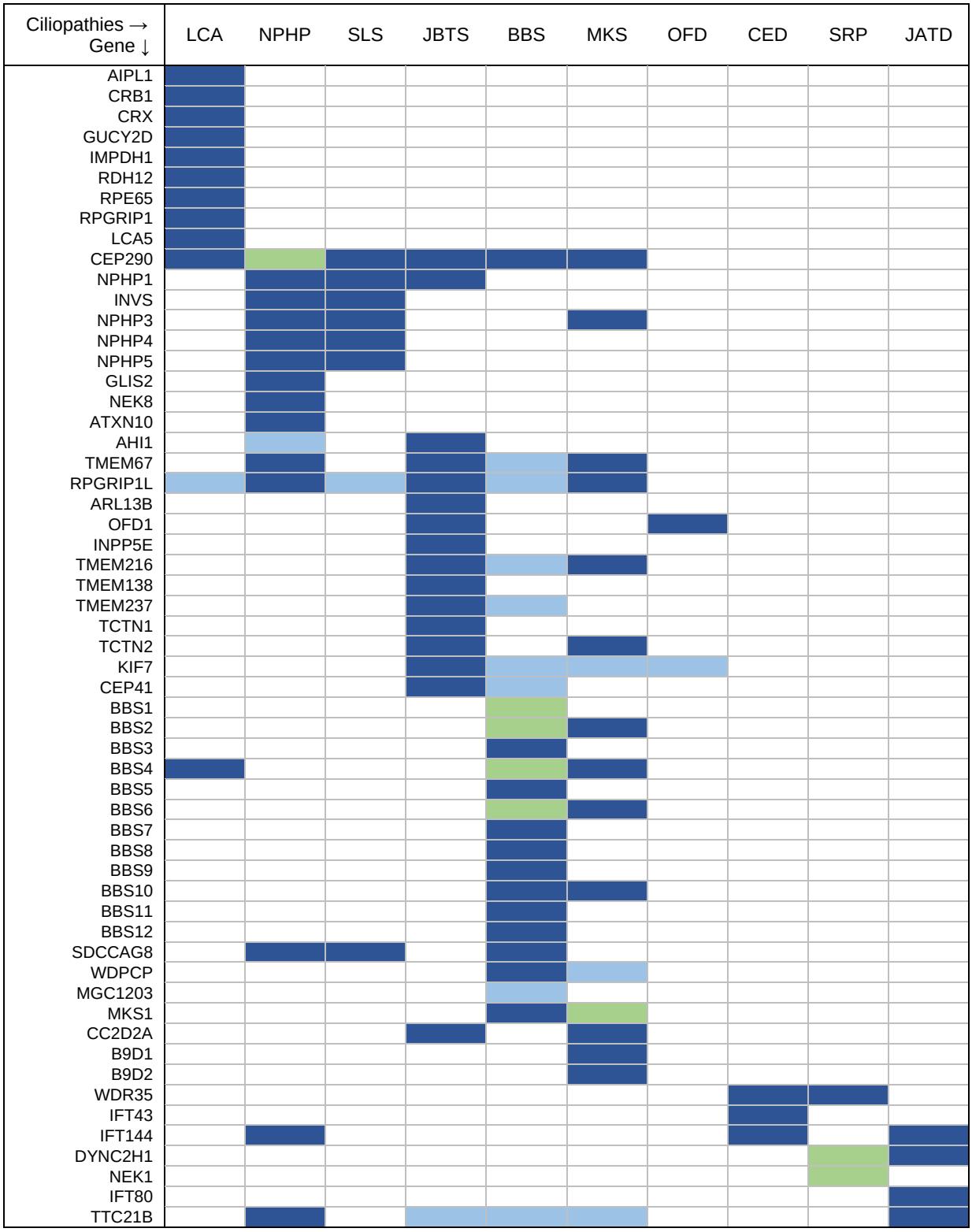

LCA: Leber congenital amaurosis, NPHP: Nephronophthisis, SLS: Senior-Loken Syndrome, JBTS: Joubert Syndrome, BBS: Bardet-Biedl Syndrome, MKS: Meckel-Grüber Syndrome, OFD: Orofaciodigital Syndrome, CED: Sensenbrenner Syndrome, SRP: Short rib polydactyly, JATD: Jeune Asphyxiating Thoracic Dystrophy. Primary locus, modifier locus, both. Adapted from [182].

Table 1 gives an overview of the genetic complexity of ciliopathies: while hypomorphic mutations in *ARL13B* are associated strictly with Joubert syndrome, the implication of null alleles of *CEP290* in five different ciliopathies with a wide range of severity, from Leber congenital amaurosis to Meckel-Grüber syndrome, strongly argues against a model of monogenic disease [185]. Hypotheses to explain the variation in the clinical manifestation are the presence of modifier genes and increased mutational burden in ciliary protein encoding genes.

Modifier genes. Several modifiers of ciliary phenotypes have been reported (**Table 1**). For instance, a common allele in *RPGRIP1L* has been proposed to be a modifier of the retinopathy observed in ciliopathies with support from genetics, biochemical and *in vivo* modeling data [225]. Additional examples in the literature include: heterozygous deleterious variants in *TTC21B/IFT139* which might act as modifiers of polycystic kidney disease [226], and some *IFT140* alleles which might act as modifiers of short-rib thoracic dysplasia [219]. The identification of modifier genes is not only key to better understand the genetics behind ciliopathies and improve prognosis but it also has the potential to offer additional therapeutic targets which might be more accessible than the primary pathogenic cause. However, identification of phenotype modifiers using human genetic data remains challenging because it requires large cohort numbers (intractable in the individually rare ciliopathies), and the modifier locus must be common enough to be detected (with sufficient statistical power). To bypass these limitations and to identify candidate modifiers which may not be naturally occurring, researchers have deployed new techniques such as suppressor screens and the use of model organisms. Suppressor screens aim to identify mutations and genes which can modulate the phenotype of a disease causing mutation and thus uncover potential modifiers. A suppressor screen performed on mouse models of Rett syndrome, a severe form of autism, identified cholesterol homeostasis as a potential treatment target for patients [227], and we postulate that the same powerful approach could prove to be informative in a ciliopathy context. The zebrafish has been proven to not only be a robust model to test human allele pathogenicity but also to investigate genetic interactions [228]. This approach allows

exploration of genetic interactions by knocking down, knocking out or over-expressing several genes in parallel. One example is the identification of *vangl2* as a modifier of connecting cilia length in the photoreceptors of *arl13b* zebrafish mutants, thus proposing that PCP genes should be considered for modifiers of Joubert syndrome and other ciliopathies [229].

Oligogenic phenomena and mutational burden. BBS was among the first documented disorders wherein some pedigrees required three alleles (the recessive locus plus an additional heterozygous pathogenic variant) to manifest the syndrome [230]. The study showed that two siblings carried compound heterozygous nonsense mutations in *BBS2* but that only the child bearing a third nonsense mutation in *BBS6* was affected. Although this phenomenon was observed in thirteen BBS families [231] and was also suspected for nephronophthisis [232], the rarity of this inheritance model has made it subject to controversy [224,233]. Nonetheless, these initial reports of oligogenic alleles paved the way to a new revised hypothesis to explain phenotype variability within and among affected individuals; mutational burden at other ciliary loci can influence ciliopathy phenotype. This paradigm was already observed in two non-ciliopathic disorders includingCharcot-Marie-Tooth disease [234] and hypogonadotropic hypogonadism [235]. By revisiting this hypothesis directed at BBS, it was found that copy-number variations could also contribute to the mutational burden as secondary sites in addition to a recessive BBS locus [236]. Moreover, recent work suggests that additive and multiplicative effects of recessive variants with deleterious heterozygous variants inside a same biochemical module (BBSome) is enriched in BBS [237]. Replication of this study by evaluating the IFT, NPHP or other recently characterized modules [238] could refine further our understanding of ciliopathies as well as other Mendelian disorders hallmarked by phenotypic variation and genetic heterogeneity.

Genetics of ciliary modules. Prior to genetic studies that sought to quantify mutational burden, ciliary modules and interactome maps had gained interest through the concept of systems-biology. The characterization of the different ciliary modules and their components enabled the identification of candidate ciliopathy genes and brought insights into

the pathomechanisms of ciliopathies. The first characterization of the BBSome showed that seven of the twelve *BBS* genes known at the time were coding for members of the same complex which illustrates the relationship between functional module and phenotype [73]. The study of the proteins mutated in Meckel-Grüber syndrome and nephronophthisis which present overlapping symptoms, allowed the identification of the MKS and NPHP modules. The characterization of those modules enabled us to understand the role of the TZ as a selective gate operated by the MKS and NPHP modules [239]. By using those modules as baits in proteomics analysis, in combination with linkage and sequencing analysis of patients affected by nephronophthisis and Joubert syndrome, *Sang et al.* identified *ATXN10* and *TCTN2* as novel ciliopathy genes [240]. A study on the members of the IFT-B complex identified *IFT172* as a novel gene for short-rib thoracic dysplasia, and suggested a relationship between members of the IFT-B complex and skeletal ciliopathies, similar to what was already observed for the members of the IFT-A complex [241]. A yeast two-hybrid assay enabled to understand the function of FAM161A which is lost in recessive forms of retinitis pigmentosa [242]. Indeed, only the localization of FAM161A at the connecting cilium of photoreceptors was known, but the identification of its interacting partners enabled to elucidate its function in the Golgi-centrosomal network [242]. Those different studies and work from other groups allowed Reiter & Leroux to dissect the structural network of motile *versus* non-motile cilia, the ciliogenesis temporal network, and the ciliary trafficking network to build maps of proteins and ciliopathies [3]. This visualization can inform on symptoms being linked to defect in a specific compartment such as hearing loss being associated to early defects in basal body maturation, or organ sensitivity such as the kidney being affected exclusively in case of ciliary transport defects.

3. Spinocerebellar ataxia 7, a candidate ciliopathy?

By evaluating the function of a protein or the clinical manifestations of a syndrome, several reviews have proposed inclusion of some human genetic disorders in the spectrum of ciliopathies [180,243]. For instance, short-rib thoracic dysplasia syndrome was proposed to be a ciliopathy based on its clinical manifestation before the ciliary defect was identified as the cause of the disease [243]. Spinocerebellar ataxia 7 (SCA7) is an autosomal dominant neurodegenerative disorder caused by a mutation in Ataxin-7 (ATXN7) and characterized by progressive cerebellar ataxia and retinal degeneration [244,245] (**Figure 6**). These hallmark cerebellar and retinal features resemble characteristics listed among the top nine relevant features to predict ciliopathies [243]. Further, ATXN7 has been shown to interact with the centrosomal/BB proteins CEP70 and CEP72 [246]. These observations have led us to hypothesize that SCA7 could be part of the ciliopathy spectrum.

The well-characterized genetics of SCA7. The expansion of the polyglutamine (polyQ) tract [244] and the gene [245] causing SCA7 were identified in 1995 and 1998 respectively. Based on the mutational mechanism, SCA7 has been classified as one of nine polyQ expansion disorders which also include spinocerebellar ataxias 1, 2, 3, 6 and 17, dentatorubralpallidoluysian atrophy, spinal-bulbal muscular atrophy and Huntington's disease. They are autosomal dominant diseases (with the exception of X-linked spinal-bulbal muscular atrophy) caused by an expansion of cytosine-adenine-guanine (CAG) repeats in their corresponding genes coding for polyQ in unrelated proteins [247]. Common features and differences between polyQ disorders are summarized in **Table 2**. Healthy individuals typically carry 4 to 35 CAG repeats in *ATXN7* while expansion above this threshold is pathogenic. There is a strong positive correlation between the length of the repeat and the severity of the disease. Indeed, alleles with 38-70 repeats lead to the classic progressive adult form of SCA7 and larger expansions lead to accelerated juvenile forms (70-100), and infantile forms (>100) which are lethal soon after birth [248]. The largest number of repeats reported in a SCA7 patient to date is 460 repeats [249], highlighting the fact that CAG repeats in SCA7 are the

most unstable. Indeed, the anticipation observed in SCA7 pedigrees is strong with a decrease of the age of onset of 20 years between each generation and there is a bias towards paternal transmission [250].

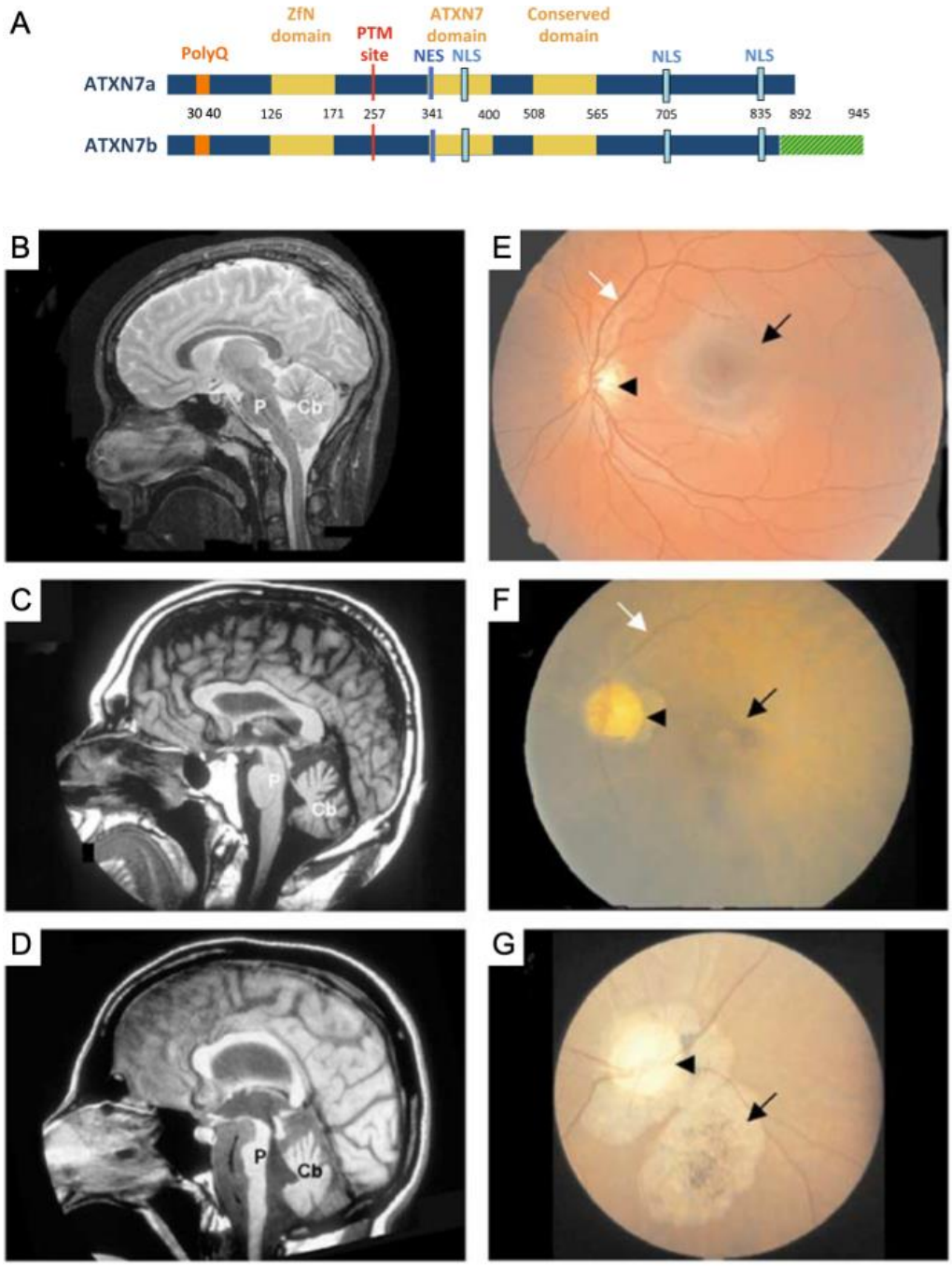

Figure 6: ATXN7 is mutated in spinocerebellar ataxia 7.

A. ATXN7a and b isoforms with a wild-type allele (10 polyQ). Conserved domains (yellow) are: a typical C2H2 zinc-finger (ZnF) motif, an atypical Cys-X9–10–Cys-X5–Cys-X2-His motif known as ATXN7 domain, and a third conserved domain. ATXN7 isoforms have 3 nuclear localization signals (NLS), 1 nuclear export signal (NES) and 1 site (lysine 257) for post-

translational modifications including acetylation and SUMOylation, but differ at their carboxy-terminal end. **B-D.** Magnetic resonance imaging of a control individual (**B**) and two SCA7 patients (**C**, **D**). The patient in (**C**) (38 polyQ, examined at 60 years and showed mild unsteadiness of gait) displays severe atrophy of the cerebellum (Cb), but almost complete sparing of the pons (P). In contrast, the patient in (**D**) (52 polyQ, examined at 40 years), shows severe cerebellar atrophy, as well as marked atrophy of the pons (P). **E-G** Fundoscopy images of a control individual (**E**) and two SCA7 patients (**F**, **G**). Normal appearance of the macula (black arrow) and the optic disk (arrowhead), and the well-developed vasculature (white arrow) in the control individual (**E**). On the contrary, the retina of patient (**F**) (52 polyQ, examined at 40 years) displays an atrophic macula (black arrow), very pale optic disk (arrowhead), and poor vasculature (white arrow). Moreover, the retina of patient (**G**) (unknown CAG repeats, examined at 20 years and showed gait ataxia, dysarthria, and decreased eyesight). Figures A from [251], B adapted from [248] with legend shortened.

Pathomechanisms of SCA7. Although not fully understood, we know the baseline pathomechanism of SCA7 and polyQ disorders (**Figure 7**). The polyQ expansion has a gain-of-function effect where the mutant protein assembles in toxic aggregates not only with itself but also to trap additional proteins [252]. ATXN7 is part of the chromatin remodeling and transcription coactivator of RNA polymerase II SAGA [253], thus its localization is mostly nuclear. Several studies showed the absence of correlation between the abundance of ATXN7 transcripts and protein suggesting that a rapid protein turnover is necessary for proper regulation of gene expression [254-256]. In the context of SCA7, mutant ATXN7 (mATXN7) is cleaved by caspase-7 which releases a smaller peptide containing the polyQ and a zinc-finger domain but deprived of the putative nuclear exportation signal and SCA7 domain [257]. The polyQ seems to stabilize the protein which results in altered transcriptional programs and neurodegeneration [258-261]. Additionally, a nuclear clearance system through clastosomes is quickly overwhelmed by the accumulation of the toxic fragments in nuclear inclusions. Those nuclear inclusions, hallmarks of the disease, are found ubiquitously in post-mortem brains [262] but seem to accumulate faster in the SCA7 hallmark tissues of SCA7 mouse models [256].

Table 2: Overview of polyglutamine disorders

Disease	Gene	pLI[1]	Protein function[2]	Wild-type allele[3]	Pathogenic allele[3]
Spinocerebellar ataxia 1	*ATXN1*	0.97	Ataxin-1: chromatin-binding factor, repressor of Notch signaling, may be involved in RNA metabolism and brain development	6-39	45-91
Spinocerebellar ataxia 2	*ATXN2*	0.85	Ataxin-2: acts as a negative regulator of endocytic EGFR internalization at the plasma membrane	14-31	35-500
Spinocerebellar ataxia 3	*ATXN3*	0.97	Ataxin-3: deubiquitinating enzyme involved in protein homeostasis maintenance, transcription, cytoskeleton regulation, myogenesis and degradation of misfolded chaperone substrates	11-44	61-87
Spinocerebellar ataxia 6	*CACNA1A*	1.00	Voltage-dependent P/Q-type calcium channel subunit α-1A: mediate the entry Ca2+ into excitable cells and is involved in a variety of calcium-dependent processes	4-18	20-33
Spinocerebellar ataxia 7	*ATXN7*	0.96	Ataxin-7: component of the SAGA transcription coactivator-HAT complex, mediates the interaction of SAGA complex with CRX, necessary for microtubule cytoskeleton stabilization	4-35	36-460
Spinocerebellar ataxia 17	*TBP*	0.02	TATA box binding protein: general transcription factor, functions at the core of the DNA-binding multiprotein factor TFIID to activate RNA polymerase II transcription of eukaryotic genes	25-42	49-66
Huntington's disease	*HTT*	1.00	Huntingtin: may play a role in microtubule-mediated transport or vesicle function	9-35	>40
Dentatorubralpalli doluysian atrophy	*ATN1*	1.00	Atrophin-1: transcriptional corepressor	6-35	49-93
Spinalbulbal muscular atrophy	*AR*	0.99	Androgen receptor: steroid hormone-activated transcription factor that regulates eukaryotic gene expression and affects cellular proliferation and differentiation in target tissues	9-34	38-62

Information compiled in this table is from the following online databases: [1] Probability of being loss-of-function intolerant from gnomAD (the closer the pLI is to 1, the more intolerant it is), [2] Uniprot, and [3] OMIM.

Neurodegeneration in SCA7. In the classic adult form, SCA7 first manifests as a cerebellar pathology. Patients progressively lose coordination of balance, gait and speech and present with pyramidal signs due to neuronal degeneration in the cerebellum, in the Purkinje cell layer and in the dentate nuclei especially, but also in other brain structures [248,263]. Cerebellar atrophy can be visualized through magnetic resonance imaging (**Figure 6**). SCA7 retinopathy usually appears second and manifests as dyschromatopsia followed by decreased central visual acuity (loss of cone photoreceptors). The degeneration progresses into a cone-rod dystrophy until the loss of the entire visual field and complete blindness (**Figure 6**). SCA7 disease progresses over several decades and most patients die from pneumonia caused by dysphagia [264]. In the most severe form of SCA7, the retinopathy manifests prior to spinocerebellar ataxia.

Neurodevelopmental component. In the past two decades, the definition of late onset diseases evolved due to accumulating evidence of developmental components to degenerative manifestations. A well-known example is the observation that post-mortem tissues from schizophrenia patients revealed brain developmental anomalies which were not related to neurodegeneration [265,266]. More closely related to SCA7, subtle brain differences were observed in individuals who were at risk for Huntington's disease [267,268]. A possible explanation for those early manifestations could be a partial loss-of-function of the protein. Indeed, overexpression of wild-type *HTT* and *ATXN3* ameliorated some phenotypes of a mouse model of Huntington's disease [269,270], and the neurodegeneration of a *Drosophila* model of SCA3 [271] respectively. Further lines of support include the high probability of being Loss-of-function Intolerant (pLI) of the genes mutated in polyQ disorders (**Table 2**) and the non-viability of *HTT* knockout mice. More recently, we showed that *atxn7* plays a role in the development of the eyes and brain of the zebrafish ([272] with results description in section Results III.2).

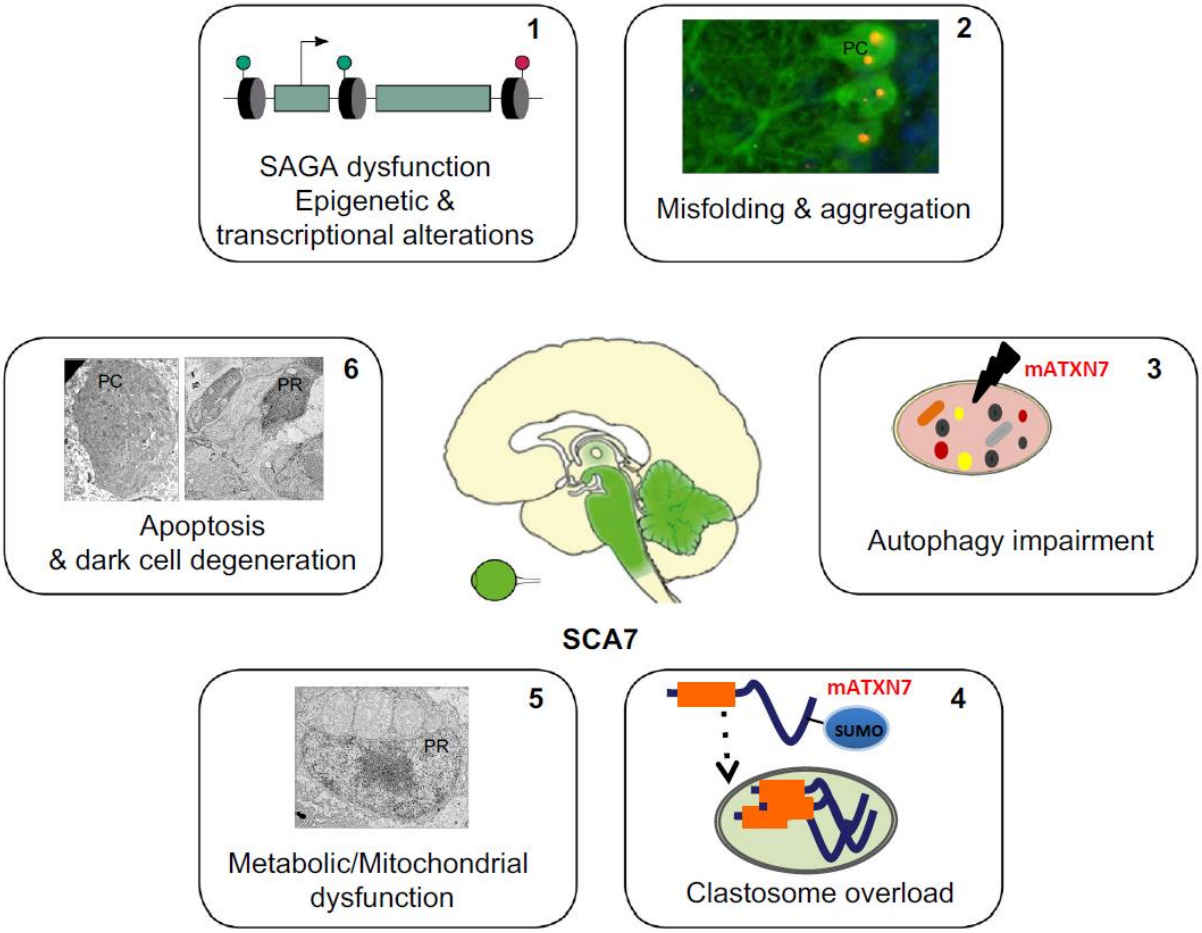

Figure 7: Pathomechanisms of SCA7.

SCA7 pathogenesis triggers multiple pathogenic cascades that cause cellular dysfunctions and lead to cell death. (1) Mutant ATXN7 causes gene deregulation by altering transcription and epigenetics through different mechanisms, including sequestration of SAGA components in nuclear inclusions, alteration of SAGA integrity, and aberrant interaction with SAGA components or with promoter bound transcription factors such as CRX. (2) Mutant ATXN7 misfolds, accumulates in nucleus and forms aggregates that sequester a large number of cellular proteins, which may therefore lose their biological functions and contribute to the pathogenesis (Fluorescent image of section of SCA7 mouse cerebellum with mATXN7 aggregates (red) in the nuclei of Purkinje cells (green)). (3) Mutant ATXN7 can be degraded by autophagy; however, studies of SCA7 cells, mice and human brains indicate that autophagy is impaired in the disease. (4) Mutant ATXN7 is also degraded by nuclear clastosomes, which might prevent its accumulation for several decades before onset of aggregation. Over time, the degradation activity of clastosomes might be overwhelmed by the aggregation process. (5) SCA7 mitochondria show morphological enlargement and dysfunction, and several lines of evidence indicate metabolic deficits in SCA7 (electron micrograph showing large mitochondria in photoreceptor (PR) of SCA7 mouse). (6) SCA7 patients loose neurons in retina, cerebellum, brainstem and other brain structures. In SCA7 mice, neuronal loss occurs through apoptosis and dark cell degeneration (electron micrographs showing dark degeneration of Purkinje cell (PC) and photoreceptor (PR)). Figure and adapted legend from [273]

ATXN7 and cilia. One of the possible implications of the wild-type ATXN7 being lost is a putative impact in ciliary function. ATXN7 is found in both the nucleus and the cytoplasm in many human tissues [274]. Consistently, a study aiming to build an ataxia interactome map used ATXN7 as a bait in a yeast two-hybrid screen and identified multiple interactions between ATXN7 and nuclear or cytoplasmic proteins [246]. Of interest was the interaction between ATXN7 and the two centrosomal/BB proteins CEP70 and CEP72. Furthermore, ATXN7 was shown to associate with and stabilize the microtubule cytoskeleton *in vitro* [275]. A number of experiments performed in our lab showed that 1) ATXN7 and CEP72 indeed colocalize to the centrosome in human telomerase-immortalized retinal pigmented epithelial (htRPE-1) cells; 2) ATXN7 can be observed at the base of the primary cilia in mouse primary cortical and hippocampal neurons, as well as in IMCD3 cells and embryonic rat cardiomyocytes (H9c2 cells); and 3) ATXN7 colocalizes to the BB of connecting cilia of photoreceptors in the retina of wild-type mice (**Figure 8**, [276]). Together, these data show that ATXN7 can associate with two ciliary components: the centrosome/BB and tubulin, and could suggest a role for ATXN7 in ciliary biology. However, further functional studies are required to characterize this putative and unexpected role of ATXN7.

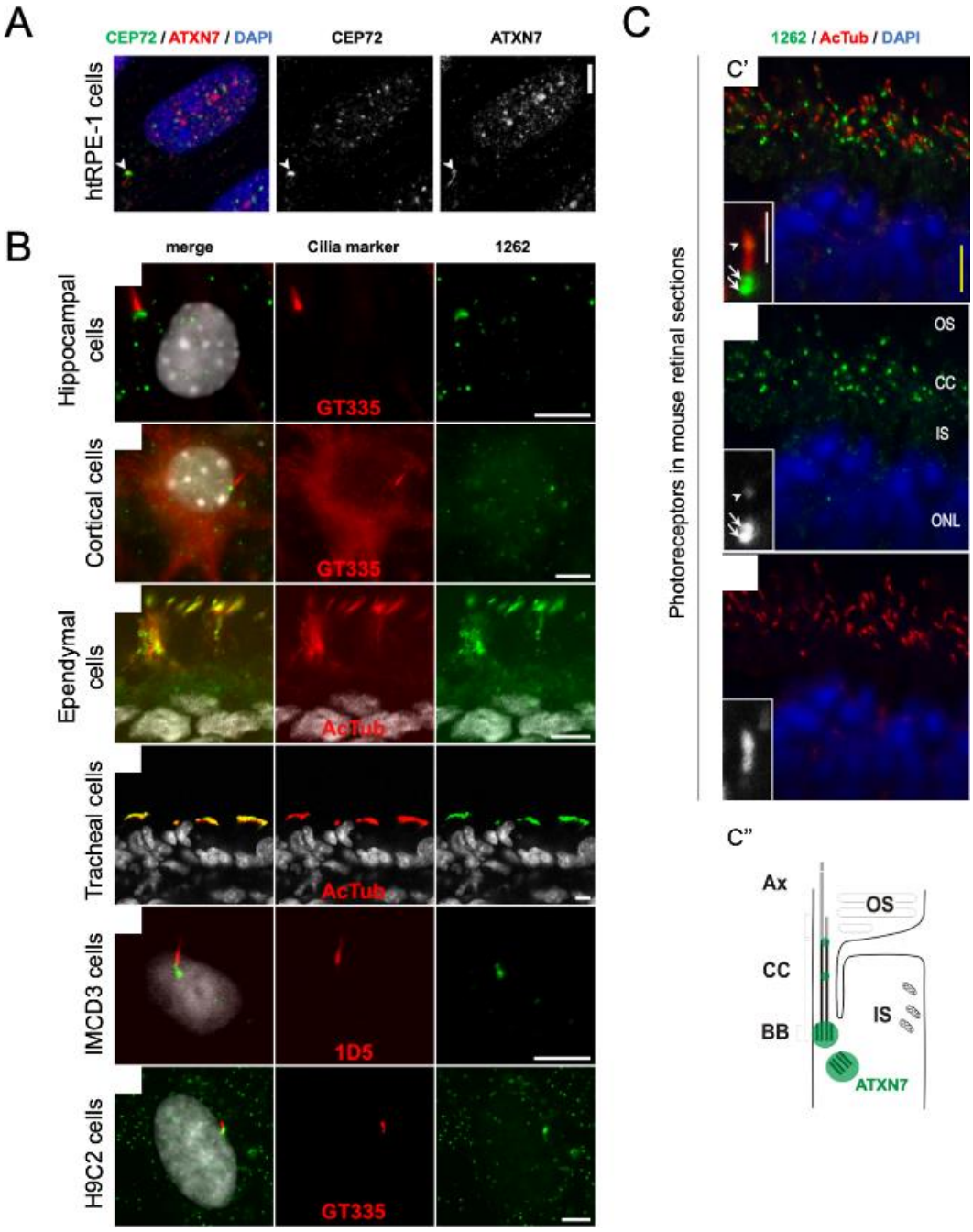

Figure 8: ATXN7 localizes at the centrosome and is present at the base of primary cilia.

A. Co-immunolabeling of htRPE-1 cells showing the colocalization of endogenous ATXN7 with its centrosomal CEP72 interactor (arrowhead). **B.** Co-immunostaining of ATXN7 (1262 polyclonal antibody against N-terminus fragment of the protein) and cilia markers (polyglutamylation modification, GT335; acetylated α-tubulin, AcTub; or tubulin,1D5). ATXN7 is present at the base of primary cilia of cultured primary neurons of mouse hippocampus and cortex. ATXN7 is detected in the shaft of motile cilia of ependymal and tracheal epithelium of 14-day old mice. ATXN7 is detected at the base of primary cilia of IMCD3 and H9c2 cells. **C.** Retinal sections of 3-week old mice were labeled with the 1262 antibody. Cilia were detected with anti-acetylated α-tubulin (AcTub) which labels the connecting cilum (CC) (**C'**). **C''** is a schematic map of ATXN7 localization in photoreceptors. Scale bars 5 µm. Figure and adapted legend from [276]

Scientific progress and next challenges. Our understanding of ciliopathies has greatly increased in the past two decades. Even if some aspects of these disorders are now well documented, such as the cause and progression of retinal degeneration through the impairment of connecting cilia [277], there are a number of symptoms which are not fully understood. For instance, the mechanisms leading to the kidney pathology in autosomal dominant polycystic kidney disease remain unsolved despite the different hypotheses to explain the formation of cysts [278]. Perhaps the non-ciliary roles of ciliary proteins and the ciliary roles of hitherto unknown ciliary proteins could explain knowledge gaps. Establishment of a comprehensive “ciliary landscape” integrating data from gene location and regulation to protein maturation, localization, interactions and functions would considerably improve the diagnosis and prognosis of ciliopathies [279,280]. Thus, an emergent trend is a systems-level approach integrating proteomics and patients’ data aiming to capture ciliary protein networks. One example includes the identification of *KIAA0586* as the causative gene for 5% of unexplained Joubert syndrome cases through combinatorial approaches of siRNA screening, proteomics data integration and whole-exome sequencing [281]. Another recent report has documented the simultaneous identification of *ADAMTS9* as the causative gene for a form of nephronophthisis [282] and the role of ADAMTS9 in ciliary growth [283].

V. Challenges and opportunities

1. Non-coding RNAs and cilia

The first ciliary proteome database contained more than 1,200 proteins selected through multiple approaches, including data on gene expression and proteins from different organisms [284]. The most recent databases of ciliary and centrosomal genes and proteins (including data from multiple species) include: the original SYSCILIA Gold Standard (1,319 proteins, [238,285]), Cildb3.1 [286,287] and CiliaCarta which integrates data from the SYSCILIA Gold Standard (836 genes, [288]). However, those resources focused primarily on proteins because of technical choice (yeast-two hybrid screens, whole exome sequencing, mass spectrometry, etc). Despite playing a substantial role on regulating cell biology, non-coding RNAs have not been integrated in the ciliary databases. This mostly unexplored molecular repertoire offers us the opportunity to contribute to the building of the "ciliary landscape".

The candidacy of microRNAs. microRNAs (miRNA) are short (about 20 nucleotides long) non-coding RNAs which act as post-transcriptional regulators of messenger RNA (mRNA) expression that bind to complementary regions in their 3'UTR [289]. They are involved in almost every biological process and are highly conserved across species. miRNAs are scattered throughout the genome in both intergenic regions and introns and are often present in paralogous copies coding for miRNAs of a same family. For instance, *let-7* was the second miRNA to be discovered, is highly conserved, and has been established as a key promoter of differentiation in *C. elegans*, *Drosophila*, mouse and human cell types [290]. There are twelve *let-7* loci in the human genome: three give rise to *let-7a*, two to *let-7f* and the others code for *let-7b*, *c*, *d*, *e*, *g*, *i*, and *miR-28* [291]. They exist in three forms: the immature pri-miRNA, the pre-miRNA hairpin and the mature miRNA. Pri-miRNAs are transcribed in the nucleus by the RNA polymerase II and bear a 5' cap and a polyA tail, similar to mRNAs [292]. In cases where miRNAs are located in introns, pri-miRNAs are released as part of the splicing

process allowing maturation of both mRNAs and miRNAs. The Microprocessor complex formed by the nuclear RNase III Drosha and its cofactor DGCR8 can crop pri-miRNAs and release pre-miRNA hairpins which can then be exported to the cytoplasm by Exportin5/Ran-GTP complexes located at the nuclear envelope (**Figure 9**) [293,294]. The cytoplasmic RNase III Dicer and TRBP further crop the hairpin to release a small double strand fragment [295]. One hairpin can hold 2 mature miRNAs: one on its 5' strand and the other on its 3' strand. However, only one mature miRNA can then be incorporated to the RISC (RNA-induced silencing complex) at a time, alongside with AGO, to target mRNAs for degradation or repress their translation [289] (**Figure 9**). Regulation of miRNAs can occur at several levels: through regulation of the processing proteins necessary for miRNA maturation or through post-transcriptional modifications such as miRNA tailing and methylation [296]. LIN28 is a well-studied regulator of the *let-7* family: it can bind to the pri-miRNAs to prevent the first maturation step by the Microprocessor, or recruit TUT4 to add uridylyl to the 3' end of pre-let-7 to prevent processing by Dicer and target them for degradation. Because *LIN28* transcripts harbor *let-7* targets in their 3'UTR, LIN28 and *let-7* are mutual repressors [297].

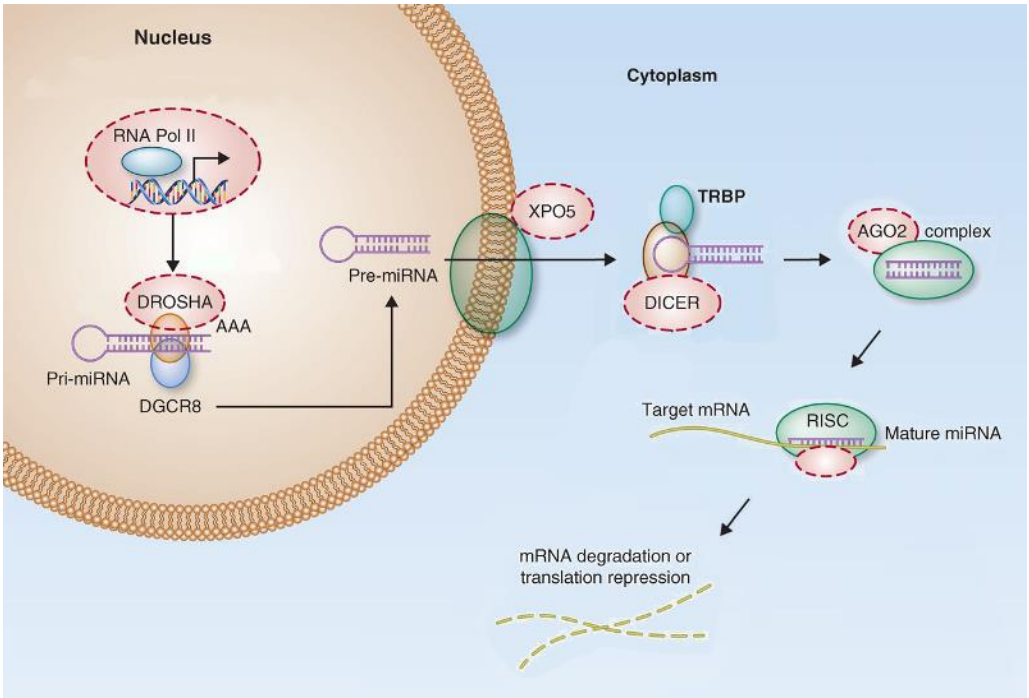

Figure 9: Summary of canonical miRNA biogenesis pathway.

Figure 9: Summary of canonical miRNA biogenesis pathway.

miRNA genes are transcribed from intergenic or intragenic regions of noncoding RNA transcripts mediated by RNA polymerase II, called pri-miRNA. These long pri-miRNAs are processed by the DROSHA–DGCR8 complex to form pre-miRNAs (~60 nucleotides long). XPO5 mediates the export of these pre-miRNAs to the cytoplasm for further processing by DICER. DICER cleaves pre-miRNAs to form mature miRNAs of ~20 nucleotides long. One of the strands of mature miRNA (guide strand) gets incorporated into RISC involving DICER and AGO2 enzymes to target mRNAs to cause degradation or translational suppression of the target gene. Figure and legend adapted from [298].

Paucity of studies on microRNAs and cilia. Despite the regulatory role of miRNAs and their potential effect on the expression of ciliary genes, there have been few studies connecting miRNAs and cilia. In particular, the *miR-34/miR-449* family has been implicated in several mechanisms linked to reduced ciliogenesis such as the direct repression of the Delta/Notch signaling pathway and the relocalization of actin binding protein Filamin-A in human airway epithelium and embryonic *Xenopus* epidermis [299,300]; the repression of CP110 in mouse and *Xenopus* models [301]; and the inhibition of cell cycle genes in a *miR-34/miR-449* knockout mouse model [302]. Another study has reported that *miR-129-3p* can also control ciliogenesis through the direct repression of CP110, as well as by repressing F-actin formation [303]. These different studies showed a role for *miR-34/miR-449* and *miR-129-3p* in the initiation of ciliogenesis and suggest that other miRNAs could contribute to ciliary biology.

***let-7b* identified as a modulator of ciliogenesis**. In 2010, our group (CHDM) performed a medium throughput screen, testing approximately 800 miRNA inhibitors, to identify miRNAs that could significantly induce or suppress ciliogenesis. The top candidate predicted to enhance ciliogenesis was the *let-7* family with *let-7b* showing the most substantial effect. It was further shown that *let-7b* could promote ciliogenesis and increase cilia length independent of its role on the cell cycle (**Figure 9**). However, these preliminary *in vitro* data required validation in an *in vivo* developmental context.

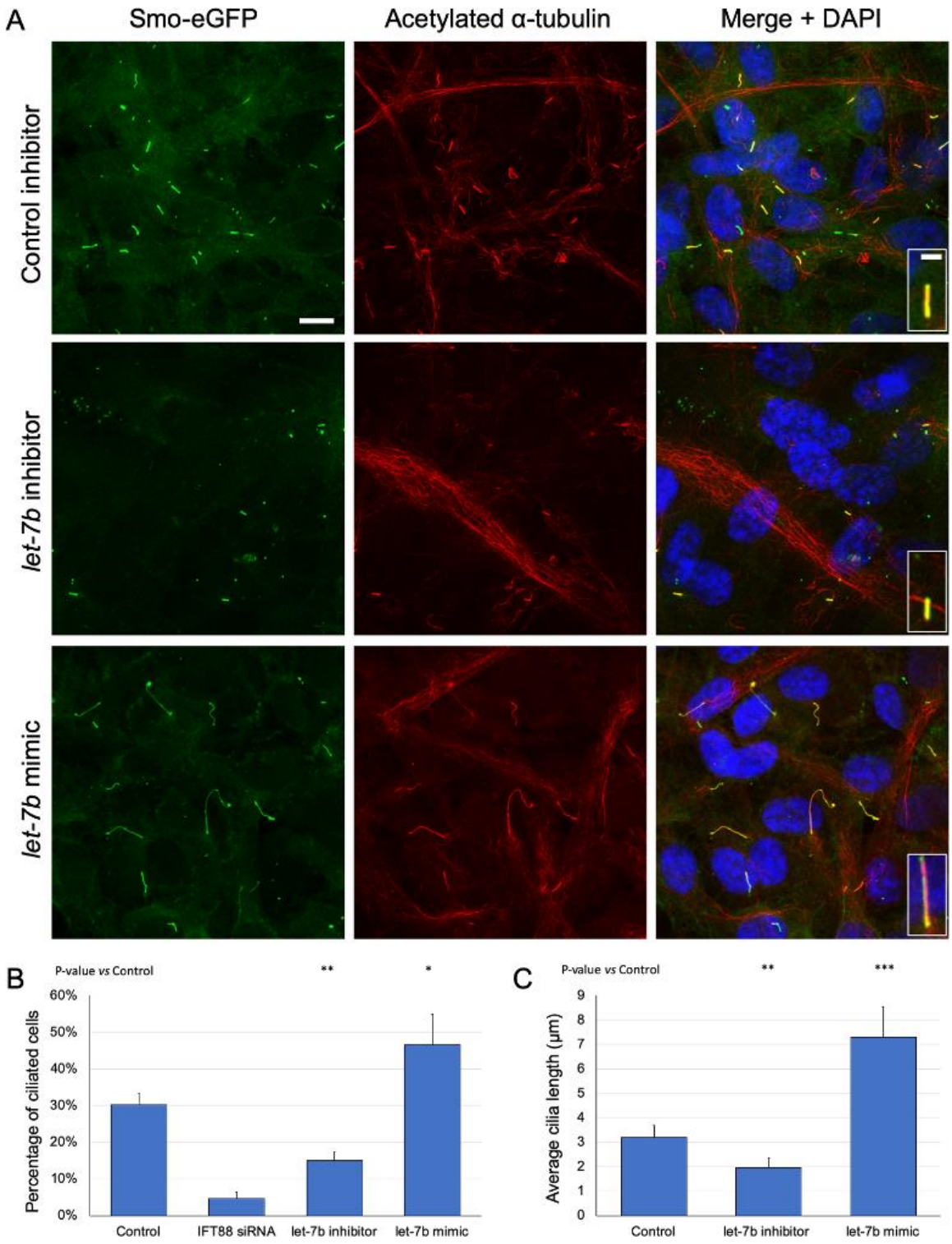

Figure 10: *let-7b* is a positive regulator of ciliogenesis.

A. Immunofluorescence of htRPE-1 cells stably expressing Smo-EGFP (green) and stained for acetylated α-tubulin (red). Cells transfected with *let-7b* miRIDIAN inhibitor (middle panel) show a marked reduction in the number of cilia in comparison to a control inhibitor (top panel). Elevation of *let-7* levels by transfecting a *let-7b* mimic (bottom panel) results in a greater fraction of ciliated cells and significantly longer cilia. **B.** Quantification of the fraction of ciliated cells and **C.** ciliary length. Statistics two-tailed t-test, ****p<0.0001, ***p<0.001; *p<0.05. Scale bars=10µm, 2µm in insets. (Jon Robinson's thesis; [304])

THESIS AIM 1

The first objective of this work is to validate the potential role of *let-7b* on ciliogenesis using three approaches: 1) the suppression and overexpression of *let-7b* in the zebrafish model organism to monitor ciliary defect *in vivo*; 2) identification of *let-7b* target genes which are negative regulators of ciliogenesis using transcriptomic data; and 3) exploration of the hypothesis that human ciliopathy cohorts might harbor an enrichment of variation in the 3'UTRs of *let-7b* target genes. Outcomes of this work could contribute to the "ciliary landscape" and help to explain the phenotypic variability observed in patients, but could also improve diagnostics and prognostics of ciliopathies.

2. New ciliary role for an already characterized protein

The observation that there are ciliary proteins with non-ciliary roles and non-ciliary proteins with ciliary roles has challenged the mapping of the "ciliary landscape". ATXN7 has been characterized previously to participate to the mediation of transcription through the SAGA complex [305]. However, protein interaction and localization experiments suggest a novel role linked to cilia. Thus, ATXN7 is suspected to be a non-ciliary protein with a ciliary role.

Primary cilia in brain development. Primary cilia play an important role in brain development not only through the transduction of signaling pathways but also through regulated autophagy [306]. In particular, they are involved in the morphogenesis of the cerebellum, which is severely affected in SCA7, through HH signaling [307,308]. Sonic HH is secreted by the Purkinje cells in the cerebellum and allows the proliferation of cerebellar neuronal precursors including in the granule cell layer [309,310]. Defects in primary cilia have been observed in olfactory neuronal precursors obtained from patients affected with late onset disorders, including schizophrenia and bipolar disorder [311,312].

SCA7, a second-order ciliopathy? Considering: 1) the probable developmental component of SCA7 with a role for ATXN7 in brain and eye development [272]; 2) the putative

ciliary role of ATXN7; and 3) the role of primary cilia in cerebellum development, it is possible that SCA7 first manifests through subtle brain anomalies caused by a partial loss of ATXN7's putative ciliary role.

THESIS AIM 2

The second objective of this thesis is to explore the potential link between ATXN7 and cilia in the development of SCA7 by overexpressing wild-type and mutant *ATXN7* in the developing zebrafish. The zebrafish offers an opportunity to evaluate the brain of a transparent vertebrate with *ex vivo* development and is also a model of choice to observe potential ciliary defects [313]. A zebrafish model of SCA7 would be a relevant tool not only to understand the disease by complementing mouse models, which are more expensive and take 5 weeks to 11 months to develop relevant phenotypes [251], but would also have the potential to be used in therapeutic screens to test compounds such as anti-aggregation molecules identified *in vitro* by our group (IGBMC) [314].

3. Exploring other aspects of ciliopathies and SCA7

The zebrafish model organism presented an opportunity to explore phenotypic aspects of ciliopathies and to study the role of ATXN7 in development. Indeed, the zebrafish produces a large amount of offspring, develops externally and rapidly, is transparent during development [315] and 70% of its genome is conserved with the one of humans [316].

THESIS AIM 3

The third objective is to broaden my range of technical skills by participating in other projects lead in my host laboratories. Notably, by exploiting the zebrafish model organism to study organs which are typically affected in ciliopathies (kidney [317] and retina (manuscript submitted)) and to contribute to the study on the consequences of *atxn7* inactivation on development [272].

MATERIAL AND METHODS

Material and Methods

Material and methods for the two attached publications (chapter III of the results) are included in the publications and are not mentioned here.

Zebrafish maintenance

Zebrafish adults from the Duke University facility or IGBMC facility were maintained at 28°C. Embryos were maintained at 28.5°C in egg water (0.55mM $CaSO_4$, 0.45mM $CHNaO_3$, 5.13mM NaCl). Wild-type embryos were from the ZDR strain (*let-7b* chapter) or AB strain (ATXN7 chapter), and transgenic SoFa1 strain was kindly provided by Dr. William A. Harris [318]. Embryos were staged in somite-stage (ss), hours-post-fertilization (hpf) or days-post-fertilization (dpf) as described [315].

CRISPR/Cas9 genome editing of *let-7b* in zebrafish

We used ChopChop to design a guide RNA (gRNA) targeting the Drosha processing site required for *let-7b* pri-miRNA maturation into pre-miRNA (miRBase ID: MI0001865; 5′-AGTGGTGTTCGGACAGGGTGAGG-3′). We synthesized the gRNA using the Gene Art precision gRNA synthesis Kit (Invitrogen) according to manufacturer's instructions. To test our gRNA efficiency, we co-injected 100pg of gRNA with 200pg of Cas9 protein (PNA Bio) in the cell of 1-cell stage zebrafish embryos (1nL/embryo). We extracted the genomic DNA at 1dpf, amplified the region targeted by the gRNA and loaded the product on a 15% polyacrylamide gel to visualize heteroduplexes after a denaturation-reannealing treatment. PCR products from different embryos were cloned and Sanger sequenced. Percent mosaicism was calculated by counting the percentage of mutant clones per total clones and averaging across all embryos tested.

Transient suppression and overexpression of *let-7b* in zebrafish

The mature sequence of human *let-7-b-5p* (miRbase ID: MI0000063) is 100% conserved in zebrafish. We designed a morpholino (MO) complementary to the mature sequence of *let-7b*

to inhibit its activity (5'- AAACCACACAACCTACTACCTCACC -3'; GeneTools), and obtained a dsRNA *let-7b-5p* mimic from Dharmacon (5'- UGAGGUAGUAGGUUGUGUGGUU -3'). We first titrated our MO by injecting increasing concentrations of MO (2, 4 and 6ng/nL) and mimic (0.2 and 0.8µM) in the cell of 1-cell stage zebrafish embryos (1nL/embryo) then used 6ng/nL of MO and 0.08µM of *let-7b-5p* mimic to perform the rescue experiments.

RT-qPCR on zebrafish embryos

Total RNA was extracted from 30hpf embryos with TRIzol (Invitrogen) according to manufacturer's instructions. Total RNA was reverse transcribed with either the miRNA 1st-Strand cDNA Synthesis Kit (Agilent) or the QuantiTect Reverse Transcription Kit (Qiagen), from 800ng or 500ng of total RNA, respectively, according to manufacturer's instructions. qPCR was performed with Power SYBR Green PCR Master Mix (Applied Biosystems) according to manufacturer's instructions. *let-7b* levels were normalized to *miR-206* and *limk2* levels were normalized to *gapdh*. qPCR data were analyzed with the $2^{-\Delta\Delta CT}$ method [319] and statistical analyses were performed with a two-tailed t-tests (GraphPad PRISM software; version 8.0). The following primers were used: *let-7b*: 5'-TGAGGTAGTAGGTTGTGTGGTT-3'; *miR-206*: 5'-TGGAATGTAAGGAAGTGTGTGG-3'; universal reverse primer from the Agilent kit; *limk2*-F: 5'-CCATGGTGGCAGGAGACTAT-3' and *limk2*-R: 5'-GGACCACCTGCTTGT AGCAT-3'; *gapdh*-F: 5'- TTGTAAGCAATGCCTCCTGC-3' and *gapdh*-R:5'-CTGTGTTGCTGT GATGGCAT-3'.

Brightfield examination of zebrafish embryos

let-7b chapter: Embryos at the desired developmental stage were anesthetized with 0.02% Tricaine (A5040, SigmaAldrich) and positioned in a 2% agarose mold. Heart looping assessment was performed when the embryos were still in their chorion to facilitate manipulation. Statistical comparison was performed with a two-tailed Fisher's exact test (GraphPad online QuickCalcs tool). Images were acquired using a Nikon SMZ745 stereoscope equipped with a Digital Sight camera and with NIS-Elements software. The background of the images was normalized with Gimp software.

ATXN7 chapter: Embryos older than or at the 24hpf stage were anesthetized with 0.02% Tricaine (A5040, SigmaAldrich) and imaged in egg water or in a 1.5% agarose mold. Images were captured with a M420 Macroscope (Leica) with COOLSNAP coupled camera and analyzed using FiJi software (NIH).

spaw whole mount _in situ_ hybridization

18ss embryos were fixed in 4% paraformaldehyde (PFA) at 4°C overnight. *in situ* hybridization on whole-mount embryos was performed as described [320]. Statistical comparison was performed with a two-tailed Fisher's exact test (GraphPad online QuickCalcs tool). Images were acquired using a Nikon SMZ745 stereoscope equipped with a Digital Sight camera and with NIS-Elements software. The background of the pictures was normalized with Gimp software.

Cilia measurement in the Kupffer's vesicle of zebrafish embryos

Embryos were reared at 23°C and fixed at the 10ss in Dent's solution (80% methanol, 20% dimethylsulfoxide) overnight at 4°C. Embryos were rehydrated with a decreasing series of methanol and phosphate-buffered saline with 0.1% Tween-20 (PBST); washed with PBST and dechorionated. Cilia were stained with acetylated tubulin primary antibody (T745, Sigma Aldrich, 1:1000 dilution) and goat anti-mouse IgG secondary antibody (488 Alexa Fluor, Invitrogen; 1:500 dilution). The tail buds were dissected and mounted in 50% glycerol on a slide prior imaging with a 90i fluorescent microscope (Nikon) at 60x magnification, a digital black and white camera (Nikon), and the NIS Elements software (Nikon). Z-stacks were combined using the Maximum Intensity projection in FiJi (NIH) and cilia were measured with the Segmented Line tool. Statistical comparisons were performed with a non-parametric one-way ANOVA followed by Tukey's multiple comparison (GraphPad PRISM software; version 8.0).

Evaluation of convergent-extension

let-7b chapter: Convergent-extension (CE) was assessed at the 10ss. Images were acquired with an Axio Zoom V16 (Zeiss) at 80x magnification, and the ZEN Blue software (Zeiss).

ATXN7 chapter: Fixed (4% PFA overnight at 4°C) embryos at the 10-11ss were imaged in a 1.5% agarose mold with a M420 Macroscope (Leica) coupled to a COOLSNAP camera. Images were analyzed in ImageJ software (NIH) where the body-gap angle was measured using the zebrafish head (before the polster) and tail tip as landmarks. Statistical comparison was performed with a non-parametric one-way ANOVA followed by Tukey's multiple comparison (GraphPad PRISM software; version 8.0).

Targeted sequencing of a ciliopathy cohort and analysis

Human gDNA was quantified using fluorometric quantification with the Quant-iT PicoGreen dsDNA kit according to manufacturer's instruction on a FLUOStar Omega plate reader (BMG Labtech). For each sample, gDNA was subsequently diluted to 2.5ng/µL to a final volume of 10µL, and transferred to the Duke sequencing core. Raw sequencing results were analyzed by the Duke bioinformatics Core which produced an Excel file the filtered data. Detailed methods of the targeted sequencing and bioinformatics analysis can be found in the annex. Each variant was manually verified in the Integrative Genomics Viewer version 2.4.10 (Broad Institute) and variants were called at a cutoff value of 20%. Ethnicity, sex, and primary causal mutation were reattributed to each patient as well as the variants detected in the targeted sequencing. Variants were then manually counted and we used control data from the Genome Aggregation Database (gnomAD; https://gnomad.broadinstitute.org/) to perform the enrichment analysis. Statistical comparisons were performed with a Chi-square test with Yates' correction (GraphPad online QuickCalcs tool) and Bonferroni correction was applied to the p-values.

Cloning and construct preparation

Truncated ATXN7 constructs were obtained as follows: 4xnrUAS-Ataxin (wild-type or mutant)-P2A-mCherry vectors obtained from the AMAGEN platform (Gif-sur-Yvette) were digested with *Nhe*I and *Xma*I to extract the coding sequences of truncated ATXN7 which was then purified by gel electrophoresis and ligated back into pCS2+_ATXN7a vector after digestion by the same enzyme to remove the sequence coding for the full-length wild-type protein. The addition of eGFP downstream of truncated wild-type and mutant *ATXN7* sequence was performed as follows: the sequence coding for eGFP was amplified from a pEGFP-N2 plasmid using the following primers 5'-GAATTCTGCAGTCGACGGTA-3' and 5'-TATGTTCTAGAG TCGCGGCC-3' because the *Xba*I site was methylated and could not be used for digestion, the PCR product was then cloned in a p-GMT vector and recovered by digestion with *Xma*I and *Xba*I, finally the eGFP fragment was cloned into the pCS2+_wild-type/mutant-ATXN7Δ vectors which were first digested with *Xma*I and *Xba*I. The addition of eGFP downstream of full-length wild-type and mutant *ATXN7* sequence was performed using a three-fragment strategy to increase specificity as follows: pCS2+_wild-type/mutant-ATXN7Δ-eGFP vectors were digested with *Nhe*I, *Xma*I and *Dra*I and the *Xma*I-*Dra*III and *Dra*III-*Nhe*I fragments were gel purified, in parallel, the pCS2+_ATXN7 (wild-type, with 60 CAG repeats and with 104 CAG repeats) vectors were digested with *Nde*I, *Nhe*I and *Xma*I and only the *Nhe*I-*Xma*I fragments were gel purified, finally the three purified fragments were ligated all together. Removal of the STOP codon which was kept between *ATXN7* and *eGFP* sequences was achieved by amplifying the 3' region of *ATXN7* sequence with a forward primer upstream of the *Xho*I digestion site 5'-CCTGTCAACTCCCACGGCAG TTTTTCCCACTCAC-3' and a reverse primer overlapping the *Xma*I digestion site but excluding the STOP codon 3'-CCGGTGGATCCCGGGACGTGCCTTTGGC TGATGA-5', the amplicon was then digested with *Xho*I and *Xma*I and used to replace the faulty fragment containing the STOP codon.

Mature mRNA synthesis and microinjection into zebrafish embryos

pCS2+ vectors containing a SP6 promoter upstream of the sequence of interest were linearized with *Kpn*I then capped mRNAs were prepared according to manufacturer's intructions using the mMessage mMachine SP6 Transcription kit (AM1340, ThermoFisher). mRNAs were aliquoted to prevent freeze-thaw cycles and stored at -80°C. Injection cocktails were prepared with Phenol red and nuclease-free water. Injection cocktails were injected in the cell of one-cell stage zebrafish embryo using a Picospritzer III microinjector (Parker Hannifin) in Duke University facilities or in the yolk of one- to two-cell stage zebrafish embryo using a Nanoject II micro-injector (Drummond Scientific) in IGBMC facilities.

Cerebellum immunostaining

Embryos were anesthetized and fixed in Dent's solution (80% methanol, 20% dimethylsulfoxide) at 3 dpf. Whole-mount immunostaining was performed as described [321]. Briefly, embryos were rehydrated with a decreasing series of methanol and phosphate-buffered saline with 0.1% TWEEN-20 (PBST), washed with PBST, bleached (with 3% H_2O_2/0.5% KOH) and permeabilized with Proteinase K at 10µg/mL (25530-049, ThermoFisher). Embryos were then incubated with primary antibody anti-acetylated α-tubulin (T7451, mouse, Sigma-Aldrich, dilution 1:1000) and then secondary antibody Alexa Fluor 488 goat anti-mouse IgG (ThermoFisher, 1:500). Dorsal images were acquired with an AZ100 fluorescent microscope (Nikon), digital sight black and white camera (Nikon), and NIS Elements software (Nikon) at 7X magnification. The area of the cerebellum was measured with ImageJ (NIH) and statistical differences between conditions were determined with a non-parametric one-way ANOVA followed by Tukey's multiple comparison (GraphPad PRISM software; version 8.0).

SoFa1 retina imaging

Embryos were kept in egg water with 0.003% 1-phenyl-2-thiourea (PTU, P7629-10G, Sigma-Aldrich) starting at 24hpf to prevent pigment formation. Embryos were manually dechorionated if younger than 50hpf, anesthetized with 0.02% Tricaine (A5040, SigmaAldrich)

and mounted into 3%-methylcellulose (M0387, SigmaAldrich) on depression slides. Pictures were captured with a DM 400B microscope (Leica) with COOLSNAP coupled camera.

Cryo-sections

Embryos were fixed at 24hpf in 4% paraformaldehyde (PFA) for 10 min at room-temperature to preserve the eGFP, washed in PBST, incubated in 30% sucrose overnight then mounted in optimal cutting temperature compound (OCT; AGR1180; Agar scientific) and stored at -80°C until ready for sectioning. 7µm-thick sections were cut using a CM3050 S cryostat (Leica).

Comparisons of eGFP kinetics

Live embryos were mounted in 3%-methylcellulose (M0387, SigmaAldrich) after being anesthetized with 0.02% Tricaine (A5040, SigmaAldrich). If older than 24hpf, images were captured with a DM 400B microscope (Leica) with COOLSNAP coupled camera. Images were then analyzed in ImageJ (NIH). To calculate the Corrected Total Embryo Fluorescence (CTEF), I traced the contour of each embryo using the brightfield picture and measured the area and integrated density using the fluorescent image. Then I used the following formula adapted from [322]: CTEF = Integrated density – (Area of embryo X Mean fluorescence of background reading) where the mean fluorescence of uninjected controls was used as the mean fluorescence of background reading. For the first experiment (II. **Figure 5A**), a defined exposure time was set too high which is why saturation was observed in the eGFP injected embryos. For the second experiment (II. **Figure 5B**), the exposure time was not set but recorded and used to adjust the integrated density. Statistical differences between the CTEF of embryos injected with ATXN7 constructs were determined with two-way ANOVA followed by Tukey's multiple comparison.

Immunostaining of the proximal convoluted tubule

Embryos were anesthetized and fixed in Dent's solution (80% methanol, 20% dimethylsulfoxide) at 4 dpf. Whole-mount immunostaining was performed as follows: embryos were rehydrated with a decreasing series of methanol and phosphate-buffered saline with

0.1% TWEEN-20 (PBST), washed with PBST, bleached (with 3% H_2O_2/0.5% KOH) and permeabilized with 1% Triton X-100 (85112, ThermoFisher). Embryos were then incubated with primary antibody anti-Na^+/K^+/ATPase alpha-1 subunit (a6F, mouse, Developmental Studies Hybridoma B, 1:20 dilution) and then secondary antibody Alexa Fluor 488 goat anti-mouse IgG (ThermoFisher, 1:500). Lateral images were acquired with an AZ100 fluorescent microscope (Nikon), digital sight black and white camera (Nikon), and NIS Elements software (Nikon) at 4X magnification. The area of the proximal convoluted tubule was measured with ImageJ (NIH) and statistical differences between conditions were determined with a non-parametric one-way ANOVA followed by Tukey's multiple comparison (GraphPad PRISM software; version 8.0).

RESULTS

Results

I. The microRNA *let-7b* can modulate ciliogenesis

A medium throughput screen conducted on htRPE-1 cells in our group (CHDM) enabled the identification of the *let-7* family of miRNAs to significantly induce or suppress ciliogenesis. To validate further the role of *let-7* on ciliary biology, we chose to test *let-7 in vivo*.

1. Use of zebrafish for *in vivo* validation of the effect of *let-7b* on ciliogenesis

We used zebrafish as a model organism to test whether *let-7* has similar effects on cilia *in vivo*. *let-7* miRNAs are conserved in zebrafish and expressed at low levels in early embryogenesis [291,323]. Based on conservation, number of copies, and ranking from our *in vitro* screen, the most experimentally tractable *let-7* member is *let-7b* (100% identity, single copy and top hit) (**Table1**).

Suppression of *let-7b* results in established ciliary phenotypes in zebrafish

We designed a guide RNA (gRNA) with 100% efficiency targeting the Drosha processing site required for *let-7b* pri-miRNA maturation into pre-miRNA (**Supp. Figure 1A,D, E**). We co-injected 100pg of gRNA with 200pg of Cas9 enzyme into zebrafish embryos to generate *let-7b* mosaic F0, and we measured a 36% reduction of mature *let-7b* via RT-qPCR (p=1.62E-4; **Supp. Figure 1B**). Next, we examined the mosaic *let-7b* F0 at different developmental stages. Left-right defects are a hallmark of ciliopathies and can be assessed in the zebrafish by the directionality of the heart looping at 2 days post-fertilization (dpf) [324,325]. We

observed minimal abnormal cardiac looping among our injected embryos with a greater extent in embryos injected with gRNA+Cas9 (5.3%) compared to their siblings injected with gRNA alone (2.4%; not significant) or uninjected (0%; p<0.0001; **Figure 1A, B**). Left-right patterning during embryogenesis is governed by spatially restricted expression of nodal genes, such as *southpaw* (*spaw*) [326], so we performed RNA *in situ* hybridization to assess the expression pattern of this gene. 59.3% of mutants presented either bilateral, contralateral or absent expression of *spaw* compared to 8.3% in embryos injected with gRNA alone (p=0.0001) and 3.3% in uninjected embryos (p<0.0001; **Figure 1C, D**). The increased number of affected embryos can be explained by the fact that bilateral or absent expression of *spaw* could give rise to normal looping by chance. We raised the zebrafish embryos up to 4dpf and noticed that 18% of mosaic *let-7b* F0 were smaller, lacked a swim bladder and had cardiac edema. Less than 3% of such embryos were found in the control conditions (**Supp. Figure 2**).

Suppression of *let-7b* leads to shorter cilia in the zebrafish Kupffer's vesicle

The asymmetrical expression of nodal genes is created by the detection of a flow generated by the motile cilia in the Kupffer's vesicle (KV) which forms at approximately the 4-5ss somite-stage and persists until 18ss. Thus, we hypothesized that the left-right defects observed in the *let-7b* mosaic F0 were caused by ciliary defects in the KV. We stained 10ss embryos using an antibody against acetylated α-tubulin and examined the KV. The size of KV is naturally variable from one embryo to another [327] and we observed a trend toward a smaller KV in injected embryos (**Supp. Figure 3A**). To account for this variability, we measured the number of cilia per μm^2 of the KV lumen for each condition. We did not observe a change in the cilia density (**Figure 1F**), but cilia were significantly shorter in the KV of embryos injected with gRNA+Cas9 (4.3µm) compared to their siblings injected with gRNA alone (4.9µm; p<0.0001) or uninjected controls (5.1µm; p<0.0001; **Figure 1G**). These results suggest that suppression of *let-7b* in zebrafish embryos does not affect the number of ciliated cells but leads to shorter

cilia in the KV. This defect might prevent the generation of a proper flow to trigger restricted asymmetrical expression of laterality genes and could explain the heterotaxia phenotypes.

Cilia defects were recapitulated in *let-7b* morphants and were partially rescued when the morpholino was co-injected with *let-7b-5p* mimic

To validate further the effect of *let-7b* on cilia length, we injected a morpholino (MO) against *let-7b* or a *let-7b-5p* mimic (**Supp. Figure 1A, Figure 2**). Injection of increasing concentrations of *let-7b* MO from 2ng/µL to 6ng/µL led to a significant reduction of mature *let-7b* (2ng: 47% reduction, p=7.08E-5; 4ng: 48% reduction, p=9.31E-5; 6ng: 53% reduction, p=6.63E-6), while injection of the mimic at 0.2µM and 0.8µM led to a significant increase (0.2µM: 287% increase, p=1.57E-8; 0.8µM: 902% increase, p=2.64E-7) (**Supp. Figure 1C**). The injection of the MO recapitulated the heart looping anomalies (5.4-9.6%, p≤0.0001; **Figure 2A**), the *spaw* expression defects (36.8-65.3%, p-values<0.0001; **Figure 2B**), and cilia length defects (3.5-4.5µm, p<0.0001; **Figure 2F**) in a dose dependent manner. The KV tended to be smaller but the cilia density in the KV lumen was not affected (p>0.5, except for 2ngMO, p=0.02; **Supp. Figure 3B**, **Figure 2G**). Longer cilia have also been shown to affect left-right development in zebrafish [328] so we expected to see similar phenotypes in the embryos injected with the *let-7-5p* mimic. The injection of the *let-7b-5p* mimic led to dose-dependent heart looping anomalies (3.3% at 0.2µM, p=0.0001; and 25.3% at 0.8µM, p<0.0001) and *spaw* expression defects (30.6% at 0.2µM, p=0.0004; and 54.3% at 0.8µM, p<0.0001) (**Figure 2A, B**). However, we found no effect on the cilia density or length in the KV (**Figure 2F, G**). There was a trend for a smaller KV lumen in the embryos injected with the mimic but differences were not statistically significant (**Supp. Figure 3B**). The absence of cilia phenotypes in fixed samples, despite the presence of ciliary phenotypes, could suggest a mechanical or a signaling defect in embryos injected with the mimic. It is also possible that the left-right anomalies are caused by imbalance in cell differentiation due to excessive levels of *let-7b-5p* at these developmental stages.

Next, we co-injected *let-7b* MO with *let-7b-5p* mimic to see whether we could rescue the ciliary phenotypes observed in the morphants. All observed phenotypes were partially rescued when the MO was co-injected with 0.08µM of *let-7b-5p* mimic suggesting specificity: the heart looping anomalies were improved by 7.3% (from 9% in the morphants to 1.7% in the rescued embryos, p<0.0001; **Figure 2C**), the *spaw* expression defects were improved by 41.9% (from 64.9% to 23%, p =5.8E-3; **Figure 2D**), and the cilia length by 0.6 µm (from 3.7µm to 4.3µm, p<0.0001; **Figure 2H**). The cilia density calculated based on the size of the KV lumen (**Supp. Figure 3C**) and the number of cilia showed no difference (**Figure 2I**).

Suppression of *let-7b* in zebrafish also leads to phenotypes related to primary cilia defects

Convergent-extension (CE) is a process where cells migrate collectively and intercalate to allow body axis elongation in the developing zebrafish. The main pathway regulating CE is the cilia-dependent Wnt/PCP pathway and CE defects have been observed in several zebrafish ciliopathy models [313,329]. Thus, we examined 10ss *let-7b* mosaic F0, morphants and embryos expressing *let-7b-5p* mimic. We observed a significant increase of the angle between the anterior- and posterior-most ends of *let-7b* mosaic F0 (64.5°, p<0.0001), *let-7b* morphants (57,6° at 2ng/µL, 60.3° at 4ng/µL, and 77° at 6ng/µL, all p<0.0001) compared to controls (45° in embryos injected with gRNA alone, and 39.2 - 46,6° in uninjected siblings) suggesting a defect in primary cilia (**Supp. Figure 4**). Embryos injected with *let-7b-5p* mimic did not show a significant increase of their body-gap angle compared to uninjected siblings (51.8° at 0.2µM, p=0.21; and 52.2° at 0.8µM, p=0.14; **Supp. Figure 4**). This suggests that the overexpression of *let-7b-5p* in zebrafish embryos does not affect ciliary signaling.

2. Identification of possible *let-7b* targets which might act on ciliogenesis

Both *in vitro* and *in vivo* results support the candidacy of *let-7b* as a positive regulator of ciliogenesis but its mechanism of action remains unclear. To identify candidate genes that are regulated by *let-7b* and could influence ciliogenesis, we used the online prediction tool TargetScan and RNA-seq data performed on htRPE-1 cells treated with *let-7b* inhibitor or mimic.

Target gene predicting tool and database: TargetScan

The fewer and shorter cilia observed upon knockdown of *let-7b in vitro* and *in vivo* suggest that *let-7b* targets transcripts which negatively regulate ciliogenesis and cilia maintenance (**Figure 3A**), thus we looked in the literature for either validated or predicted negative regulators of ciliogenesis and identified 213 genes (**Supp. Table 1**). Next, we looked at the TargetScan database [330] which predicted 1207 target genes for the *let-7* family based on the presence of conserved sites matching the seed region and experimental evidence (**Supp. Table 2**). We found an overlap of 21 genes between the TargetScan predicted targets and the list of confirmed or predicted negative regulators: *MDM4*, *DUSP16*, *PBX1*, *PLA2G3*, *ARL4D*, *EIF4G2*, *ELOVL4*, *RTCA*, *ABL2*, *KDM3A*, *DUSP9*, *CCND1*, *SLC6A15*, *LIMK2*, *APC2*, *RASGRP1*, *EIF2S2*, *UTP15*, *B3GALT1*, *SCARA3*, and *MTDH* (**Figure 3B, Table 2**). Of note, *ARL4D* codes for an ADP Ribosylation Factor Like GTPase protein, and *ARL6*/*BBS3* codes for a protein of the same family and has been associated with BBS [331]. Since *let-7b* was the *let-7* family member which had the most marked effect *in vitro*, we filtered the predicted target genes by preferred *let-7* member and obtained a list of 60 genes which were *let-7b* preferred targets (**Supp. Table 2**). None of them were known or predicted negative regulators of ciliogenesis.

Insights from transcriptomics data from cells treated with *let-7b* inhibitor or mimic

Next, we switched from an *in silico* approach to an *in vitro* approach to account for the gene expression in the context of the htRPE-1 cells which allowed the identification of *let-7* as a candidate regulator of ciliogenesis. We hypothesized that the negative regulators of ciliogenesis targeted by the *let-7* family, and *let-7b* in particular, would be up-regulated in the context of *let-7b* inhibitor and down-regulated in the context of *let-7b* mimic. RNA-seq on htRPE-1 cells that were treated with *let-7b* inhibitor or *let-7b-5p* mimic was previously performed at CHDM. Transcriptomic data analysis led to the identification of 1,221 genes (1,152 were protein coding) of which expression was significantly increased when the cells were treated with the inhibitor and significantly decreased in the context of the mimic (FDR<0.05) (see methods in the annex). There was an overlap of 18 genes with the list of validated or predicted negative regulators of ciliogenesis, and 5 were also predicted with TargetScan (**Figure 3C, Table 3**). Functional annotation using the DAVID bioinformatics resource 6.8 [332] showed an enrichment in KEGG pathways related to proteoglycans in cancer and cell adhesion, the first term being expected considering the characterized function of *let-7* (**Figure 3D**). The Gene Ontology term analysis of biological processes replicated the enrichment in cell adhesion pathways and also suggested an enrichment for terms associated to the vesicle trafficking between the endoplasmic reticulum and the Golgi apparatus, and the extracellular matrix organization (**Figure 3**). However, it has been shown that endocardial-derived cells of conditional *Ift88* knock-out mice, which lack cilia in the heart, produce significantly more collagen and versican than their control littermates [333]. This indicated that the enrichment analyses might reveal consequences of the loss of cilia (increased protein synthesis and trafficking to the extracellular matrix) rather than *let-7b* direct upstream effect. Therefore, we further filtered our list of candidate targets.

Identifying direct targets of *let-7b*

It is likely that some gene expression alteration is an indirect effect of the modulation of *let-7b* levels. Therefore, we combined both *in silico* and *in vitro* approaches by using the TargetScan search tool on the transcriptomic data. We identified a total of 3,882 *let-7* seed targets on 1,979 transcripts and only retained the 1,526 transcripts coding for proteins. After consolidating the multiple isoforms, we obtained a list of 733 genes of which expression was perturbed in cells treated with *let-7b* inhibitor and mimic, and bearing at least one *let-7* target (interactive **Table 4** mentioned in the annex). When we restricted the search to *let-7b-5p* targets to be consistent with the *let-7b-5p* mimic treatment, we narrowed down the list of candidate genes to 499 (**Table 4**). Ten genes were overlapping with the list of negative regulators of ciliogenesis: *ARL4D*, *EIF4G2*, *ELOVL4*, *RTCA*, *LIMK2*, *CXXC4*, *RIOK2*, *PARVA*, *NCK2*, and *TEAD1*, of which 5 were also predicted targets by TargetScan (**Figure 3E, Table 4**). To guide our filtering, we also noted whether the gene was associated with cilia based on different studies including the SYSCILIA lists [285], our own data obtained from the ciliary proteome [284] and ciliopathy patients sequencing [334], the ciliary landscape study [238], and OMIM database (**Table 4, Supp. Table 3**). The small number of genes prevented us from reaching statistical significance in an enrichment analysis, however, manual review of the genes enabled the identification of three different patterns which could link the transcript regulation by *let-7b* and ciliogenesis: cell cycle regulation, actin cytoskeleton remodeling and the PI3K/Akt pathway.

We identified a number of candidates, including *CDC25A*, *CXXC4* and *RIOK2*, which are involved in the regulation of the cell cycle which ultimately affects ciliogenesis. However, those genes do not fit the model where *let-7* regulates ciliogenesis in a cell cycle-independent manner (Jon Robinson's thesis, [304]). Thus, those genes were not further explored.

Among the validated negative regulators, we found the actin regulator *PARVA* which has been identified in a RNAi screen where authors further demonstrated the inhibitory effect of the actin cytoskeleton on ciliogenesis [335]. Additionally, LIMK2 was shown to

phosphorylate CFL to inactivate its actin-depolarization activity which blocks vesicle trafficking to the BB, but also allows nuclear translocation of YAP/TAZ, complexing with TEAD4, and transcription of *AURKA* and *PLK1* [92]. Since *TEAD1* is closely related to *TEAD4 [336]*, it is possible that it plays a role in this cascade as well. Among the candidate genes not established or predicted negative regulators of ciliogenesis, we found *NRK*, which is predicted to play a similar role *as LIMK2* [337], *ACTR2* and a number of genes coding for cytoplasmic membrane proteins which serves as anchor for the actin cytoskeleton. These genes include *VCL*, *RDX*, *EZR*, *MSN*, *TPM1*, *DAG1*, *PVRL2* and three genes coding for integrins: *ITGA11*, *ITGAV*, *ITGB3*.

We found 15 genes coding for proteins stimulating the PI3K/AKT pathway: *PDGFB*, *GNB4*, *CDKN1A*, *NGF*, *TLR4*, *THBS1*, *ITGA11*, *ITGAV*, *OSMR*, *YWHAZ*, *IRS1*, *GNG5*, *CREB3L2*, *NRAS*, and *ITGB3*. It has recently been shown that the PI3K/AKT pathway is activated by lysophosphatidic acid present in the serum delivered to htRPE-1 cells in culture, and that it leads to the phosphorylation of WDR44. WDR44 then binds to RAB11 to prevent it from initiating the preciliary trafficking [338].

Verifying *LIMK2* candidacy in zebrafish

LIMK2 was the top candidate as it was selected by TargetScan, by our transcriptomics analysis with low FDRs ($FDR_{Inhibitor}$=6.53E-46, FDR_{Mimic}=1.65E-5) and high fold changes (Log_2 $(FoldChange)_{Inhibitor}$=1.50 and Log_2 $(FoldChange)_{Mimic}$=-0.47), had three *let-7b-5p* target sites, and is a validated negative regulator of ciliogenesis (**Table 4, Figure 4A**). Thus, we asked whether we could detect an increase in the level of *limk2* in *let-7b* F0 mosaic zebrafish and morphants, and a decrease of *limk2* in the embryos expressing *let-7b-5p* mimic. We did not detect significant changes in the expression of *limk2* in our injected embryos at 30hpf (**Figure 4B,C**). However, this does not exclude the possibility that *let-7b* modulates ciliogenesis through LIMK2 and the regulation of the actin cytoskeleton in another context. It is possible that LIMK2 played a role in the htRPE-1 cells *in vitro* but not in the developing zebrafish

embryos at the observed stage. It would be relevant to knock down *limk2* in *let-7b* F0 mosaic and morphants to see if it rescues the cilia length phenotype. Phenocopy could also be tested by overexpressing *limk2* by mRNA injection in the zebrafish embryo.

3. Explore the hypothesis that the *let*-7 family of miRNAs is a modifier gene of ciliopathies

To explore the hypothesis that the *let-7* family of miRNAs acts as a modifier of ciliopathies, we proposed that ciliopathy patients might harbor an enrichment of variants in the 3'UTR of *let-7* target genes. We selected a cohort of 185 ciliopathy patients affected with a severe or a milder form of ciliopathy (68 with Meckel-Grüber syndrome, and 117 with BBS). Patients were from different ethnicities and split into two groups in accordance with the gnomAD for the downstream analysis: North European (Non-Finnish) or other (Latino, African, East Asian, and other). First, we Sanger sequenced the *let-7b* locus and confirmed that there was no mutation in any sample from our cohort.

Identification of the target loci for sequencing

We built a list of *let-7b* targets to sequence based on the filtered data obtained from RNA-seq data and the TargetScan tool. Here, we decided to focus on genes associated with ciliopathies or established ciliary genes. Thus, we filtered the list of 733 genes (dysregulated in treated htRPE-1 cells and containing at least one *let-7b-5p* or *let-7b-3p* binding site) with a list of genes which have an established ciliary role obtained from the SYSCILIA list [285], and genes associated with ciliopathies (our own data obtained from patients sequencing [334], and OMIM database, **Supp. Table 3**). We identified 42 genes with 113 *let-7b* target loci (*let-7b-5p* or *let-7b-3p*, **Table 5**) and performed targeted sequencing on our cohort of 185 ciliopathy patients. The mean target coverage was 1,369 reads across all samples.

Analysis of variants

We looked for rare homozygous variants in *let7b* target sites which might contribute to recessive ciliopathies but we found no such variant. Next, we ask whether there were more variants in the 3'UTR of Meckel-Grüber patients compared to BBS patients to investigate a correlation between mutational burden and disease severity. We observed no enrichment at a 5% or 1% minor allele frequency (MAF) suggesting no mutational burden at the sequenced loci in these patients (**Table 6**). Then, we used the controls from the gnomAD to ask whether there was an enrichment or depletion of the variants we identified through targeted sequencing. We identified 2 variants which were significantly depleted or enriched in our ciliopathy cohort. rs6679100 (1-198288709-A-G, MAF=0.70%) in the 3'UTR of *NEK7* was significantly depleted in our ciliopathy cohort (p=0.02; **Table 7**). *NEK7* codes for NIMA related kinase 7 which accelerates microtubule shrinkage speed [339] and is related to NEK2, a protein mutated in Retinitis pigmentosa [340]. On the other hand, rs182129505 (10-113912476-C-T; MAF=8.22E-5) in the 3'UTR of *GPAM* was significantly enriched in our cohort (p <0.01; **Table 7**). *GPAM* codes for a glycerol-3-phosphate acyltransferase located in mitochondria and has been associated with primary cilia but its function in relation to cilia biology remains unclear [341]. Those 2 variants were confirmed by Sanger sequencing. **Figure 5** shows where the variants are located relative to *let-7* seed target sequence. It is possible that the depletion of rs6679100 observed in our ciliopathy cohort is due to an ethnicity bias. Indeed, 37% of our ethnicity group "Other" is composed of patients of Pakistani origin and gnomAD lacks data on individuals from South Asia at this particular region in the genome. This potential population bias and the fact that the variants were not directly disrupting the seed target sequence dissuaded us from pursuing validation *in vitro*.

4. Summary and concluding remarks

Following a medium-throughput screen *in vitro* suggesting that *let-7* is a positive regulator of ciliogenesis and cilia maintenance, we further validated the function of *let-7b in vivo*.

Consistent with the shorter cilia observed in the htRPE-1 cells treated with *let-7b* inhibitor, we showed that knocking down *let-7b* in the zebrafish embryos using two different methods, namely the CRISPR/Cas9 genome editing technology and the injection of MO, leads to shorter cilia in the KV and associated ciliary phenotypes. We did not observe a decrease in the fraction of ciliated cells measured by cilia density in the KV lumen, which might be due to differences between *in vitro* and *in vivo* models. The overexpression of *let-7b-5p* mimic *in vivo* did not recapitulate the increased cilia length and fraction of ciliated cells observed *in vitro*. However, the presence of left-right patterning defects at the concentrations of 0.2µM and 0.8µM suggests that cilia might be affected in a different way, perhaps in their beating capacity.

By combining *in silico* and *in vitro* data with a thorough literature search, we obtained a list of 499 candidate targets which could link the transcript regulation activity of *let-7* and the downstream effect on ciliogenesis and cilia maintenance. We identified two networks of genes which could contribute to the cilia phenotypes observed *in vitro* and *in vivo*: the actin cytoskeleton remodeling and the PI3K/Akt pathway. When focusing on single genes, we identified ten strong candidates which have already been associated with roles of negative regulators of ciliogenesis and five of them were also present in the TargetScan database which lists predicted and validated targets of *let-7*. *LIMK2* was our top candidate but could not be validated *in vivo*. However, further experiments are needed to conclude with certainty on the relationship between *let-7*, *LIMK2*, and ciliogenesis.

Finally, to explore the hypothesis that *let-7* is a modifier gene of ciliopathies, we performed targeted sequencing on *let-7* targets in the 3'UTR of fourty ciliary genes of which expression was showed to be disturbed through transcriptomic analysis of htRPE-1 cells. We did not find variants in the seed targets that we sequenced in our ciliopathy cohort at an allele balance cut-off of 20%, nor strong candidate variants for enrichment analysis. A possible explanation is the small size of our cohort once split according to ethnicity groups. However, this study as a whole revealed the potential of non-coding RNA in affecting ciliogenesis and

cilia maintenance, and suggests a need to include the UTRs in whole-exome sequencing (WES) analysis performed on patients. Once more UTRs are available, it would be worthwhile to reevaluate the *let-7* targets across all genes.

Table 1: Intra- and inter-species conservation of *let-7b* miRNAs

miRNA	Human loci	Human mature sequence	Zebrafish loci	Zebrafish mature sequence
let-7a*	*let-7a-1,2,3*	UGAGGUAGU**AGG**UUG**UAUA**GUU	*let-7a-1,2,3,4,5,6*	UGAGGUAGU**AGG**UUG**UAUA**GUU
let-7b*	*let-7b*	UGAGGUAGU**AGG**UUG**UGUG**GUU	*let-7b*	UGAGGUAGU**AGG**UUG**UGUG**GUU
let-7c*	*let-7c*	UGAGGUAGU**AGG**UUG**UAUG**GUU	*let-7c-1,2*	UGAGGUAGU**AGG**UUG**UAUG**GUU
let-7d	*let-7d*	**A**GAGGUAGU**AGG**UUG**CAUA**GUU	*let-7d-1,2*	UGAGGUAGU**UGG**UUG**UAUG**GUU
let-7e	*let-7e*	UGAGGUAGG**AGG**UUG**UAUA**GUU	*let-7e*	UGAGGUAGU**AGA**UUG**AAUA**GUU
let-7f*	*let-7f-1,2*	UGAGGUAGU**AGA**UUG**UAUA**GUU	*let-7f*	UGAGGUAGU**AGA**UUG**UAUA**GUU
let-7g	*let-7g*	UGAGGUAGU**AGU**UUG**UACA**GUU	*let-7g1,2*	UGAGGUAGU**AGU**UUG**UAUA**GUU
let-7h			*let-7h*	UGAGGUAGU**AAG**UUG**UGUU**GUU
let-7i*	*let-7i*	UGAGGUAGU**AGU**UUG**UGCU**GUU	*let-7i*	UGAGGUAGU**AGU**UUG**UGCU**GUU
let-7j			*let-7j*	UGAGGUAGU**UGU**UUG**UACA**GUU
miR-98	*miR-98*	UGAGGUAGU**AAG**UUG**UAUU**GUU		

miRNA mature sequences which are 100% conserved between human and zebrafish are indicated with *. miRNA seed is underlined. Nucleotides which differ from one *let-7* member to another are indicated in bold.

Table 2: *let-7* targets and negative regulators of ciliogenesis

Ensembl ID	Gene Name	Gene Description	TCS	Negative Regulator Reference (PMID)
ENSG00000198625	MDM4	Mdm4 p53 binding protein homolog (mouse)	-0.84	26026149
ENSG00000185630	PBX1	pre-B-cell leukemia homeobox 1	-0.7	26026149
ENSG00000111266	DUSP16	dual specificity phosphatase 16	-0.68	26026149
ENSG00000182541	LIMK2	LIM domain kinase 2	-0.48	26026149
ENSG00000100078	PLA2G3	phospholipase A2, group III	-0.45	20393563
ENSG00000175906	ARL4D	ADP-ribosylation factor-like 4D	-0.42	26026149
ENSG00000172575	RASGRP1	RAS guanyl releasing protein 1 (calcium and DAG-regulated)	-0.42	26026149
ENSG00000125977	EIF2S2	eukaryotic translation initiation factor 2, subunit 2 beta, 38kDa	-0.41	26026149
ENSG00000110321	EIF4G2	eukaryotic translation initiation factor 4 gamma, 2	-0.4	26026149
ENSG00000110092	CCND1	cyclin D1	-0.4	26026149
ENSG00000118402	ELOVL4	ELOVL fatty acid elongase 4	-0.39	26167768
ENSG00000147649	MTDH	metadherin	-0.39	26026149
ENSG00000137996	RTCA	RNA 3'-terminal phosphate cyclase	-0.37	26026149
ENSG00000164338	UTP15	UTP15, U3 small nucleolar ribonucleoprotein, homolog (S. cerevisiae)	-0.37	26026149
ENSG00000143322	ABL2	c-abl oncogene 2, non-receptor tyrosine kinase	-0.36	26026149
ENSG00000115548	KDM3A	lysine (K)-specific demethylase 3A	-0.33	28246120
ENSG00000130829	DUSP9	dual specificity phosphatase 9	-0.31	26026149
ENSG00000072041	SLC6A15	solute carrier family 6 (neutral amino acid transporter), member 15	-0.27	26026149
ENSG00000172318	B3GALT1	UDP-Gal:betaGlcNAc beta 1,3-galactosyltransferase, polypeptide 1	-0.26	26026149
ENSG00000115266	APC2	adenomatosis polyposis coli 2	-0.13	26026149
ENSG00000168077	SCARA3	scavenger receptor class A, member 3	-0.05	26026149

TCS: Total Context++ Score is based on several parameters such as the type of the binding site and the length of the 3'UTR [342]. It measures the strength of a miRNA inhibition on a particular transcript, the lower the score the stronger the predicted inhibition.

Table 3: Genes with altered expression in the cells treated with *let-7b* inhibitor or mimic, and which are also negative regulators of ciliogenesis

Ensembl ID	Gene Name	Gene Description	$Log(FC)_{inhibitor}$	$FDR_{inhibitor}$	$Log(FC)_{mimic}$	FDR_{mimic}	Negative Regulator Reference (PMID)
ENSG00000182541	LIMK2	LIM domain kinase 2	1.5	6.53E-46	-0.47	1.65E-05	25849865
ENSG00000120708	TGFBI	transforming growth factor beta induced	1.05	6.26E-21	-0.75	1.86E-11	26026149
ENSG00000141524	TMC6	transmembrane channel like 6	1.15	5.64E-18	-1.01	3.22E-10	26026149
ENSG00000197702	PARVA	parvin alpha	0.61	8.95E-15	-0.36	5.89E-06	20393563
ENSG00000110321	EIF4G2	eukaryotic translation initiation factor 4 gamma 2	0.42	7.59E-09	-0.67	3.58E-22	26026149
ENSG00000188488	SERPINA5	serpin family A member 5	1.23	1.26E-06	-4	9.64E-26	26026149
ENSG00000168772	CXXC4	CXXC finger protein 4	0.73	1.58E-05	-0.55	2.03E-03	26026149
ENSG00000115091	ACTR3	actin related protein 3	0.35	3.18E-05	-0.49	4.39E-10	20393563
ENSG00000187079	TEAD1	TEA domain transcription factor 1	0.29	6.16E-05	-0.23	1.01E-03	26026149
ENSG00000168615	ADAM9	ADAM metallopeptidase domain 9	0.3	3.84E-04	-0.37	4.88E-06	26026149
ENSG00000118402	ELOVL4	ELOVL fatty acid elongase 4	0.28	7.19E-04	-0.81	1.19E-24	26167768
ENSG00000027847	B4GALT7	beta-1,4-galactosyltransferase 7	0.28	8.45E-04	-0.19	1.79E-02	26026149
ENSG00000162302	RPS6KA4	ribosomal protein S6 kinase A4	0.3	1.33E-03	-0.29	1.21E-03	26026149
ENSG00000058729	RIOK2	RIO kinase 2	0.25	3.72E-03	-0.25	2.13E-03	26026149
ENSG00000175906	ARL4D	ADP ribosylation factor like GTPase 4D	0.31	1.03E-02	-1.15	5.68E-24	26026149
ENSG00000119326	CTNNAL1	catenin alpha like 1	0.28	1.22E-02	-0.91	7.13E-20	20393563
ENSG00000071051	NCK2	NCK adaptor protein 2	0.26	2.66E-02	-0.45	2.41E-05	26026149
ENSG00000137996	RTCA	RNA 3'-terminal phosphate cyclase	0.18	3.32E-02	-1.07	5.95E-46	26026149

FC: fold change; FDR: false discovery rate

Table 4: Final list of *let-7b* candidate targets

Ensembl ID	Gene Name	Number of *-3p* Sites	Number of *-5p* Sites	TargetScan TCS	Preferred *let-7*	L2FC (IC)	FDR (IC)	L2FC (MC)	FDR (MC)	Negative Regulator Reference (PMID)	Ciliary Gene
ENSG00000197702	PARVA	0	1	N/A	N/A	0.61	8.95E-15	-0.36	5.89E-06	20393563	FALSE
ENSG00000182541	LIMK2	0	3	-0.48	hsa-miR-98-5p	1.50	6.53E-46	-0.47	1.65E-05	25849865	FALSE
ENSG00000110321	EIF4G2	0	1	-0.4	hsa-let-7d-5p	0.42	7.59E-09	-0.67	3.58E-22	26026149	FALSE
ENSG00000168772	CXXC4	6	2	N/A	N/A	0.73	1.58E-05	-0.55	2.03E-03	26026149	FALSE
ENSG00000187079	TEAD1	6	1	N/A	N/A	0.29	6.16E-05	-0.23	1.01E-03	26026149	FALSE
ENSG00000058729	RIOK2	2	2	N/A	N/A	0.25	3.72E-03	-0.25	2.13E-03	26026149	FALSE
ENSG00000175906	ARL4D	0	1	-0.42	hsa-let-7a-5p	0.31	1.03E-02	-1.15	5.68E-24	26026149	FALSE
ENSG00000071051	NCK2	0	1	N/A	N/A	0.26	2.66E-02	-0.45	2.41E-05	26026149	FALSE
ENSG00000137996	RTCA	0	1	-0.37	hsa-let-7d-5p	0.18	3.32E-02	-1.07	5.95E-46	26026149	FALSE
ENSG00000118402	ELOVL4	1	1	-0.39	hsa-let-7f-5p	0.28	7.19E-04	-0.81	1.19E-24	26167768	FALSE
ENSG00000159217	IGF2BP1	0	6	-1.51	hsa-let-7d-5p	2.42	2.39E-148	-0.42	2.38E-05	N/A	FALSE
ENSG00000078401	EDN1	0	1	-0.54	hsa-let-7d-5p	4.51	4.46E-98	-1.16	1.64E-05	N/A	FALSE
ENSG00000011201	KAL1	4	2	N/A	N/A	2.07	3.45E-97	-1.87	4.33E-56	N/A	FALSE
ENSG00000001617	SEMA3F	0	1	N/A	N/A	1.81	1.50E-93	-1.59	4.97E-70	N/A	FALSE
ENSG00000100311	PDGFB	1	1	-0.32	hsa-let-7f-5p	3.71	4.19E-85	-1.08	1.79E-05	N/A	FALSE
ENSG00000173065	FAM222B	0	4	-1.03	hsa-let-7d-5p	1.33	3.16E-80	-0.67	1.15E-19	N/A	FALSE
ENSG00000100697	DICER1	3	3	-0.96	hsa-let-7d-5p	1.56	1.53E-76	-0.29	1.15E-03	N/A	FALSE
ENSG00000144057	ST6GAL2	4	2	N/A	N/A	2.84	2.06E-76	-2.14	2.98E-34	N/A	FALSE
ENSG00000134198	TSPAN2	5	1	-0.28	hsa-let-7g-5p	3.04	1.14E-66	-2.18	1.83E-20	N/A	FALSE
ENSG00000099337	KCNK6	0	1	-0.47	hsa-let-7d-5p	1.78	1.43E-59	-1.40	1.44E-32	N/A	FALSE
ENSG00000143641	GALNT2	1	1	-0.29	hsa-let-7g-5p	1.10	4.81E-59	-1.06	8.22E-54	N/A	FALSE
ENSG00000137801	THBS1	1	2	-0.3	hsa-let-7c-5p	2.14	7.26E-56	-1.14	9.76E-18	N/A	FALSE
ENSG00000099953	MMP11	1	1	-0.36	hsa-let-7d-5p	2.28	9.75E-53	-1.59	4.84E-24	N/A	FALSE
ENSG00000004399	PLXND1	0	1	-0.32	hsa-let-7d-5p	1.22	3.27E-50	-0.80	2.49E-21	N/A	FALSE
ENSG00000122367	LDB3	1	1	N/A	N/A	2.78	3.25E-49	-1.31	5.82E-05	N/A	FALSE
ENSG00000158258	CLSTN2	4	3	N/A	N/A	1.80	9.58E-48	-1.35	6.00E-28	N/A	FALSE
ENSG00000136603	SKIL	2	3	-0.77	hsa-let-7d-5p	0.99	6.95E-46	-1.00	2.12E-44	N/A	FALSE
ENSG00000128510	CPA4	0	2	-0.57	hsa-let-7d-5p	3.25	1.07E-44	-0.74	1.02E-03	N/A	FALSE
ENSG00000149948	HMGA2	5	10	-2.69	hsa-let-7d-5p	2.26	3.06E-43	-0.65	8.01E-05	N/A	FALSE
ENSG00000164292	RHOBTB3	5	2	N/A	N/A	1.12	4.98E-41	-0.65	9.64E-15	N/A	FALSE
ENSG00000205978	NYNRIN	0	3	-0.4	hsa-let-7d-5p	2.14	1.28E-40	-0.85	2.83E-05	N/A	FALSE
ENSG00000060718	COL11A1	3	1	-0.26	hsa-let-7d-5p	2.56	9.81E-40	-1.48	7.45E-14	N/A	FALSE
ENSG00000204516	MICB	0	1	N/A	N/A	0.95	8.04E-39	-1.19	2.00E-51	N/A	FALSE
ENSG00000151233	GXYLT1	3	2	-0.63	hsa-let-7d-5p	1.14	1.78E-38	-0.39	2.74E-05	N/A	FALSE
ENSG00000129657	SEC14L1	1	1	-0.26	hsa-let-7d-5p	0.99	4.70E-38	-0.48	1.12E-09	N/A	FALSE
ENSG00000241852	C8orf58	0	1	-0.65	hsa-let-7d-5p	1.13	6.20E-37	-0.65	4.17E-11	N/A	FALSE
ENSG00000173706	HEG1	1	1	N/A	N/A	1.35	6.54E-37	-0.54	5.85E-07	N/A	FALSE
ENSG00000135912	TTLL4	0	2	-0.87	hsa-let-7d-5p	0.81	1.25E-36	-0.34	4.95E-07	N/A	FALSE
ENSG00000035403	VCL	3	1	N/A	N/A	1.02	9.97E-36	-1.37	6.84E-64	N/A	Ciliary-landscape_2016
ENSG00000119927	GPAM	2	2	N/A	N/A	1.09	1.39E-35	-0.19	4.92E-02	N/A	Katsanis_2006
ENSG00000185909	KLHDC8B	0	1	-0.57	hsa-let-7d-5p	1.11	2.17E-35	-1.04	5.30E-27	N/A	FALSE
ENSG00000090097	PCBP4	0	1	N/A	N/A	0.87	3.15E-35	-1.19	1.74E-60	N/A	FALSE
ENSG00000156466	GDF6	1	1	-0.51	hsa-let-7d-5p	2.34	1.47E-34	-0.48	1.74E-02	N/A	FALSE
ENSG00000197930	ERO1L	3	3	-0.63	hsa-let-7a-5p	0.88	2.21E-34	-0.92	5.80E-37	N/A	FALSE
ENSG00000130958	SLC35D2	0	1	-0.92	hsa-let-7d-5p	0.77	1.06E-33	-0.79	1.27E-32	N/A	FALSE
ENSG00000182054	IDH2	0	1	-0.36	hsa-let-7d-5p	0.96	5.69E-33	-1.96	8.72E-115	N/A	FALSE
ENSG00000166897	ELFN2	0	1	N/A	N/A	1.05	1.26E-32	-0.74	1.09E-14	N/A	FALSE
ENSG00000141429	GALNT1	1	2	-0.69	hsa-let-7d-5p	1.13	2.14E-32	-0.33	9.08E-04	N/A	Katsanis_2006
ENSG00000182752	PAPPA	3	3	-0.81	hsa-miR-98-5p	1.96	6.00E-32	-1.20	2.75E-13	N/A	FALSE
ENSG00000073792	IGF2BP2	1	2	-0.54	hsa-let-7d-5p	0.98	2.24E-31	-1.14	5.25E-42	N/A	FALSE
ENSG00000196428	TSC22D2	6	1	-0.31	hsa-let-7d-5p	0.92	2.85E-30	-0.48	5.96E-09	N/A	FALSE
ENSG00000144810	COL8A1	2	1	N/A	N/A	0.94	4.07E-30	-0.70	2.03E-17	N/A	FALSE
ENSG00000139719	VPS33A	1	1	N/A	N/A	1.12	1.80E-29	-0.51	2.86E-06	N/A	FALSE
ENSG00000075420	FNDC3B	6	3	-0.36	hsa-let-7d-5p	0.85	2.71E-29	-0.27	7.01E-04	N/A	Katsanis_2006

Ensembl ID	Gene Name	Number of *-3p* Sites	Number of *-5p* Sites	TargetScan TCS	Preferred *let-7*	L2FC (IC)	FDR (IC)	L2FC (MC)	FDR (MC)	Negative Regulator Reference (PMID)	Ciliary Gene
ENSG00000135622	SEMA4F	1	1	-0.38	hsa-let-7d-5p	0.84	4.43E-29	-1.04	4.28E-41	N/A	FALSE
ENSG00000106080	FKBP14	4	1	N/A	N/A	0.76	6.62E-29	-0.39	3.39E-08	N/A	FALSE
ENSG00000015532	XYLT2	0	1	N/A	N/A	0.83	1.31E-28	-0.57	5.96E-14	N/A	Ciliary-landscape_2016
ENSG00000129128	SPCS3	2	2	N/A	N/A	0.95	7.15E-26	-0.99	4.54E-28	N/A	FALSE
ENSG00000164574	GALNT10	1	1	N/A	N/A	0.84	2.61E-25	-1.36	1.59E-64	N/A	FALSE
ENSG00000126003	**PLAGL2**	**1**	**1**	**-0.41**	**hsa-let-7b-5p**	**0.84**	**2.84E-25**	**-1.03**	**3.04E-32**	**N/A**	**FALSE**
ENSG00000168256	NKIRAS2	0	1	-0.3	hsa-let-7d-5p	0.65	3.75E-25	-0.47	3.98E-13	N/A	FALSE
ENSG00000114302	PRKAR2A	2	1	-0.44	hsa-let-7d-5p	0.84	5.84E-25	-1.01	3.04E-34	N/A	Katsanis_2006
ENSG00000130508	PXDN	1	3	-0.54	hsa-let-7d-5p	1.12	8.61E-24	-1.27	4.91E-31	N/A	FALSE
ENSG00000259207	ITGB3	1	4	-0.46	hsa-let-7d-5p	1.57	1.08E-23	-3.77	9.92E-38	N/A	FALSE
ENSG00000179361	ARID3B	0	5	-1.68	hsa-let-7d-5p	1.72	3.33E-23	-0.80	2.95E-05	N/A	FALSE
ENSG00000158156	XKR8	0	3	-0.77	hsa-let-7d-5p	0.73	2.44E-22	-1.05	2.24E-39	N/A	FALSE
ENSG00000136295	TTYH3	0	2	N/A	N/A	1.12	3.07E-22	-0.54	2.78E-06	N/A	FALSE
ENSG00000174695	TMEM167A	4	2	-0.62	hsa-let-7d-5p	0.78	3.13E-22	-0.49	2.46E-09	N/A	FALSE
ENSG00000114554	PLXNA1	1	1	N/A	N/A	0.66	6.82E-22	-0.84	4.00E-35	N/A	FALSE
ENSG00000183023	SLC8A1	8	3	N/A	N/A	0.92	4.55E-21	-0.78	1.08E-14	N/A	FALSE
ENSG00000114115	RBP1	0	1	N/A	N/A	0.88	4.55E-21	-1.50	1.64E-45	N/A	FALSE
ENSG00000060982	BCAT1	1	1	-0.42	hsa-let-7d-5p	1.06	9.53E-21	-0.90	1.03E-15	N/A	FALSE
ENSG00000112763	BTN2A1	0	1	N/A	N/A	0.64	1.67E-20	-0.61	5.45E-18	N/A	FALSE
ENSG00000085491	SLC25A24	1	1	-0.4	hsa-let-7a-5p	0.81	2.41E-20	-1.10	1.10E-35	N/A	FALSE
ENSG00000080493	SLC4A4	7	1	-0.25	hsa-let-7d-5p	1.19	2.41E-20	-1.12	1.60E-13	N/A	FALSE
ENSG00000104660	LEPROTL1	4	2	-0.59	hsa-let-7d-5p	0.73	3.15E-20	-0.81	3.35E-23	N/A	FALSE
ENSG00000177058	SLC38A9	1	1	-0.31	hsa-let-7d-5p	0.77	4.05E-20	-0.29	1.21E-03	N/A	FALSE
ENSG00000065308	TRAM2	0	1	N/A	N/A	0.83	5.60E-20	-0.70	6.23E-15	N/A	FALSE
ENSG00000180758	GPR157	0	2	-0.36	hsa-let-7f-5p	0.85	5.78E-20	-0.33	1.27E-03	N/A	FALSE
ENSG00000119681	LTBP2	1	1	N/A	N/A	0.95	5.94E-20	-0.78	3.94E-14	N/A	FALSE
ENSG00000134871	COL4A2	0	1	-0.32	hsa-miR-98-5p	1.06	1.76E-19	-0.70	1.79E-09	N/A	FALSE
ENSG00000196923	PDLIM7	0	1	N/A	N/A	0.71	2.45E-19	-0.91	4.74E-31	N/A	Ciliary-landscape_2016
ENSG00000105419	MEIS3	0	3	N/A	N/A	0.96	2.52E-19	-1.28	4.56E-28	N/A	FALSE
ENSG00000078804	TP53INP2	1	1	N/A	N/A	0.71	2.67E-19	-0.78	2.69E-22	N/A	FALSE
ENSG00000114268	PFKFB4	0	1	N/A	N/A	0.83	3.88E-19	-0.78	2.79E-15	N/A	FALSE
ENSG00000107443	CCNJ	1	2	-0.63	hsa-let-7d-5p	0.70	4.43E-19	-0.74	4.24E-19	N/A	FALSE
ENSG00000134762	DSC3	4	1	N/A	N/A	0.63	4.45E-19	-0.74	1.28E-25	N/A	FALSE
ENSG00000173473	SMARCC1	0	2	-0.31	hsa-let-7g-5p	0.70	7.58E-19	-0.92	4.92E-32	N/A	FALSE
ENSG00000154678	PDE1C	4	1	N/A	N/A	0.87	1.12E-18	-1.12	1.47E-29	N/A	Katsanis_2006
ENSG00000159263	SIM2	0	1	N/A	N/A	0.70	1.42E-18	-0.26	1.45E-03	N/A	FALSE
ENSG00000058799	YIPF1	0	1	N/A	N/A	0.67	5.20E-18	-0.88	7.05E-27	N/A	FALSE
ENSG00000173641	HSPB7	3	1	N/A	N/A	1.29	6.22E-18	-1.47	5.63E-15	N/A	FALSE
ENSG00000130021	HDHD1	2	2	-0.46	hsa-let-7d-5p	1.20	6.58E-18	-1.61	2.16E-26	N/A	FALSE
ENSG00000163362	C1orf106	1	1	N/A	N/A	2.09	6.58E-18	-0.95	1.26E-02	N/A	FALSE
ENSG00000126067	PSMB2	0	1	N/A	N/A	0.60	2.92E-17	-0.57	4.25E-16	N/A	FALSE
ENSG00000164741	DLC1	2	2	-0.36	hsa-let-7d-5p	0.93	3.89E-17	-1.45	1.27E-39	N/A	FALSE
ENSG00000164294	GPX8	1	2	N/A	N/A	0.62	4.28E-17	-1.38	3.88E-79	N/A	FALSE
ENSG00000165072	MAMDC2	2	1	N/A	N/A	1.04	4.80E-17	-0.40	1.76E-03	N/A	FALSE
ENSG00000166086	JAM3	0	1	N/A	N/A	0.66	5.31E-17	-1.63	5.16E-91	N/A	FALSE
ENSG00000172548	NIPAL4	0	1	-0.3	hsa-let-7d-5p	1.24	1.07E-16	-2.34	2.07E-32	N/A	FALSE
ENSG00000088854	C20orf194	1	2	-0.48	hsa-let-7d-5p	0.66	1.29E-16	-0.44	9.54E-08	N/A	FALSE
ENSG00000121058	COIL	1	1	-0.63	hsa-let-7f-5p	0.65	4.27E-16	-0.20	2.34E-02	N/A	FALSE
ENSG00000160094	**ZNF362**	**1**	**2**	**-0.26**	**hsa-let-7b-5p**	**0.69**	**6.51E-16**	**-0.67**	**9.78E-14**	**N/A**	**FALSE**
ENSG00000154380	ENAH	2	3	N/A	N/A	0.60	1.04E-15	-0.29	1.63E-04	N/A	FALSE
ENSG00000107551	RASSF4	0	2	N/A	N/A	0.94	1.10E-15	-1.16	8.89E-21	N/A	FALSE
ENSG00000054983	GALC	1	1	-0.43	hsa-let-7f-5p	1.10	1.47E-15	-1.61	3.93E-25	N/A	FALSE
ENSG00000106799	TGFBR1	4	3	-0.76	hsa-let-7d-5p	0.66	1.62E-15	-1.15	2.23E-43	N/A	FALSE
ENSG00000146109	ABT1	0	1	N/A	N/A	0.70	1.64E-15	-0.50	5.07E-08	N/A	FALSE
ENSG00000166860	ZBTB39	3	2	-0.28	hsa-let-7d-5p	0.72	1.72E-15	-0.35	3.42E-04	N/A	FALSE
ENSG00000196233	LCOR	9	3	-0.51	hsa-let-7d-5p	0.62	2.49E-15	-0.49	6.57E-10	N/A	FALSE

Ensembl ID	Gene Name	Number of *-3p* Sites	Number of *-5p* Sites	TargetScan TCS	Preferred *let-7*	L2FC (IC)	FDR (IC)	L2FC (MC)	FDR (MC)	Negative Regulator Reference (PMID)	Ciliary Gene
ENSG00000213281	NRAS	2	2	-0.7	hsa-let-7f-5p	0.57	2.72E-15	-0.63	2.06E-18	N/A	FALSE
ENSG00000156140	ADAMTS3	1	1	N/A	N/A	0.87	3.09E-15	-1.16	1.02E-20	N/A	FALSE
ENSG00000169612	FAM103A1	0	2	-0.74	hsa-let-7d-5p	1.19	3.14E-15	-0.50	3.99E-03	N/A	FALSE
ENSG00000184117	NIPSNAP1	0	1	N/A	N/A	0.55	5.69E-15	-1.42	1.68E-90	N/A	Ciliary-landscape_2016
ENSG00000125170	DOK4	0	1	N/A	N/A	0.56	6.59E-15	-0.66	3.14E-18	N/A	FALSE
ENSG00000154813	DPH3	1	1	-0.77	hsa-let-7d-5p	0.71	8.52E-15	-0.87	3.17E-21	N/A	FALSE
ENSG00000170185	USP38	1	2	-0.49	hsa-let-7g-5p	0.49	1.61E-14	-0.79	1.76E-34	N/A	FALSE
ENSG00000204304	PBX2	1	2	-0.54	hsa-let-7d-5p	0.63	1.86E-14	-0.68	2.22E-16	N/A	FALSE
ENSG00000113657	DPYSL3	1	1	-0.25	hsa-let-7d-5p	0.82	2.70E-14	-0.50	4.10E-06	N/A	FALSE
ENSG00000248905	FMN1	4	3	N/A	N/A	1.64	3.88E-14	-1.13	4.21E-07	N/A	FALSE
ENSG00000175727	MLXIP	0	4	-0.17	hsa-let-7f-5p	0.49	4.70E-14	-0.45	4.83E-12	N/A	FALSE
ENSG00000092531	SNAP23	0	2	-0.38	hsa-let-7d-5p	0.50	5.02E-14	-0.71	1.13E-26	N/A	FALSE
ENSG00000166349	RAG1	0	1	-0.25	hsa-let-7a-5p	1.39	5.58E-14	-1.18	1.06E-06	N/A	FALSE
ENSG00000128487	SPECC1	1	2	N/A	N/A	0.67	5.60E-14	-0.83	5.52E-21	N/A	FALSE
ENSG00000040487	PQLC2	0	2	-0.68	hsa-let-7d-5p	0.62	8.89E-14	-0.35	5.82E-05	N/A	FALSE
ENSG00000196663	TECPR2	1	3	-0.37	hsa-let-7d-5p	0.55	1.26E-13	-1.34	1.57E-68	N/A	FALSE
ENSG00000134986	NREP	3	1	N/A	N/A	1.22	1.33E-13	-0.69	4.01E-05	N/A	FALSE
ENSG00000168672	FAM84B	1	2	-0.23	hsa-let-7g-5p	1.40	1.63E-13	-0.95	5.57E-07	N/A	FALSE
ENSG00000163900	TMEM41A	0	1	-0.41	hsa-let-7d-5p	0.71	2.19E-13	-0.77	4.47E-15	N/A	FALSE
ENSG00000137075	RNF38	3	1	-0.26	hsa-let-7g-5p	0.51	2.27E-13	-0.19	1.08E-02	N/A	FALSE
ENSG00000176697	BDNF	2	1	N/A	N/A	1.02	3.49E-13	-0.99	2.04E-12	N/A	FALSE
ENSG00000174600	CMKLR1	1	1	N/A	N/A	1.82	3.53E-13	-2.34	3.18E-18	N/A	FALSE
ENSG00000083454	P2RX5	0	1	N/A	N/A	1.25	4.71E-13	-1.19	1.01E-08	N/A	FALSE
ENSG00000095539	SEMA4G	0	1	-0.22	hsa-let-7d-5p	0.89	6.33E-13	-2.06	1.18E-33	N/A	FALSE
ENSG00000126768	TIMM17B	0	1	-0.36	hsa-let-7f-5p	0.56	7.17E-13	-1.19	1.22E-48	N/A	Ciliary-landscape_2016
ENSG00000072682	P4HA2	1	2	-0.49	hsa-let-7d-5p	0.63	1.02E-12	-0.87	9.87E-24	N/A	FALSE
ENSG00000138131	LOXL4	0	1	-0.29	hsa-let-7a-5p	3.40	1.19E-12	-2.14	4.59E-02	N/A	FALSE
ENSG00000169857	AVEN	0	1	N/A	N/A	0.59	3.53E-12	-1.49	2.91E-59	N/A	FALSE
ENSG00000111642	CHD4	0	1	-0.28	hsa-let-7a-5p	0.54	3.84E-12	-0.92	1.85E-34	N/A	SYSCILIA_potential
ENSG00000120868	APAF1	0	1	N/A	N/A	0.63	4.01E-12	-0.43	4.17E-06	N/A	FALSE
ENSG00000185127	C6orf120	3	1	N/A	N/A	0.58	5.04E-12	-0.32	1.57E-04	N/A	FALSE
ENSG00000120925	RNF170	1	2	-0.52	hsa-let-7d-5p	0.68	5.88E-12	-0.39	1.06E-04	N/A	FALSE
ENSG00000132000	PODNL1	0	1	N/A	N/A	1.28	6.22E-12	-3.55	1.03E-57	N/A	FALSE
ENSG00000142623	PADI1	0	1	N/A	N/A	1.16	7.32E-12	-1.05	1.09E-08	N/A	FALSE
ENSG00000047230	CTPS2	1	1	N/A	N/A	0.54	7.86E-12	-0.71	1.75E-18	N/A	FALSE
ENSG00000170153	RNF150	5	5	N/A	N/A	0.92	8.30E-12	-0.57	8.04E-05	N/A	FALSE
ENSG00000148154	UGCG	2	2	-0.48	hsa-let-7d-5p	0.99	1.24E-11	-1.07	1.28E-13	N/A	FALSE
ENSG00000150593	PDCD4	0	2	N/A	N/A	0.52	1.26E-11	-0.25	1.82E-03	N/A	FALSE
ENSG00000171302	**CANT1**	**0**	**1**	**-0.41**	**hsa-let-7b-5p**	**0.46**	**2.05E-11**	**-1.32**	**5.52E-82**	**N/A**	**FALSE**
ENSG00000196182	STK40	1	2	-0.37	hsa-let-7d-5p	0.48	2.10E-11	-0.41	2.18E-08	N/A	FALSE
ENSG00000073969	NSF	1	1	N/A	N/A	0.54	4.05E-11	-0.22	8.68E-03	N/A	Ciliary-landscape_2016
ENSG00000171877	FRMD5	2	1	-0.33	hsa-let-7d-5p	0.50	4.41E-11	-0.52	5.39E-12	N/A	FALSE
ENSG00000134259	NGF	0	1	-0.79	hsa-let-7d-5p	0.66	5.13E-11	-0.79	7.39E-15	N/A	FALSE
ENSG00000087095	NLK	1	2	-0.29	hsa-miR-98-5p	0.45	5.14E-11	-0.40	8.16E-09	N/A	FALSE
ENSG00000170442	KRT86	1	1	N/A	N/A	1.14	6.75E-11	-1.61	1.27E-11	N/A	FALSE
ENSG00000026103	FAS	0	2	-0.58	hsa-let-7d-5p	0.69	8.04E-11	-0.75	1.39E-12	N/A	FALSE
ENSG00000168872	DDX19A	0	1	-0.77	hsa-let-7g-5p	0.46	8.61E-11	-0.22	2.87E-03	N/A	FALSE
ENSG00000117500	TMED5	1	1	-0.39	hsa-let-7f-5p	0.45	8.89E-11	-0.37	7.48E-08	N/A	FALSE
ENSG00000117335	CD46	5	1	N/A	N/A	0.49	9.51E-11	-0.21	6.27E-03	N/A	FALSE
ENSG00000164976	KIAA1161	0	2	-0.24	hsa-let-7f-5p	1.33	1.19E-10	-1.65	1.67E-14	N/A	FALSE
ENSG00000127452	FBXL12	0	1	N/A	N/A	0.61	1.21E-10	-0.41	2.59E-05	N/A	FALSE
ENSG00000213190	MLLT11	0	1	N/A	N/A	0.77	1.33E-10	-0.34	5.89E-03	N/A	FALSE
ENSG00000224531	SMIM13	2	1	-0.26	hsa-let-7d-5p	0.52	1.93E-10	-0.62	6.33E-14	N/A	FALSE
ENSG00000153317	ASAP1	2	1	-0.34	hsa-let-7d-5p	0.54	2.73E-10	-0.72	5.78E-18	N/A	SYSCILIA_2019
ENSG00000181026	AEN	0	2	-0.59	hsa-let-7g-5p	0.57	2.95E-10	-0.24	1.17E-02	N/A	FALSE
ENSG00000123572	NRK	2	2	-0.39	hsa-let-7d-5p	1.24	3.12E-10	-1.44	5.04E-12	N/A	FALSE

Ensembl ID	Gene Name	Number of *-3p* Sites	Number of *-5p* Sites	TargetScan TCS	Preferred *let-7*	L2FC (IC)	FDR (IC)	L2FC (MC)	FDR (MC)	Negative Regulator Reference (PMID)	Ciliary Gene
ENSG00000221866	PLXNA4	3	3	-0.32	hsa-let-7d-5p	0.58	3.81E-10	-1.82	1.23E-85	N/A	FALSE
ENSG00000092841	MYL6	1	2	N/A	N/A	0.55	5.45E-10	-0.24	7.89E-03	N/A	Ciliary-landscape_2016
ENSG00000144655	CSRNP1	0	1	N/A	N/A	0.87	5.63E-10	-0.49	4.86E-04	N/A	FALSE
ENSG00000107719	PALD1	0	1	-0.42	hsa-let-7d-5p	0.94	5.89E-10	-0.80	3.03E-06	N/A	Ciliary-landscape_2016
ENSG00000163904	SENP2	0	2	-0.65	hsa-let-7d-5p	0.45	5.94E-10	-0.84	1.90E-31	N/A	FALSE
ENSG00000156017	C9orf41	0	1	-0.32	hsa-let-7f-5p	0.62	6.13E-10	-0.43	2.65E-05	N/A	FALSE
ENSG00000198959	TGM2	1	1	N/A	N/A	0.69	7.36E-10	-1.03	3.69E-21	N/A	FALSE
ENSG00000151414	NEK7	2	1	N/A	N/A	0.43	9.95E-10	-0.67	2.19E-22	N/A	Ciliary-landscape_2016
ENSG00000222047	C10orf55	1	1	N/A	N/A	1.13	1.19E-09	-0.72	6.34E-04	N/A	FALSE
ENSG00000114529	C3orf52	1	1	-0.33	hsa-let-7c-5p	0.60	1.63E-09	-0.29	5.00E-03	N/A	FALSE
ENSG00000135535	CD164	1	2	N/A	N/A	0.47	2.15E-09	-0.84	2.95E-28	N/A	FALSE
ENSG00000076685	NT5C2	5	1	N/A	N/A	0.51	2.69E-09	-0.40	1.58E-06	N/A	SYSCILIA_potential
ENSG00000108679	LGALS3BP	0	1	N/A	N/A	0.55	3.05E-09	-0.24	1.24E-02	N/A	FALSE
ENSG00000174437	ATP2A2	1	1	-0.34	hsa-let-7d-5p	0.42	3.28E-09	-0.34	5.82E-07	N/A	FALSE
ENSG00000171992	SYNPO	3	2	N/A	N/A	0.88	3.46E-09	-0.69	3.29E-06	N/A	FALSE
ENSG00000131236	CAP1	0	1	N/A	N/A	0.46	3.53E-09	-1.29	5.86E-66	N/A	FALSE
ENSG00000103066	**PLA2G15**	**0**	**1**	**-0.26**	**hsa-let-7b-5p**	**0.64**	**6.15E-09**	**-1.63**	**1.46E-49**	**N/A**	**FALSE**
ENSG00000174021	GNG5	0	1	-0.63	hsa-let-7a-5p	0.42	7.40E-09	-1.55	3.18E-104	N/A	FALSE
ENSG00000133997	MED6	2	1	-0.35	hsa-let-7d-5p	0.63	8.62E-09	-0.54	2.84E-06	N/A	FALSE
ENSG00000184988	TMEM106A	0	1	N/A	N/A	0.64	1.04E-08	-1.50	1.27E-32	N/A	FALSE
ENSG00000181027	FKRP	1	1	-0.27	hsa-let-7d-5p	0.58	1.13E-08	-0.92	9.39E-20	N/A	FALSE
ENSG00000087152	ATXN7L3	0	1	-0.23	hsa-let-7d-5p	0.36	1.21E-08	-0.14	3.24E-02	N/A	FALSE
ENSG00000110881	ASIC1	2	1	N/A	N/A	0.46	1.25E-08	-1.01	4.69E-38	N/A	FALSE
ENSG00000221988	PPT2	0	1	N/A	N/A	0.50	1.34E-08	-0.74	1.75E-15	N/A	FALSE
ENSG00000152683	SLC30A6	0	1	-0.4	hsa-let-7d-5p	0.46	1.61E-08	-0.35	1.98E-05	N/A	FALSE
ENSG00000168758	SEMA4C	0	1	-0.35	hsa-let-7d-5p	0.45	1.71E-08	-0.25	1.64E-03	N/A	FALSE
ENSG00000101367	MAPRE1	0	1	N/A	N/A	0.36	1.87E-08	-0.64	8.81E-25	N/A	SYSCILIA_2019
ENSG00000123684	LPGAT1	0	4	-0.88	hsa-let-7g-5p	0.38	2.27E-08	-0.41	4.38E-10	N/A	FALSE
ENSG00000156990	RPUSD3	0	2	N/A	N/A	0.53	2.50E-08	-0.77	4.76E-16	N/A	FALSE
ENSG00000254986	DPP3	0	1	-0.48	hsa-let-7d-5p	0.61	3.43E-08	-0.75	4.45E-12	N/A	FALSE
ENSG00000153310	FAM49B	1	1	N/A	N/A	0.42	4.00E-08	-0.41	5.81E-08	N/A	FALSE
ENSG00000175697	GPR156	1	1	-0.3	hsa-let-7g-5p	1.08	5.94E-08	-0.60	1.72E-02	N/A	FALSE
ENSG00000135083	CCNJL	0	1	-0.31	hsa-let-7d-5p	0.57	7.15E-08	-0.30	6.17E-03	N/A	FALSE
ENSG00000130202	PVRL2	0	1	N/A	N/A	0.39	7.15E-08	-0.70	2.20E-23	N/A	FALSE
ENSG00000188112	C6orf132	3	1	N/A	N/A	0.48	7.17E-08	-0.52	5.85E-09	N/A	FALSE
ENSG00000049239	H6PD	0	2	N/A	N/A	0.45	7.22E-08	-0.31	1.79E-04	N/A	FALSE
ENSG00000164100	NDST3	2	2	N/A	N/A	0.81	7.45E-08	-1.31	7.44E-16	N/A	FALSE
ENSG00000128606	LRRC17	1	1	N/A	N/A	0.66	7.84E-08	-1.44	4.28E-34	N/A	FALSE
ENSG00000112186	CAP2	0	1	N/A	N/A	0.53	9.17E-08	-0.99	2.31E-25	N/A	FALSE
ENSG00000105556	MIER2	0	1	N/A	N/A	0.42	9.59E-08	-1.18	5.13E-50	N/A	FALSE
ENSG00000160208	RRP1B	0	1	-0.23	hsa-let-7d-5p	0.35	1.01E-07	-0.46	5.48E-13	N/A	FALSE
ENSG00000196839	ADA	0	1	N/A	N/A	0.83	1.15E-07	-1.22	3.97E-15	N/A	FALSE
ENSG00000100364	KIAA0930	0	2	-0.36	hsa-let-7d-5p	0.34	1.22E-07	-0.42	3.49E-11	N/A	Ciliary-landscape_2016
ENSG00000142252	GEMIN7	0	1	-0.71	hsa-let-7d-5p	0.64	1.34E-07	-0.57	5.06E-06	N/A	FALSE
ENSG00000100599	RIN3	0	1	N/A	N/A	0.53	1.53E-07	-0.32	2.90E-03	N/A	FALSE
ENSG00000140950	TLDC1	2	2	N/A	N/A	0.51	1.57E-07	-0.80	3.54E-17	N/A	FALSE
ENSG00000099804	CDC34	0	2	-0.92	hsa-let-7d-5p	0.43	1.79E-07	-1.34	2.21E-61	N/A	FALSE
ENSG00000119231	SENP5	0	1	-0.28	hsa-let-7d-5p	0.39	1.90E-07	-0.45	5.92E-10	N/A	FALSE
ENSG00000148843	PDCD11	0	1	N/A	N/A	0.37	1.98E-07	-0.45	1.07E-10	N/A	FALSE
ENSG00000169047	IRS1	10	2	N/A	N/A	0.40	2.03E-07	-0.30	5.53E-05	N/A	FALSE
ENSG00000164054	SHISA5	1	1	N/A	N/A	0.38	2.08E-07	-1.21	7.35E-68	N/A	FALSE
ENSG00000174840	PDE12	5	2	-0.65	hsa-let-7a-5p	0.40	2.18E-07	-0.30	1.16E-04	N/A	FALSE
ENSG00000197183	C20orf112	1	1	-0.34	hsa-let-7d-5p	0.47	3.21E-07	-1.64	9.28E-71	N/A	FALSE
ENSG00000102158	MAGT1	4	1	N/A	N/A	0.34	3.33E-07	-1.08	2.54E-62	N/A	Ciliary-landscape_2016
ENSG00000046604	DSG2	3	1	N/A	N/A	0.46	3.52E-07	-0.90	3.78E-26	N/A	FALSE
ENSG00000105245	NUMBL	0	1	-0.22	hsa-let-7d-5p	0.36	4.37E-07	-0.59	1.53E-17	N/A	Ciliary-landscape_2016

Ensembl ID	Gene Name	Number of *-3p* Sites	Number of *-5p* Sites	TargetScan TCS	Preferred *let-7*	L2FC (IC)	FDR (IC)	L2FC (MC)	FDR (MC)	Negative Regulator Reference (PMID)	Ciliary Gene
ENSG00000072501	SMC1A	4	4	-0.7	hsa-let-7a-5p	0.51	5.11E-07	-0.76	8.98E-15	N/A	Ciliary-landscape_2016
ENSG00000102781	KATNAL1	7	2	-0.3	hsa-let-7d-5p	0.36	5.56E-07	-0.97	4.88E-44	N/A	FALSE
ENSG00000086544	ITPKC	0	2	N/A	N/A	0.38	6.75E-07	-1.05	1.27E-42	N/A	FALSE
ENSG00000114026	OGG1	0	1	N/A	N/A	0.42	7.04E-07	-0.55	1.55E-10	N/A	FALSE
ENSG00000160325	CACFD1	1	1	-0.3	hsa-let-7a-5p	0.55	8.13E-07	-0.84	2.62E-13	N/A	FALSE
ENSG00000164023	SGMS2	0	2	N/A	N/A	0.56	9.23E-07	-0.35	1.64E-03	N/A	FALSE
ENSG00000155034	FBXL18	1	1	N/A	N/A	0.36	1.26E-06	-0.26	5.37E-04	N/A	FALSE
ENSG00000108433	GOSR2	0	1	N/A	N/A	0.44	1.36E-06	-0.33	2.73E-04	N/A	SYSCILIA_potential
ENSG00000122482	ZNF644	1	2	-0.48	hsa-let-7d-5p	0.35	1.82E-06	-0.17	2.07E-02	N/A	FALSE
ENSG00000131446	MGAT1	0	1	N/A	N/A	0.34	2.30E-06	-0.70	4.81E-25	N/A	FALSE
ENSG00000097033	SH3GLB1	4	2	N/A	N/A	0.33	2.34E-06	-0.26	8.21E-05	N/A	Ciliary-landscape_2016
ENSG00000132017	**DCAF15**	**0**	**1**	**-0.37**	**hsa-let-7b-5p**	**0.40**	**2.93E-06**	**-1.01**	**4.67E-33**	**N/A**	**FALSE**
ENSG00000115486	GGCX	0	3	N/A	N/A	0.34	3.14E-06	-0.32	5.73E-06	N/A	FALSE
ENSG00000155016	CYP2U1	3	1	N/A	N/A	0.37	3.45E-06	-0.68	9.62E-19	N/A	FALSE
ENSG00000115318	LOXL3	0	2	N/A	N/A	0.66	3.64E-06	-1.27	6.20E-17	N/A	FALSE
ENSG00000087303	NID2	0	2	-0.36	hsa-let-7d-5p	0.66	3.90E-06	-1.30	1.73E-21	N/A	FALSE
ENSG00000167595	C19orf55	0	1	N/A	N/A	0.54	4.05E-06	-0.38	1.39E-03	N/A	FALSE
ENSG00000163214	DHX57	2	1	-0.37	hsa-let-7i-5p	0.36	4.47E-06	-0.47	1.24E-09	N/A	FALSE
ENSG00000123191	ATP7B	0	1	N/A	N/A	0.52	4.68E-06	-1.10	3.23E-21	N/A	FALSE
ENSG00000146828	SLC12A9	0	1	-0.37	hsa-let-7d-5p	0.41	5.18E-06	-0.41	2.16E-06	N/A	FALSE
ENSG00000244242	IFITM10	0	1	N/A	N/A	0.54	5.58E-06	-1.61	1.64E-41	N/A	FALSE
ENSG00000120913	PDLIM2	0	1	N/A	N/A	0.47	6.58E-06	-0.61	1.30E-09	N/A	FALSE
ENSG00000180914	OXTR	1	1	N/A	N/A	1.12	7.82E-06	-2.00	2.78E-16	N/A	FALSE
ENSG00000087266	SH3BP2	2	3	N/A	N/A	0.34	8.26E-06	-0.83	1.75E-29	N/A	FALSE
ENSG00000187867	**PALM3**	**0**	**1**	**-0.33**	**hsa-let-7b-5p**	**1.67**	**8.31E-06**	**-1.46**	**8.45E-03**	**N/A**	**FALSE**
ENSG00000106636	YKT6	0	1	N/A	N/A	0.38	8.46E-06	-0.39	1.89E-06	N/A	FALSE
ENSG00000127946	HIP1	1	1	-0.28	hsa-let-7d-5p	0.48	8.51E-06	-1.20	2.48E-31	N/A	FALSE
ENSG00000158769	F11R	0	1	N/A	N/A	0.45	8.83E-06	-0.23	2.66E-02	N/A	FALSE
ENSG00000177374	HIC1	1	1	-0.24	hsa-let-7i-5p	0.56	1.03E-05	-0.86	3.37E-11	N/A	FALSE
ENSG00000068383	INPP5A	1	1	-0.28	hsa-let-7d-5p	0.63	1.05E-05	-0.49	5.40E-04	N/A	Katsanis_2006
ENSG00000167889	MGAT5B	0	1	N/A	N/A	0.60	1.09E-05	-1.18	3.82E-19	N/A	FALSE
ENSG00000171365	CLCN5	1	8	-0.87	hsa-let-7d-5p	0.54	1.09E-05	-0.73	2.34E-09	N/A	FALSE
ENSG00000101856	PGRMC1	0	2	-0.73	hsa-let-7d-5p	0.36	1.19E-05	-1.90	5.03E-120	N/A	FALSE
ENSG00000142687	KIAA0319L	0	1	N/A	N/A	0.31	1.30E-05	-0.42	2.48E-10	N/A	FALSE
ENSG00000164045	CDC25A	0	3	-0.59	hsa-let-7d-5p	0.77	1.33E-05	-1.09	1.07E-09	N/A	FALSE
ENSG00000143816	WNT9A	2	1	-0.45	hsa-let-7d-5p	0.74	1.39E-05	-1.15	2.03E-11	N/A	FALSE
ENSG00000175376	EIF1AD	4	1	N/A	N/A	0.37	1.41E-05	-0.68	9.24E-17	N/A	FALSE
ENSG00000108039	XPNPEP1	0	1	N/A	N/A	0.36	1.51E-05	-0.71	7.18E-20	N/A	FALSE
ENSG00000108582	CPD	4	1	-0.29	hsa-let-7i-5p	0.43	1.54E-05	-0.38	5.65E-05	N/A	SYSCILIA_potential
ENSG00000102034	ELF4	0	1	-0.33	hsa-let-7a-5p	0.46	1.68E-05	-1.85	5.59E-72	N/A	FALSE
ENSG00000137710	RDX	3	1	-0.53	hsa-let-7d-5p	0.32	1.76E-05	-0.94	4.83E-40	N/A	FALSE
ENSG00000163359	COL6A3	0	1	N/A	N/A	0.82	1.79E-05	-1.78	1.18E-18	N/A	FALSE
ENSG00000111711	GOLT1B	1	2	-0.59	hsa-let-7d-5p	0.41	1.92E-05	-1.08	1.25E-32	N/A	FALSE
ENSG00000153404	PLEKHG4B	0	2	N/A	N/A	0.94	2.13E-05	-1.48	3.90E-07	N/A	FALSE
ENSG00000128791	TWSG1	0	1	N/A	N/A	0.34	2.15E-05	-0.90	1.17E-32	N/A	FALSE
ENSG00000108829	LRRC59	0	1	-0.22	hsa-let-7d-5p	0.44	2.32E-05	-0.87	5.35E-19	N/A	SYSCILIA_potential
ENSG00000106460	TMEM106B	1	1	N/A	N/A	0.32	2.53E-05	-0.22	2.96E-03	N/A	FALSE
ENSG00000164086	DUSP7	1	1	-0.23	hsa-let-7d-5p	0.36	2.86E-05	-0.93	1.58E-29	N/A	FALSE
ENSG00000175130	MARCKSL1	0	1	N/A	N/A	0.42	2.94E-05	-0.49	2.64E-07	N/A	FALSE
ENSG00000104131	EIF3J	1	2	N/A	N/A	0.33	3.05E-05	-0.26	8.24E-04	N/A	FALSE
ENSG00000122863	CHST3	1	3	-0.27	hsa-let-7d-5p	0.68	3.08E-05	-1.05	1.17E-11	N/A	Ciliary-landscape_2016
ENSG00000131791	PRKAB2	2	2	-0.25	hsa-let-7a-5p	0.33	3.08E-05	-0.55	9.82E-13	N/A	FALSE
ENSG00000106829	TLE4	3	1	N/A	N/A	0.28	3.10E-05	-0.29	1.02E-05	N/A	FALSE
ENSG00000167977	KCTD5	1	1	N/A	N/A	0.31	3.13E-05	-1.00	8.91E-43	N/A	Ciliary-landscape_2016
ENSG00000138193	PLCE1	3	1	N/A	N/A	0.31	3.21E-05	-1.32	7.78E-77	N/A	SYSCILIA_potential
ENSG00000164933	SLC25A32	0	1	-0.33	hsa-miR-98-5p	0.36	3.23E-05	-0.73	1.12E-18	N/A	FALSE

Ensembl ID	Gene Name	Number of *-3p* Sites	Number of *-5p* Sites	TargetScan TCS	Preferred *let-7*	L2FC (IC)	FDR (IC)	L2FC (MC)	FDR (MC)	Negative Regulator Reference (PMID)	Ciliary Gene
ENSG00000090971	NAT14	0	2	N/A	N/A	0.38	3.25E-05	-0.90	5.05E-25	N/A	Ciliary-landscape_2016
ENSG00000166171	DPCD	0	1	N/A	N/A	0.39	3.33E-05	-0.74	8.14E-16	N/A	SYSCILIA_2019
ENSG00000147533	GOLGA7	2	1	-0.34	hsa-let-7d-5p	0.32	3.35E-05	-0.35	2.33E-06	N/A	FALSE
ENSG00000149313	AASDHPPT	2	2	N/A	N/A	0.33	3.57E-05	-0.96	3.03E-36	N/A	FALSE
ENSG00000164924	YWHAZ	2	1	N/A	N/A	0.31	3.92E-05	-0.82	9.54E-33	N/A	FALSE
ENSG00000010270	STARD3NL	0	1	-0.35	hsa-let-7d-5p	0.32	4.28E-05	-1.09	6.61E-50	N/A	FALSE
ENSG00000115540	MOB4	7	1	-0.33	hsa-let-7a-5p	0.34	4.43E-05	-0.40	9.86E-07	N/A	FALSE
ENSG00000198108	CHSY3	0	1	-0.27	hsa-let-7d-5p	0.78	4.49E-05	-1.45	3.29E-13	N/A	FALSE
ENSG00000165915	SLC39A13	1	2	N/A	N/A	0.29	4.50E-05	-0.16	2.81E-02	N/A	FALSE
ENSG00000136869	TLR4	3	2	N/A	N/A	0.57	4.69E-05	-0.52	1.23E-04	N/A	FALSE
ENSG00000205213	LGR4	3	1	-0.49	hsa-let-7f-5p	0.28	4.75E-05	-0.48	2.37E-13	N/A	FALSE
ENSG00000006695	COX10	0	2	N/A	N/A	0.47	4.87E-05	-0.53	3.48E-06	N/A	FALSE
ENSG00000095139	ARCN1	1	1	N/A	N/A	0.36	4.92E-05	-1.18	5.21E-45	N/A	FALSE
ENSG00000198862	LTN1	1	1	-0.27	hsa-let-7d-5p	0.32	5.40E-05	-0.63	4.08E-17	N/A	FALSE
ENSG00000091527	CDV3	0	1	-0.46	hsa-let-7d-5p	0.31	5.80E-05	-0.59	4.45E-16	N/A	FALSE
ENSG00000172113	NME6	0	1	-0.45	hsa-let-7f-5p	0.40	6.38E-05	-0.59	3.34E-09	N/A	FALSE
ENSG00000177119	ANO6	0	3	N/A	N/A	0.40	6.54E-05	-1.32	1.73E-44	N/A	FALSE
ENSG00000141699	FAM134C	0	1	N/A	N/A	0.29	6.95E-05	-0.40	5.27E-09	N/A	FALSE
ENSG00000204682	CASC10	0	2	N/A	N/A	0.64	7.19E-05	-0.67	1.20E-04	N/A	FALSE
ENSG00000137809	ITGA11	0	1	N/A	N/A	0.94	7.39E-05	-1.21	9.76E-08	N/A	FALSE
ENSG00000105229	PIAS4	1	2	-0.24	hsa-let-7a-5p	0.32	7.77E-05	-0.31	6.47E-05	N/A	FALSE
ENSG00000138316	ADAMTS14	0	2	-0.25	hsa-let-7d-5p	1.09	7.82E-05	-1.35	3.47E-07	N/A	FALSE
ENSG00000173166	RAPH1	6	2	N/A	N/A	0.47	8.20E-05	-0.54	1.71E-06	N/A	FALSE
ENSG00000128590	DNAJB9	1	1	-0.3	hsa-let-7d-5p	0.35	8.46E-05	-0.40	3.57E-06	N/A	FALSE
ENSG00000162104	ADCY9	1	3	-0.18	hsa-let-7d-5p	0.31	8.53E-05	-0.62	1.98E-16	N/A	FALSE
ENSG00000140406	MESDC1	0	1	-0.32	hsa-let-7d-5p	0.39	8.64E-05	-1.09	1.03E-29	N/A	FALSE
ENSG00000133056	PIK3C2B	0	1	N/A	N/A	0.67	8.95E-05	-0.51	3.14E-03	N/A	FALSE
ENSG00000111319	SCNN1A	0	1	N/A	N/A	0.77	9.32E-05	-1.24	1.08E-07	N/A	FALSE
ENSG00000087502	ERGIC2	0	1	-0.36	hsa-let-7g-5p	0.40	9.66E-05	-1.27	2.37E-40	N/A	FALSE
ENSG00000242265	PEG10	2	3	-0.36	hsa-let-7d-5p	0.78	9.68E-05	-1.28	1.33E-11	N/A	FALSE
ENSG00000172687	ZNF738	4	3	N/A	N/A	0.59	1.00E-04	-0.65	6.46E-05	N/A	FALSE
ENSG00000162980	ARL5A	7	2	-0.32	hsa-let-7d-5p	0.29	1.01E-04	-0.91	2.54E-38	N/A	FALSE
ENSG00000128595	CALU	1	1	-0.31	hsa-let-7d-5p	0.41	1.03E-04	-0.85	1.99E-18	N/A	FALSE
ENSG00000133740	E2F5	1	1	-0.47	hsa-let-7a-5p	0.49	1.06E-04	-1.28	2.77E-26	N/A	FALSE
ENSG00000124762	CDKN1A	0	1	-0.46	hsa-let-7d-5p	0.41	1.07E-04	-0.50	5.69E-07	N/A	FALSE
ENSG00000143324	XPR1	3	2	N/A	N/A	0.29	1.08E-04	-0.68	3.98E-22	N/A	FALSE
ENSG00000153006	SREK1IP1	3	3	-0.78	hsa-let-7d-5p	0.36	1.14E-04	-0.74	1.48E-16	N/A	FALSE
ENSG00000006831	ADIPOR2	1	2	-0.32	hsa-let-7d-5p	0.29	1.17E-04	-0.42	5.85E-09	N/A	FALSE
ENSG00000103202	NME4	0	1	-0.45	hsa-let-7d-5p	0.28	1.17E-04	-1.01	7.70E-49	N/A	FALSE
ENSG00000163171	CDC42EP3	2	1	N/A	N/A	0.44	1.20E-04	-0.49	6.09E-06	N/A	FALSE
ENSG00000181619	GPR135	1	2	N/A	N/A	0.56	1.20E-04	-0.70	2.58E-06	N/A	FALSE
ENSG00000126785	RHOJ	0	1	N/A	N/A	0.42	1.24E-04	-1.33	2.33E-38	N/A	FALSE
ENSG00000141179	PCTP	1	3	-0.55	hsa-let-7d-5p	0.52	1.24E-04	-0.37	7.08E-03	N/A	FALSE
ENSG00000134243	SORT1	2	2	N/A	N/A	0.37	1.26E-04	-0.64	2.11E-12	N/A	FALSE
ENSG00000123159	GIPC1	0	2	-0.49	hsa-let-7d-5p	0.29	1.27E-04	-1.03	3.62E-47	N/A	FALSE
ENSG00000152767	FARP1	1	2	-0.28	hsa-let-7d-5p	0.30	1.30E-04	-0.60	1.62E-16	N/A	FALSE
ENSG00000166471	TMEM41B	1	1	N/A	N/A	0.35	1.39E-04	-0.36	4.57E-05	N/A	Ciliary-landscape_2016
ENSG00000136014	USP44	3	5	-1.3	hsa-let-7d-5p	0.70	1.60E-04	-0.46	2.28E-02	N/A	FALSE
ENSG00000102100	SLC35A2	0	1	N/A	N/A	0.42	1.74E-04	-1.29	2.37E-33	N/A	FALSE
ENSG00000183762	KREMEN1	1	2	-0.37	hsa-let-7i-5p	0.70	1.97E-04	-0.83	2.83E-05	N/A	FALSE
ENSG00000196814	MVB12B	3	2	-0.19	hsa-let-7d-5p	0.39	2.00E-04	-0.33	1.76E-03	N/A	FALSE
ENSG00000128829	EIF2AK4	0	1	N/A	N/A	0.28	2.00E-04	-0.52	3.31E-13	N/A	FALSE
ENSG00000002834	LASP1	1	2	N/A	N/A	0.29	2.13E-04	-0.46	1.50E-10	N/A	FALSE
ENSG00000131069	ACSS2	0	1	N/A	N/A	0.28	2.22E-04	-0.43	9.27E-10	N/A	FALSE
ENSG00000106948	AKNA	3	3	N/A	N/A	0.39	2.30E-04	-0.75	1.60E-13	N/A	Katsanis_2006
ENSG00000107021	TBC1D13	0	1	N/A	N/A	0.31	2.31E-04	-0.26	1.52E-03	N/A	FALSE

Ensembl ID	Gene Name	Number of *-3p* Sites	Number of *-5p* Sites	TargetScan TCS	Preferred *let-7*	L2FC (IC)	FDR (IC)	L2FC (MC)	FDR (MC)	Negative Regulator Reference (PMID)	Ciliary Gene
ENSG00000167695	FAM57A	0	1	N/A	N/A	0.34	2.75E-04	-0.96	3.66E-26	N/A	FALSE
ENSG00000077585	GPR137B	2	1	N/A	N/A	0.37	2.77E-04	-0.57	3.11E-09	N/A	FALSE
ENSG00000146476	C6orf211	0	1	-0.3	hsa-let-7a-5p	0.32	3.16E-04	-0.60	3.56E-13	N/A	FALSE
ENSG00000176986	SEC24C	1	1	N/A	N/A	0.28	3.37E-04	-0.35	1.59E-06	N/A	FALSE
ENSG00000125970	RALY	0	1	N/A	N/A	0.25	3.47E-04	-0.84	3.16E-40	N/A	FALSE
ENSG00000205726	ITSN1	6	2	-0.27	hsa-let-7d-5p	0.28	3.61E-04	-0.19	1.30E-02	N/A	FALSE
ENSG00000176771	NCKAP5	1	1	N/A	N/A	0.69	3.92E-04	-1.55	4.69E-16	N/A	FALSE
ENSG00000146555	SDK1	1	2	-0.21	hsa-let-7f-5p	1.07	3.95E-04	-1.50	3.04E-04	N/A	FALSE
ENSG00000156709	AIFM1	0	2	-0.77	hsa-let-7d-5p	0.27	4.23E-04	-0.25	8.74E-04	N/A	FALSE
ENSG00000115419	GLS	5	2	N/A	N/A	0.38	4.24E-04	-0.23	2.66E-02	N/A	FALSE
ENSG00000104081	BMF	1	2	N/A	N/A	0.68	4.32E-04	-0.45	1.39E-02	N/A	FALSE
ENSG00000160688	FLAD1	0	1	N/A	N/A	0.33	4.66E-04	-0.46	2.77E-07	N/A	FALSE
ENSG00000103591	AAGAB	0	1	N/A	N/A	0.28	4.71E-04	-0.38	4.64E-07	N/A	FALSE
ENSG00000138448	ITGAV	6	2	N/A	N/A	0.30	5.14E-04	-0.71	1.62E-19	N/A	FALSE
ENSG00000102898	NUTF2	0	1	N/A	N/A	0.26	5.18E-04	-0.66	3.43E-21	N/A	SYSCILIA_potential
ENSG00000166145	SPINT1	0	2	N/A	N/A	1.86	5.36E-04	-2.64	2.17E-03	N/A	FALSE
ENSG00000141542	RAB40B	1	1	N/A	N/A	0.40	5.49E-04	-0.68	2.54E-09	N/A	FALSE
ENSG00000109066	TMEM104	0	1	N/A	N/A	0.38	5.71E-04	-0.55	1.36E-07	N/A	FALSE
ENSG00000172731	LRRC20	0	3	-0.27	hsa-let-7a-5p	0.33	5.82E-04	-0.90	2.15E-23	N/A	SYSCILIA_potential
ENSG00000225830	ERCC6	0	1	-0.38	hsa-let-7d-5p	0.47	6.59E-04	-0.42	1.37E-03	N/A	FALSE
ENSG00000185551	NR2F2	4	1	N/A	N/A	0.52	6.98E-04	-1.25	3.99E-19	N/A	FALSE
ENSG00000172936	MYD88	0	2	N/A	N/A	0.46	7.75E-04	-0.62	4.58E-06	N/A	FALSE
ENSG00000063601	MTMR1	1	1	N/A	N/A	0.25	8.28E-04	-0.52	8.49E-14	N/A	FALSE
ENSG00000196230	TUBB	1	1	N/A	N/A	0.30	8.39E-04	-1.38	3.56E-64	N/A	Katsanis_2006
ENSG00000137073	UBAP2	0	1	N/A	N/A	0.25	8.87E-04	-0.63	1.69E-19	N/A	FALSE
ENSG00000170266	GLB1	0	1	N/A	N/A	0.44	8.88E-04	-1.80	5.55E-48	N/A	Ciliary-landscape_2016
ENSG00000139977	NAA30	4	5	-0.77	hsa-let-7d-5p	0.23	9.09E-04	-0.34	2.06E-07	N/A	FALSE
ENSG00000049449	RCN1	1	1	-0.34	hsa-let-7d-5p	0.28	9.41E-04	-0.36	5.89E-06	N/A	FALSE
ENSG00000106692	FKTN	1	4	N/A	N/A	0.32	9.84E-04	-0.68	5.08E-14	N/A	FALSE
ENSG00000143845	ETNK2	0	1	-0.27	hsa-let-7d-5p	0.57	1.16E-03	-0.86	1.66E-05	N/A	FALSE
ENSG00000138768	USO1	0	2	N/A	N/A	0.26	1.17E-03	-1.12	1.23E-53	N/A	FALSE
ENSG00000044574	HSPA5	0	1	N/A	N/A	0.40	1.26E-03	-0.74	5.10E-11	N/A	SYSCILIA_potential
ENSG00000180182	MED14	5	1	N/A	N/A	0.26	1.26E-03	-0.72	2.83E-22	N/A	FALSE
ENSG00000115084	SLC35F5	2	2	N/A	N/A	0.32	1.33E-03	-0.66	3.95E-13	N/A	FALSE
ENSG00000148358	GPR107	0	2	N/A	N/A	0.27	1.34E-03	-0.28	4.20E-04	N/A	FALSE
ENSG00000159479	MED8	0	1	-0.65	hsa-let-7d-5p	0.33	1.47E-03	-0.92	1.94E-21	N/A	FALSE
ENSG00000130311	DDA1	0	3	N/A	N/A	0.26	1.48E-03	-0.58	5.21E-14	N/A	FALSE
ENSG00000144231	**POLR2D**	**0**	**1**	**-0.5**	**hsa-let-7b-5p**	**0.27**	**1.59E-03**	**-0.70**	**2.32E-18**	**N/A**	**FALSE**
ENSG00000182389	CACNB4	2	1	-0.27	hsa-let-7a-5p	0.35	1.59E-03	-0.42	9.39E-05	N/A	FALSE
ENSG00000104067	TJP1	3	1	N/A	N/A	0.25	1.63E-03	-0.32	1.18E-05	N/A	FALSE
ENSG00000147065	**MSN**	**0**	**1**	**-0.23**	**hsa-let-7b-5p**	**0.27**	**1.64E-03**	**-0.62**	**3.10E-15**	**N/A**	**FALSE**
ENSG00000131941	RHPN2	1	1	N/A	N/A	0.34	1.69E-03	-0.79	1.73E-13	N/A	FALSE
ENSG00000182197	EXT1	3	2	N/A	N/A	0.32	1.83E-03	-0.51	8.99E-08	N/A	Katsanis_2006
ENSG00000196591	HDAC2	7	1	N/A	N/A	0.23	1.86E-03	-0.59	4.18E-19	N/A	Ciliary-landscape_2016
ENSG00000168005	C11orf84	1	3	-0.3	hsa-let-7g-5p	0.26	1.97E-03	-1.61	6.44E-89	N/A	FALSE
ENSG00000121578	B4GALT4	1	2	N/A	N/A	0.27	2.00E-03	-0.68	3.15E-17	N/A	FALSE
ENSG00000059804	SLC2A3	0	1	N/A	N/A	0.37	2.03E-03	-0.72	9.31E-11	N/A	FALSE
ENSG00000164970	FAM219A	3	4	N/A	N/A	0.23	2.10E-03	-0.64	7.07E-21	N/A	FALSE
ENSG00000005238	FAM214B	0	1	-0.45	hsa-let-7d-5p	0.26	2.18E-03	-0.86	3.69E-28	N/A	FALSE
ENSG00000137076	TLN1	0	1	N/A	N/A	0.24	2.27E-03	-0.70	1.34E-22	N/A	FALSE
ENSG00000198933	TBKBP1	0	2	-0.44	hsa-let-7d-5p	0.30	2.34E-03	-0.26	6.70E-03	N/A	Ciliary-landscape_2016
ENSG00000156966	B3GNT7	0	2	-0.32	hsa-let-7d-5p	0.62	2.42E-03	-0.73	5.01E-04	N/A	FALSE
ENSG00000161558	TMEM143	0	1	-0.35	hsa-let-7a-5p	0.51	2.48E-03	-0.85	1.14E-07	N/A	FALSE
ENSG00000146267	FAXC	11	3	-0.26	hsa-let-7d-5p	0.49	2.50E-03	-0.62	1.14E-04	N/A	FALSE
ENSG00000074047	GLI2	2	1	N/A	N/A	0.39	2.52E-03	-0.76	8.73E-10	N/A	SYSCILIA_2019
ENSG00000082805	ERC1	0	3	N/A	N/A	0.27	2.55E-03	-0.48	4.96E-09	N/A	Ciliary-landscape_2016

Ensembl ID	Gene Name	Number of *-3p* Sites	Number of *-5p* Sites	TargetScan TCS	Preferred *let-7*	L2FC (IC)	FDR (IC)	L2FC (MC)	FDR (MC)	Negative Regulator Reference (PMID)	Ciliary Gene
ENSG00000112679	DUSP22	0	2	-0.44	hsa-let-7d-5p	0.37	2.89E-03	-0.45	1.00E-04	N/A	FALSE
ENSG00000145194	ECE2	0	1	N/A	N/A	0.51	3.00E-03	-0.55	2.32E-03	N/A	FALSE
ENSG00000137166	FOXP4	0	1	N/A	N/A	0.23	3.10E-03	-1.15	4.48E-60	N/A	FALSE
ENSG00000100379	KCTD17	0	1	-0.55	hsa-let-7d-5p	0.26	3.24E-03	-0.91	1.48E-28	N/A	FALSE
ENSG00000221914	PPP2R2A	1	1	-0.34	hsa-let-7a-5p	0.20	3.39E-03	-0.27	1.89E-05	N/A	FALSE
ENSG00000127463	EMC1	2	2	N/A	N/A	0.23	3.43E-03	-0.59	4.49E-16	N/A	FALSE
ENSG00000149541	B3GAT3	1	1	-0.32	hsa-let-7a-5p	0.28	3.76E-03	-0.70	1.85E-15	N/A	FALSE
ENSG00000123178	SPRYD7	0	2	N/A	N/A	0.31	4.05E-03	-0.84	2.23E-16	N/A	FALSE
ENSG00000171793	CTPS1	0	1	-0.28	hsa-let-7a-5p	0.33	4.31E-03	-0.28	1.03E-02	N/A	FALSE
ENSG00000136888	ATP6V1G1	1	1	N/A	N/A	0.28	4.47E-03	-0.49	4.66E-08	N/A	FALSE
ENSG00000145996	CDKAL1	1	1	N/A	N/A	0.29	4.53E-03	-0.98	3.12E-24	N/A	FALSE
ENSG00000138071	ACTR2	1	1	N/A	N/A	0.22	4.63E-03	-0.45	2.64E-10	N/A	FALSE
ENSG00000168924	LETM1	0	1	N/A	N/A	0.23	4.66E-03	-0.35	3.83E-06	N/A	FALSE
ENSG00000198925	ATG9A	0	1	N/A	N/A	0.20	4.69E-03	-0.31	1.58E-06	N/A	FALSE
ENSG00000132953	XPO4	2	1	N/A	N/A	0.31	4.70E-03	-0.75	1.11E-13	N/A	FALSE
ENSG00000204291	COL15A1	1	1	-0.3	hsa-let-7d-5p	1.44	4.88E-03	-1.41	3.76E-02	N/A	FALSE
ENSG00000116396	**KCNC4**	**0**	**1**	**-0.07**	**hsa-let-7b-5p**	**0.61**	**4.99E-03**	**-2.18**	**1.09E-18**	**N/A**	**FALSE**
ENSG00000185009	AP3M1	0	1	N/A	N/A	0.20	5.16E-03	-0.65	1.80E-23	N/A	FALSE
ENSG00000160404	TOR2A	0	1	N/A	N/A	0.41	5.23E-03	-0.45	1.49E-03	N/A	FALSE
ENSG00000058335	RASGRF1	1	1	N/A	N/A	0.62	5.49E-03	-1.02	1.07E-04	N/A	FALSE
ENSG00000196588	MKL1	1	1	N/A	N/A	0.23	5.94E-03	-0.32	2.75E-05	N/A	FALSE
ENSG00000113569	NUP155	1	1	-0.49	hsa-let-7g-5p	0.26	5.97E-03	-0.57	2.37E-11	N/A	FALSE
ENSG00000166479	TMX3	0	2	N/A	N/A	0.19	6.61E-03	-0.46	4.91E-13	N/A	FALSE
ENSG00000129925	TMEM8A	0	1	N/A	N/A	0.34	6.73E-03	-1.92	5.16E-64	N/A	FALSE
ENSG00000171303	KCNK3	0	2	N/A	N/A	0.61	7.13E-03	-2.52	1.02E-27	N/A	FALSE
ENSG00000028203	VEZT	0	1	-0.54	hsa-let-7g-5p	0.18	7.18E-03	-0.85	1.60E-46	N/A	FALSE
ENSG00000239672	NME1	0	1	N/A	N/A	0.35	7.24E-03	-0.26	3.49E-02	N/A	Katsanis_2006
ENSG00000134874	DZIP1	1	1	-0.3	hsa-let-7d-5p	0.23	7.95E-03	-0.46	4.99E-09	N/A	FALSE
ENSG00000104886	PLEKHJ1	0	1	N/A	N/A	0.24	8.45E-03	-0.29	7.81E-04	N/A	FALSE
ENSG00000142178	SIK1	1	1	N/A	N/A	0.34	8.54E-03	-0.71	1.12E-09	N/A	FALSE
ENSG00000165195	PIGA	1	1	-0.42	hsa-let-7a-5p	0.29	8.56E-03	-0.24	2.56E-02	N/A	FALSE
ENSG00000104611	SH2D4A	0	1	N/A	N/A	0.26	8.56E-03	-0.68	2.58E-14	N/A	FALSE
ENSG00000113070	HBEGF	1	1	-0.26	hsa-miR-98-5p	0.30	8.95E-03	-1.13	1.05E-27	N/A	FALSE
ENSG00000177425	PAWR	4	3	-0.43	hsa-let-7g-5p	0.26	9.06E-03	-0.28	2.07E-03	N/A	FALSE
ENSG00000094916	CBX5	4	3	-0.96	hsa-let-7d-5p	0.33	9.12E-03	-0.77	8.55E-12	N/A	FALSE
ENSG00000164073	MFSD8	2	3	N/A	N/A	0.33	9.26E-03	-0.44	1.86E-04	N/A	FALSE
ENSG00000181192	DHTKD1	0	1	N/A	N/A	0.25	9.42E-03	-0.76	9.79E-18	N/A	FALSE
ENSG00000148248	SURF4	0	1	-0.34	hsa-let-7d-5p	0.22	9.45E-03	-0.91	7.32E-35	N/A	FALSE
ENSG00000102317	RBM3	0	1	N/A	N/A	0.25	1.00E-02	-0.85	6.25E-23	N/A	FALSE
ENSG00000134717	BTF3L4	2	2	-0.41	hsa-let-7g-5p	0.19	1.05E-02	-0.17	1.67E-02	N/A	Katsanis_2006
ENSG00000170085	SIMC1	0	1	N/A	N/A	0.29	1.07E-02	-1.23	4.96E-30	N/A	FALSE
ENSG00000196313	POM121	1	1	N/A	N/A	0.23	1.10E-02	-1.29	4.16E-55	N/A	FALSE
ENSG00000133872	TMEM66	1	1	N/A	N/A	0.21	1.15E-02	-0.74	3.01E-24	N/A	FALSE
ENSG00000115107	STEAP3	1	1	-0.31	hsa-let-7d-5p	0.29	1.15E-02	-0.36	4.95E-04	N/A	Katsanis_2006
ENSG00000136052	SLC41A2	0	3	N/A	N/A	0.29	1.16E-02	-0.40	2.55E-04	N/A	FALSE
ENSG00000008838	MED24	1	1	N/A	N/A	0.20	1.17E-02	-0.48	5.76E-12	N/A	FALSE
ENSG00000123728	RAP2C	2	1	N/A	N/A	0.18	1.18E-02	-0.41	1.97E-10	N/A	Katsanis_2006
ENSG00000106367	AP1S1	0	2	-0.67	hsa-let-7a-5p	0.20	1.24E-02	-1.19	4.72E-64	N/A	FALSE
ENSG00000094880	CDC23	2	2	N/A	N/A	0.19	1.27E-02	-0.53	2.64E-14	N/A	FALSE
ENSG00000113621	TXNDC15	1	1	N/A	N/A	0.17	1.29E-02	-0.23	3.39E-04	N/A	FALSE
ENSG00000167065	DUSP18	1	2	N/A	N/A	0.35	1.29E-02	-0.46	4.33E-04	N/A	FALSE
ENSG00000161791	FMNL3	3	2	N/A	N/A	0.22	1.33E-02	-0.44	5.59E-08	N/A	FALSE
ENSG00000151693	ASAP2	4	1	N/A	N/A	0.22	1.41E-02	-0.43	4.21E-08	N/A	Ciliary-landscape_2016
ENSG00000072849	DERL2	3	2	N/A	N/A	0.18	1.59E-02	-0.20	3.84E-03	N/A	FALSE
ENSG00000156853	ZNF689	0	2	-0.43	hsa-let-7d-5p	0.24	1.59E-02	-0.65	1.21E-12	N/A	FALSE
ENSG00000260027	HOXB7	0	1	N/A	N/A	0.49	1.64E-02	-1.27	7.66E-09	N/A	FALSE

Ensembl ID	Gene Name	Number of *-3p* Sites	Number of *-5p* Sites	TargetScan TCS	Preferred *let-7*	L2FC (IC)	FDR (IC)	L2FC (MC)	FDR (MC)	Negative Regulator Reference (PMID)	Ciliary Gene
ENSG00000188501	LCTL	2	1	N/A	N/A	0.48	1.76E-02	-0.80	2.36E-05	N/A	FALSE
ENSG00000173406	DAB1	1	2	-0.28	hsa-let-7d-5p	0.69	1.85E-02	-1.95	1.46E-10	N/A	FALSE
ENSG00000198467	TPM2	0	1	N/A	N/A	0.26	1.86E-02	-0.55	8.11E-09	N/A	FALSE
ENSG00000173226	IQCB1	0	1	-0.46	hsa-let-7f-5p	0.28	1.86E-02	-0.74	5.04E-12	N/A	SYSCILIA_2019
ENSG00000145623	OSMR	0	1	-0.36	hsa-let-7d-5p	0.24	1.89E-02	-0.46	4.65E-07	N/A	FALSE
ENSG00000130309	COLGALT1	0	1	N/A	N/A	0.19	1.93E-02	-0.41	2.34E-08	N/A	FALSE
ENSG00000151553	FAM160B1	5	1	N/A	N/A	0.22	1.98E-02	-0.61	1.31E-13	N/A	FALSE
ENSG00000132256	TRIM5	2	1	N/A	N/A	0.20	1.99E-02	-0.63	6.90E-16	N/A	FALSE
ENSG00000149809	TM7SF2	0	1	N/A	N/A	0.27	2.00E-02	-0.26	1.86E-02	N/A	FALSE
ENSG00000186073	**C15orf41**	**1**	**1**	**-0.41**	**hsa-let-7b-5p**	**0.24**	**2.04E-02**	**-0.83**	**5.23E-18**	**N/A**	**FALSE**
ENSG00000166908	PIP4K2C	0	1	N/A	N/A	0.20	2.06E-02	-0.19	1.35E-02	N/A	FALSE
ENSG00000068438	FTSJ1	0	1	N/A	N/A	0.17	2.10E-02	-0.42	3.19E-10	N/A	FALSE
ENSG00000160218	TRAPPC10	3	1	N/A	N/A	0.17	2.13E-02	-0.29	1.15E-05	N/A	SYSCILIA_2019
ENSG00000129515	SNX6	0	1	-0.38	hsa-let-7c-5p	0.21	2.50E-02	-0.45	3.01E-08	N/A	FALSE
ENSG00000182158	CREB3L2	3	2	N/A	N/A	0.26	2.65E-02	-0.93	2.64E-19	N/A	FALSE
ENSG00000072736	NFATC3	1	1	N/A	N/A	0.19	2.65E-02	-0.44	4.54E-09	N/A	FALSE
ENSG00000114450	GNB4	2	1	N/A	N/A	0.20	2.67E-02	-0.26	1.68E-03	N/A	FALSE
ENSG00000122176	FMOD	1	2	N/A	N/A	0.41	2.77E-02	-3.22	1.08E-49	N/A	FALSE
ENSG00000143815	LBR	1	1	-0.4	hsa-let-7d-5p	0.28	2.79E-02	-0.35	3.15E-03	N/A	Katsanis_2006
ENSG00000187244	BCAM	0	2	N/A	N/A	0.24	2.88E-02	-0.58	8.94E-10	N/A	FALSE
ENSG00000101654	RNMT	3	3	N/A	N/A	0.19	2.93E-02	-0.30	1.02E-04	N/A	FALSE
ENSG00000090924	PLEKHG2	0	1	N/A	N/A	0.29	3.02E-02	-0.48	7.66E-05	N/A	FALSE
ENSG00000163602	RYBP	2	3	N/A	N/A	0.21	3.07E-02	-0.45	2.70E-07	N/A	FALSE
ENSG00000163697	APBB2	2	2	N/A	N/A	0.24	3.07E-02	-0.34	8.23E-04	N/A	FALSE
ENSG00000065060	UHRF1BP1	1	1	N/A	N/A	0.21	3.15E-02	-0.21	2.18E-02	N/A	Ciliary-landscape_2016
ENSG00000107949	BCCIP	1	2	N/A	N/A	0.17	3.19E-02	-0.17	2.41E-02	N/A	FALSE
ENSG00000010704	HFE	3	1	N/A	N/A	0.22	3.22E-02	-0.57	9.65E-10	N/A	FALSE
ENSG00000204138	PHACTR4	4	3	N/A	N/A	0.17	3.23E-02	-0.36	4.87E-07	N/A	FALSE
ENSG00000124783	SSR1	2	1	N/A	N/A	0.18	3.36E-02	-0.84	6.90E-31	N/A	FALSE
ENSG00000144043	TEX261	0	2	-0.35	hsa-let-7d-5p	0.18	3.37E-02	-0.44	4.57E-09	N/A	FALSE
ENSG00000145545	SRD5A1	0	1	N/A	N/A	0.22	3.41E-02	-1.12	1.70E-31	N/A	FALSE
ENSG00000135503	ACVR1B	1	4	-0.29	hsa-let-7c-5p	0.22	3.43E-02	-1.21	3.29E-40	N/A	FALSE
ENSG00000089723	OTUB2	0	1	-0.21	hsa-let-7d-5p	0.36	3.46E-02	-0.53	9.03E-04	N/A	FALSE
ENSG00000128989	ARPP19	3	2	-0.56	hsa-miR-98-5p	0.16	3.57E-02	-0.51	3.89E-15	N/A	FALSE
ENSG00000167118	URM1	0	1	N/A	N/A	0.16	3.58E-02	-0.39	1.83E-08	N/A	FALSE
ENSG00000063587	**ZNF275**	**0**	**2**	**-0.52**	**hsa-let-7b-5p**	**0.20**	**3.60E-02**	**-0.74**	**3.95E-19**	**N/A**	**FALSE**
ENSG00000125871	MGME1	0	1	N/A	N/A	0.23	3.66E-02	-0.43	1.29E-05	N/A	FALSE
ENSG00000110917	MLEC	2	2	N/A	N/A	0.20	3.73E-02	-1.03	4.18E-35	N/A	SYSCILIA_potential
ENSG00000137941	TTLL7	3	2	N/A	N/A	0.21	4.01E-02	-0.25	5.96E-03	N/A	Katsanis_2006
ENSG00000168297	PXK	1	1	N/A	N/A	0.17	4.12E-02	-0.77	1.04E-27	N/A	FALSE
ENSG00000158863	FAM160B2	0	1	-0.2	hsa-let-7d-5p	0.19	4.18E-02	-0.54	1.67E-11	N/A	FALSE
ENSG00000136492	BRIP1	1	1	N/A	N/A	0.34	4.21E-02	-0.98	6.10E-11	N/A	FALSE
ENSG00000129493	HEATR5A	1	1	N/A	N/A	0.19	4.22E-02	-0.34	6.17E-05	N/A	FALSE
ENSG00000049245	VAMP3	0	1	N/A	N/A	0.16	4.25E-02	-1.17	1.82E-64	N/A	FALSE
ENSG00000168016	**TRANK1**	**1**	**1**	**-0.4**	**hsa-let-7b-5p**	**0.52**	**4.31E-02**	**-0.55**	**4.14E-02**	**N/A**	**SYSCILIA_potential**
ENSG00000166986	MARS	0	1	N/A	N/A	0.16	4.50E-02	-0.68	8.86E-24	N/A	FALSE
ENSG00000156162	DPY19L4	2	2	N/A	N/A	0.17	4.52E-02	-0.41	4.94E-08	N/A	FALSE
ENSG00000204308	RNF5	0	1	N/A	N/A	0.18	4.53E-02	-0.55	2.89E-12	N/A	FALSE
ENSG00000124571	XPO5	0	1	N/A	N/A	0.16	4.75E-02	-0.65	1.07E-19	N/A	FALSE
ENSG00000136731	UGGT1	0	3	-0.29	hsa-let-7d-5p	0.21	4.76E-02	-0.76	4.96E-17	N/A	FALSE
ENSG00000134490	TMEM241	1	1	N/A	N/A	0.25	4.92E-02	-0.77	1.93E-11	N/A	FALSE
ENSG00000125447	GGA3	0	1	N/A	N/A	0.16	4.99E-02	-0.22	4.02E-03	N/A	FALSE
ENSG00000197702	PARVA	0	1	N/A	N/A	0.61	8.95E-15	-0.36	5.89E-06	20393563	FALSE

TCS: Total Context++ Score; L2FC: Log_2(FoldChange); IC: inhibitor *versus* control condition; MC: mimic *versus* control condition; FDR: False Discovery Rate; N/A: not applicable; Negative regulator of ciliogenesis are highlighted in light gray or dark grey when they also have a TCS score; *let-7b-5p* preferred targets are indicated in bold

Table 5: Genes with *let-7b* target sites selected for targeted sequencing in the ciliopathy cohort

Ensembl ID	Gene Name	L2FC(IC)	FDR(IC)	L2FC(MC)	FDR(MC)	Number of *-3p* sites	Number of *-5p* sites
ENSG00000106948	AKNA	0.39	2.30E-04	-0.75	1.60E-13	3	3
ENSG00000153317	ASAP1	0.54	2.73E-10	-0.72	5.78E-18	2	1
ENSG00000134717	BTF3L4	0.19	1.05E-02	-0.17	1.67E-02	2	2
ENSG00000165376	CLDN2	2.07	1.92E-25	-1.67	4.78E-09	1	0
ENSG00000166171	DPCD	0.39	3.33E-05	-0.74	8.14E-16	0	1
ENSG00000182197	EXT1	0.32	1.83E-03	-0.51	8.99E-08	3	2
ENSG00000092820	EZR	0.20	3.62E-02	-0.67	1.15E-16	2	0
ENSG00000088832	FKBP1A	0.49	1.26E-13	-0.18	7.10E-03	1	0
ENSG00000075420	FNDC3B	0.85	2.71E-29	-0.27	7.01E-04	6	3
ENSG00000141429	GALNT1	1.13	2.14E-32	-0.33	9.08E-04	1	2
ENSG00000090863	GLG1	0.20	3.00E-02	-0.49	1.52E-09	2	0
ENSG00000111087	GLI1	0.41	1.01E-02	-0.41	6.46E-03	2	0
ENSG00000074047	GLI2	0.39	2.52E-03	-0.76	8.73E-10	2	1
ENSG00000119927	GPAM	1.09	1.39E-35	-0.19	4.92E-02	2	2
ENSG00000107937	GTPBP4	0.33	3.94E-05	-0.29	2.10E-04	1	0
ENSG00000061918	GUCY1B3	0.36	1.67E-03	-1.33	1.36E-33	5	0
ENSG00000155304	HSPA13	0.18	3.87E-02	-0.60	1.77E-16	4	0
ENSG00000044574	HSPA5	0.40	1.26E-03	-0.74	5.10E-11	0	1
ENSG00000068383	INPP5A	0.63	1.05E-05	-0.49	5.40E-04	1	1
ENSG00000132321	IQCA1	0.60	5.06E-04	-0.44	1.42E-02	2	0
ENSG00000173226	IQCB1	0.28	1.86E-02	-0.74	5.04E-12	0	1
ENSG00000143815	LBR	0.28	2.79E-02	-0.35	3.15E-03	1	1
ENSG00000108829	LRRC59	0.44	2.32E-05	-0.87	5.35E-19	0	1
ENSG00000101367	MAPRE1	0.36	1.87E-08	-0.64	8.81E-25	0	1
ENSG00000110917	MLEC	0.20	3.73E-02	-1.03	4.18E-35	2	2
ENSG00000100345	MYH9	0.64	1.09E-15	-0.76	3.38E-22	1	0
ENSG00000151414	NEK7	0.43	9.95E-10	-0.67	2.19E-22	2	1
ENSG00000239672	NME1	0.35	7.24E-03	-0.26	3.49E-02	0	1
ENSG00000154678	PDE1C	0.87	1.12E-18	-1.12	1.47E-29	4	1
ENSG00000114302	PRKAR2A	0.84	5.84E-25	-1.01	3.04E-34	2	1
ENSG00000104388	RAB2A	0.24	4.70E-03	-0.37	2.24E-06	5	0
ENSG00000108774	RAB5C	0.24	2.48E-03	-0.17	3.05E-02	1	0
ENSG00000123728	RAP2C	0.18	1.18E-02	-0.41	1.97E-10	2	1
ENSG00000168385	SEPT2	0.33	2.60E-05	-0.19	1.10E-02	1	0
ENSG00000099956	SMARCB1	0.40	9.09E-06	-0.61	7.86E-13	1	0
ENSG00000115107	STEAP3	0.29	1.15E-02	-0.36	4.95E-04	1	1
ENSG00000119977	TCTN3	0.17	4.94E-02	-0.17	3.44E-02	1	0
ENSG00000041982	TNC	2.38	6.25E-48	-0.37	2.55E-02	1	0
ENSG00000160218	TRAPPC10	0.17	2.13E-02	-0.29	1.15E-05	3	1
ENSG00000137941	TTLL7	0.21	4.01E-02	-0.25	5.96E-03	3	2
ENSG00000196230	TUBB	0.30	8.39E-04	-1.38	3.56E-64	1	1
ENSG00000152763	WDR78	0.24	3.81E-02	-0.44	4.16E-05	4	0

L2FC: Log_2(FoldChange); IC: inhibitor *versus* control condition; MC: mimic *versus* control condition; FDR: False Discovery Rate

Table 6: Burden analysis between Meckel-Grüber and Bardet-Biedl syndrome patients

<5% MAF	Number of patients	Number of alleles	Number of variants	P-Value (Bonferroni correction)
European (Non-Finnish)				
BBS	102	204	14	
MKS	28	56	11	2.61
Other				
BBS	15	30	1	
MKS	40	80	16	7.88

<1% MAF	Number of patients	Number of alleles	Number of variants	P-Value (Bonferroni correction)
European (Non-Finnish)				
BBS	102	204	11	
MKS	28	56	10	1.49
Other				
BBS	15	30	1	
MKS	40	80	15	13.12

MAF: Minor Allele Frequency; BBS: Bardet-Biedl Syndrome; MKS: Meckel-Grüber Syndrome

Table 7: Depletion or enrichment analysis of candidate variants

Other (Other, Latino, African and East Asian)

rs6679100 (1-198288709-A-G)

Clinical diagnosis	N	Genotype Counts			Genotype Frequency			Allele Count		Allele Frequency		P-value (Bonferroni)	
		AA	AG	GG	AA	AG	GG	A	G	A	G	Case *vs* Controls	BBS *vs* MKS
Controls	6068	604	2383	3081	0.10	0.39	0.51	3591	8545	0.30	0.70		
BBS	15	2	9	4	0.13	0.60	0.27	13	17	0.43	0.57	16.7353	
MKS	40	12	14	14	0.30	0.35	0.35	38	42	0.48	0.53	0.0791	
Ciliopathy	55	14	23	18	0.25	0.42	0.33	51	59	0.46	0.54	**0.0226**	97.2478

rs182129505 (10-113912476-C-T)

Clinical diagnosis	N	Genotype Counts			Genotype Frequency			Allele Count		Allele Frequency		P-value (Bonferroni)	
		CC	CT	TT	CC	CT	TT	C	T	C	T	Case *vs* Controls	BBS *vs* MKS
Controls	6082	6081	1	0	1.00	0.00	0.00	12163	1.00	1.00	0.00		
BBS	15	15	0	0	1.00	0.00	0.00	30	0.00	1.00	0.00	108.5252	
MKS	40	39	1	0	0.98	0.03	0.00	79	1.00	0.99	0.01	**<0.01**	
Ciliopathy	55	54	1	0	0.98	0.02	0.00	109	1.00	0.99	0.01	0.339	61.9692

BBS: Bardet-Biedl Syndrome; MKS: Meckel-Grüber Syndrome; significant P-values are indicated in bold

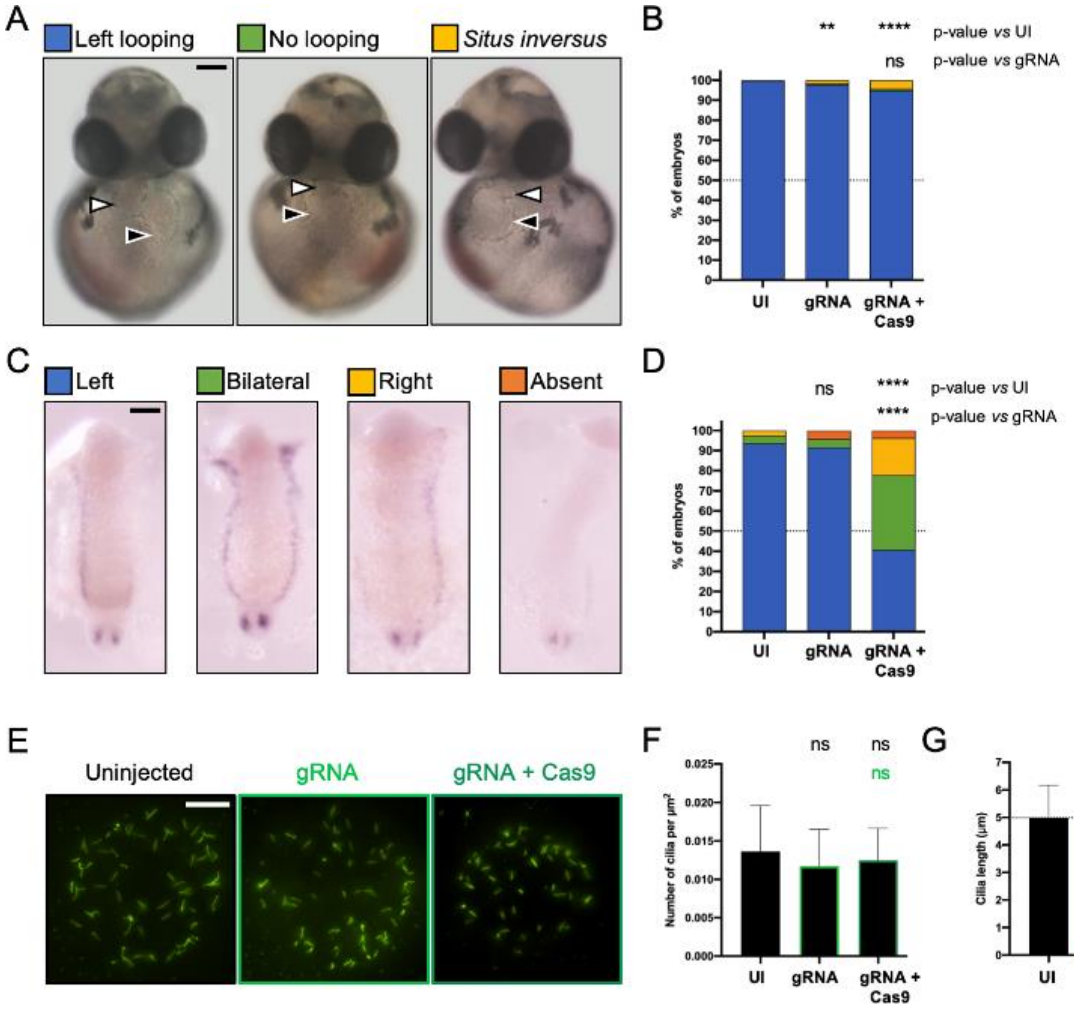

Figure 1: Suppression of *let-7b* leads to cilia defects in zebrafish

A. Representative images of 2 days-post-fertilization (dpf) embryos with normal leftward heart looping, no looping and *situs inversus*. White and black arrowheads indicate the ventricle and atrium respectively. **B.** Percentage of embryos with each type of heart looping at 2dpf. n=84-112 embryos per condition, N=3 biological replicates. **C.** Dorsal view of whole-mount *in situ* hybridization showing normal left-side restricted expression of *spaw*, and abnormal bilateral, contralateral or absent expression at the 18 somites-stage (ss). **D.** Percentage of embryos with each pattern of *spaw* expression at 18ss. n=17-32 embryos per condition, N=2 biologiccal replicates. **E.** Kupffer's vesicle (KV) of 10ss embryos stained with anti-acetylated α-tubulin to label cilia. Density (**F**) and length (**G**) of cilia in the KV at 10ss. n=20-27 KV, 416-865 cilia/condition, N=3 biological replicates. Error bars indicate standard deviation. ****p≤0.0001; ns: not significant; UI: uninjected control. Black scale bars=100µm, white scale bar=20µm.

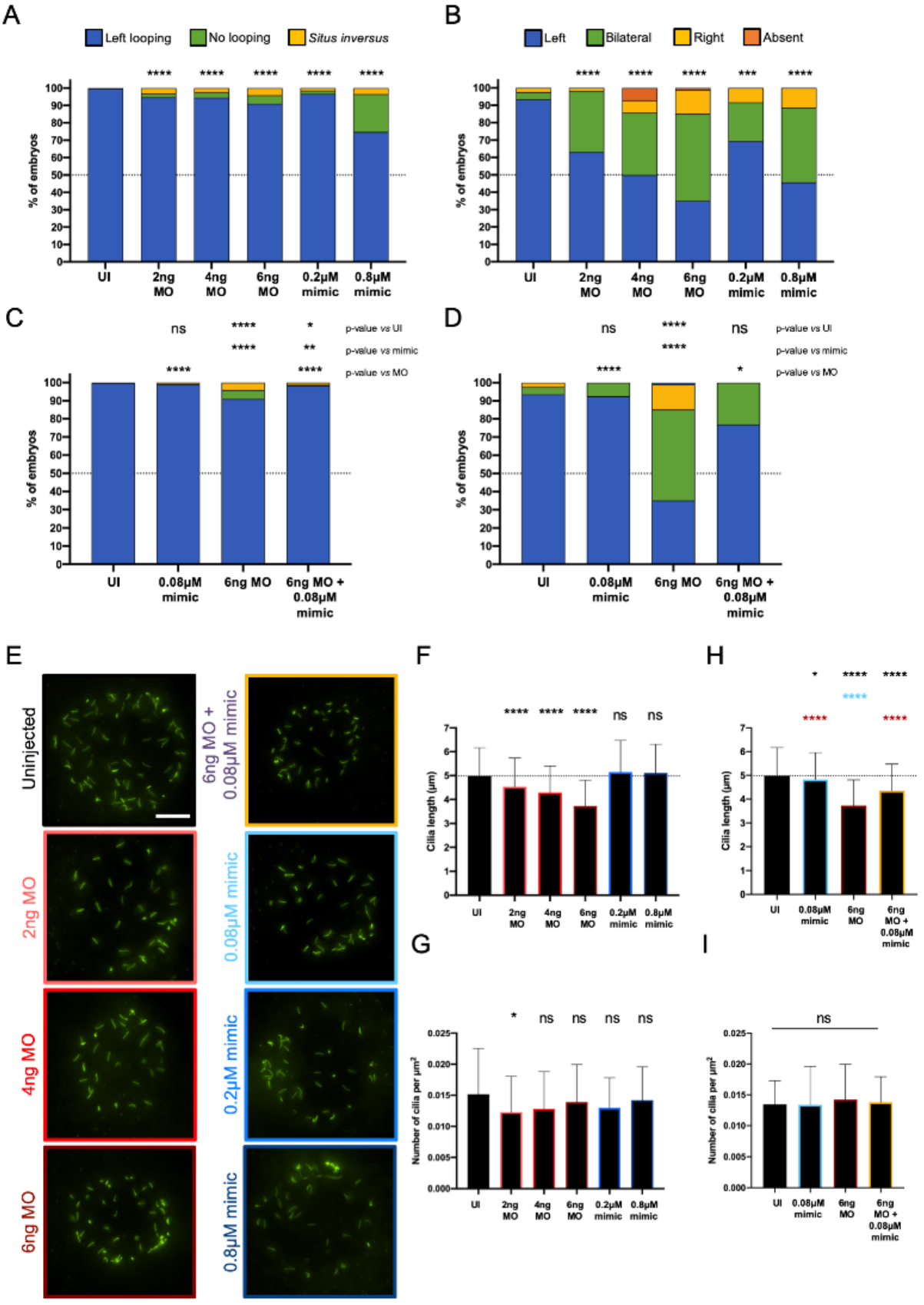

Figure 2: Ciliary phenotypes are recapitulated in *let-7b* morphants but overexpression of *let-7b* does not lead to opposite cilia defects

Figure 2: Ciliary phenotypes are recapitulated in *let-7b* morphants but overexpression of *let-7b* does not lead to opposite cilia defects

A. Percentage of embryos with each type of heart looping at 2 days-post-fertilization (dpf). n=90-110 embryos per condition, N=3. **B.** Percentage of embryos with each pattern of *spaw* expression at the 18 somites-stage (ss). n=35-72 embryos per condition, N=2 biological replicates. Co-injection of 6ng MO + 0.08µM mimic partially rescues the heart looping phenotype (**C**) and *spaw* expression defects (**D**). n=35-72 embryos per condition, N=2 biological replicates. **E.** KV of 10ss embryos stained with anti-acetylated α-tubulin to label cilia. Measurements (**F**) and density (**G**) of cilia in the KV at 10ss. n=11-16 KV, 233-629 cilia/condition, N=3 biological replicates. Co-injection of 6ng MO + 0.08µM mimic partially rescues the cilia length anomaly (**H**) and does not affect the cilia density (**I**). n=21-31 embryos per condition, N=3 biological replicates. Error bars indicate standard deviation. *p≤0.05; **p≤0.01; ****p≤0.0001; ns: not significant; UI: uninjected controls; MO: morpholino. Scale bar=20µm.

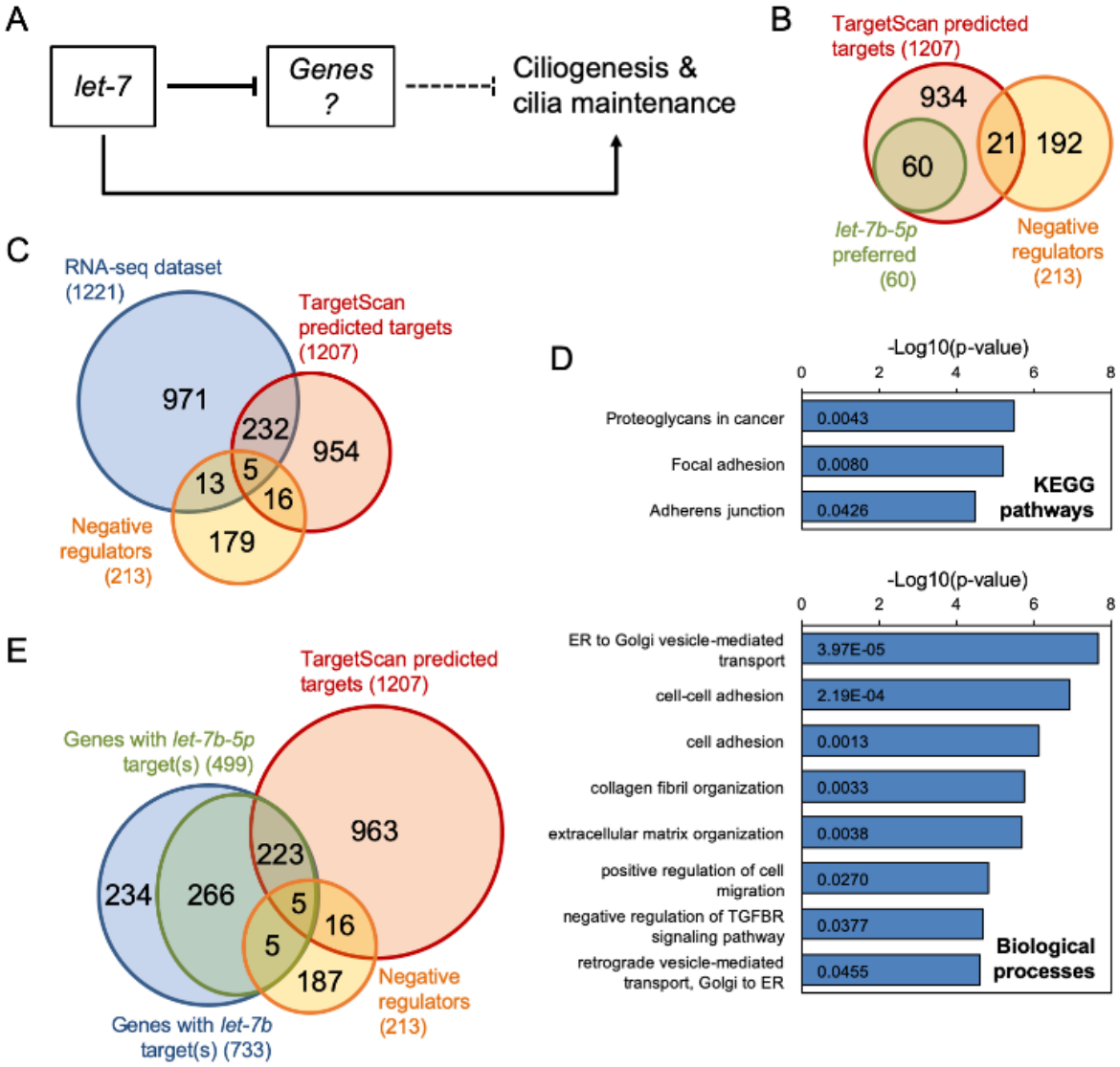

Figure 3: Filtering strategy to identify *let-7* candidate targets with a role of negative regulator of ciliogenesis

A. Expected mechanism of action of *let-7b* on ciliogenesis and cilia maintenance. **B.** Venn diagram representing the overlap between different lists of genes. **C.** Venn diagram showing the restricted overlap between the transcriptomic data, the TargetScan predicted *let-7* targets, and the list of negative regulators of ciliogenesis. **D.** Functional enrichment analysis for KEGG pathways and biological processes (Gene Ontology). Terms with an FDR<0.5 are displayed (values indicated on histograms). **E.** Venn diagram showing the overlap between the different filters applied to identify *let-7b-5p* target genes.

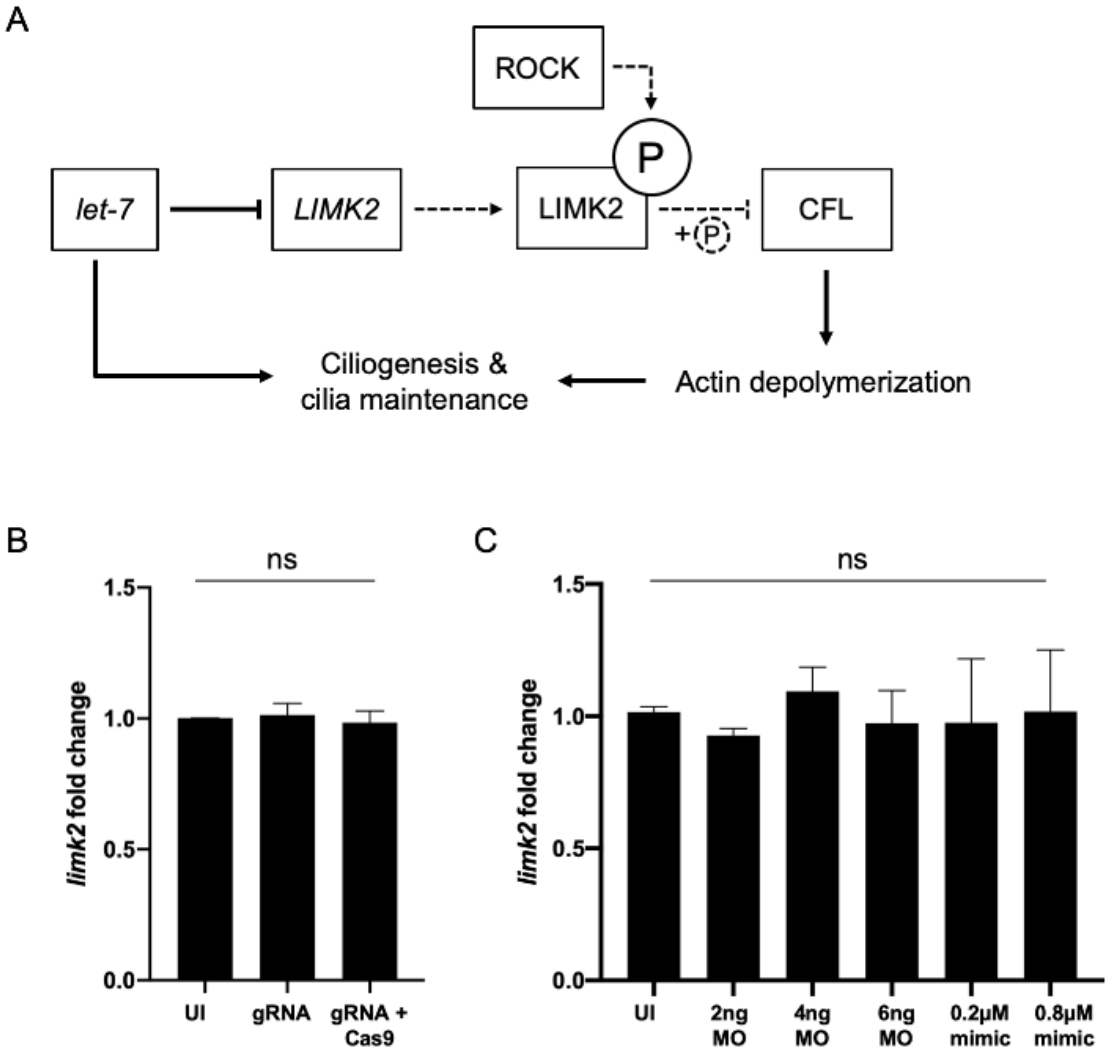

Figure 4: Testing the candidacy of *LIMK2* in zebrafish

A. Putative mechanism of action of *let-7* and *LIMK2* on ciliogenesis. Dashed lines indicate weak effect in the presence of *let-7*, P indicate phosphorylation events: ROCK phosphorylates LIMK2 to activate the protein but LIMK2 phosphorylates CFL to inactivate it. **B.** Expression of *limk2* measured in *let-7b* mosaic F0 and controls at 30hpf. **C.** Expression of *limk2* measured in *let-7b* morphants and embryos overexpressing *let-7b-5p* at 30hpf. Error bars indicated standard deviation. ns: not significant; UI: uninjected control; MO: morpholino; ROCK: Rho associated coiled-coil Containing protein Kinase; CFL: cofilin.

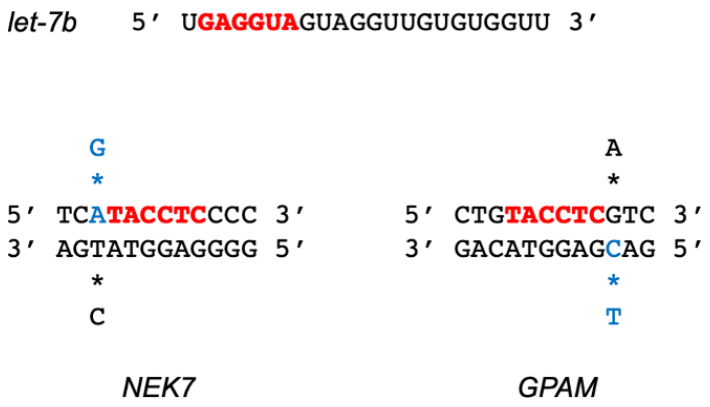

Figure 5: Representation of variants relative to the *let-7* seed target

Schematic of *let-7b* mature miRNA and map of the variants identified in our ciliopathy cohort. *let-7* seed is indicated in red and bold. Variants are indicated in blue, asterisks indicate the position of the variant and the protruding letter indicates the alternative allele.

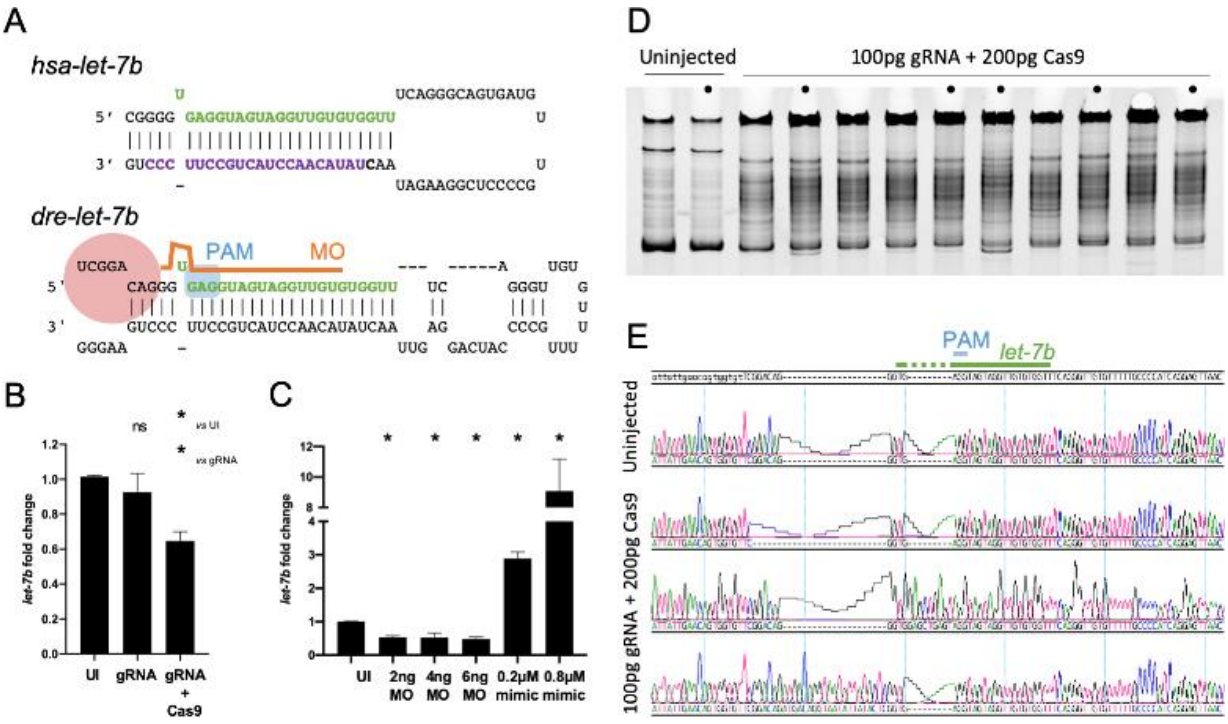

Supplementary Figure 1: Validation of *let-7b* knockdown and overexpression

A. Schematics of human and zebrafish *let-7b* immature stem-loops. *let-7b-5p* is indicated in green and *let-7b-3p* is indicated in purple. The Protospacer Adjacent Motif (PAM) targeted for cleavage by the CRISPR system is indicated in light blue, and the Drosha processing site predicted to be altered after DNA repair is highlighted in red. The target sequence of the morpholino (MO) is indicated in orange. **B.** and **C.** indicate the level of mature *let-7b* measured in a pool of 50 embryos for each condition at 30 hours-post-fertilization. **D.** Heteroduplex analysis of 2 uninjected controls and 10 embryos injected with gRNA + Cas9 protein and harvested for genomic DNA extraction at 2 days-post-fertilization. The 15% polyacrylamide gel was loaded with denatured-reannealed PCR products flanking the gRNA target. **E.** Representative chromatograms of PCR products that were cloned and sequenced from uninjected controls or *let-7b* mosaic F0 (individuals marked with a black dot in (**D**)). *let-7b* mature sequence is indicated in green and the PAM in light blue.

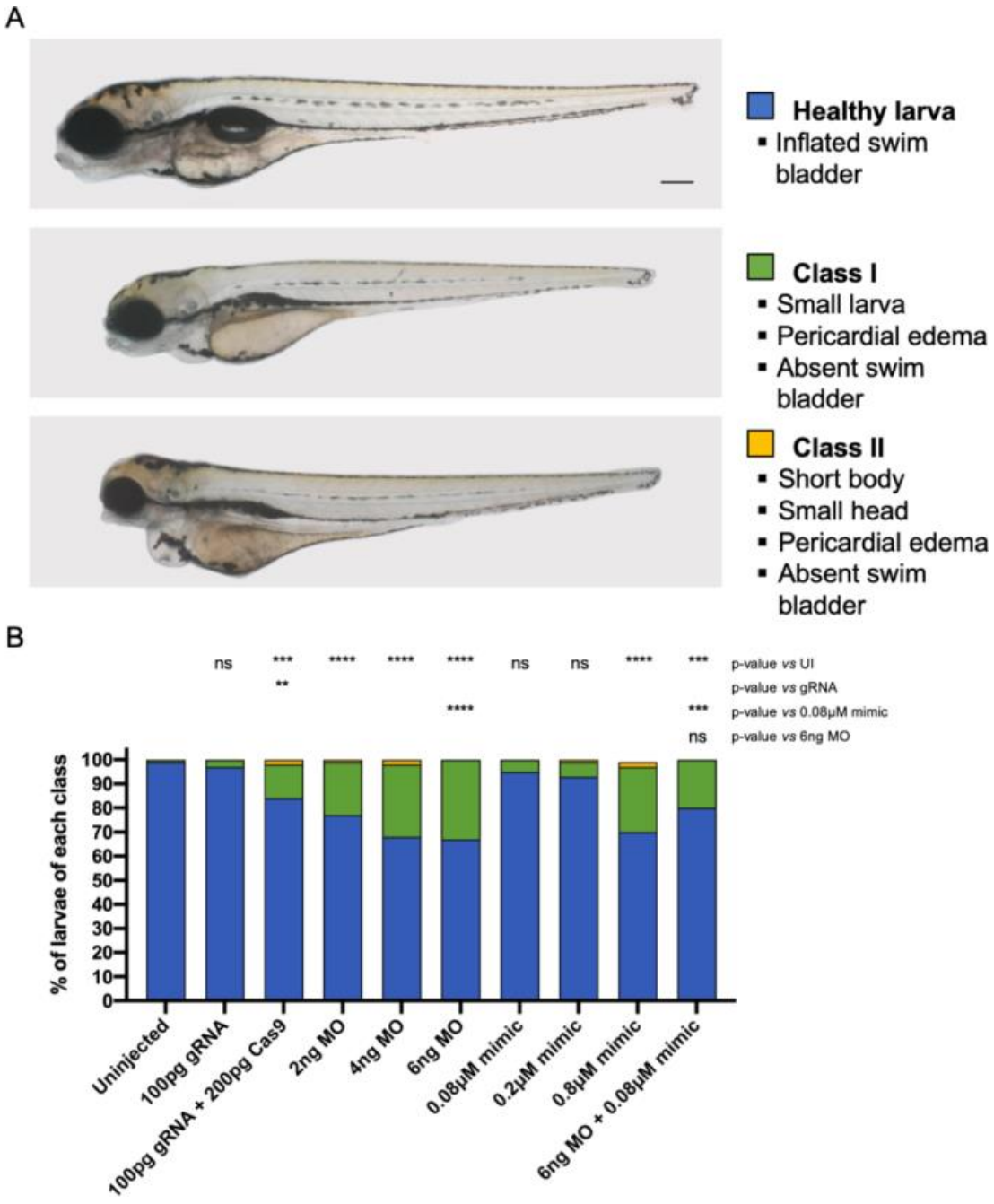

Supplementary Figure 2: Quantification of developmental defects at 4 days-post-fertilization.

A. Representative pictures of 4 days-post-fertilization (dpf) larvae for each observed class. **B.** Quantification of the different phenotype class at 4dpf for each condition. n=47-113, N=2-3 biological replicates. **p≤0.01; ***p≤0.001; ****p≤0.0001; ns: not significant. Scale bar =100µm.

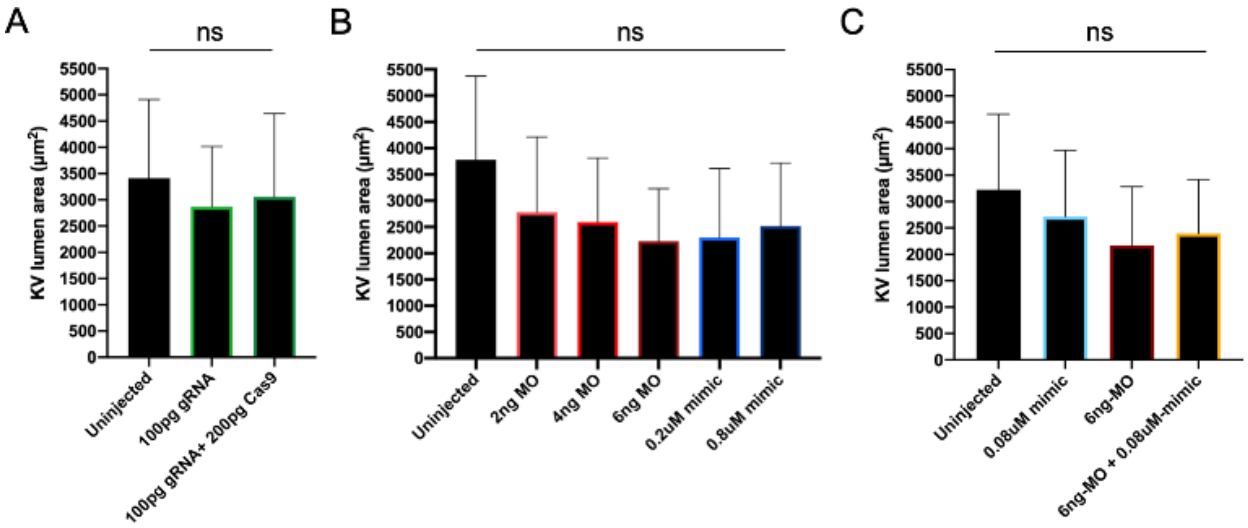

Supplementary Figure 3: Kupffer's vesicles tend to be smaller in injected embryos.

The area of the Kupffer's vesicle (KV) lumen at 10 somites-stage is variable in *let-7b* mosaic F0 (**A**), embryos injected with *let-7b* morpholino (MO) or mimic (**B**), and embryos co-injected with *let-7b* MO and mimic (**C**). n=11-27, N=3 biological replicates. ns: not significant.

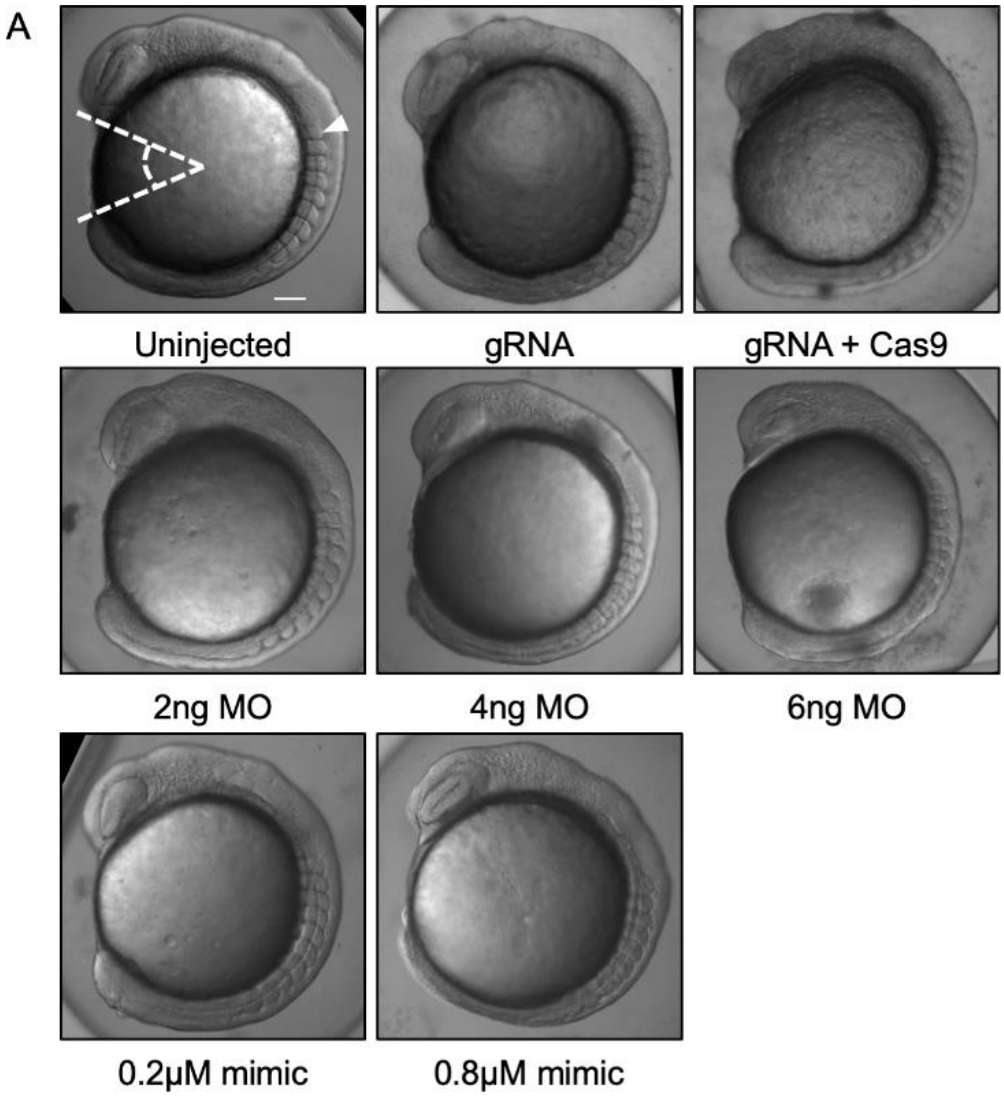

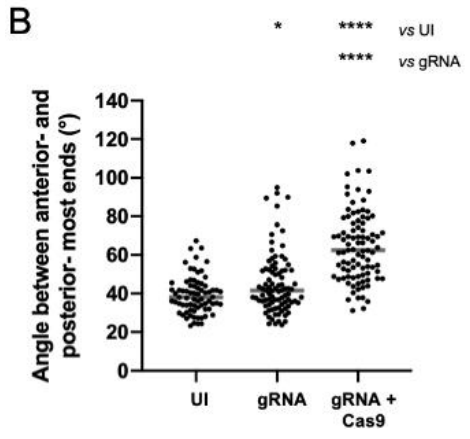

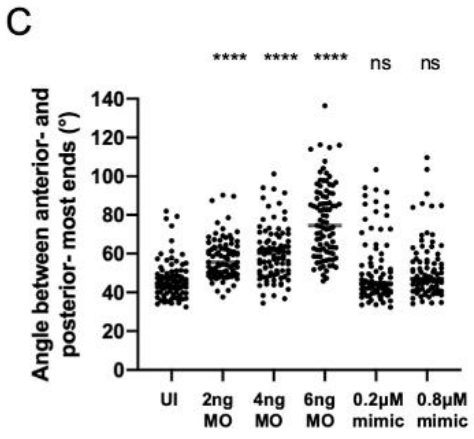

Supplementary Figure 4: Suppression but not overexpression of *let-7b* leads to convergent-extension defects

Supplementary Figure 4: Suppression but not overexpression of *let-7b* leads to convergent-extension defects

A. Lateral view of 10 somites-stage embryos. Angle between the anterior- and posterior-most ends of the embryo (white dashed lines) was used for the convergent-extension assay. White arrowhead indicates first somite. **B.** Plot of the angles measured for each embryo. n=73-92 embryos per condition, pool of 3 independent experiments. **C.** Plot of the angles measured for each morphant and embryos overexpressing *let-7b-5p* compared to control embryos. n=83-91 embryos per condition, pool of 3 independent experiments. *p≤0.05; ****p≤0.0001; ns: not significant; UI: uninjected controls. Scale bar=100µm.

II. Developing a zebrafish model for spinocerebellar ataxia 7 to explore the link between Ataxin-7 and cilia

To investigate the interplay between ATXN7 and cilia in the context of SCA7, we first attempted to develop a zebrafish model of the disease. Our approach consisted of overexpressing human ATXN7 in zebrafish embryos by injecting mRNA.

Human *ATXN7* has a single ortholog in the zebrafish genome encoded by *atxn7*. The zebrafish Atxn7 protein shares 46% identity and 59% similarity with human ATXN7. All domains are conserved, including the polyQ stretch which is shorter with only 5Q [272].

1. A SCA7 zebrafish model with phenotypes characteristic of ciliary defects

Preliminary results show cilia-related phenotypes in a zebrafish model of SCA7

pCS2+ vectors containing cDNA encoding wild-type (WT) ATXN7 with 10Q (N10; normal 10) and for two forms of mutant (m) ATXN7 with 60Q (E60; expanded 60) and 104 or 106Q (E104 or E106; expanded 104 or 106) were used to generated mature mRNA coding for the human proteins. Preliminary injections performed in our group produced embryos with several cilia-related phenotypes such as body curvature, otolith defects, cardiac edema and kidney cysts [343,344], which seemed polyQ dependent when the embryos were injected with E60 and E106 mRNAs at concentrations ranging from 250 to 400ng/µL (**Figure 1A-D**). At 2dpf, approximately 10% of embryos injected with E60 mRNA presented with otolith defects and cardiac edemas and almost 30% had a curved body. Embryos injected with mRNA coding for E106 mRNA presented with the same phenotype at higher frequencies: 35% with otolith defects, almost 40% with cardiac edema and nearly 80% with body curvature. Less than 5% of uninjected siblings showed those defects (**Figure 1D**). Although not counted, few cyclops were observed among embryos injected with mRNA coding for E106 (**Figure 1B**).

Discrepancy between preliminary and new experiments

Contrary to our expectations, the injections of the same concentrations of the original mRNAs, or freshly prepared mRNAs from the same vectors, did not recapitulate those phenotypes. We first compared the embryos injected with 250ng/µL of fresh mRNA with the images obtained from preliminary data at 4dpf but 95% of injected embryos looked like uninjected controls (**Figure 1B, E**). Next, we repeated the injections but included a control mRNA and monitored the development of the embryos at earlier time points in case affected embryos might have died before 4dpf. The control mRNA was injected at 10ng/µL and coded for the fusion protein Histone 2B-GFP (H2B-GFP) and enabled to control for the injection and mRNA expression. Every injection generated more than 98% fluorescent embryos (**Supp. Figure 1**). At 2dpf with 250ng/µL of *ATXN7* mRNA, less than 6% of injected embryos presented with no phenotype while control embryos, including H2B-GFP mRNA injected and uninjected siblings, had a phenotype (**Figure 1G**). The injection of mRNA at 400ng/µL triggered more phenotypes but the proportions of affected embryos were still minimal compared to preliminary experiments (**Figure 1D, H**). For instance, body curvature was found in 16% and 8% of embryos injected with E60 and E104 respectively (**Figure 1H**). At 3dpf, the mortality in embryos injected with 250ng/µL of mRNA did not exceed 6% but it augmented up to 38% in embryos injected with 400ng/µL of E104 mRNA (**Figure 1F**). The latest is exceptionally high and might explain the discrepancy between the preliminary and new injections, however a mortality rate of 35% as early as at 1dpf prevents any characterization of the phenotypes of interest. Next, we compared the injection of mature mRNA with the injection of plasmids which is a technique preferentially used by colleagues [345]. We used plasmids containing either eGFP alone as a control, or eGFP fused to WT ATXN7 or mATXN7 (pEGFP, pEGFP-N10 and pEGFP-E104 respectively). The injection of 30 or 100ng/µL of pEGFP-N10 and pEGFP-E104 lead to 23-53% mortality at 2dpf, which was surprising as the fluorescence evidenced low expression (**Supp. Figure 2**). Besides, pEGFP-N10 and pEGFP-E104 were equally toxic. Surviving embryos looked delayed and had gnarled tails which are two signs of non-specific toxicity [346] (**Supp. Figure 2**). pEGFP, and second control pCS2+ H2B-GFP, were correctly

expressed as evidenced by fluorescence in about half of the injected embryos. The mortality was also high in embryos injected with control plasmids. Therefore, this approach raised more questions than brought solutions and we chose to pursue with the mRNA injection strategy. The lower mortality and increased percentage of fluorescent embryos observed in experiments conducted with the injection of mRNA suggest that this tool is more appropriate for our experiments.

Evaluation of organs affected in SCA7

We did not detect significant phenotypes at the level of the whole body in the embryos injected with mRNA coding for mATXN7, however, the hallmarks of SCA7 are neurodegeneration in the cerebellum and in the retina [248], and Atxn7 is known to play a role in the development of the brain and eye of the zebrafish [272]. Thus, we asked whether the injected embryos had more subtle phenotypes in each respective cell type. We used an anti-acetylated α-tubulin antibody to label the cerebellum (**Figure 2A**) and the transgenic zebrafish SoFa1 line which highlights the retinal neurons [318] (**Figure 2D**). We did not detect any significant hypoplasia of the cerebellum in the embryos injected with E104 compared to the embryos injected with N10 or uninjected siblings at 3dpf (**Figure 2A-C**). Observation of retinas at 48 and 72hpf did not show any anomalies: retinas of embryos injected with mRNA coding for WT or mATXN7 were indistinguishable from uninjected controls with defined retinal neuron layers (**Figure 2E**). Retinas from embryos injected with H2B-GFP mRNA were saturated with GFP and were not imaged. We concluded that the injection of mRNA coding for ATXN7 at concentrations ranging from 100ng/µL to 400ng/µL in our zebrafish lines was not sufficient to generate a robust zebrafish SCA7 model. Knowing that embryos used for preliminary experiments were obtained from adult fish of almost 2-years of age, we hypothesized that they might have been more sensitive to proteotoxicity.

Shorter peptides with predicted augmentation of proteotoxicity

To address the possibility of variable proteotoxic sensitivity, we injected mRNAs coding for a fragment of ATXN7 (ATXN7Δ) predicted to be more toxic than the full-length proteins [257]. Previous studies showed that expanded-polyQ-eGFP was sufficient to cause protein aggregation, nuclear inclusion and death in zebrafish [347,348]. Therefore, we cloned WT and mutant ATXN7Δ (WT ATXN7Δ coding for 10Q and mATXN7Δ coding for 104Q respectively) constructs into pCS2+ vectors to produce mRNA. The injection of mRNA coding for WT ATXN7Δ and mATXN7Δ at concentrations ranging from 10ng/µL up to 400ng/µL did not lead to significant phenotypes. Less than 10% of embryos presented with anomalies in every condition. For instance, no more than 6% embryos injected with 400ng/µL of mATXN7Δ mRNA had a cardiac edema at 2dpf (**Figure 3A**), and mortality was at 10% at 3dpf (**Figure 3B**). Like in the preliminary injections, we noted few cyclops but we did not count them because of their rarity. At the concentration of 1000ng/µL, which was used in [348], we observed up to 35% of cardiac edemas in embryos injected with WT ATXN7Δ and high mortality rates (27-58%) (**Figure 3A, B**). The phenotype frequencies being higher in the embryos injected with WT ATXN7Δ compared to mATXN7Δ, and the high mortality rate dissuaded us from pursuing the characterization of these embryos. Because embryos injected with mATXN7Δ mRNA showed less phenotypes compared to embryos injected with WT ATXN7Δ mRNA despite the predicted proteotoxicity of the mATXN7Δ, we decided to control the expression of the injected mRNAs.

2. Spatio-temporal expression pattern of *ATXN7* mRNAs

Despite our positive control H2B-GFP suggesting a proper expression of the injected mRNA, we wanted to verify the expression of the mRNA coding for ATXN7. We generated fluorescent fusion proteins by adding an eGFP in the C-terminus of the ATXN7Δ peptides. To do so, we amplified the eGFP coding sequence from a pEGFP-N2 vector and cloned it downstream of the ATXN7Δ sequences and upstream of the STOP codon.

Fluorescent fusion protein to monitor expression

We followed the evolution of the fluorescent signal of WT ATXN7ΔeGFP, mATXN7ΔeGFP and of an eGFP control in live embryos injected with 400ng/µL from 4hpf to 7dpf. Fluorescence was detectable as early as 4hpf in all injected embryos suggesting that all mRNAs were correctly expressed (**Figure 4A**). However, we observed a strong decrease of fluorescence after 24hpf in the embryos injected with WT ATXN7ΔeGFP and mATXN7ΔeGFP mRNAs while the fluorescence in control embryos injected with eGFP mRNA lasted until the experimental endpoint at 7dpf (**Figure 4A** and data not shown). This suggested that either the ATXN7ΔeGFP were degraded too quickly or that the produced proteins were very unstable. Less than 10% of injected embryos had a body curvature, cardiac edema or otolith defect and we noted a low but constant appearance of cyclops (<5%) at 2dpf (**Figure 4D**). The mortality was less than 10% at 3dpf (**Figure 4E**).

Insights from the cellular level

To investigate if the injection of ATXN7ΔeGFP mRNAs at 400ng/µL triggered protein aggregation, we fixed embryos at 24hpf, the latest stage with visible fluorescence, and prepared cryo-sections of the heads to look for nuclear inclusions. We observed fluorescence in both the nucleus and the cytoplasm despite all nuclear localization and exportation signals being ablated in ATXN7Δ constructs, with a preference for the nucleus in the cells from embryos injected with WT ATXN7ΔeGFP and mATXN7ΔeGFP mRNAs (**Figure 4C**). Cells from the control embryos injected with eGFP mRNA had a strong cytoplasmic signal (**Figure 4C**). The absence of puncta at 24hpf characteristic of protein aggregation indicated that the amount of available protein was not enough to cause proteotoxicity at this stage.

Kinetic studies to define expression timeline

To better understand the expression timeline of the injected mRNAs and to determine the developmental stage with the peak of mRNA expression and potentially protein aggregation, we performed comparative analyses of eGFP kinetics. We first cloned eGFP in C-terminus of the full-length ATXN7 proteins to compare them with the ATXN7ΔeGFP. Then we injected equimolar concentrations of mRNA (0.7mM) to facilitate the comparison of signal intensity, and imaged six live embryos for each condition from the cleavage period at 1hpf to protruding mouth at 72hpf (**Figure 5A**). The fluorescence intensity for each embryo was measured and corrected in Image J software and called Corrected Total Embryo Fluorescence (CTEF). We first compared WT ATXN7 full-length and WT ATXN7Δ with the eGFP control and observed that the highest CTEF was measured in eGFP controls at 18hpf ($77x10^6$ a.u.) (**Figure 5A**). However, images of embryos injected with eGFP mRNA were saturated between 6hpf and 18hpf suggesting that the real fluorescence peak was probably reached at one of these time points (**Figure 5A**). CTEF from embryos injected with WT ATXN7ΔeGFP mRNA were much lower with a peak at 10hpf of $50x10^6$ a.u., and CTEF from embryos injected with WT ATXN7eGFP mRNA was even lower with a peak at 10hpf of $5x10^6$ a.u. (**Figure 5A**). This experiment suggests that mRNA coding for ATXN7Δ is more highly expressed or that the produced peptide is more stable, and thus that the overexpression of ATXN7Δ is a better approach to develop the SCA7 model rather than the overexpression of the full-length proteins. Therefore, we repeated this kinetic study and compared WT ATXN7ΔeGFP with mATXN7ΔeGFP kinetics (**Figure 5B**). We did not detect significant difference between the CTEF of embryos injected with ATXN7ΔeGFP or mATXN7ΔeGFP but we confirmed that both mRNAs were correctly expressed. This time the highest CTEF was detected at 24hpf which might be due to the more accurate method used for these measurements (see methods).

To conclude, the spatio-temporal tracking of ATXN7 mRNA expression showed that: 1) small levels of protein were present at the observed stages (50% less than eGFP protein according

to the CTEF) suggesting a problem in the translation of the mRNAs coding for ATXN7, or the instability of the produced proteins; and that 2) even the polyQ peptide predicted to be the most toxic did not aggregate in cells. The low levels, the short time window of expression (increasing CTEF until 24hpf then drop of fluorescence) and the absence of aggregates can nevertheless explain the absence of significant phenotype in all conditions analyzed.

3. Early cilia defects and protein context

The kinetic analyses indicated that the peak of protein accumulation occurred between 6hpf and 24hpf and that the amount of protein quickly dropped after that stage. Therefore, we established a new time point to phenotype zebrafish embryos.

Convergent-extension assay enables detection of ciliary defects at an early stage

The convergent-extension (CE) assay is performed at the 8-12ss (corresponds to ~14hpf at 28.5°C or ~24hpf at 23°C) and enables the assessment of collective cell migration movements orchestrated by PCP which is a ciliary dependent pathway. It involves the assessment of the body-gap angle during zebrafish embryo segmentation and has been used to measure cilia defects in zebrafish in several studies [313,329]. We first performed this assay on embryos injected with 100 and 200ng/µL of mRNA coding for the full-length ATXN7 N10 or E104 to verify if those constructs could trigger an early ciliary phenotype despite producing small amounts of proteins. We observed a significant increase in the body-gap angle of embryos injected with 100 and 200ng/µL of N10 or E104 mRNA compared to H2B-GFP injected controls and uninjected siblings (**Figure 6A, B**). There was a significant increase in the body-gap angle of E104 injected embryos compared to N10 injected embryos at 200ng/µL but not at 100ng/µL (**Figure 6B**) suggesting that the overexpression of E104 is more pathogenic than N10 at 200ng/µL and that it might interfere with PCP signaling at this concentration. We monitored the development of the siblings of the embryos evaluated for CE

until 3dpf and confirmed the absence of significant phenotypes in accordance with our first experiments.

Co-injection of human WT and mutant mRNA

The analysis of nuclear inclusions found in mammalian cells overexpressing mATXN7 revealed that they contained not only truncated polyQ expanded ATXN7 but also additional proteins including WT ATXN7 [252] and USP22, another component of SAGA [349]. Therefore, we hypothesized that the absence of aggregate and phenotype in the injected embryos might be due to unfavorable context such as the lack of human WT ATXN7 or the 48% of difference in the protein sequence of human ATXN7 and its zebrafish ortholog which might be necessary for interactions. Thus, we compared the injection of 100 or 200ng/µL of mRNA coding for N10 or E104 alone with the co-injection of 100 or 200ng/µL of each mRNA in zebrafish embryos (**Figure 6A**). We performed the CE assay and followed the development of the injected siblings until 3dpf. We measured a significant difference in the body-gap angle of embryos co-injected with 100 or 200ng/µL of N10 and E104 (average of 51.6° and 58.9° at 100 or 200ng/µL respectively) compared to H2B-GFP injected (45°) and uninjected controls (43.7°) (**Figure 6B**). However, the co-injection of N10 and E104 mRNAs were not significantly different from the injection of N10 mRNA alone. We concluded that the co-injection of mRNA coding for WT and mutant ATXN7 did not increase proteotoxicity. At later stages, we observed few cyclops (1-6%) but no significant phenotypes.

Injection of zebrafish mRNA to favor endogenous interactions

To favor interactions with endogenous proteins, we switched to ATXN7 of zebrafish origin. Therefore, we prepared mRNA coding for WT Atxn7 mRNA (bearing 5 CAG repeats) and performed injections and phenotyping. The CE assay showed a significant increase in the body-gap angle of embryos injected with Atxn7 mRNA (83.7°) compared to embryos injected with H2B-GFP mRNA (41.4°) and uninjected siblings (41.3°) (**Figure 6C**). Observations at

later stages showed low frequencies of eye phenotypes at 24hpf: 0% and 6% of cyclopia, and 4% and 9% of unilateral ano- or microphthalmia at the concentrations of 100 and 200ng/uL of mRNA respectively (**Supp. Figure 3A**). We prepared mutant *atxn7* construct (bearing 61 CAG repeats; mAtxn7; Eurofins) and the preliminary injections of 100 and 200ng/uL of mRNA did not lead to any significant phenotype, no more than 1% of the injected embryos presented with defects in the assessed organs (**Supp. Figure 3A**). Mortality was low in every condition (≤1%) (**Supp. Figure 3B**). Because embryos injected with *mAtxn7* mRNA were indistinguishable from uninjected siblings at 2dpf, we decided not to perform the CE assay. Considering the strong effect of WT Atxn7 mRNA on the body-gap angle, we would have first needed to titrate down the mRNA to find a concentration where WT *Atxn7* mRNA would not trigger a phenotype to allow interpretation.

4. Summary and concluding remarks

The injection of dose curves of human WT and mutant *ATXN7* mRNA, which were shown to be expressed properly via the visualization of fluorescence, were not sufficient to trigger protein aggregation or significant ciliary phenotypes that could be characterized further in our zebrafish models. The co-injection of both WT and mutant ATXN7 mRNA did not exacerbate proteotoxicity as assessed by the CE experiment and the general aspect of the embryos until 3dpf. We suspect that no aggregates were formed and this was verified in cryo-sections from early stage injected embryos (<24hpf). The injection of zebrafish mRNA generated encouraging results and further work could inform on the relationship between Atxn7 and cilia. However, the absence of striking phenotypes at 2dpf diminishes the potential of a zebrafish developmental model to study SCA7. Now that the SCA7 knock-in mouse model SCA7$^{104Q/5Q}$ is available in our group, investigation of cilia anomalies can be performed in a mammalian model which is more relevant to SCA7 disease and therapeutic opportunities. Therefore, efforts were concentrated towards the other projects.

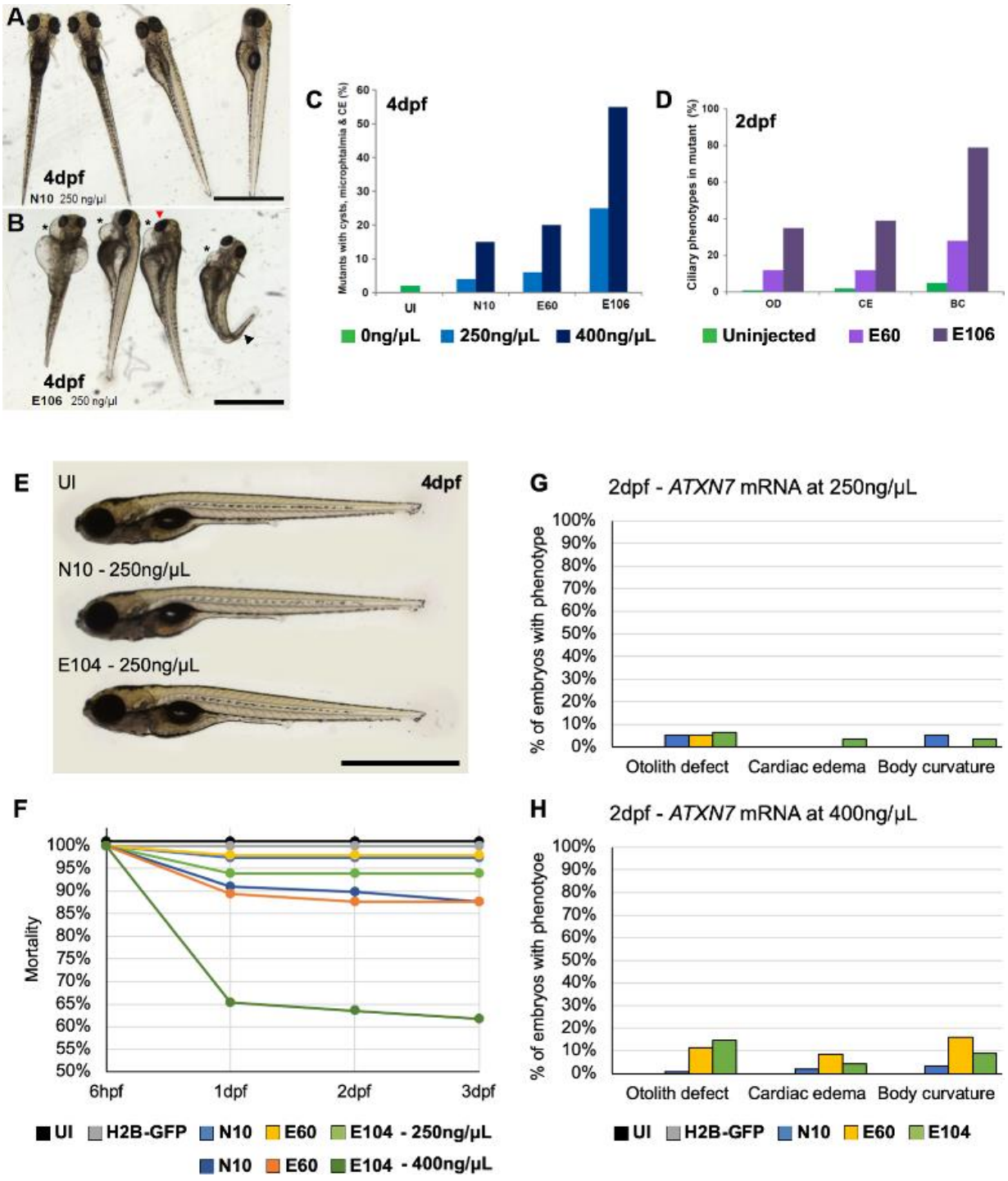

Figure 1: Discrepancy in SCA7 models from mRNA injections.

Figure 1: Discrepancy in SCA7 models from mRNA injections.

A. Dorsal and lateral views of zebrafish injected with 250ng/µL of human WT *ATXN7* mRNA (N10), and **B.** human mutant *ATXN7* mRNA (E106). A portion of E106-injected embryos have cardiac edema (CE, *) a dorsal body curvature (BC, ▼) and otolith defects (not visible at this magnification). Rare cyclops were observed (▼) **C.** Quantification of 4 days-post-fertilization (dpf) larvae with phenotypes to show dose dependency. n=80 larvae/condition. **D.** Quantification of 2dpf embryos with phenotypes to show polyQ dependency. n=60 embryos per group. **E.** Lateral view of 4dpf newly injected embryos with 250ng/µL of human *ATXN7* mRNA, more than 90% of injected embryos looked like uninjected controls. **F.** Mortality showing an increase in embryo death as the concentration of mRNA increases. **G., H.** Quantification of 2dpf embryos with phenotypes when injected with 250ng/µL of ATXN7 mRNAs (**G**) and 400ng/µL of ATXN7 mRNAs (**H**). n=50-100 embryo per condition, representative experiments showed, N=2 biological replicates. Scale bars = 1mm. UI: uninjected. Figures A-E and legends are adapted from [276].

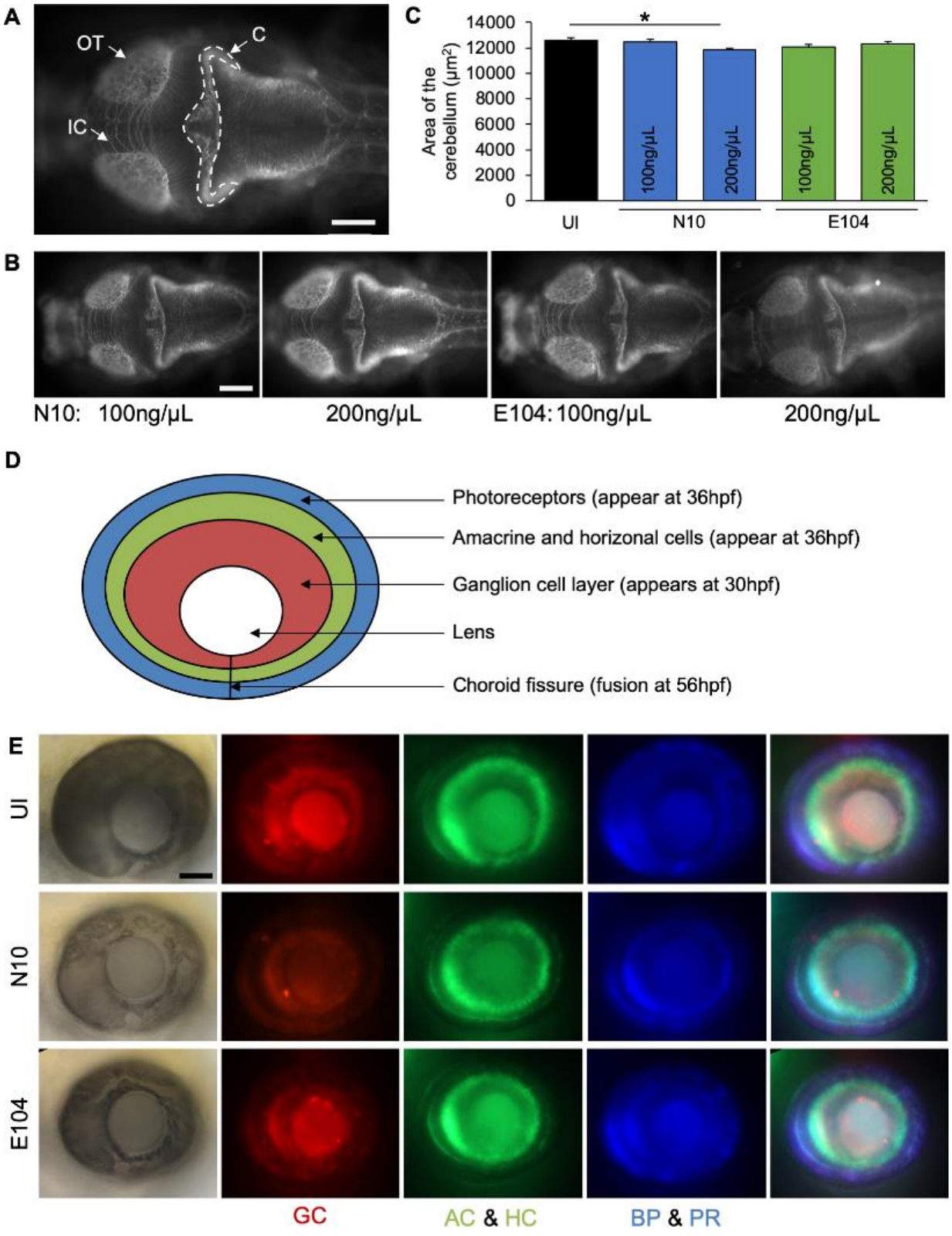

Figure 2: Characterization of the cerebellum and retina of SCA7 larvae.

Figure 2: Characterization of the cerebellum and retina of SCA7 larvae**.**

A. Dorsal view of an uninjected control stained with anti-acetylated α-tubulin to highlight the brain structures of the larva: OT: optic tectum, IC: intertectal connections and C: cerebellum. **B.** Dorsal views of stained larva injected with *ATXN7* mRNAs. **C.** Quantification of the cerebellum area (dashed area in **A**) for all conditions. n=39-48 embryos per condition, repeated. Error bars indicate standard error of the mean. *p<0.05. **D.** Schematic of the retina of a SoFa1 embryo showing the different fluorescent layers of retinal neurons and when they first differentiate. **E.** Lateral views of the eyes of 3dpf zebrafish embryos injected with 400ng/µL of human *ATXN7* mRNA. UI: uninjected, GC: ganglion cell layer, AC: amacrine cells, HC: horizontal cells, BP: bipolar cells, PR: photoreceptors. White scale bars = 100µm, black scale bars = 50µm.

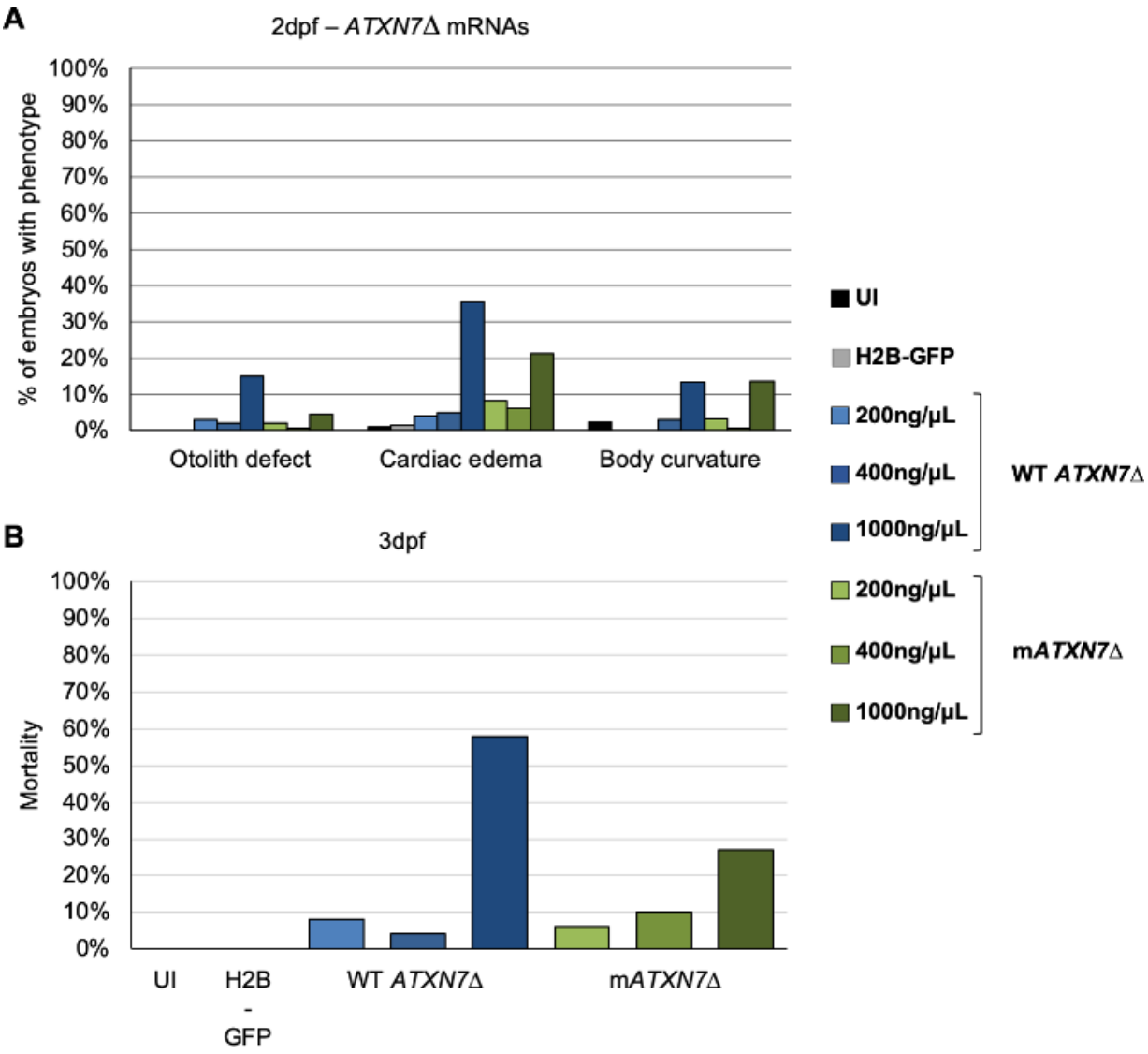

Figure 3: Injection of *ATXN7*Δ mRNA does not trigger more phenotypes in a dose-dependent manner.

A. Quantification of 2dpf embryos with phenotypes when injected with increasing concentrations of mRNA. **B.** Cumulative mortality at 3dpf shows that 1000ng/µL of ATXN7Δ mRNA is highly toxic. n=60-100 embryos per condition, representative experiments are shown, N=2 biological replicates.

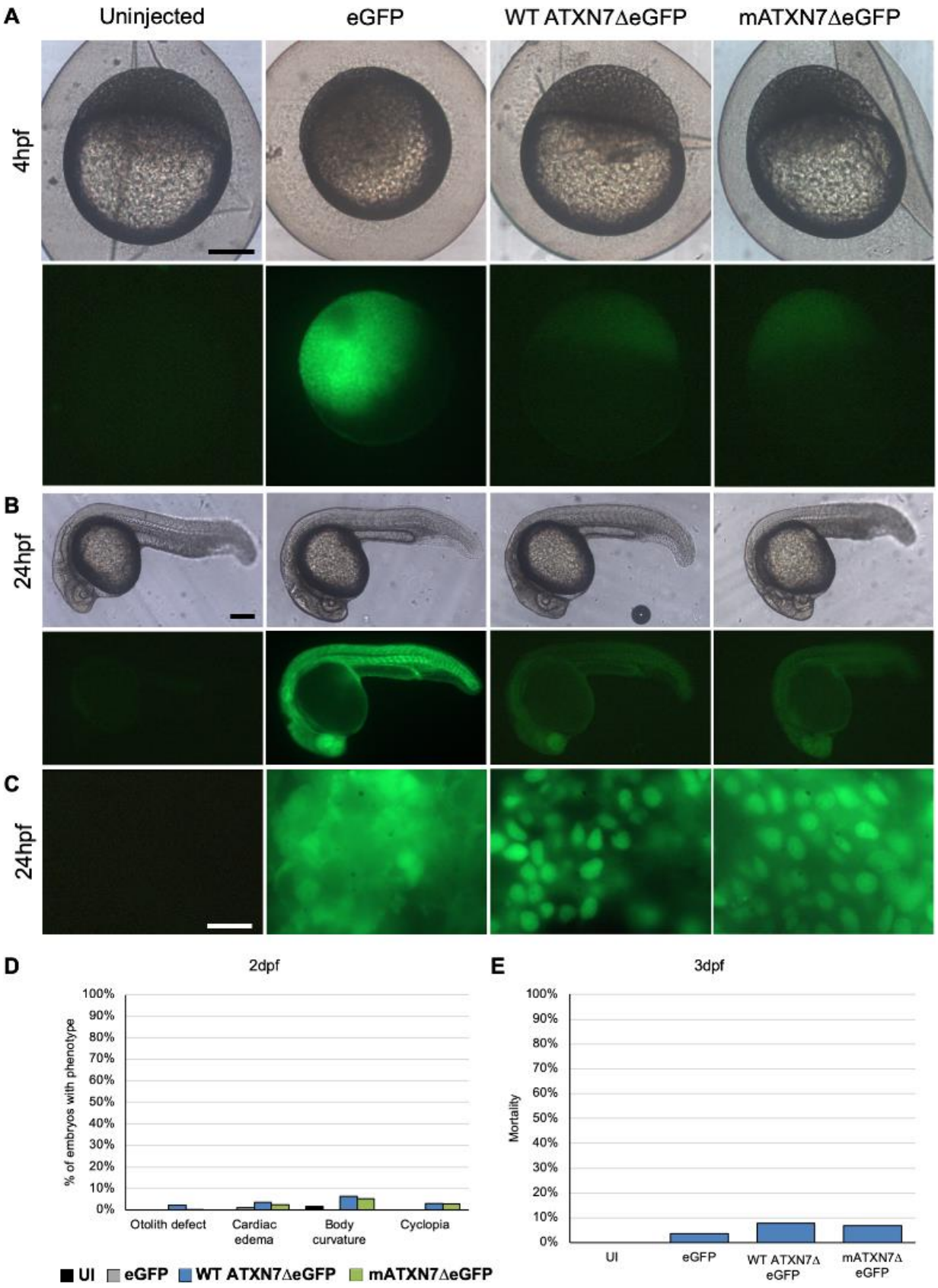

Figure 4: Injection of mRNAs coding for fusion fluorescent ATXN7 proteins to control for expression.

Figure 4: Injection of mRNAs coding for fusion fluorescent ATXN7 proteins to control for expression.

A. Images showing that eGFP is visible at 4 hours-post-fertilization (hpf) in embryos injected with 400ng/µL of mRNA coding for control eGFP, wild-type and mutant ATXN7ΔeGFP (mATXN7ΔeGFP). **B.** The fluorescent signal remains at 24hpf, embryos injected with mRNA coding for eGFP are the brightest. **C.** Cryo-sections of 24hpf embryos showing fluorescence in cerebellar cells. **D.** Quantification of 2 days-post-fertilization (dpf) embryos with phenotypes. WT ATXN7ΔeGFP and mATXN7ΔeGFP mRNAs injected at 400ng/µL. **E.** Quantification of the mortality at 3dpf. n=60-150 embryos per condition, N=2 biological replicates, representative experiments are shown. Black scale bars = 200µm, white scale bars = 10µm. UI: uninjected.

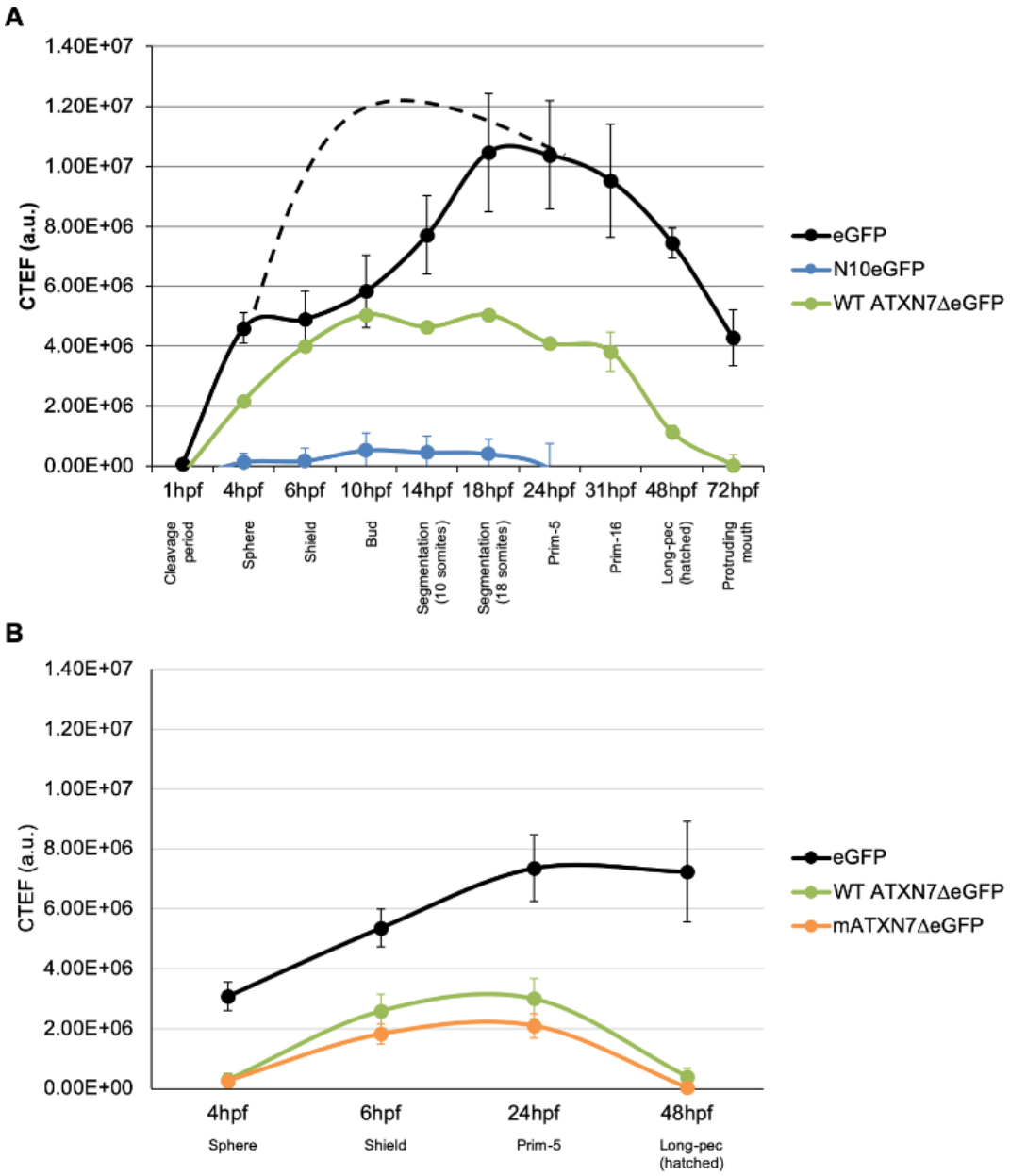

Figure 5: eGFP kinetic comparison studies.

A. Plot of the average CTEF of 6 live embryos per condition followed during development. Saturation was observed in images of eGFP injected embryos between 4hpf and 24hpf suggesting that the true CTEF is higher than what was calculated (dashed line). **B.** Comparison between the CTEF of ATXN7ΔeGFP and mATXN7ΔeGFP injected embryos revealed no significant differences.

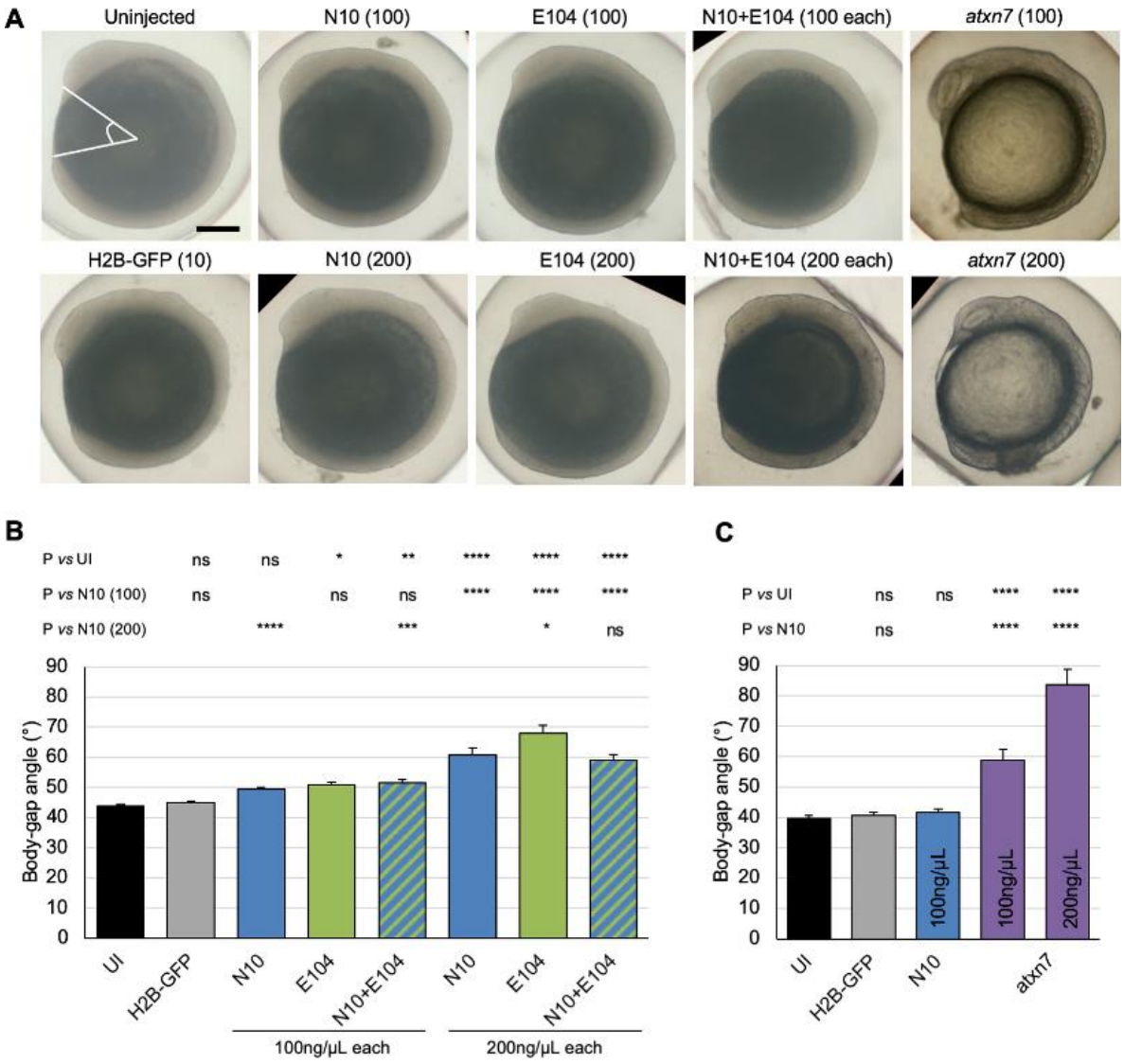

Figure 6: Convergent-extension assay.

A. Images of fixed (controls and human mRNA) and live (zebrafish mRNA) 10 somites-stage embryos. Concentration of mRNA in ng/µL injected indicated in brackets. The body-gap angle measured for this assay is indicated in white. Scale bar = 200µm. **B.** Quantification of the body-gap angle of control embryos and embryos injected with human ATXN7 mRNA. n=98-100 embryos per condition, repeated. **C.** Quantification of the body-gap angle of control embryos and embryos injected with zebrafish *atxn7* mRNA. n=25-60 embryos per condition, representative experiments are showen, N=2 biological replicates. Error bars indicate standard error of the mean. *p<0.05, **p<0.01, ****p<0.0001, ns: not significant. UI: uninjected.

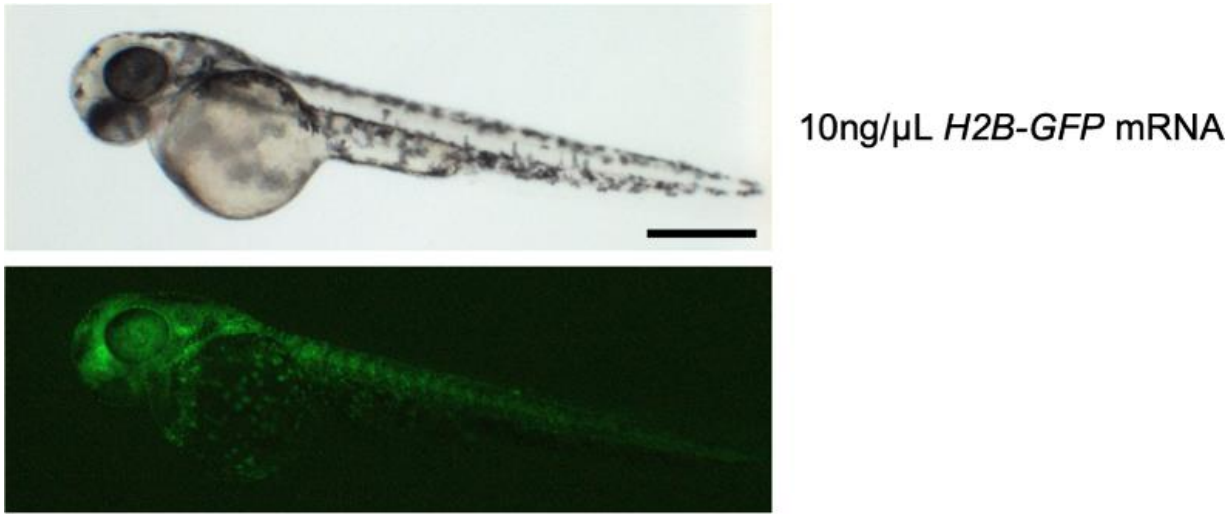

Supplementary Figure 1: Embryos injected with H2B-GFP mRNA are fluorescent.

Representative image of a 2 days-post-fertilization embryo injected with 10ng/µL of mRNA coding for H2B-GFP. No apparent phenotype is visible and fluorescence can be detected which confirms the expression of the injected mRNA. Scale bar = 500µm.

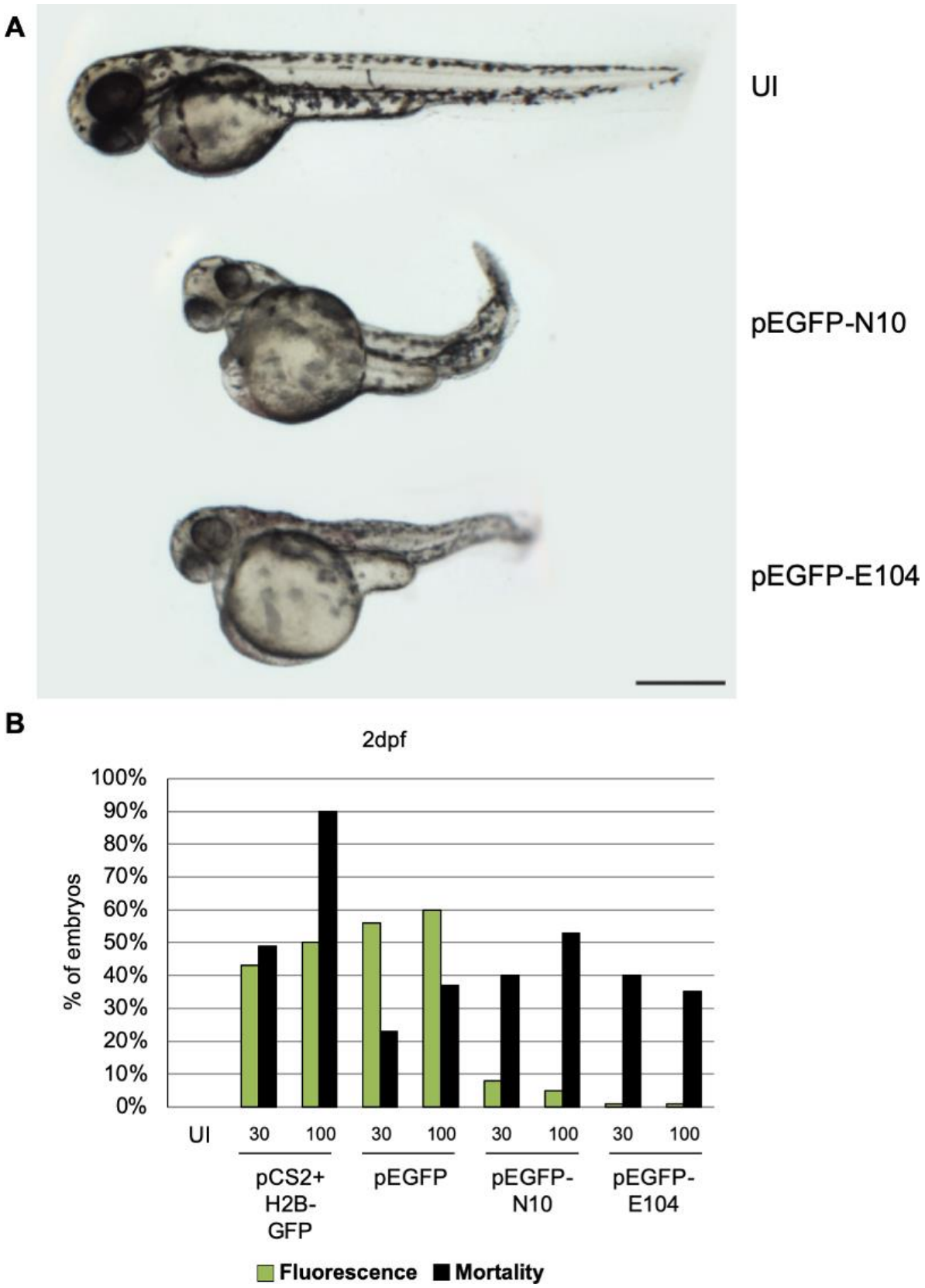

Supplementary Figure 2: Embryos injected with plasmids coding for ATXN7 proteins are severely affected.

Supplementary Figure 2: Embryos injected with plasmids coding for ATXN7 proteins are severely affected.

A. Representative images of a 2 days-post-fertilization uninjected (UI) zebrafish embryo and siblings injected with 30ng/µL of expression plasmids coding for WT ATXN7 (pEGFP-N10) and mATXN7 (pEGFP-E104) fused to eGFP. Surviving embryos have small heads and eyes, are developmentally delayed and have gnarled tails which are signs of non-specific toxicity. Scale bar = 500µm. **B.** Quantification of fluorescent and dead embryos at 2dpf. Concentrations of injected plasmids in ng/µL are indicated below the histogram. n=60-95 embryos per condition.

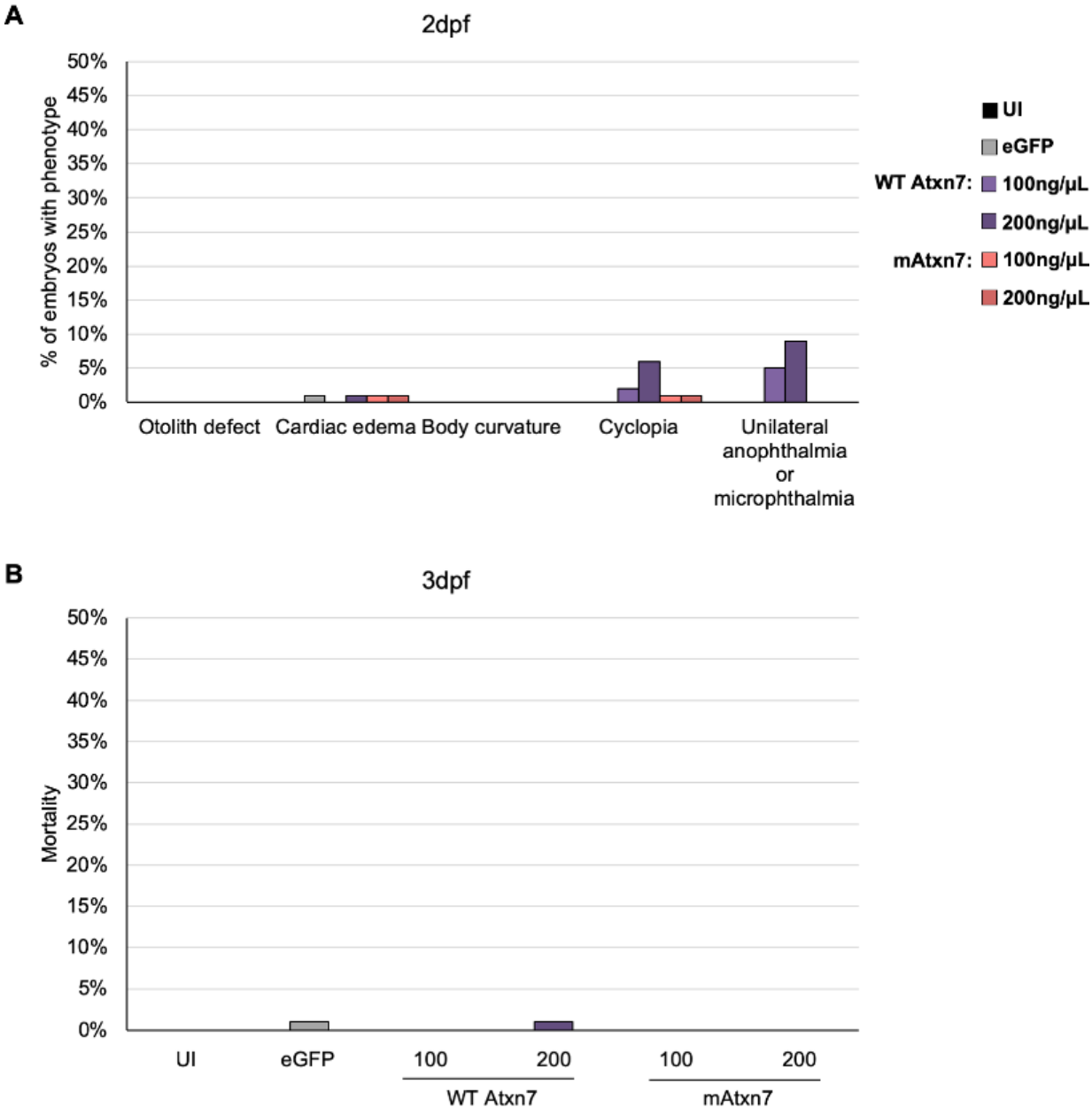

Supplementary Figure 3: Embryos injected with mRNA coding for zebrafish Atxn7 do not present the expected ciliary-phenotypes.

A. Quantification of embryos with a phenotype observed at 2 days-post-fertilization. **B.** Mortality at 3dpf, concentrations of injected mRNA in ng/µL are indicated below the histogram. n=60-135 embryos per condition, N=2 biological replicates, representative experiments are shown.

III. Other opportunities to explore the advantages of the zebrafish to model human genetic diseases,

1. Studying organs in zebrafish embryos which are typically affected in ciliopathies

An overarching mission of the CHDM is to understand the genetic architecture of rare human genetic disorders. Thus, I had the opportunity to work on two additional projects: the first one focused on an autosomal dominant retinal ciliopathy, and the second one focused on congenital kidney malformations which are commonly found in ciliopathies. My contribution to both studies consisted of characterization of the affected organs in zebrafish models.

1.1 Mutations in the Kinesin-2 motor KIF3B cause an autosomal dominant ciliopathy

Our collaborators identified two families with typical ciliopathy symptoms including retinal degeneration and polydactyly. WES enabled to identification of candidate variants in the Kinesin-2 motor KIF3B which were inherited in an autosomal dominant manner in one pedigree, and appeared *de novo* in the proband of the second pedigree. Analysis of patients' fibroblasts from a single proband revealed longer primary cilia. To functionally confirm the variants *in vivo*, we injected wild-type and mutated human *KIF3B* mRNA into zebrafish embryos and monitored their development. We were especially interested in characterizing their eye phenotypes. I participated to this project by 1) performing cryo-sections of 5dpf embryos; 2) staining retina sections with antibodies labelling cilia to measure the connecting cilia in photoreceptors; 3) performing TUNEL on retina sections to measure cell death; and 4) editing the manuscript (results are shown in **Figure 4 D,E**, **Figure S3** and **Figure S4** of the following manuscript). This work lead to the preparation of a manuscript which is in revision at the *American Journal of Human Genetics*.

In this study, we show that the variants identified in patients lead to longer cilia *in vitro* and *in vivo*; and that rhodopsin, which is transported via the connecting cilium from the inner to the outer segments of photoreceptors, is mis-localized in rod inner segments of zebrafish embryos injected with human mutated *KIF3B* mRNA. Considering that most ciliopathies are inherited in an autosomal recessive pattern, this study represents a rare example of an autosomal dominant ciliopathy. Our work also shows that perturbation of KIF3B can result in either dominant toxic effects as shown here for humans, or it can result in recessive disease as reported previously for multiple mutant model organisms including mouse and zebrafish [8,350].

1.2 Association study identifies GREB1L mutations in congenital kidney malformations

Kidney defects are one of the hallmarks of ciliopathies and can be found through the whole spectrum of ciliopathies: from some severe forms of Senior-Loken syndrome to perinatal lethal Meckel-Grüber cases [351]. Although the cellular defect did not involve ciliary dysfunction, this project was an opportunity to learn how to stain, measure and interpret data regarding the zebrafish pronephros. Because this study is less closely related to the topic of this thesis manuscript, the publication will not be included.

Renal agenesis and hypodysplasia are severe conditions which affect about 0.5% of the population, but only 15% of the cases have known genetic causes. Our collaborators identified a candidate gene which could contribute to kidney anomalies in cohorts of patients with renal agenesis and hypodysplasia. To further validate the candidacy of *GREB1L,* we characterized renal phenotypes in zebrafish mutants and morphants and performed functional testing of the missense variants identified in patient cohorts. I contributed to this project by 1) providing support to Kamal Khan to characterize the loss of function models and to test the different variants; 2) preparing **Figure 2**, **Figure 3**, **Figure S3**, **Figure S4** and **Table S7**; and 3) editing the manuscript. I performed whole-mount immunostaining of 4dpf larvae and imaged them (results are showed in **Figure 3**, **S3**, **S4** and **Table S7** of the publication: [317]).

This work enabled the identification of *GREB1L* as a new gene contributing to renal agenesis and hypodysplasia which improves our understanding of the complex genetics behind these conditions, and will inform future diagnosis of kidney malformations.

2. The role of Atxn7 in the development of the zebrafish brain and eye

The primary research interest of Dr. Yvon Trottier's laboratory is to understand the pathomechanisms underlying two polyglutamine expansion diseases: Huntington's disease and SCA7. Therefore, the thesis project led by Dr. Samantha Carrillo-Rosas was to develop and characterize a model of *ATXN7* loss of function with a focus on the photoreceptor.

Because the *Atxn7* knockout mouse was not available, the zebrafish offered a quick and relevant alternative to generate this model. Indeed, the use of morpholinos and CRISPR/Cas9 tools enabled the partial and complete loss-of-function of *atxn7* and the rapid development of the embryos enabled monitoring of the development of the retina, a major affected structure in SCA7, over the course of a week. Humans and mice have an overall similar cone-rod ratio in their retina (mouse: 97:3, human:95:5). However, humans are diurnal and their fovea is enriched in cones. As the fovea corresponds to the site where neurodegeneration initiates in SCA7, diurnal zebrafish with a cone-rod ratio of 65:35 are relevant to model SCA7 retinopathy [352]. I contributed to this project by 1) performing preliminary ISH; 2) titrating the splice-blocking morpholino as well as the human wild-type ATXN7 mRNA to perform the rescue experiments; and 3) editing the manuscript. This work led to a publication which has been cited in this manuscript: [272].

In this paper, we show that Atxn7 plays an important role in the development of the zebrafish eye and brain. In particular, we show that Atxn7 is required for the proximo-distal patterning of the optic stalk and vesicle, as well as for the closure of the choroid fissure. Deeper characterization of the loss of function models (morphants and CRISPR mutants) suggests that Atxn7 is an indirect negative regulator of the members of the Hedgehog family and that it is required for morphogenesis of the photoreceptor outer segment through the control of *crx* expression. The latest being directly correlated with SCA7 retinopathy and suggesting that partial loss of function of normal ATXN7 in SCA7 patients could account for the retinal degeneration.

DISCUSSION AND PERSPECTIVES

Discussion and Perspectives

In this study, we explored functional links between cilia, a non-coding RNA, and a protein mainly characterized for its role in transcriptional regulation. We used a broad range of techniques which was complemented by the participation in additional projects. From genetic manipulation *in vivo* to immunostaining and targeted sequencing, we investigated ciliary biology from different angles and dissected contributing mechanisms to ciliogenesis and pathogenic consequences of ciliary defects. We validated the role of *let-7b* as a positive regulator of ciliogenesis *in vivo* after previous identification of this miRNA through a medium-throughput *in vitro* screen, and we identified 499 potential *let-7b* targets which could explain its mechanism of action. Despite the non-validation of our hypothesis of *let-7* as a modifier of ciliopathies in our targeted sequencing experiment, we will pursue this work in expanded cohorts and/or candidate target sites. Publication of the results obtained on *let-7* will likely motivate the community to include UTRs in their WES analyses. The ATXN7 study confronted biological obstacles that we could not overcome despite our diverse approaches. However, the hypothesis of a putative role for ATXN7 was neither confirmed nor refuted and further work in SCA7 mouse models is ongoing in our group (IGBMC).

The zebrafish model in comparison to other model organisms to explore ciliary biology

Aside from cilia, the common theme among the different studies described was the use of the zebrafish model organism to explore questions around the cilium. From the characterization of immotile flagella in *Chlamydomonas* mutants which highlighted the role of the central pair of tubules cilia motility [353], to the mouse model of primary ciliary dyskinesia [11], a collection of model organisms contributed to the expansion of our understanding of ciliary biology and ciliopathies.

Chlamydomonas is a unicellular algae which can explore its environment by propelling itself with its two flagella [354]. It presents several advantages to study motile cilia: flagella are long (12µm) and can be easily isolated for proteomics analyses [355], and it is inexpensive to maintain. Although mostly used in fundamental research, there are several examples where studies in *Chlamydomonas* enabled to explore ciliopathy mechanisms. For instance, Miertzschke *et al.* used the crystal structure of arl13b to predict the functional effect of the mutation p.R79Q identified in *ARL13B* in patients affected with Joubert syndrome. They concluded that the arginine residue was playing an important role in the protein conformation and that the mutation was probably leading to a loss of the protein function [356]. Perhaps the most famous contribution of *Drosophila* to the field of cilia research is the study of morphogenes which function through the primary cilium. Close to five decades after the first observation of PCP defects [114], we are still learning from *Drosophila* about Wnt mechanisms. Indeed, recent work showed that the polarization of centrioles in *Drosophila* wings depended on two different PCP protein complexes: the Frizzled-PCP and the Fat-PCP [357].

As more genetic manipulations and imaging technologies became available, more complex organisms including zebrafish [313], mice [95,96], rabbits [19] and even hamsters [55] were used to study cilia. Mice remain the favored model to study underlying mechanisms of ciliopathy due to their closest relationship to humans (99% of their genes possess a human homolog [358]). However, zebrafish are less expensive to maintain and are transparent, with ciliated organs which are easily accessible. The KV mentioned in this study is an examplar. Additionally, the *ex vivo* development of zebrafish and shorter generation time allow easy gene manipulations. Zebrafish also present the opportunity to screen therapeutic compounds [359].

In this work, zebrafish appeared as a powerful tool by successfully replicating *in vitro* observations such as the cilia shortening in the *let-7b* experiments or the cilia lengthening in the *KIF3B* experiments. It was also shown to be relevant in modeling human diseases such as the eye anomalies caused by dominant mutations in *KIF3B*, and the kidney developmental

defects caused by loss of function of *GREB1L*. However, the zebrafish also showed limitations in the modeling of SCA7 where low protein expression could not trigger relevant phenotypes. Nonetheless, zebrafish remains a relevant organism to model neurological disorders [360,361].

on let-7b miRNA

Strengths and limits of the zebrafish depleted in *let-7b* or overexpressing *let-7b-5p*

To validate further the effect of *let-7b* on ciliogenesis and cilia maintenance, we used the zebrafish to test *let-7b in vivo*. We recapitulated the decrease in cilia length: we measured a decrease of 0.6µm in the *let-7b* mosaic F0, and 1.49µm in *the let-7b* morphants. Those reductions are comparable to the decrease of 1.23µm observed *in vitro* which highlights the strength of our model.

The mild cilia length decrease observed in the *let-7b* mosaic F0 correlates with the mild knockdown measured by RT-qPCR despite the guide efficiency calculated at 100%. It is common to observe milder phenotypes in mosaic F0 compared to morphants due to three factors. First, we cannot certify the disruptive nature of the mutations generated by CRISPR/CAS9 technology in our organ of interest, and some mutations might not lead to a complete loss of function of a gene. Second, it has been shown in zebrafish how compensatory mechanisms can arise after a gene ablation but not in the case of a gene knockdown [362]. It is thus possible that cells which completely lost *let-7b* and contributed to form the KV, triggered a compensatory mechanism. Third, the genome manipulation is permanent but does not affect maternal transcripts which are actively expressed until 4hpf. Whereas morpholinos regulate expression of all transcripts. In the case of the *let-7b* mosaic F0, the hypothesis of the maternal transcript to explain mild phenotypes is unlikely since it is

crucial for the zebrafish embryonic cells to maintain their proliferative capacity and pluripotency until at least 6hpf [363], and that *let-7* is known to contribute to cell differentiation [364]. We targeted only the *let-7b* locus, and within that strategy, our gRNA targeted the Drosha processing site and not the mature sequence directly due to technical constraints. It is thus likely that the mild effect observed in *let-7b* mosaic F0 is caused by the two other possible explanations. There might be compensation from the 17 other *let-7* loci coding for the nine other members of the *let-7* family, and/or the mutations affecting the Drosha processing site might not all be disruptive and some mature *let-7b* might still be produced in some cells. Future work on the *let-7b* F3 knockout will ensure stability of the mutation and absence of any potential maternal transcripts. The F1 generation has just reached maturity and should be propagated for eventual further experiments, including the phenotyping of other ciliated organs such as the retina and the kidney.

Other approaches to obtain stable mutants depleted of *let-7* consist of either knocking down all *let-7* members, or a subset of them since all *let-7* members were shown to affect ciliogenesis *in vitro*. A previous study demonstrated that it is possible to knockdown the 10 members of the *let-7* family in zebrafish, however the embryos were only used for genotyping at 1dpf or sensor assays at 2dpf and were not characterized [365]. Since the loss of *let-7* is lethal in *C. elegans*, it is likely that the F0 would not survive to adulthood for propagation and that studies might be restricted to mosaic F0. Alternatively, targeting a cluster of *let-7* members might have allowed us to observe stronger phenotypes such as shorter cilia and associated developmental defects including retinal degeneration and kidney cysts [344]. This approach was used by a group who observed an increased activation of B cells in a *let-7adf* knockout mouse model [366]. In their study, authors targeted one *let-7* cluster and knocked out three *let-7* genes altogether.

A limitation of our *in vivo* study of the role of *let-7b* is the normal length and normal cilia density observed in the embryos injected with the *let-7b-5p* mimic despite the observed left-right anomalies. After the striking increase in ciliation and cilia length observed *in vitro* upon transfection of *let-7b-5p* mimic, it was reasonable to expect a similar pattern *in vivo*. The

presence of left-right defects could suggest an anomaly at the level of the beating mechanism. To test this hypothesis, future studies should monitor ciliary beating in the KV of live embryos injected with *let-7b-5p* mimic by either using transgenic zebrafish with a cilia reporter Tg(βact::Arl13b–GFP), or fluorescent beads directly injected in the KV lumen [367]. Another possible explanation is that the RISC was overwhelmed with the quantity of *let-7b-5p* which led to a global dysregulation gene expression and the observed phenotypes. However, this is unlikely as the over-expression of *miR-145* mimic, *miR-203a* mimic, and *miR-210* mimic did not trigger toxicity in zebrafish embryos [368-370]. *miR-145*, *miR-203a*, and *miR-210* are involved in gut and heart development, myelopoiesis, and muscle development respectively, and are expressed at similar levels with that of *let-7b* in the developing zebrafish [323]. *miR-203a* mimic was injected at a concentration as high as 20µM and generated a 46-fold expression increase which is far superior to the 9-fold increase obtained with the injection of 0.8µM of *let-7b-5p* mimic. These observations, and the partial rescue of the left-right asymmetry patterning defect when the mimic was co-injected with *let-7b* morpholino, argue against a toxicity effect via RISC.

Understanding the biological processes targeted by *let-7b* which affect ciliogenesis

To validate further *let-7b* role on ciliogenesis and cilia maintenance, and to understand the level at which *let-7b* is operating to regulate cilia biology, we could perform rescue experiments in different models harboring longer cilia. Depending on the mechanisms leading to longer cilia, such rescue experiments will help identify the steps in cilia biology where *let-7b* intervenes. The zebrafish model developed in the *KIF3B* study represents an opportunity to test whether *let-7b* operates at the level the axoneme elongation. Indeed, KIF3B is involved in anterograde transport of tubulin to the tip of the cilium [371]. To refine the chronology of *let-7b* intervention in ciliogenesis, we could compare this experiment with another model where an earlier step in ciliogenesis is affected. Ciliary membrane elongation occurs prior axoneme elongation and ARL13B is one actor of this initial step. Its over-expression in zebrafish and

mammalian cells leads to longer cilia [372]. Thus, we could test whether *let-7b* intervenes early in ciliogenesis by co-injecting *let-7b* MO with *arl13b* mRNA in zebrafish. We could also focus on ciliary modules such as the BBSome. The over-expression of mutant *BBS3* (p.T31R or p.Q73L) leads to a higher proportion of ciliated htRPE-1 cells in culture [373]. There is a collection of additional models harboring longer cilia such as cultured renal epithelial cells from both *Bbs4* [97] and *Nek8* knockout mice [374], or *Rpgrip1l* knockout mice [375]. However, the longer cilia are generated by the loss of a protein in those cases and it would be challenging to track multiple inhibitory relationships.

Challenges in identifying *let-7b* direct targets

The *in vitro* cilia length data in the context of *let-7* modulation and the recapitulation of the cilia length phenotype *in vivo* strongly support the candidacy of *let-7*, especially *let-7b*, as a positive regulator of ciliogenesis and cilia maintenance. The subsequent identification of direct targets of *let-7b* remains challenging. Indeed, it is possible that the transcripts targeted by *let-7* that function to inhibit ciliogenesis are individually weakly modulated. Only the cumulative knockdown would regulate ciliogenesis rather than the strong negative regulation of a single transcript [376]. Moreover, the study is limited by our current knowledge on both miRNAs and cilia. Those different aspects are discussed below. However, we identified 499 candidates and possible regulatory networks providing a partial answer to the complex role of *let-7*.

Gene network. Since miRNAs have many different target transcripts, it is likely that *let-7* regulates not only the expression of one negative regulator of ciliogenesis, but a network of genes which act together. The functional enrichment analysis we performed on the transcriptomic data suggested a role for *let-7b* on cell adhesion and organization of the extracellular matrix. However, extracellular matrix changes, including excessive secretion of collagen, were observed in the heart of conditional *Ift88* knockout mice lacking cilia in this organ [333]. Additionally, collagen is known to interact with integrins which represents a significant proportion of cell adhesion molecules detected in our study [377]. Thus, we

hypothesized that the enrichment analysis showed pathways stimulated as a consequence of cilia loss, and not pathways directly controlled by *let-7b*. Review of our list of 499 candidates obtained after further filtering enabled confirmation of the enrichment in cell adhesion proteins. However, we also found actin-interacting proteins which shape the actin cytoskeleton for cell motility; these are associated with tumor invasiveness (*ENAH*, *AFAP1*, *FSCN1*). Thus, we focused on the actin anchoring property of the cell adhesion molecules rather than their extra cellular matrix interaction properties. It has been shown at different levels how the actin cytoskeleton can interfere with ciliogenesis [92,303,335], therefore, we propose that *let-7* is a modulator of the actin cytoskeleton at the expression level. To validate this hypothesis, we could first use phalloidin dye to stain actin in the htRPE-1 cells and compare the cytoskeleton between control cells and cells treated with either *let-7b* inhibitor and *let-7b-5p* mimic. Of note, the cytoskeleton dynamics are crucial to cell motility and a role for *let-7* on the regulation of actin could bring insights in the mechanism behind metastasis observed in cancers where *let-7* is mis-regulated [378,379].

***let-7b* specificity.** The knockdown of each *let-7* member in htRPE-1 cells led to fewer ciliated cells and shorter cilia, and loss of *let-7b* had the most marked effect. This suggests that *let-7b* has a specific affinity for a gene, or a network of genes, regulating ciliogenesis and cilia maintenance. When we used this affinity criterion which was available in the TargetScan database, we did not find an overlap with our list of predicted and validated negative regulators of ciliogenesis. There are two possible explanations for this result. First, the list of predicted and validated negative regulators is non-exhaustive and is likely to grow in the future as our knowledge of cilia extends. Second, the measurement of the affinity of the *let-7* members is based on the sequences on the 5’ arm of their coding stem-loop. Indeed, the scientific community has gathered much more data on the miRNAs coded on the guide strand which are considered to be the primary active miRNA compared to the other strand of the stem-loop [380]. Thus, we are lacking information on the repression capacity of *let-7b-3p* which could contribute to the regulation of gene expression through *let-7b*. However, the

strong effect obtained *in vitro* from overexpressing only *let-7b-5p* supports a major role for *let-7b-5p* and a minor role for *let-7b-3p*.

Atypical regulation by miRNAs. The mechanism by which a miRNA regulates gene expression at the level of the transcripts depends partly on the type of binding between the seed sequence and the 3'UTR of a mRNA. Perfect base-pairing usually leads to mRNA degradation while imperfect base-pairing leads to translational repression [381]. This has been confirmed for *let-7* in human cultured HeLa cells where constructs bearing perfect base-pairing were degraded, while constructs with imperfect base-pairing were repressed from translation and stored in P bodies (membrane-less organelles with a concentration of RNA-protein complexes for RNA decay) [382]. This is why we performed RNA-seq on htRPE-1 cells and prioritized transcripts which were 1) up-regulated in the context of *let-7b* inhibitor; 2) down-regulated in the context of *let-7b-5p* mimic; and 3) bearing at least one seed complementary sequence. However, it is possible that *let-7* acts through translational repression in htRPE-1 cells, or in zebrafish, to regulate ciliogenesis. It this case, the RNA-seq dataset might not reflect the regulation by *let-7b*. Despite not being translated, mRNAs would still be present in the cytoplasm. In this instance, proteomic analysis would be more relevant to identify miRNA targets. Finally, although this mechanism has not been reported for the *let-7* family of miRNA, some miRNAs can positively regulate gene expression by binding to the 3'UTR of target transcripts and competing with TTP to prevent AU-rich element mediated mRNA decay [383,384]. Notably, we obtained a list of 910 genes which were down-regulated in the context of *let-7b* inhibitor and up-regulated in the context of *let-7b-5p* mimic. It could be relevant to analyze this list of genes and identify possible networks stimulating ciliogenesis.

Further validation of best candidates

Our final list of 499 candidate *let-7b* targets can be refined once we intersect it with the list generated by TargetSan and the list of predicted and validated negative regulators of ciliogenesis. We have tools available to validate and further study the 5 top candidates *LIMK2*,

EIF4G2, *ARL4D*, *RTCA* and *ELOVL4*. Indeed, we could perform rescue experiments by knocking down those genes in htRPE-1 cells, zebrafish stable mutants or *let-7b* morphants with siRNAs or MO depending on the model. We could also perform phenocopy experiments where we would overexpress those genes and see if it recapitulates the cilia defects.

Lessons from the targeted sequencing

To test whether *let-7* could be a modifier gene of ciliopathies, we sequenced *let-7* targets in the 3'UTR of 40 cilia-associated genes, which were selected after analysis of the RNA-seq analysis and contained one or multiple *let-7b-5p* or *let-7b-3p* targets sequences. A mutational burden analysis requires individual data and not aggregated data like the one available in the gnomAD. Indeed, we need to be able to count and compare the number of rare variants (MAF<5% or 1%) in *let-7* target sequences for each individual. It would have thus required the sequencing of a control cohort. However, the paucity of rare variants detected in our patients dissuaded us from performing this financially burdensome experiment. This observation suggests a high conservation of those sites which actually strengthen our hypothesis that miRNA regulation could play an important role in determining the expressivity of a ciliopathy. As the cost of WES decreases every year, it would be relevant to include UTRs to complement WES without necessarily doing whole-genome sequencing.

In our study, we were confronted to a potential population substructure bias which we were unable to overcome. Indeed, a significant portion of our cohort was of Pakistani origin and the gnomAD lacks data on controls from South Asia, at least at the site of the variants investigated. An alternative database is the Great Middle East (GME) variome (http://igm.ucsd.edu/gme/) which is composed of exomes of controls from North Africa, Middle East and South-West Asia which includes Pakistan. However, this database contains exclusively exome data and no UTR.

In the scenario wherein we would have identified candidate variants in *let-7* targets, we would have first validated the effect of the mutation on *let-7* binding *in vitro* through a GFP

sensor assay [385]. We would have transfected cells with *let-7b-5p* mimic alongside with mRNA coding for eGFP associated to the 3'UTR containing the mutation in *let-7* target. We would have measured the resulting fluorescence and compared it to cells transfected with the same reagents but with a corrected *let-7* target. Next, we would have validated the effect of the overexpression of the gene with the mutated 3'UTR by over-expressing it in the htRPE-1 cells and quantifying the fraction of ciliated cells as well as the cilia length.

on ATXN7 and cilia

The injection of our different human constructs did not generate SCA7-related phenotypes (protein aggregation) nor did it reproduce the cilia-related phenotypes obtained in preliminary experiments (otolith defects, cardiac edema, kidney cysts and body curvature). This can be due to an anomaly relative to the injected mRNA or resulting protein, but it could also be due to the model itself. Indeed, some model organisms can be more or less appropriate to the *in vivo* analysis of human diseases. Here, we will discuss both of these aspects, starting with the reagents used to generate the SCA7 zebrafish model.

High concentration of mRNA but low level of accumulated protein

By controlling the expression of the injected mRNA with a fluorescent tag, we understood that little protein was accumulated in the embryos and that it could explain the absence of phenotypic manifestations. However, the reasons for low protein accumulation remain unclear. Our two control mRNAs *H2B-GFP* and *eGFP* were expressed normally as indicated by fluorescence that was visible up to 7dpf, suggesting that the anomaly was specific to *ATXN7* mRNAs. We propose two hypotheses: 1) there is a problem in the translation or

stability of the mRNAs; and 2) the produced protein is unstable and quickly degraded. Inefficient mRNA translation can arise from errors in the 5'UTR while mRNA instability can be due to missing 5'cap and missing or short polyA tail [386,387]. Since all mRNAs, including controls, were generated from the same pCS2+ backbone and SP6 polymerase kit, we can speculate that the difference in expression is not caused by anomalies of the cap, UTR, or polyA tail. There is an inter- and intra-species codon bias affecting translation efficiency [388-390] and zebrafish are no exception [391]. To investigate if a codon bias could explain translation inefficacy of the ATXN7 mRNAs, we uploaded the human and zebrafish ATXN7 coding sequences to the Integrated DNA Technologies (IDT) online tool for codon optimization (https://www.idtdna.com/CodonOpt) and simulated a codon optimization for expression in the zebrafish. About 28% of each sequence (human: 27.7%, zebrafish: 28.2%) required codon optimization according to the Integrated DNA Technologies online tool, which suggests that codons from the human and zebrafish ATXN7 coding sequences are equally efficient. Thus, the hypothesis of the protein instability remains. To test the protein stability of human ATXN7 and H2B, we could use the technique of fluorescence decay after photoconversion [392] on injected embryos younger than 24hpf (before the drop of fluorescence) to calculate the half-life of each protein.

The observation that ATXN7ΔeGFP mRNAs enable more protein accumulation than the mRNAs coding for ATXN7 full-length was an encouraging step in our development of a zebrafish SCA7 model. Even though we were not able to observe the phenotypes noted during the preliminary experiments, we were confident that the mRNAs were expressed correctly. As mentioned in the introduction on SCA7 disease, ATXN7 has a rapid turnover which seems to be necessary for its proper function. According to the fluorescent tag, WT ATXN7ΔeGFP has a longer half-life than N10eGFP, but WT and mutant ATXN7ΔeGFP behave similarly in terms of protein accumulation. Since WT ATXN7Δ lacks the functional domains of ATXN7 which are required for its function within the SAGA complex, it is not surprising that its turnover is different than the full-length protein. However, in the context of SCA7, the polyQ in mATXN7 stabilizes the protein so we could have expected stronger

fluorescence from embryos injected with mATXN7ΔeGFP mRNA compared to WT ATXN7ΔeGFP mRNA.

Zebrafish Atxn7 and cilia

The injection of WT and mutant zebrafish Atxn7 at 100 and 200ng/µL did not trigger the expected cilia-related phenotypes at 2dpf including otolith defects, cardiac edema and body curvature. A small fraction of embryos (less than 10%) presented an anomaly in the formation of the eyes: either cyclopia or unilateral ano- or microphthalmia, which is consistent with the presence of cyclops among embryos injected with human mRNA. However, the injection of zebrafish mRNA generated a CE phenotype while the human WT ATXN7 mRNA did not trigger defects at the same concentration of 100ng/µL. As discussed above, differences in the manifestation of a mRNA over-expression can be caused by anomalies at the level of the translation, or at the level of the protein. Because the same tools were used to prepare the different mRNAs, we concluded that the differences might arise from the level of the synthesized protein instead. Atxn7 is more likely to localize properly and interact with its appropriate partners in the zebrafish embryo compared to the human ATXN7. Indeed, there is 41% of sequence difference between the human and zebrafish ATXN7.

Nonetheless, the CE assay suggests that WT Atxn7 can interfere with PCP, and thus cilia, when overexpressed at early stages of development. To determine with whether Atxn7 interacts with cilia, one should first confirm its expression through quantification or visualization. The preferred technique for protein quantification is the Western blot, however, this technique is challenging because of the lack of an efficient Atxn7 antibody. Therefore, a protein tag could be used to monitor the protein level. We previously chose a fluorescent tag eGFP to follow the course of the expression in real-time. An alternative would be a smaller tag, such as a Flag, Myc or PA tag, which are predicted to be less disruptive than a fluorophore [393]. A small tag presents additional advantages such as the flexibility to choose the detection method: Western blot, whole-mount immunostaining and immunostaining on

cryo-sections with the choice of fluorophore. Furthermore, a Flag tag in N- and C-termini would allow us to account for protein cleavage and investigate the fate of each peptide. Once the expression is confirmed, we could investigate whether Atxn7 participates in ciliary biology. As seen in the *let-7b* morphants, it is possible that cilia defects do not lead to body curvature or otolith defects. Consequently, it is possible that Atxn7 interacts with cilia in zebrafish and further experiments are required to resolve this possibility. We could analyze the KV of the injected animals and label the cilia, the basal body and Atxn7 to look for cilia anomalies, and see if Atxn7 colocalizes with the BB as seen *in vitro*. Then, to characterize the role of Atxn7 in the context of SCA7, we could perform parallel injections of WT and mutant Atxn7 and assess cilium morphology in the retina and cerebellum. A concentration where mAtxn7 triggers cilia anomalies but not WT Atxn7 would be ideal to generate a SCA7-ciliopathy model.

eno2:gal4 x 4xnrUAS-Ataxin-P2A-mCherry transgenic zebrafish

We hypothesized that the low accumulation of the ATXN7 was the reason for the absence of SCA7 phenotype in our injected embryos. Regardless of the protein stability, the stock of injected mRNA is degraded over time which also limits protein aggregation. Thus, an alternative would be the use of a transgenic zebrafish line to allow a continuous production and gradual accumulation of protein. This would also give us the opportunity to analyze more timepoints and organs. Such transgenics would not only have the potential to study the relationship between ATNX7 and cilia but could also be used for the discovery of small compounds which could ameliorate SCA7 phenotypes. To identify drugs capable of improving symptoms of amyotrophic lateral sclerosis, McGown *et al.* have developed a drug screen on 6dpf zebrafish model [394] which corresponds to a stage where we could expect protein aggregation. At the onset of this work, we had ordered a transgenic zebrafish line with a UAS responder module: 4xnrUAS-Ataxin-P2A-mCherry (AMAGEN). When crossed with the GAL4 driver line eno2:gal4 [395], those fish stably overexpress human ATXN7Δ specifically in mature neurons. ATXN7Δ is fused to mCherry through a P2A peptide, which enables the

release of mCherry after synthesis, to monitor expression but to limit interference with ATXN7Δ conformation. The purpose of these fish is to study the interplay of ATXN7 and cilia specifically in the neurons which are more sensitive to mATXN7 proteotoxicity. They are now available but have not been characterized yet. Considering the role of Atxn7 in the differentiation of the photoreceptors [272], it would be appropriate to start with retinal sections and evaluate the presence of anomalies of the connecting cilium.

The choice of the model organism

Rather than a technical issue, it is possible that the observed levels of protein are representative of the rapid turnover of ATXN7, which could be accelerated and polyQ-independent in the context of the zebrafish. Indeed, some model organisms can be more or less appropriate to the modeling of human diseases and there are several instances where humans and model organisms react differently to a pathogenic mutation. For example, there are at least 20 pathogenic variants reported in patients which are fixed in mice [396], which highlights the importance of the context of a variant (whole protein sequence, interactors). More relevant is the collection of Huntington's disease models which are necessary to study the different aspects of the disease [397]. Thus, it is possible that the zebrafish might not develop SCA7 phenotypes with a human protein but remains relevant to study the interplay between Atxn7 and cilia.

Putative ciliary role for ATXN7

Despite the lack of *in vivo* data on the interaction between ATXN7 and cilia at the onset of this work, the strong *in vitro* data and the accumulated observations in SCA7 mouse models support this relationship. As mentioned in the introduction, labelling ATXN7, cilia axonemes and BB in different cell types cultured *in vitro* showed that ATXN7 colocalizes with the BB and is also present in the ciliary compartment. Recently, our group showed that knocking down ATXN7 via siRNA in cultured ARPE-19 cells leads to longer cilia while ATXN7 overexpression

leads to shorter cilia suggesting that ATXN7 could act as a negative regulator of ciliogenesis (**Figure Annex**; Yvon Trottier, unpublished data). Furthermore, we have observed kidney cysts in the SCA7$^{104Q/5Q}$ knock-in mice (**Figure Annex**; Yvon Trottier, unpublished data) which can also be found in a mouse model of Bardet-Biedl syndrome (*Bbs4* knock-out mice, [398]). Cilia were found on podocytes in adult SCA7$^{104Q/5Q}$ knock-in mice while those cells should not be ciliated at this stage (Yvon Trottier, unpublished data) [399].

Interestingly, a function for ATXN7 at the primary cilium could provide a mechanistic explanation for the Shh disturbance observed in the *atxn7* zebrafish morphants. Indeed, we showed in [272] that the loss of function of endogenous Atxn7 leads to increased Shh levels and coloboma, and suggested that Atxn7 indirectly and negatively regulates Shh levels. Since, HH pathway functions through the cilia in zebrafish [118], it is reasonable to hypothesize that Atxn7 might regulate Shh through cilia. This would be consistent with the rare but consistent presence of cyclops in embryos overexpressing ATXN7 as cyclopia is an expected outcome of Shh downregulation [400]. Thus, the level of Atxn7 negatively correlates with the level of Shh. To validate the specificity of this rare but constant phenotype, we would need to show that *ATXN7* expression is higher in the cyclops than in their siblings. This could be achieved by Western blot by using an antibody against the human protein or by introducing a tag in our constructs. To further validate our hypothesis, we could perform an ISH or a RT-qPCR on cyclops and siblings to measure the level of Shh in those animals. Alternatively, it is possible that ATXN7 influences the level of Shh through its role in SAGA and transcription regulation.

The microtubule-binding and -stabilizing properties of ATXN7 [275] represent a possible avenue of investigation for the functional link between this protein and cilia. In their study, Nakamura *et al.*, prepared different constructs to identify the ATXN7 residues involved in the binding to microtubules. Although they concluded that the full protein was most likely necessary for an optimal binding, they identified the amino acid residues 120 to 400 to play a major role in the binding to α-tubulin. It would be relevant to 1) investigate which of these constructs maintain their BB colocalization in different cell types; and 2) test these constructs

in the ARPE-19 cells treated with ATXN7 siRNA to see which constructs would rescue the cilia length phenotype. These experiments will help to determine whether ATXN7 affects ciliogenesis through its microtubule binding property.

ANNEX

Annex

An Excel version of **Table 4** and the four supplementary tables attached to the results part on the miRNA can be read as Excel files:

Table 4: Final list of *let-7b* candidate targets sorted by evidence for being a negative regulator, then by FDR(IC).

Supp Table 1: Validated and predicted negative regulators of ciliogenesis

Supp Table 2: *let-7* targets according to TargetScan database (last download on 06/10/2019)

Supp Table 3: List of cilia-associated genes

Supp Table 4: List of genes which are up-regulated in htRPE-1 cells treated with *let-7b* inhibitor and down-regulated in htRPE-1 cells treated with *let-7b-5p* mimic

Supp Table 5: Loci targeted for sequencing in our ciliopathy cohort

Supplementary information include methods on RNA-seq and targeted sequencing performed in collaboration with Duke sequenging and bioinformatics core, and a figure to illustrate the discussion on the putative ciliary role of ATXN7.

Supplementary methods

RNA-sequencing on htRPE-1 cells

Total RNA was isolated from htRPE-1 cells with TRIzol (Invitrogen) following manufacturer's instructions. RNA-seq data was processed using the TrimGalore toolkit (1), which employs Cutadapt (2) to trim low quality bases and Illumina sequencing adapters from the 3' end of the reads. Only reads that were 20nt or longer were kept for further analysis. Reads were mapped to the GrCh37v75 version of the human genome and transcriptome (3) using the STAR RNA-seq alignment tool (4). Reads were kept for subsequent analysis if they mapped to a single genomic location. Gene counts were compiled using the HTSeq tool (5). Only genes that had at least 10 reads in any given library were used in subsequent analysis. Normalization and differential expression was carried out using the EdgeR (6) Bioconductor (7) package with the R statistical programming environment (8). Because a batch effect was observed in the data, we included batch as a cofactor in the linear model when calculating the significance of the differential expression.

Targeted sequencing

Human gDNA was quantified using fluorometric quantitation on the Qubit 2.0 (ThermoFisher Scientific). Diluted gDNA was then hybridized with a mix of oligos designed to amplify regions of interests across the genome. This amplicon-based assay is designed to capture multiple targets of interest simultaneously and sequence up to 1,536 amplicons in a single pool, using a single reaction. The custom set of oligos used for this study was designed using Illumina Design Studio (9). The list of targeted regions can be found in **Supp. Table 5**. The Illumina TruSeq Custom Amplicon Low Input Library Prep Kit was used to generate the libraries and the manufacturer protocol was followed. After unbound oligos are removed, bound oligos are extended and ligated. A PCR reaction then amplifies the regions of interest while also adding indexes to each library. Amplified and indexed libraries are cleaned and quantified using Qubit. Before pooling and sequencing, fragment length distribution is first assessed on a

2100 Bioanalyzer using the High Sensitivity DNA Kit (Agilent Technologies). Each pool contained a total of ninety-six libraries and were sequenced on a Illumina MiSeq instrument using a 150bp PE protocol. Sequence data was demultiplexed and Fastq files generated using Bcl2Fastq conversion software provided by Illumina.

1. http://www.bioinformatics.babraham.ac.uk/projects/trim_galore
2. Martin, M. Cutadapt removes adapter sequences from high-throughput sequencing reads. EMBnet.journal 17, 10–12 (2011).
3. Kersey, P. J. et al. Ensembl Genomes: an integrative resource for genome-scale data from non-vertebrate species. Nucleic Acids Res. 40, D91–D97 (2011).
4. Dobin, A. et al. STAR: ultrafast universal RNA-seq aligner. Bioinformatics 29, 15–21 (2012).
5. Anders S, Pyl PT, Huber W. HTSeq-a Python framework to work with high-throughput sequencing data. Bioinformatics. 2015 Jan 15;31(2):166-9.
6. Robinson, M. D., McCarthy, D. J. & Smyth, G. K. edgeR: a Bioconductor package for differential expression analysis of digital gene expression data. Bioinformatics 26, 139–140 (2009).
7. Gentleman, R. C. et al. Bioconductor: open software development for computational biology and bioinformatics. Genome Biol. 5, R80 (2004).
8. www.r-project.org
9. https://www.illumina.com/informatics/sample-experiment-management/custom-assay-design.html

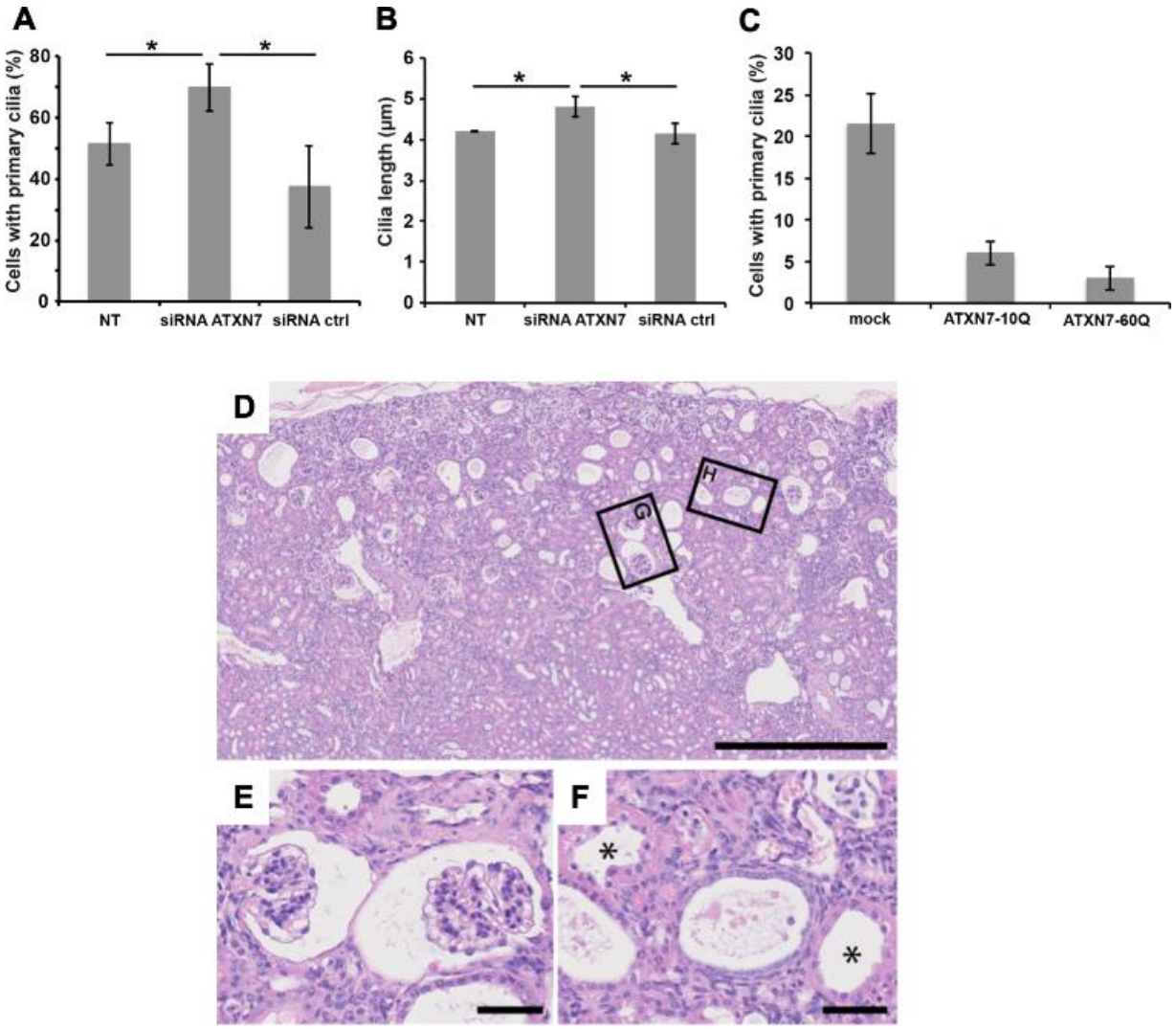

Figure Annex: Recently acquired data supporting a ciliary role for ATXN7.

A. Primary cilia formation in ARPE19 cells treated with ATXN7 siRNA, control (ctrl) siRNA or not treated (NT). 72h-starved cells were immunostained with GT335 antibody to label primary cilia. Percentage of ciliated cells were determined from three independent experiments performed in triplicates (n>900 cells counted per condition; * $p<0.05$). **B.** Quantification of primary cilium length performed in three independent experiments (n>850 cilia per condition; * $p<0.05$). **C.** Primary cilia formation in ARPE19 cells transfected with ATXN7-10Q or ATXN7-60Q expression vectors or empty vector (mock) as control. Percentage of ciliated cells were determined from 2 independent experiments performed in triplicates (n>425 cells per condition). Error bars are standard deviation. **D.** A lower magnification showing the density of cysts. Boxes in (**D**) show higher magnifications of glomerular cysts (**E**) and proximal (asterisks) and distal tubular cysts (**F**). Scale bars: D: 500 µm; E, F: 50 µm. (Yvon Trottier, unpublished data)

BIBLIOGRAPHY

Bibliography

1. Goetz SC, Anderson KV: **The primary cilium: a signalling centre during vertebrate development**. *Nat Rev Genet* 2010, **11**:331-344.

2. Gerdes JM, Davis EE, Katsanis N: **The vertebrate primary cilium in development, homeostasis, and disease**. *Cell* 2009, **137**:32-45.

3. Reiter JF, Leroux MR: **Genes and molecular pathways underpinning ciliopathies**. *Nat Rev Mol Cell Biol* 2017, **18**:533-547.

4. Satir P: **Landmarks in cilia research from Leeuwenhoek to us**. *Cell Motil Cytoskeleton* 1995, **32**:90-94.

5. Worthington WC, Jr., Cathcart RS, 3rd: **Ependymal cilia: distribution and activity in the adult human brain**. *Science* 1963, **139**:221-222.

6. Tilley AE, Walters MS, Shaykhiev R, Crystal RG: **Cilia dysfunction in lung disease**. *Annu Rev Physiol* 2015, **77**:379-406.

7. Whitfield TT: **Development of the inner ear**. *Curr Opin Genet Dev* 2015, **32**:112-118.

8. Nonaka S, Tanaka Y, Okada Y, Takeda S, Harada A, Kanai Y, Kido M, Hirokawa N: **Randomization of left-right asymmetry due to loss of nodal cilia generating leftward flow of extraembryonic fluid in mice lacking KIF3B motor protein**. *Cell* 1998, **95**:829-837.

9. Bloodgood RA: **From central to rudimentary to primary: the history of an underappreciated organelle whose time has come. The primary cilium**. *Methods Cell Biol* 2009, **94**:3-52.

10. Pazour GJ, Dickert BL, Vucica Y, Seeley ES, Rosenbaum JL, Witman GB, Cole DG: **Chlamydomonas IFT88 and its mouse homologue, polycystic kidney disease gene tg737, are required for assembly of cilia and flagella**. *J Cell Biol* 2000, **151**:709-718.

11. Schrick JJ, Onuchic LF, Reeders ST, Korenberg J, Chen XN, Moyer JH, Wilkinson JE, Woychik RP: **Characterization of the human homologue of the mouse Tg737 candidate polycystic kidney disease gene**. *Hum Mol Genet* 1995, **4**:559-567.

12. Huangfu D, Liu A, Rakeman AS, Murcia NS, Niswander L, Anderson KV: **Hedgehog signalling in the mouse requires intraflagellar transport proteins**. *Nature* 2003, **426**:83-87.

13. Nauli SM, Alenghat FJ, Luo Y, Williams E, Vassilev P, Li X, Elia AE, Lu W, Brown EM, Quinn SJ, et al.: **Polycystins 1 and 2 mediate mechanosensation in the primary cilium of kidney cells**. *Nat Genet* 2003, **33**:129-137.

14. Singla V, Reiter JF: **The primary cilium as the cell's antenna: signaling at a sensory organelle**. *Science* 2006, **313**:629-633.

15. Wheway G, Nazlamova L, Hancock JT: **Signaling through the Primary Cilium**. *Front Cell Dev Biol* 2018, **6**:8.

16. Heydeck W, Fievet L, Davis EE, Katsanis N: **The complexity of the cilium: spatiotemporal diversity of an ancient organelle**. *Curr Opin Cell Biol* 2018, **55**:139-149.

17. Ishikawa H, Marshall WF: **Ciliogenesis: building the cell's antenna**. *Nat Rev Mol Cell Biol* 2011, **12**:222-234.

18. Malicki JJ, Johnson CA: **The Cilium: Cellular Antenna and Central Processing Unit**. *Trends Cell Biol* 2017, **27**:126-140.

19. Feistel K, Blum M: **Three types of cilia including a novel 9+4 axoneme on the notochordal plate of the rabbit embryo**. *Dev Dyn* 2006, **235**:3348-3358.

20. Marshall WF: **Basal bodies platforms for building cilia**. *Curr Top Dev Biol* 2008, **85**:1-22.

21. Janke C: **The tubulin code: molecular components, readout mechanisms, and functions**. *J Cell Biol* 2014, **206**:461-472.

22. Tanos BE, Yang HJ, Soni R, Wang WJ, Macaluso FP, Asara JM, Tsou MF: **Centriole distal appendages promote membrane docking, leading to cilia initiation**. *Genes Dev* 2013, **27**:163-168.

23. Mazo G, Soplop N, Wang WJ, Uryu K, Tsou MF: **Spatial Control of Primary Ciliogenesis by Subdistal Appendages Alters Sensation-Associated Properties of Cilia**. *Dev Cell* 2016, **39**:424-437.

24. Clare DK, Magescas J, Piolot T, Dumoux M, Vesque C, Pichard E, Dang T, Duvauchelle B, Poirier F, Delacour D: **Basal foot MTOC organizes pillar MTs required for coordination of beating cilia**. *Nat Commun* 2014, **5**:4888.

25. Gilula NB, Satir P: **The ciliary necklace. A ciliary membrane specialization**. *J Cell Biol* 1972, **53**:494-509.

26. Szymanska K, Johnson CA: **The transition zone: an essential functional compartment of cilia**. *Cilia* 2012, **1**:10.

27. Gupta GD, Coyaud E, Goncalves J, Mojarad BA, Liu Y, Wu Q, Gheiratmand L, Comartin D, Tkach JM, Cheung SW, et al.: **A Dynamic Protein Interaction Landscape of the Human Centrosome-Cilium Interface**. *Cell* 2015, **163**:1484-1499.

28. Hartill V, Szymanska K, Sharif SM, Wheway G, Johnson CA: **Meckel-Gruber Syndrome: An Update on Diagnosis, Clinical Management, and Research Advances**. *Front Pediatr* 2017, **5**:244.

29. Goetz SC, Bangs F, Barrington CL, Katsanis N, Anderson KV: **The Meckel syndrome-associated protein MKS1 functionally interacts with components of the BBSome and IFT complexes to mediate ciliary trafficking and hedgehog signaling**. *PLoS One* 2017, **12**:e0173399.

30. Li C, Jensen VL, Park K, Kennedy J, Garcia-Gonzalo FR, Romani M, De Mori R, Bruel AL, Gaillard D, Doray B, et al.: **MKS5 and CEP290 Dependent Assembly Pathway of the Ciliary Transition Zone**. *PLoS Biol* 2016, **14**:e1002416.

31. Chavez M, Ena S, Van Sande J, de Kerchove d'Exaerde A, Schurmans S, Schiffmann SN: **Modulation of Ciliary Phosphoinositide Content Regulates Trafficking and Sonic Hedgehog Signaling Output**. *Dev Cell* 2015, **34**:338-350.

32. Garcia-Gonzalo FR, Phua SC, Roberson EC, Garcia G, 3rd, Abedin M, Schurmans S, Inoue T, Reiter JF: **Phosphoinositides Regulate Ciliary Protein Trafficking to Modulate Hedgehog Signaling**. *Dev Cell* 2015, **34**:400-409.

33. Molla-Herman A, Ghossoub R, Blisnick T, Meunier A, Serres C, Silbermann F, Emmerson C, Romeo K, Bourdoncle P, Schmitt A, et al.: **The ciliary pocket: an endocytic membrane domain at the base of primary and motile cilia**. *J Cell Sci* 2010, **123**:1785-1795.

34. Caspary T, Larkins CE, Anderson KV: **The graded response to Sonic Hedgehog depends on cilia architecture**. *Dev Cell* 2007, **12**:767-778.

35. Han S, Miyoshi K, Shikada S, Amano G, Wang Y, Yoshimura T, Katayama T: **TULP3 is required for localization of membrane-associated proteins ARL13B and INPP5E to primary cilia**. *Biochem Biophys Res Commun* 2019, **509**:227-234.

36. Garcia G, 3rd, Raleigh DR, Reiter JF: **How the Ciliary Membrane Is Organized Inside-Out to Communicate Outside-In**. *Curr Biol* 2018, **28**:R421-R434.

37. Corbit KC, Aanstad P, Singla V, Norman AR, Stainier DY, Reiter JF: **Vertebrate Smoothened functions at the primary cilium**. *Nature* 2005, **437**:1018-1021.

38. Humbert MC, Weihbrecht K, Searby CC, Li Y, Pope RM, Sheffield VC, Seo S: **ARL13B, PDE6D, and CEP164 form a functional network for INPP5E ciliary targeting**. *Proc Natl Acad Sci U S A* 2012, **109**:19691-19696.

39. Young RW, Bok D: **Participation of the retinal pigment epithelium in the rod outer segment renewal process**. *J Cell Biol* 1969, **42**:392-403.

40. Hogan MC, Manganelli L, Woollard JR, Masyuk AI, Masyuk TV, Tammachote R, Huang BQ, Leontovich AA, Beito TG, Madden BJ, et al.: **Characterization of PKD protein-positive exosome-like vesicles**. *J Am Soc Nephrol* 2009, **20**:278-288.

41. Hogan MC, Bakeberg JL, Gainullin VG, Irazabal MV, Harmon AJ, Lieske JC, Charlesworth MC, Johnson KL, Madden BJ, Zenka RM, et al.: **Identification of Biomarkers for PKD1 Using Urinary Exosomes**. *J Am Soc Nephrol* 2015, **26**:1661-1670.

42. Hoang-Minh LB, Dutra-Clarke M, Breunig JJ, Sarkisian MR: **Glioma cell proliferation is enhanced in the presence of tumor-derived cilia vesicles**. *Cilia* 2018, **7**:6.

43. Nager AR, Goldstein JS, Herranz-Perez V, Portran D, Ye F, Garcia-Verdugo JM, Nachury MV: **An Actin Network Dispatches Ciliary GPCRs into Extracellular Vesicles to Modulate Signaling**. *Cell* 2017, **168**:252-263 e214.

44. Satir P, Christensen ST: **Overview of structure and function of mammalian cilia**. *Annu Rev Physiol* 2007, **69**:377-400.

45. Falk N, Losl M, Schroder N, Giessl A: **Specialized Cilia in Mammalian Sensory Systems**. *Cells* 2015, **4**:500-519.

46. Xu Z, Schaedel L, Portran D, Aguilar A, Gaillard J, Marinkovich MP, Thery M, Nachury MV: **Microtubules acquire resistance from mechanical breakage through intralumenal acetylation**. *Science* 2017, **356**:328-332.

47. Eshun-Wilson L, Zhang R, Portran D, Nachury MV, Toso DB, Lohr T, Vendruscolo M, Bonomi M, Fraser JS, Nogales E: **Effects of alpha-tubulin acetylation on microtubule structure and stability**. *Proc Natl Acad Sci U S A* 2019, **116**:10366-10371.

48. Lee JE, Silhavy JL, Zaki MS, Schroth J, Bielas SL, Marsh SE, Olvera J, Brancati F, Iannicelli M, Ikegami K, et al.: **CEP41 is mutated in Joubert syndrome and is required for tubulin glutamylation at the cilium**. *Nat Genet* 2012, **44**:193-199.

49. Satir P, Heuser T, Sale WS: **A Structural Basis for How Motile Cilia Beat**. *Bioscience* 2014, **64**:1073-1083.

50. Ibanez-Tallon I, Heintz N, Omran H: **To beat or not to beat: roles of cilia in development and disease**. *Hum Mol Genet* 2003, **12 Spec No 1**:R27-35.

51. Soares H, Carmona B, Nolasco S, Viseu Melo L, Goncalves J: **Cilia Distal Domain: Diversity in Evolutionarily Conserved Structures**. *Cells* 2019, **8**.

52. Dalen H: **An ultrastructural study of the tracheal epithelium of the guinea-pig with special reference to the ciliary structure**. *J Anat* 1983, **136**:47-67.

53. Fisch C, Dupuis-Williams P: **Ultrastructure of cilia and flagella - back to the future!** *Biol Cell* 2011, **103**:249-270.

54. Dirksen ER, Satir P: **Ciliary activity in the mouse oviduct as studied by transmission and scanning electron microscopy**. *Tissue Cell* 1972, **4**:389-403.

55. Lam X, Gieseke C, Knoll M, Talbot P: **Assay and importance of adhesive interaction between hamster (Mesocricetus auratus) oocyte-cumulus complexes and the oviductal epithelium**. *Biol Reprod* 2000, **62**:579-588.

56. Wilsman NJ, Farnum CE, Reed-Aksamit DK: **Incidence and morphology of equine and murine chondrocytic cilia**. *Anat Rec* 1980, **197**:355-361.

57. Gluenz E, Hoog JL, Smith AE, Dawe HR, Shaw MK, Gull K: **Beyond 9+0: noncanonical axoneme structures characterize sensory cilia from protists to humans**. *FASEB J* 2010, **24**:3117-3121.

58. Nir I, Cohen D, Papermaster DS: **Immunocytochemical localization of opsin in the cell membrane of developing rat retinal photoreceptors**. *J Cell Biol* 1984, **98**:1788-1795.

59. Maskey D, Marlin MC, Kim S, Kim S, Ong EC, Li G, Tsiokas L: **Cell cycle-dependent ubiquitylation and destruction of NDE1 by CDK5-FBW7 regulates ciliary length**. *EMBO J* 2015, **34**:2424-2440.

60. Inoko A, Matsuyama M, Goto H, Ohmuro-Matsuyama Y, Hayashi Y, Enomoto M, Ibi M, Urano T, Yonemura S, Kiyono T, et al.: **Trichoplein and Aurora A block aberrant primary cilia assembly in proliferating cells**. *J Cell Biol* 2012, **197**:391-405.

61. Lee J, Chung YD: **Ciliary subcompartments: how are they established and what are their functions?** *BMB Rep* 2015, **48**:380-387.

62. Fonte VG, Searls RL, Hilfer SR: **The relationship of cilia with cell division and differentiation**. *J Cell Biol* 1971, **49**:226-229.

63. Tucker RW, Pardee AB, Fujiwara K: **Centriole ciliation is related to quiescence and DNA synthesis in 3T3 cells**. *Cell* 1979, **17**:527-535.

64. Shahid U, Singh P: **Emerging Picture of Deuterosome-Dependent Centriole Amplification in MCCs**. *Cells* 2018, **7**.

65. Nanjundappa R, Kong D, Shim K, Stearns T, Brody SL, Loncarek J, Mahjoub MR: **Regulation of cilia abundance in multiciliated cells**. *Elife* 2019, **8**.

66. Doxsey S, Zimmerman W, Mikule K: **Centrosome control of the cell cycle**. *Trends Cell Biol* 2005, **15**:303-311.

67. Schmidt KN, Kuhns S, Neuner A, Hub B, Zentgraf H, Pereira G: **Cep164 mediates vesicular docking to the mother centriole during early steps of ciliogenesis**. *J Cell Biol* 2012, **199**:1083-1101.

68. Hehnly H, Chen CT, Powers CM, Liu HL, Doxsey S: **The centrosome regulates the Rab11- dependent recycling endosome pathway at appendages of the mother centriole**. *Curr Biol* 2012, **22**:1944-1950.

69. Kuhns S, Schmidt KN, Reymann J, Gilbert DF, Neuner A, Hub B, Carvalho R, Wiedemann P, Zentgraf H, Erfle H, et al.: **The microtubule affinity regulating kinase MARK4 promotes axoneme extension during early ciliogenesis**. *J Cell Biol* 2013, **200**:505-522.

70. Cajanek L, Nigg EA: **Cep164 triggers ciliogenesis by recruiting Tau tubulin kinase 2 to the mother centriole**. *Proc Natl Acad Sci U S A* 2014, **111**:E2841-2850.

71. Kasahara K, Kawakami Y, Kiyono T, Yonemura S, Kawamura Y, Era S, Matsuzaki F, Goshima N, Inagaki M: **Ubiquitin-proteasome system controls ciliogenesis at the initial step of axoneme extension**. *Nat Commun* 2014, **5**:5081.

72. Lu Q, Insinna C, Ott C, Stauffer J, Pintado PA, Rahajeng J, Baxa U, Walia V, Cuenca A, Hwang YS, et al.: **Early steps in primary cilium assembly require EHD1/EHD3-dependent ciliary vesicle formation**. *Nat Cell Biol* 2015, **17**:228-240.

73. Nachury MV, Loktev AV, Zhang Q, Westlake CJ, Peranen J, Merdes A, Slusarski DC, Scheller RH, Bazan JF, Sheffield VC, et al.: **A core complex of BBS proteins cooperates with the GTPase Rab8 to promote ciliary membrane biogenesis**. *Cell* 2007, **129**:1201-1213.

74. Rosenbaum JL, Child FM: **Flagellar regeneration in protozoan flagellates**. *J Cell Biol* 1967, **34**:345-364.

75. Katoh Y, Terada M, Nishijima Y, Takei R, Nozaki S, Hamada H, Nakayama K: **Overall Architecture of the Intraflagellar Transport (IFT)-B Complex Containing Cluap1/IFT38 as an Essential Component of the IFT-B Peripheral Subcomplex**. *J Biol Chem* 2016, **291**:10962-10975.

76. Cole DG, Chinn SW, Wedaman KP, Hall K, Vuong T, Scholey JM: **Novel heterotrimeric kinesin-related protein purified from sea urchin eggs**. *Nature* 1993, **366**:268-270.

77. Stepanek L, Pigino G: **Microtubule doublets are double-track railways for intraflagellar transport trains**. *Science* 2016, **352**:721-724.

78. Jordan MA, Diener DR, Stepanek L, Pigino G: **The cryo-EM structure of intraflagellar transport trains reveals how dynein is inactivated to ensure unidirectional anterograde movement in cilia**. *Nat Cell Biol* 2018, **20**:1250-1255.

79. Haycraft CJ, Schafer JC, Zhang Q, Taulman PD, Yoder BK: **Identification of CHE-13, a novel intraflagellar transport protein required for cilia formation**. *Exp Cell Res* 2003, **284**:251-263.

80. Morris RL, Scholey JM: **Heterotrimeric kinesin-II is required for the assembly of motile 9+2 ciliary axonemes on sea urchin embryos**. *J Cell Biol* 1997, **138**:1009-1022.

81. Mueller J, Perrone CA, Bower R, Cole DG, Porter ME: **The FLA3 KAP subunit is required for localization of kinesin-2 to the site of flagellar assembly and processive anterograde intraflagellar transport**. *Mol Biol Cell* 2005, **16**:1341-1354.

82. Bre MH, Redeker V, Vinh J, Rossier J, Levilliers N: **Tubulin polyglycylation: differential posttranslational modification of dynamic cytoplasmic and stable axonemal microtubules in paramecium**. *Mol Biol Cell* 1998, **9**:2655-2665.

83. Gadadhar S, Dadi H, Bodakuntla S, Schnitzler A, Bieche I, Rusconi F, Janke C: **Tubulin glycylation controls primary cilia length**. *J Cell Biol* 2017, **216**:2701-2713.

84. He M, Subramanian R, Bangs F, Omelchenko T, Liem KF, Jr., Kapoor TM, Anderson KV: **The kinesin-4 protein Kif7 regulates mammalian Hedgehog signalling by organizing the cilium tip compartment**. *Nat Cell Biol* 2014, **16**:663-672.

85. Niwa S, Nakajima K, Miki H, Minato Y, Wang D, Hirokawa N: **KIF19A is a microtubule-depolymerizing kinesin for ciliary length control**. *Dev Cell* 2012, **23**:1167-1175.

86. Chien A, Shih SM, Bower R, Tritschler D, Porter ME, Yildiz A: **Dynamics of the IFT machinery at the ciliary tip**. *Elife* 2017, **6**.

87. Pedersen LB, Miller MS, Geimer S, Leitch JM, Rosenbaum JL, Cole DG: **Chlamydomonas IFT172 is encoded by FLA11, interacts with CrEB1, and regulates IFT at the flagellar tip**. *Curr Biol* 2005, **15**:262-266.

88. May SR, Ashique AM, Karlen M, Wang B, Shen Y, Zarbalis K, Reiter J, Ericson J, Peterson AS: **Loss of the retrograde motor for IFT disrupts localization of Smo to cilia and prevents the expression of both activator and repressor functions of Gli**. *Dev Biol* 2005, **287**:378-389.

89. Lechtreck KF, Van De Weghe JC, Harris JA, Liu P: **Protein transport in growing and steady-state cilia**. *Traffic* 2017, **18**:277-286.

90. Yoshimura S, Egerer J, Fuchs E, Haas AK, Barr FA: **Functional dissection of Rab GTPases involved in primary cilium formation**. *J Cell Biol* 2007, **178**:363-369.

91. Zuo X, Guo W, Lipschutz JH: **The exocyst protein Sec10 is necessary for primary ciliogenesis and cystogenesis in vitro**. *Mol Biol Cell* 2009, **20**:2522-2529.

92. Kim J, Jo H, Hong H, Kim MH, Kim JM, Lee JK, Heo WD, Kim J: **Actin remodelling factors control ciliogenesis by regulating YAP/TAZ activity and vesicle trafficking**. *Nat Commun* 2015, **6**:6781.

93. Follit JA, Tuft RA, Fogarty KE, Pazour GJ: **The intraflagellar transport protein IFT20 is associated with the Golgi complex and is required for cilia assembly**. *Mol Biol Cell* 2006, **17**:3781-3792.

94. Fogelgren B, Lin SY, Zuo X, Jaffe KM, Park KM, Reichert RJ, Bell PD, Burdine RD, Lipschutz JH: **The exocyst protein Sec10 interacts with Polycystin-2 and knockdown causes PKD-phenotypes**. *PLoS Genet* 2011, **7**:e1001361.

95. Nishimura DY, Fath M, Mullins RF, Searby C, Andrews M, Davis R, Andorf JL, Mykytyn K, Swiderski RE, Yang B, et al.: **Bbs2-null mice have neurosensory deficits, a defect in social dominance, and retinopathy associated with mislocalization of rhodopsin**. *Proc Natl Acad Sci U S A* 2004, **101**:16588-16593.

96. Uytingco CR, Williams CL, Xie C, Shively DT, Green WW, Ukhanov K, Zhang L, Nishimura DY, Sheffield VC, Martens JR: **BBS4 is required for intraflagellar transport coordination and basal body number in mammalian olfactory cilia**. *J Cell Sci* 2019, **132**.

97. Mokrzan EM, Lewis JS, Mykytyn K: **Differences in renal tubule primary cilia length in a mouse model of Bardet-Biedl syndrome**. *Nephron Exp Nephrol* 2007, **106**:e88-96.

98. Mukhopadhyay S, Wen X, Chih B, Nelson CD, Lane WS, Scales SJ, Jackson PK: **TULP3 bridges the IFT-A complex and membrane phosphoinositides to promote trafficking of G protein-coupled receptors into primary cilia**. *Genes Dev* 2010, **24**:2180-2193.

99. Kim M, Kim M, Lee MS, Kim CH, Lim DS: **The MST1/2-SAV1 complex of the Hippo pathway promotes ciliogenesis**. *Nat Commun* 2014, **5**:5370.

100. Schou KB, Mogensen JB, Morthorst SK, Nielsen BS, Aleliunaite A, Serra-Marques A, Furstenberg N, Saunier S, Bizet AA, Veland IR, et al.: **KIF13B establishes a CAV1-enriched microdomain at the ciliary transition zone to promote Sonic hedgehog signalling**. *Nat Commun* 2017, **8**:14177.

101. Eguether T, San Agustin JT, Keady BT, Jonassen JA, Liang Y, Francis R, Tobita K, Johnson CA, Abdelhamed ZA, Lo CW, et al.: **IFT27 links the BBSome to IFT for maintenance of the ciliary signaling compartment**. *Dev Cell* 2014, **31**:279-290.

102. Tang Z, Lin MG, Stowe TR, Chen S, Zhu M, Stearns T, Franco B, Zhong Q: **Autophagy promotes primary ciliogenesis by removing OFD1 from centriolar satellites**. *Nature* 2013, **502**:254-257.

103. Wang S, Livingston MJ, Su Y, Dong Z: **Reciprocal regulation of cilia and autophagy via the MTOR and proteasome pathways**. *Autophagy* 2015, **11**:607-616.

104. Sanchez de Diego A, Alonso Guerrero A, Martinez AC, van Wely KH: **Dido3-dependent HDAC6 targeting controls cilium size**. *Nat Commun* 2014, **5**:3500.

105. Pugacheva EN, Jablonski SA, Hartman TR, Henske EP, Golemis EA: **HEF1-dependent Aurora A activation induces disassembly of the primary cilium**. *Cell* 2007, **129**:1351-1363.

106. Kim S, Lee K, Choi JH, Ringstad N, Dynlacht BD: **Nek2 activation of Kif24 ensures cilium disassembly during the cell cycle**. *Nat Commun* 2015, **6**:8087.

107. Anvarian Z, Mykytyn K, Mukhopadhyay S, Pedersen LB, Christensen ST: **Cellular signalling by primary cilia in development, organ function and disease**. *Nat Rev Nephrol* 2019, **15**:199-219.

108. Nusslein-Volhard C, Wieschaus E: **Mutations affecting segment number and polarity in Drosophila**. *Nature* 1980, **287**:795-801.

109. Liu A, Wang B, Niswander LA: **Mouse intraflagellar transport proteins regulate both the activator and repressor functions of Gli transcription factors**. *Development* 2005, **132**:3103-3111.

110. Haycraft CJ, Banizs B, Aydin-Son Y, Zhang Q, Michaud EJ, Yoder BK: **Gli2 and Gli3 localize to cilia and require the intraflagellar transport protein polaris for processing and function**. *PLoS Genet* 2005, **1**:e53.

111. Petrov K, Wierbowski BM, Salic A: **Sending and Receiving Hedgehog Signals**. *Annu Rev Cell Dev Biol* 2017, **33**:145-168.

112. Bangs F, Anderson KV: **Primary Cilia and Mammalian Hedgehog Signaling**. *Cold Spring Harb Perspect Biol* 2017, **9**.

113. Kong JH, Siebold C, Rohatgi R: **Biochemical mechanisms of vertebrate hedgehog signaling**. *Development* 2019, **146**.

114. Sharma RP, Chopra VL: **Effect of the Wingless (wg1) mutation on wing and haltere development in Drosophila melanogaster**. *Dev Biol* 1976, **48**:461-465.

115. Nusse R, Varmus HE: **Many tumors induced by the mouse mammary tumor virus contain a provirus integrated in the same region of the host genome**. *Cell* 1982, **31**:99-109.

116. Oh EC, Katsanis N: **Context-dependent regulation of Wnt signaling through the primary cilium**. *J Am Soc Nephrol* 2013, **24**:10-18.

117. Ocbina PJ, Tuson M, Anderson KV: **Primary cilia are not required for normal canonical Wnt signaling in the mouse embryo**. *PLoS One* 2009, **4**:e6839.

118. Huang P, Schier AF: **Dampened Hedgehog signaling but normal Wnt signaling in zebrafish without cilia**. *Development* 2009, **136**:3089-3098.

119. Corbit KC, Shyer AE, Dowdle WE, Gaulden J, Singla V, Chen MH, Chuang PT, Reiter JF: **Kif3a constrains beta-catenin-dependent Wnt signalling through dual ciliary and non-ciliary mechanisms**. *Nat Cell Biol* 2008, **10**:70-76.

120. Lancaster MA, Louie CM, Silhavy JL, Sintasath L, Decambre M, Nigam SK, Willert K, Gleeson JG: **Impaired Wnt-beta-catenin signaling disrupts adult renal homeostasis and leads to cystic kidney ciliopathy**. *Nat Med* 2009, **15**:1046-1054.

121. Nusse R, Clevers H: **Wnt/beta-Catenin Signaling, Disease, and Emerging Therapeutic Modalities**. *Cell* 2017, **169**:985-999.

122. Wang Y, Zhou CJ, Liu Y: **Wnt Signaling in Kidney Development and Disease**. *Prog Mol Biol Transl Sci* 2018, **153**:181-207.

123. Park TJ, Mitchell BJ, Abitua PB, Kintner C, Wallingford JB: **Dishevelled controls apical docking and planar polarization of basal bodies in ciliated epithelial cells**. *Nat Genet* 2008, **40**:871-879.

124. Simons M, Gloy J, Ganner A, Bullerkotte A, Bashkurov M, Kronig C, Schermer B, Benzing T, Cabello OA, Jenny A, et al.: **Inversin, the gene product mutated in nephronophthisis type II, functions as a molecular switch between Wnt signaling pathways**. *Nat Genet* 2005, **37**:537-543.

125. Dawe HR, Adams M, Wheway G, Szymanska K, Logan CV, Noegel AA, Gull K, Johnson CA: **Nesprin-2 interacts with meckelin and mediates ciliogenesis via remodelling of the actin cytoskeleton**. *J Cell Sci* 2009, **122**:2716-2726.

126. Lee KH, Johmura Y, Yu LR, Park JE, Gao Y, Bang JK, Zhou M, Veenstra TD, Yeon Kim B, Lee KS: **Identification of a novel Wnt5a-CK1varepsilon-Dvl2-Plk1-mediated primary cilia disassembly pathway**. *EMBO J* 2012, **31**:3104-3117.

127. Schou KB, Pedersen LB, Christensen ST: **Ins and outs of GPCR signaling in primary cilia**. *EMBO Rep* 2015, **16**:1099-1113.

128. Ezratty EJ, Stokes N, Chai S, Shah AS, Williams SE, Fuchs E: **A role for the primary cilium in Notch signaling and epidermal differentiation during skin development**. *Cell* 2011, **145**:1129-1141.

129. Tavares B, Jacinto R, Sampaio P, Pestana S, Pinto A, Vaz A, Roxo-Rosa M, Gardner R, Lopes T, Schilling B, et al.: **Notch/Her12 signalling modulates, motile/immotile cilia ratio downstream of Foxj1a in zebrafish left-right organizer**. *Elife* 2017, **6**.

130. Wu S, Huang J, Dong J, Pan D: **hippo encodes a Ste-20 family protein kinase that restricts cell proliferation and promotes apoptosis in conjunction with salvador and warts**. *Cell* 2003, **114**:445-456.

131. Harvey KF, Pfleger CM, Hariharan IK: **The Drosophila Mst ortholog, hippo, restricts growth and cell proliferation and promotes apoptosis**. *Cell* 2003, **114**:457-467.

132. Misra JR, Irvine KD: **The Hippo Signaling Network and Its Biological Functions**. *Annu Rev Genet* 2018, **52**:65-87.

133. Clement DL, Mally S, Stock C, Lethan M, Satir P, Schwab A, Pedersen SF, Christensen ST: **PDGFRalpha signaling in the primary cilium regulates NHE1-dependent fibroblast migration via coordinated differential activity of MEK1/2-ERK1/2-p90RSK and AKT signaling pathways**. *J Cell Sci* 2013, **126**:953-965.

134. Nielsen BS, Malinda RR, Schmid FM, Pedersen SF, Christensen ST, Pedersen LB: **PDGFRbeta and oncogenic mutant PDGFRalpha D842V promote disassembly of primary cilia through a PLCgamma- and AURKA-dependent mechanism**. *J Cell Sci* 2015, **128**:3543-3549.

135. Clement CA, Ajbro KD, Koefoed K, Vestergaard ML, Veland IR, Henriques de Jesus MP, Pedersen LB, Benmerah A, Andersen CY, Larsen LA, et al.: **TGF-beta signaling is associated with endocytosis at the pocket region of the primary cilium**. *Cell Rep* 2013, **3**:1806-1814.

136. Derynck R, Gelbart WM, Harland RM, Heldin CH, Kern SE, Massague J, Melton DA, Mlodzik M, Padgett RW, Roberts AB, et al.: **Nomenclature: vertebrate mediators of TGFbeta family signals**. *Cell* 1996, **87**:173.

137. Mitchell H, Choudhury A, Pagano RE, Leof EB: **Ligand-dependent and -independent transforming growth factor-beta receptor recycling regulated by clathrin-mediated endocytosis and Rab11**. *Mol Biol Cell* 2004, **15**:4166-4178.

138. Monnich M, Borgeskov L, Breslin L, Jakobsen L, Rogowski M, Doganli C, Schroder JM, Mogensen JB, Blinkenkjaer L, Harder LM, et al.: **CEP128 Localizes to the Subdistal Appendages of the Mother Centriole and Regulates TGF-beta/BMP Signaling at the Primary Cilium**. *Cell Rep* 2018, **22**:2584-2592.

139. Koefoed K, Skat-Rordam J, Andersen P, Warzecha CB, Pye M, Andersen TA, Ajbro KD, Bendsen E, Narimatsu M, Vilhardt F, et al.: **The E3 ubiquitin ligase SMURF1 regulates cell-fate specification and outflow tract septation during mammalian heart development**. *Sci Rep* 2018, **8**:9542.

140. Laplante M, Sabatini DM: **mTOR signaling in growth control and disease**. *Cell* 2012, **149**:274-293.

141. Li Y, Corradetti MN, Inoki K, Guan KL: **TSC2: filling the GAP in the mTOR signaling pathway**. *Trends Biochem Sci* 2004, **29**:32-38.

142. Shillingford JM, Murcia NS, Larson CH, Low SH, Hedgepeth R, Brown N, Flask CA, Novick AC, Goldfarb DA, Kramer-Zucker A, et al.: **The mTOR pathway is regulated by polycystin-1, and its inhibition reverses renal cystogenesis in polycystic kidney disease**. *Proc Natl Acad Sci U S A* 2006, **103**:5466-5471.

143. Yuan S, Li J, Diener DR, Choma MA, Rosenbaum JL, Sun Z: **Target-of-rapamycin complex 1 (Torc1) signaling modulates cilia size and function through protein synthesis regulation**. *Proc Natl Acad Sci U S A* 2012, **109**:2021-2026.

144. Choksi SP, Lauter G, Swoboda P, Roy S: **Switching on cilia: transcriptional networks regulating ciliogenesis**. *Development* 2014, **141**:1427-1441.

145. Mykytyn K, Askwith C: **G-Protein-Coupled Receptor Signaling in Cilia**. *Cold Spring Harb Perspect Biol* 2017, **9**.

146. Marley A, von Zastrow M: **DISC1 regulates primary cilia that display specific dopamine receptors**. *PLoS One* 2010, **5**:e10902.

147. Mannu GS: **Retinal phototransduction**. *Neurosciences (Riyadh)* 2014, **19**:275-280.

148. Firestein S: **How the olfactory system makes sense of scents**. *Nature* 2001, **413**:211-218.

149. Masyuk AI, Huang BQ, Radtke BN, Gajdos GB, Splinter PL, Masyuk TV, Gradilone SA, LaRusso NF: **Ciliary subcellular localization of TGR5 determines the cholangiocyte functional response to bile acid signaling**. *Am J Physiol Gastrointest Liver Physiol* 2013, **304**:G1013-1024.

150. Brancati F, Iannicelli M, Travaglini L, Mazzotta A, Bertini E, Boltshauser E, D'Arrigo S, Emma F, Fazzi E, Gallizzi R, et al.: **MKS3/TMEM67 mutations are a major cause of COACH Syndrome, a Joubert Syndrome related disorder with liver involvement**. *Hum Mutat* 2009, **30**:E432-442.

151. Raychowdhury MK, Ramos AJ, Zhang P, McLaughin M, Dai XQ, Chen XZ, Montalbetti N, Del Rocio Cantero M, Ausiello DA, Cantiello HF: **Vasopressin receptor-mediated functional signaling pathway in primary cilia of renal epithelial cells**. *Am J Physiol Renal Physiol* 2009, **296**:F87-97.

152. Upadhyay VS, Muntean BS, Kathem SH, Hwang JJ, Aboualaiwi WA, Nauli SM: **Roles of dopamine receptor on chemosensory and mechanosensory primary cilia in renal epithelial cells**. *Front Physiol* 2014, **5**:72.

153. Praetorius HA, Spring KR: **Bending the MDCK cell primary cilium increases intracellular calcium**. *J Membr Biol* 2001, **184**:71-79.

154. Jin X, Mohieldin AM, Muntean BS, Green JA, Shah JV, Mykytyn K, Nauli SM: **Cilioplasm is a cellular compartment for calcium signaling in response to mechanical and chemical stimuli**. *Cell Mol Life Sci* 2014, **71**:2165-2178.

155. Bai CX, Giamarchi A, Rodat-Despoix L, Padilla F, Downs T, Tsiokas L, Delmas P: **Formation of a new receptor-operated channel by heteromeric assembly of TRPP2 and TRPC1 subunits**. *EMBO Rep* 2008, **9**:472-479.

156. Kottgen M, Buchholz B, Garcia-Gonzalez MA, Kotsis F, Fu X, Doerken M, Boehlke C, Steffl D, Tauber R, Wegierski T, et al.: **TRPP2 and TRPV4 form a polymodal sensory channel complex**. *J Cell Biol* 2008, **182**:437-447.

157. Fettiplace R, Hackney CM: **The sensory and motor roles of auditory hair cells**. *Nat Rev Neurosci* 2006, **7**:19-29.

158. Delling M, Indzhykulian AA, Liu X, Li Y, Xie T, Corey DP, Clapham DE: **Primary cilia are not calcium-responsive mechanosensors**. *Nature* 2016, **531**:656-660.

159. Ibanez-Tallon I, Pagenstecher A, Fliegauf M, Olbrich H, Kispert A, Ketelsen UP, North A, Heintz N, Omran H: **Dysfunction of axonemal dynein heavy chain Mdnah5 inhibits ependymal flow and reveals a novel mechanism for hydrocephalus formation**. *Hum Mol Genet* 2004, **13**:2133-2141.

160. Mall MA: **Role of cilia, mucus, and airway surface liquid in mucociliary dysfunction: lessons from mouse models**. *J Aerosol Med Pulm Drug Deliv* 2008, **21**:13-24.

161. Lyons RA, Saridogan E, Djahanbakhch O: **The reproductive significance of human Fallopian tube cilia**. *Hum Reprod Update* 2006, **12**:363-372.

162. Yoshiba S, Shiratori H, Kuo IY, Kawasumi A, Shinohara K, Nonaka S, Asai Y, Sasaki G, Belo JA, Sasaki H, et al.: **Cilia at the node of mouse embryos sense fluid flow for left-right determination via Pkd2**. *Science* 2012, **338**:226-231.

163. Ferreira RR, Vilfan A, Julicher F, Supatto W, Vermot J: **Physical limits of flow sensing in the left-right organizer**. *Elife* 2017, **6**.

164. Inaba K: **Molecular architecture of the sperm flagella: molecules for motility and signaling**. *Zoolog Sci* 2003, **20**:1043-1056.

165. O'Callaghan C, Sikand K, Rutman A: **Respiratory and brain ependymal ciliary function**. *Pediatr Res* 1999, **46**:704-707.

166. Mossman JA, Pearson JT, Moore HD, Pacey AA: **Variation in mean human sperm length is linked with semen characteristics**. *Hum Reprod* 2013, **28**:22-32.

167. Yang P, Fox L, Colbran RJ, Sale WS: **Protein phosphatases PP1 and PP2A are located in distinct positions in the Chlamydomonas flagellar axoneme**. *J Cell Sci* 2000, **113 (Pt 1)**:91-102.

168. Gaillard AR, Fox LA, Rhea JM, Craige B, Sale WS: **Disruption of the A-kinase anchoring domain in flagellar radial spoke protein 3 results in unregulated axonemal cAMP-dependent protein kinase activity and abnormal flagellar motility**. *Mol Biol Cell* 2006, **17**:2626-2635.

169. Gokhale A, Wirschell M, Sale WS: **Regulation of dynein-driven microtubule sliding by the axonemal protein kinase CK1 in Chlamydomonas flagella**. *J Cell Biol* 2009, **186**:817-824.

170. Seeley ES, Carriere C, Goetze T, Longnecker DS, Korc M: **Pancreatic cancer and precursor pancreatic intraepithelial neoplasia lesions are devoid of primary cilia**. *Cancer Res* 2009, **69**:422-430.

171. Menzl I, Lebeau L, Pandey R, Hassounah NB, Li FW, Nagle R, Weihs K, McDermott KM: **Loss of primary cilia occurs early in breast cancer development**. *Cilia* 2014, **3**:7.

172. Egeberg DL, Lethan M, Manguso R, Schneider L, Awan A, Jorgensen TS, Byskov AG, Pedersen LB, Christensen ST: **Primary cilia and aberrant cell signaling in epithelial ovarian cancer**. *Cilia* 2012, **1**:15.

173. Fabbri L, Bost F, Mazure NM: **Primary Cilium in Cancer Hallmarks**. *Int J Mol Sci* 2019, **20**.

174. Hassounah NB, Nunez M, Fordyce C, Roe D, Nagle R, Bunch T, McDermott KM: **Inhibition of Ciliogenesis Promotes Hedgehog Signaling, Tumorigenesis, and Metastasis in Breast Cancer**. *Mol Cancer Res* 2017, **15**:1421-1430.

175. Schmid FM, Schou KB, Vilhelm MJ, Holm MS, Breslin L, Farinelli P, Larsen LA, Andersen JS, Pedersen LB, Christensen ST: **IFT20 modulates ciliary PDGFRalpha signaling by regulating the stability of Cbl E3 ubiquitin ligases**. *J Cell Biol* 2018, **217**:151-161.

176. Afzelius BA: **A human syndrome caused by immotile cilia**. *Science* 1976, **193**:317-319.

177. Olbrich H, Fliegauf M, Hoefele J, Kispert A, Otto E, Volz A, Wolf MT, Sasmaz G, Trauer U, Reinhardt R, et al.: **Mutations in a novel gene, NPHP3, cause adolescent nephronophthisis, tapeto-retinal degeneration and hepatic fibrosis**. *Nat Genet* 2003, **34**:455-459.

178. Otto EA, Schermer B, Obara T, O'Toole JF, Hiller KS, Mueller AM, Ruf RG, Hoefele J, Beekmann F, Landau D, et al.: **Mutations in INVS encoding inversin cause nephronophthisis type 2, linking renal cystic disease to the function of primary cilia and left-right axis determination**. *Nat Genet* 2003, **34**:413-420.

179. Ansley SJ, Badano JL, Blacque OE, Hill J, Hoskins BE, Leitch CC, Kim JC, Ross AJ, Eichers ER, Teslovich TM, et al.: **Basal body dysfunction is a likely cause of pleiotropic Bardet-Biedl syndrome**. *Nature* 2003, **425**:628-633.

180. Badano JL, Mitsuma N, Beales PL, Katsanis N: **The ciliopathies: an emerging class of human genetic disorders**. *Annu Rev Genomics Hum Genet* 2006, **7**:125-148.

181. Tobin JL, Beales PL: **The nonmotile ciliopathies**. *Genet Med* 2009, **11**:386-402.

182. Davis EE, Katsanis N: **The ciliopathies: a transitional model into systems biology of human genetic disease**. *Curr Opin Genet Dev* 2012, **22**:290-303.

183. Gillespie FD: **Congenital amaurosis of Leber**. *Am J Ophthalmol* 1966, **61**:874-880.

184. Wheway G, Mitchison HM: **Opportunities and Challenges for Molecular Understanding of Ciliopathies-The 100,000 Genomes Project**. *Front Genet* 2019, **10**:127.

185. Novarino G, Akizu N, Gleeson JG: **Modeling human disease in humans: the ciliopathies**. *Cell* 2011, **147**:70-79.

186. Davis EE, Zhang Q, Liu Q, Diplas BH, Davey LM, Hartley J, Stoetzel C, Szymanska K, Ramaswami G, Logan CV, et al.: **TTC21B contributes both causal and modifying alleles across the ciliopathy spectrum**. *Nat Genet* 2011, **43**:189-196.

187. Mitchison HM, Schmidts M, Loges NT, Freshour J, Dritsoula A, Hirst RA, O'Callaghan C, Blau H, Al Dabbagh M, Olbrich H, et al.: **Mutations in axonemal dynein assembly factor DNAAF3 cause primary ciliary dyskinesia**. *Nat Genet* 2012, **44**:381-389, S381-382.

188. Noda K, Kitami M, Kitami K, Kaku M, Komatsu Y: **Canonical and noncanonical intraflagellar transport regulates craniofacial skeletal development**. *Proc Natl Acad Sci U S A* 2016, **113**:E2589-2597.

189. Jabourian Z, Lublin FD, Adler A, Gonzales C, Northrup B, Zwillenberg D: **Hydrocephalus in Kartagener's syndrome**. *Ear Nose Throat J* 1986, **65**:468-472.

190. Ruiz-Perez VL, Blair HJ, Rodriguez-Andres ME, Blanco MJ, Wilson A, Liu YN, Miles C, Peters H, Goodship JA: **Evc is a positive mediator of Ihh-regulated bone growth that localises at the base of chondrocyte cilia**. *Development* 2007, **134**:2903-2912.

191. Schock EN, Brugmann SA: **Discovery, Diagnosis, and Etiology of Craniofacial Ciliopathies**. *Cold Spring Harb Perspect Biol* 2017, **9**.

192. Tsujikawa M, Malicki J: **Intraflagellar transport genes are essential for differentiation and survival of vertebrate sensory neurons**. *Neuron* 2004, **42**:703-716.

193. Dharmat R, Eblimit A, Robichaux MA, Zhang Z, Nguyen TT, Jung SY, He F, Jain A, Li Y, Qin J, et al.: **SPATA7 maintains a novel photoreceptor-specific zone in the distal connecting cilium**. *J Cell Biol* 2018, **217**:2851-2865.

194. Forsythe E, Beales PL: **Bardet-Biedl syndrome**. *Eur J Hum Genet* 2013, **21**:8-13.

195. Youn YH, Han YG: **Primary Cilia in Brain Development and Diseases**. *Am J Pathol* 2018, **188**:11-22.

196. Beales PL, Elcioglu N, Woolf AS, Parker D, Flinter FA: **New criteria for improved diagnosis of Bardet-Biedl syndrome: results of a population survey**. *J Med Genet* 1999, **36**:437-446.

197. Bacino CA, Dhar SU, Brunetti-Pierri N, Lee B, Bonnen PE: **WDR35 mutation in siblings with Sensenbrenner syndrome: a ciliopathy with variable phenotype**. *Am J Med Genet A* 2012, **158A**:2917-2924.

198. McIntyre JC, Williams CL, Martens JR: **Smelling the roses and seeing the light: gene therapy for ciliopathies**. *Trends Biotechnol* 2013, **31**:355-363.

199. Mirra V, Werner C, Santamaria F: **Primary Ciliary Dyskinesia: An Update on Clinical Aspects, Genetics, Diagnosis, and Future Treatment Strategies**. *Front Pediatr* 2017, **5**:135.

200. McIntyre JC, Davis EE, Joiner A, Williams CL, Tsai IC, Jenkins PM, McEwen DP, Zhang L, Escobado J, Thomas S, et al.: **Gene therapy rescues cilia defects and restores olfactory function in a mammalian ciliopathy model**. *Nat Med* 2012, **18**:1423-1428.

201. Cideciyan AV, Jacobson SG, Drack AV, Ho AC, Charng J, Garafalo AV, Roman AJ, Sumaroka A, Han IC, Hochstedler MD, et al.: **Effect of an intravitreal antisense oligonucleotide on vision in Leber congenital amaurosis due to a photoreceptor cilium defect**. *Nat Med* 2019, **25**:225-228.

202. Maeder ML, Stefanidakis M, Wilson CJ, Baral R, Barrera LA, Bounoutas GS, Bumcrot D, Chao H, Ciulla DM, DaSilva JA, et al.: **Development of a gene-editing approach to restore vision loss in Leber congenital amaurosis type 10**. *Nat Med* 2019, **25**:229-233.

203. Mandai M, Watanabe A, Kurimoto Y, Hirami Y, Morinaga C, Daimon T, Fujihara M, Akimaru H, Sakai N, Shibata Y, et al.: **Autologous Induced Stem-Cell-Derived Retinal Cells for Macular Degeneration**. *N Engl J Med* 2017, **376**:1038-1046.

204. Keeling KM, Xue X, Gunn G, Bedwell DM: **Therapeutics based on stop codon readthrough**. *Annu Rev Genomics Hum Genet* 2014, **15**:371-394.

205. Goldmann T, Overlack N, Wolfrum U, Nagel-Wolfrum K: **PTC124-mediated translational readthrough of a nonsense mutation causing Usher syndrome type 1C**. *Hum Gene Ther* 2011, **22**:537-547.

206. Schwarz N, Carr AJ, Lane A, Moeller F, Chen LL, Aguila M, Nommiste B, Muthiah MN, Kanuga N, Wolfrum U, et al.: **Translational read-through of the RP2 Arg120stop mutation in patient iPSC-derived retinal pigment epithelium cells**. *Hum Mol Genet* 2015, **24**:972-986.

207. Bukowy-Bieryllo Z, Dabrowski M, Witt M, Zietkiewicz E: **Aminoglycoside-stimulated readthrough of premature termination codons in selected genes involved in primary ciliary dyskinesia**. *RNA Biol* 2016, **13**:1041-1050.

208. Mockel A, Obringer C, Hakvoort TB, Seeliger M, Lamers WH, Stoetzel C, Dollfus H, Marion V: **Pharmacological modulation of the retinal unfolded protein response in Bardet-Biedl syndrome reduces apoptosis and preserves light detection ability**. *J Biol Chem* 2012, **287**:37483-37494.

209. Torres VE, Harris PC: **Strategies targeting cAMP signaling in the treatment of polycystic kidney disease**. *J Am Soc Nephrol* 2014, **25**:18-32.

210. Kim YJ, Kim S, Jung Y, Jung E, Kwon HJ, Kim J: **Eupatilin rescues ciliary transition zone defects to ameliorate ciliopathy-related phenotypes**. *J Clin Invest* 2018, **128**:3642-3648.

211. Haws RM, Fletty KL, McIntee TJ, Green C, Pomeroy J, Hylan M, Folster C, Davis EK, Brady SM, Fiedorek FT, et al.: **Effect of the Melanocortin-4 Receptor Agonist, Setmelanotide, on Obesity and Hyperphagia in Individuals Affected by Bardet-**

Biedl Syndrome. In *European Society for Paediatric Endocrinology*. Edited by. Athens, Greece; 2018.

212. Kaye C, Lewy PR: **Congenital appearance of adult-type (autosomal dominant) polycystic kidney disease**. *J Pediatr* 1974, **85**:807-810.

213. Schermer B, Ghenoiu C, Bartram M, Muller RU, Kotsis F, Hohne M, Kuhn W, Rapka M, Nitschke R, Zentgraf H, et al.: **The von Hippel-Lindau tumor suppressor protein controls ciliogenesis by orienting microtubule growth**. *J Cell Biol* 2006, **175**:547-554.

214. Narayan D, Krishnan SN, Upender M, Ravikumar TS, Mahoney MJ, Dolan TF, Jr., Teebi AS, Haddad GG: **Unusual inheritance of primary ciliary dyskinesia (Kartagener's syndrome)**. *J Med Genet* 1994, **31**:493-496.

215. Klein D, Franceschetti A, Hussels I, Race RR, Sanger R: **X-linked retinitis pigmentosa and linkage studies with the Xg blood-groups**. *Lancet* 1967, **1**:974-975.

216. Riazuddin SA, Iqbal M, Wang Y, Masuda T, Chen Y, Bowne S, Sullivan LS, Waseem NH, Bhattacharya S, Daiger SP, et al.: **A splice-site mutation in a retina-specific exon of BBS8 causes nonsyndromic retinitis pigmentosa**. *Am J Hum Genet* 2010, **86**:805-812.

217. Murphy D, Singh R, Kolandaivelu S, Ramamurthy V, Stoilov P: **Alternative Splicing Shapes the Phenotype of a Mutation in BBS8 To Cause Nonsyndromic Retinitis Pigmentosa**. *Mol Cell Biol* 2015, **35**:1860-1870.

218. He S, Parapuram SK, Hurd TW, Behnam B, Margolis B, Swaroop A, Khanna H: **Retinitis Pigmentosa GTPase Regulator (RPGR) protein isoforms in mammalian retina: insights into X-linked Retinitis Pigmentosa and associated ciliopathies**. *Vision Res* 2008, **48**:366-376.

219. Schmidts M, Frank V, Eisenberger T, Al Turki S, Bizet AA, Antony D, Rix S, Decker C, Bachmann N, Bald M, et al.: **Combined NGS approaches identify mutations in the intraflagellar transport gene IFT140 in skeletal ciliopathies with early progressive kidney Disease**. *Hum Mutat* 2013, **34**:714-724.

220. Kyttala M, Tallila J, Salonen R, Kopra O, Kohlschmidt N, Paavola-Sakki P, Peltonen L, Kestila M: **MKS1, encoding a component of the flagellar apparatus basal body proteome, is mutated in Meckel syndrome**. *Nat Genet* 2006, **38**:155-157.

221. Leitch CC, Zaghloul NA, Davis EE, Stoetzel C, Diaz-Font A, Rix S, Alfadhel M, Lewis RA, Eyaid W, Banin E, et al.: **Hypomorphic mutations in syndromic encephalocele genes are associated with Bardet-Biedl syndrome**. *Nat Genet* 2008, **40**:443-448.

222. Otto EA, Tory K, Attanasio M, Zhou W, Chaki M, Paruchuri Y, Wise EL, Wolf MT, Utsch B, Becker C, et al.: **Hypomorphic mutations in meckelin (MKS3/TMEM67) cause nephronophthisis with liver fibrosis (NPHP11)**. *J Med Genet* 2009, **46**:663-670.

223. Bujakowska KM, Zhang Q, Siemiatkowska AM, Liu Q, Place E, Falk MJ, Consugar M, Lancelot ME, Antonio A, Lonjou C, et al.: **Mutations in IFT172 cause isolated retinal degeneration and Bardet-Biedl syndrome**. *Hum Mol Genet* 2015, **24**:230-242.

224. Shaheen R, Szymanska K, Basu B, Patel N, Ewida N, Faqeih E, Al Hashem A, Derar N, Alsharif H, Aldahmesh MA, et al.: **Characterizing the morbid genome of ciliopathies**. *Genome Biol* 2016, **17**:242.

225. Khanna H, Davis EE, Murga-Zamalloa CA, Estrada-Cuzcano A, Lopez I, den Hollander AI, Zonneveld MN, Othman MI, Waseem N, Chakarova CF, et al.: **A common allele in RPGRIP1L is a modifier of retinal degeneration in ciliopathies**. *Nat Genet* 2009, **41**:739-745.

226. Bullich G, Vargas I, Trujillano D, Mendizabal S, Pinero-Fernandez JA, Fraga G, Garcia-Solano J, Ballarin J, Estivill X, Torra R, et al.: **Contribution of the TTC21B gene to glomerular and cystic kidney diseases**. *Nephrol Dial Transplant* 2017, **32**:151-156.

227. Buchovecky CM, Turley SD, Brown HM, Kyle SM, McDonald JG, Liu B, Pieper AA, Huang W, Katz DM, Russell DW, et al.: **A suppressor screen in Mecp2 mutant mice implicates cholesterol metabolism in Rett syndrome**. *Nat Genet* 2013, **45**:1013-1020.

228. Niederriter AR, Davis EE, Golzio C, Oh EC, Tsai IC, Katsanis N: **In vivo modeling of the morbid human genome using Danio rerio**. *J Vis Exp* 2013:e50338.

229. Song P, Dudinsky L, Fogerty J, Gaivin R, Perkins BD: **Arl13b Interacts With Vangl2 to Regulate Cilia and Photoreceptor Outer Segment Length in Zebrafish**. *Invest Ophthalmol Vis Sci* 2016, **57**:4517-4526.

230. Katsanis N, Ansley SJ, Badano JL, Eichers ER, Lewis RA, Hoskins BE, Scambler PJ, Davidson WS, Beales PL, Lupski JR: **Triallelic inheritance in Bardet-Biedl syndrome, a Mendelian recessive disorder**. *Science* 2001, **293**:2256-2259.

231. Eichers ER, Lewis RA, Katsanis N, Lupski JR: **Triallelic inheritance: a bridge between Mendelian and multifactorial traits**. *Ann Med* 2004, **36**:262-272.

232. Hoefele J, Wolf MT, O'Toole JF, Otto EA, Schultheiss U, Deschenes G, Attanasio M, Utsch B, Antignac C, Hildebrandt F: **Evidence of oligogenic inheritance in nephronophthisis**. *J Am Soc Nephrol* 2007, **18**:2789-2795.

233. Mykytyn K, Nishimura DY, Searby CC, Beck G, Bugge K, Haines HL, Cornier AS, Cox GF, Fulton AB, Carmi R, et al.: **Evaluation of complex inheritance involving the most common Bardet-Biedl syndrome locus (BBS1)**. *Am J Hum Genet* 2003, **72**:429-437.

234. Gonzaga-Jauregui C, Harel T, Gambin T, Kousi M, Griffin LB, Francescatto L, Ozes B, Karaca E, Jhangiani SN, Bainbridge MN, et al.: **Exome Sequence Analysis Suggests that Genetic Burden Contributes to Phenotypic Variability and Complex Neuropathy**. *Cell Rep* 2015, **12**:1169-1183.

235. Pitteloud N, Quinton R, Pearce S, Raivio T, Acierno J, Dwyer A, Plummer L, Hughes V, Seminara S, Cheng YZ, et al.: **Digenic mutations account for variable phenotypes in idiopathic hypogonadotropic hypogonadism**. *J Clin Invest* 2007, **117**:457-463.

236. Lindstrand A, Frangakis S, Carvalho CM, Richardson EB, McFadden KA, Willer JR, Pehlivan D, Liu P, Pediaditakis IL, Sabo A, et al.: **Copy-Number Variation Contributes to the Mutational Load of Bardet-Biedl Syndrome**. *Am J Hum Genet* 2016, **99**:318-336.

237. Kousi M, Söylemez O, Ozanturk A, Akle S, Jungreis I, Muller J, Cassa CA, Brand H, Mokry JA, Wolf MY, et al.: **Evidence for secondary-variant genetic burden and non-random distribution across biological modules in a recessive ciliopathy**. *bioRXiv* 2018.

238. Boldt K, van Reeuwijk J, Lu Q, Koutroumpas K, Nguyen TM, Texier Y, van Beersum SE, Horn N, Willer JR, Mans DA, et al.: **An organelle-specific protein landscape identifies novel diseases and molecular mechanisms**. *Nat Commun* 2016, **7**:11491.

239. Williams CL, Li C, Kida K, Inglis PN, Mohan S, Semenec L, Bialas NJ, Stupay RM, Chen N, Blacque OE, et al.: **MKS and NPHP modules cooperate to establish basal body/transition zone membrane associations and ciliary gate function during ciliogenesis**. *J Cell Biol* 2011, **192**:1023-1041.

240. Sang L, Miller JJ, Corbit KC, Giles RH, Brauer MJ, Otto EA, Baye LM, Wen X, Scales SJ, Kwong M, et al.: **Mapping the NPHP-JBTS-MKS protein network reveals ciliopathy disease genes and pathways**. *Cell* 2011, **145**:513-528.

241. Halbritter J, Bizet AA, Schmidts M, Porath JD, Braun DA, Gee HY, McInerney-Leo AM, Krug P, Filhol E, Davis EE, et al.: **Defects in the IFT-B component IFT172 cause Jeune and Mainzer-Saldino syndromes in humans**. *Am J Hum Genet* 2013, **93**:915-925.

242. Di Gioia SA, Farinelli P, Letteboer SJ, Arsenijevic Y, Sharon D, Roepman R, Rivolta C: **Interactome analysis reveals that FAM161A, deficient in recessive retinitis pigmentosa, is a component of the Golgi-centrosomal network**. *Hum Mol Genet* 2015, **24**:3359-3371.

243. Baker K, Beales PL: **Making sense of cilia in disease: the human ciliopathies**. *Am J Med Genet C Semin Med Genet* 2009, **151C**:281-295.

244. Trottier Y, Lutz Y, Stevanin G, Imbert G, Devys D, Cancel G, Saudou F, Weber C, David G, Tora L, et al.: **Polyglutamine expansion as a pathological epitope in Huntington's disease and four dominant cerebellar ataxias**. *Nature* 1995, **378**:403-406.

245. David G, Abbas N, Stevanin G, Durr A, Yvert G, Cancel G, Weber C, Imbert G, Saudou F, Antoniou E, et al.: **Cloning of the SCA7 gene reveals a highly unstable CAG repeat expansion**. *Nat Genet* 1997, **17**:65-70.

246. Kahle JJ, Gulbahce N, Shaw CA, Lim J, Hill DE, Barabasi AL, Zoghbi HY: **Comparison of an expanded ataxia interactome with patient medical records reveals a relationship between macular degeneration and ataxia**. *Hum Mol Genet* 2011, **20**:510-527.

247. Zoghbi HY, Orr HT: **Glutamine repeats and neurodegeneration**. *Annu Rev Neurosci* 2000, **23**:217-247.

248. Michalik A, Martin JJ, Van Broeckhoven C: **Spinocerebellar ataxia type 7 associated with pigmentary retinal dystrophy**. *Eur J Hum Genet* 2004, **12**:2-15.

249. van de Warrenburg BP, Frenken CW, Ausems MG, Kleefstra T, Sinke RJ, Knoers NV, Kremer HP: **Striking anticipation in spinocerebellar ataxia type 7: the infantile phenotype**. *J Neurol* 2001, **248**:911-914.

250. Gouw LG, Castaneda MA, McKenna CK, Digre KB, Pulst SM, Perlman S, Lee MS, Gomez C, Fischbeck K, Gagnon D, et al.: **Analysis of the dynamic mutation in the SCA7 gene shows marked parental effects on CAG repeat transmission**. *Hum Mol Genet* 1998, **7**:525-532.

251. Karam A, Trottier Y: **Molecular Mechanisms and Therapeutic Strategies in Spinocerebellar Ataxia Type 7**. *Adv Exp Med Biol* 2018, **1049**:197-218.

252. Zander C, Takahashi J, El Hachimi KH, Fujigasaki H, Albanese V, Lebre AS, Stevanin G, Duyckaerts C, Brice A: **Similarities between spinocerebellar ataxia type 7 (SCA7) cell models and human brain: proteins recruited in inclusions and activation of caspase-3**. *Hum Mol Genet* 2001, **10**:2569-2579.

253. Bonnet J, Wang CY, Baptista T, Vincent SD, Hsiao WC, Stierle M, Kao CF, Tora L, Devys D: **The SAGA coactivator complex acts on the whole transcribed genome and is required for RNA polymerase II transcription**. *Genes Dev* 2014, **28**:1999-2012.

254. Mauger C, Del-Favero J, Ceuterick C, Lubke U, van Broeckhoven C, Martin J: **Identification and localization of ataxin-7 in brain and retina of a patient with cerebellar ataxia type II using anti-peptide antibody**. *Brain Res Mol Brain Res* 1999, **74**:35-43.

255. Yvert G, Lindenberg KS, Devys D, Helmlinger D, Landwehrmeyer GB, Mandel JL: **SCA7 mouse models show selective stabilization of mutant ataxin-7 and similar cellular responses in different neuronal cell types**. *Hum Mol Genet* 2001, **10**:1679-1692.

256. Yoo SY, Pennesi ME, Weeber EJ, Xu B, Atkinson R, Chen S, Armstrong DL, Wu SM, Sweatt JD, Zoghbi HY: **SCA7 knockin mice model human SCA7 and reveal gradual accumulation of mutant ataxin-7 in neurons and abnormalities in short-term plasticity**. *Neuron* 2003, **37**:383-401.

257. Young JE, Gouw L, Propp S, Sopher BL, Taylor J, Lin A, Hermel E, Logvinova A, Chen SF, Chen S, et al.: **Proteolytic cleavage of ataxin-7 by caspase-7 modulates cellular toxicity and transcriptional dysregulation**. *J Biol Chem* 2007, **282**:30150-30160.

258. La Spada AR, Fu YH, Sopher BL, Libby RT, Wang X, Li LY, Einum DD, Huang J, Possin DE, Smith AC, et al.: **Polyglutamine-expanded ataxin-7 antagonizes CRX function and induces cone-rod dystrophy in a mouse model of SCA7**. *Neuron* 2001, **31**:913-927.

259. Abou-Sleymane G, Chalmel F, Helmlinger D, Lardenois A, Thibault C, Weber C, Merienne K, Mandel JL, Poch O, Devys D, et al.: **Polyglutamine expansion causes neurodegeneration by altering the neuronal differentiation program**. *Hum Mol Genet* 2006, **15**:691-703.

260. Helmlinger D, Hardy S, Abou-Sleymane G, Eberlin A, Bowman AB, Gansmuller A, Picaud S, Zoghbi HY, Trottier Y, Tora L, et al.: **Glutamine-expanded ataxin-7 alters TFTC/STAGA recruitment and chromatin structure leading to photoreceptor dysfunction**. *PLoS Biol* 2006, **4**:e67.

261. Chou AH, Chen CY, Chen SY, Chen WJ, Chen YL, Weng YS, Wang HL: **Polyglutamine-expanded ataxin-7 causes cerebellar dysfunction by inducing transcriptional dysregulation**. *Neurochem Int* 2010, **56**:329-339.

262. Rub U, Brunt ER, Gierga K, Seidel K, Schultz C, Schols L, Auburger G, Heinsen H, Ippel PF, Glimmerveen WF, et al.: **Spinocerebellar ataxia type 7 (SCA7): first report of a systematic neuropathological study of the brain of a patient with a very short expanded CAG-repeat**. *Brain Pathol* 2005, **15**:287-295.

263. Horton LC, Frosch MP, Vangel MG, Weigel-DiFranco C, Berson EL, Schmahmann JD: **Spinocerebellar ataxia type 7: clinical course, phenotype-genotype correlations, and neuropathology**. *Cerebellum* 2013, **12**:176-193.

264. Rub U, Brunt ER, Petrasch-Parwez E, Schols L, Theegarten D, Auburger G, Seidel K, Schultz C, Gierga K, Paulson H, et al.: **Degeneration of ingestion-related brainstem nuclei in spinocerebellar ataxia type 2, 3, 6 and 7**. *Neuropathol Appl Neurobiol* 2006, **32**:635-649.

265. Harrison PJ: **The neuropathology of schizophrenia. A critical review of the data and their interpretation**. *Brain* 1999, **122 (Pt 4)**:593-624.

266. Schmidt MJ, Mirnics K: **Neurodevelopment, GABA system dysfunction, and schizophrenia**. *Neuropsychopharmacology* 2015, **40**:190-206.

267. Lee JK, Mathews K, Schlaggar B, Perlmutter J, Paulsen JS, Epping E, Burmeister L, Nopoulos P: **Measures of growth in children at risk for Huntington disease**. *Neurology* 2012, **79**:668-674.

268. Nopoulos PC, Aylward EH, Ross CA, Mills JA, Langbehn DR, Johnson HJ, Magnotta VA, Pierson RK, Beglinger LJ, Nance MA, et al.: **Smaller intracranial volume in prodromal Huntington's disease: evidence for abnormal neurodevelopment**. *Brain* 2011, **134**:137-142.

269. Leavitt BR, Guttman JA, Hodgson JG, Kimel GH, Singaraja R, Vogl AW, Hayden MR: **Wild-type huntingtin reduces the cellular toxicity of mutant huntingtin in vivo**. *Am J Hum Genet* 2001, **68**:313-324.

270. Van Raamsdonk JM, Pearson J, Murphy Z, Hayden MR, Leavitt BR: **Wild-type huntingtin ameliorates striatal neuronal atrophy but does not prevent other abnormalities in the YAC128 mouse model of Huntington disease**. *BMC Neurosci* 2006, **7**:80.

271. Warrick JM, Morabito LM, Bilen J, Gordesky-Gold B, Faust LZ, Paulson HL, Bonini NM: **Ataxin-3 suppresses polyglutamine neurodegeneration in Drosophila by a ubiquitin-associated mechanism**. *Mol Cell* 2005, **18**:37-48.

272. Carrillo-Rosas S, Weber C, Fievet L, Messaddeq N, Karam A, Trottier Y: **Loss of zebrafish Ataxin-7, a SAGA subunit responsible for SCA7 retinopathy, causes ocular coloboma and malformation of photoreceptors**. *Hum Mol Genet* 2018.

273. Trottier Y, Niewiadomska-Cimicka A: **Molecular Targets and Therapeutic Strategies in Spinocerebellar Ataxia Type 7**. *Neurotherapeutics* 2019.

274. Jonasson J, Strom AL, Hart P, Brannstrom T, Forsgren L, Holmberg M: **Expression of ataxin-7 in CNS and non-CNS tissue of normal and SCA7 individuals**. *Acta Neuropathol* 2002, **104**:29-37.

275. Nakamura Y, Tagawa K, Oka T, Sasabe T, Ito H, Shiwaku H, La Spada AR, Okazawa H: **Ataxin-7 associates with microtubules and stabilizes the cytoskeletal network**. *Hum Mol Genet* 2012, **21**:1099-1110.

276. Karam A: **Retinal ciliopathies in Huntington's and SCA7 disorders**. In *Genomics*. Edited by. Université de Strasbourg: Université de Strasbourg; 2013. [Trottier Y (Series Editor):

277. Pazour GJ, Baker SA, Deane JA, Cole DG, Dickert BL, Rosenbaum JL, Witman GB, Besharse JC: **The intraflagellar transport protein, IFT88, is essential for vertebrate photoreceptor assembly and maintenance**. *J Cell Biol* 2002, **157**:103-113.

278. Ghata J, Cowley BD, Jr.: **Polycystic Kidney Disease**. *Compr Physiol* 2017, **7**:945-975.

279. Mitchison HM, Valente EM: **Motile and non-motile cilia in human pathology: from function to phenotypes**. *J Pathol* 2017, **241**:294-309.

280. Lee JE, Gleeson JG: **A systems-biology approach to understanding the ciliopathy disorders**. *Genome Med* 2011, **3**:59.

281. Roosing S, Hofree M, Kim S, Scott E, Copeland B, Romani M, Silhavy JL, Rosti RO, Schroth J, Mazza T, et al.: **Functional genome-wide siRNA screen identifies KIAA0586 as mutated in Joubert syndrome**. *Elife* 2015, **4**:e06602.

282. Choi YJ, Halbritter J, Braun DA, Schueler M, Schapiro D, Rim JH, Nandadasa S, Choi WI, Widmeier E, Shril S, et al.: **Mutations of ADAMTS9 Cause Nephronophthisis-Related Ciliopathy**. *Am J Hum Genet* 2019, **104**:45-54.

283. Nandadasa S, Kraft CM, Wang LW, O'Donnell A, Patel R, Gee HY, Grobe K, Cox TC, Hildebrandt F, Apte SS: **Secreted metalloproteases ADAMTS9 and ADAMTS20 have a non-canonical role in ciliary vesicle growth during ciliogenesis**. *Nat Commun* 2019, **10**:953.

284. Gherman A, Davis EE, Katsanis N: **The ciliary proteome database: an integrated community resource for the genetic and functional dissection of cilia**. *Nat Genet* 2006, **38**:961-962.

285. van Dam TJ, Wheway G, Slaats GG, Group SS, Huynen MA, Giles RH: **The SYSCILIA gold standard (SCGSv1) of known ciliary components and its applications within a systems biology consortium**. *Cilia* 2013, **2**:7.

286. Arnaiz O, Malinowska A, Klotz C, Sperling L, Dadlez M, Koll F, Cohen J: **Cildb: a knowledgebase for centrosomes and cilia**. *Database (Oxford)* 2009, **2009**:bap022.

287. Arnaiz O, Cohen J, Tassin AM, Koll F: **Remodeling Cildb, a popular database for cilia and links for ciliopathies**. *Cilia* 2014, **3**:9.

288. van Dam TJP, Kennedy J, van der Lee R, de Vrieze E, Wunderlich KA, Rix S, Dougherty GW, Lambacher NJ, Li C, Jensen VL, et al.: **CiliaCarta: An integrated and validated compendium of ciliary genes**. *PLoS One* 2019, **14**:e0216705.

289. O'Brien J, Hayder H, Zayed Y, Peng C: **Overview of MicroRNA Biogenesis, Mechanisms of Actions, and Circulation**. *Front Endocrinol (Lausanne)* 2018, **9**:402.

290. Bussing I, Slack FJ, Grosshans H: **let-7 microRNAs in development, stem cells and cancer**. *Trends Mol Med* 2008, **14**:400-409.

291. Lee H, Han S, Kwon CS, Lee D: **Biogenesis and regulation of the let-7 miRNAs and their functional implications**. *Protein Cell* 2016, **7**:100-113.

292. Lee Y, Kim M, Han J, Yeom KH, Lee S, Baek SH, Kim VN: **MicroRNA genes are transcribed by RNA polymerase II**. *EMBO J* 2004, **23**:4051-4060.

293. Gregory RI, Yan KP, Amuthan G, Chendrimada T, Doratotaj B, Cooch N, Shiekhattar R: **The Microprocessor complex mediates the genesis of microRNAs**. *Nature* 2004, **432**:235-240.

294. Yi R, Qin Y, Macara IG, Cullen BR: **Exportin-5 mediates the nuclear export of pre-microRNAs and short hairpin RNAs**. *Genes Dev* 2003, **17**:3011-3016.

295. Chendrimada TP, Gregory RI, Kumaraswamy E, Norman J, Cooch N, Nishikura K, Shiekhattar R: **TRBP recruits the Dicer complex to Ago2 for microRNA processing and gene silencing**. *Nature* 2005, **436**:740-744.

296. Ha M, Kim VN: **Regulation of microRNA biogenesis**. *Nat Rev Mol Cell Biol* 2014, **15**:509-524.

297. Tsialikas J, Romer-Seibert J: **LIN28: roles and regulation in development and beyond**. *Development* 2015, **142**:2397-2404.

298. Rupaimoole R, Calin GA, Lopez-Berestein G, Sood AK: **miRNA Deregulation in Cancer Cells and the Tumor Microenvironment**. *Cancer Discov* 2016, **6**:235-246.

299. Marcet B, Chevalier B, Luxardi G, Coraux C, Zaragosi LE, Cibois M, Robbe-Sermesant K, Jolly T, Cardinaud B, Moreilhon C, et al.: **Control of vertebrate multiciliogenesis by miR-449 through direct repression of the Delta/Notch pathway**. *Nat Cell Biol* 2011, **13**:693-699.

300. Chevalier B, Adamiok A, Mercey O, Revinski DR, Zaragosi LE, Pasini A, Kodjabachian L, Barbry P, Marcet B: **miR-34/449 control apical actin network formation during multiciliogenesis through small GTPase pathways**. *Nat Commun* 2015, **6**:8386.

301. Song R, Walentek P, Sponer N, Klimke A, Lee JS, Dixon G, Harland R, Wan Y, Lishko P, Lize M, et al.: **miR-34/449 miRNAs are required for motile ciliogenesis by repressing cp110**. *Nature* 2014, **510**:115-120.

302. Otto T, Candido SV, Pilarz MS, Sicinska E, Bronson RT, Bowden M, Lachowicz IA, Mulry K, Fassl A, Han RC, et al.: **Cell cycle-targeting microRNAs promote differentiation by enforcing cell-cycle exit**. *Proc Natl Acad Sci U S A* 2017, **114**:10660-10665.

303. Cao J, Shen Y, Zhu L, Xu Y, Zhou Y, Wu Z, Li Y, Yan X, Zhu X: **miR-129-3p controls cilia assembly by regulating CP110 and actin dynamics**. *Nat Cell Biol* 2012, **14**:697-706.

304. Robinson JF: **Genetic and functional dissection of the mechanisms of ciliogenesis** Edited by: Johns Hopkins University; 2012. [Reed R (Series Editor):

305. Helmlinger D, Hardy S, Sasorith S, Klein F, Robert F, Weber C, Miguet L, Potier N, Van-Dorsselaer A, Wurtz JM, et al.: **Ataxin-7 is a subunit of GCN5 histone acetyltransferase-containing complexes**. *Hum Mol Genet* 2004, **13**:1257-1265.

306. Park SM, Jang HJ, Lee JH: **Roles of Primary Cilia in the Developing Brain**. *Front Cell Neurosci* 2019, **13**:218.

307. Chizhikov VV, Davenport J, Zhang Q, Shih EK, Cabello OA, Fuchs JL, Yoder BK, Millen KJ: **Cilia proteins control cerebellar morphogenesis by promoting expansion of the granule progenitor pool**. *J Neurosci* 2007, **27**:9780-9789.

308. Spassky N, Han YG, Aguilar A, Strehl L, Besse L, Laclef C, Ros MR, Garcia-Verdugo JM, Alvarez-Buylla A: **Primary cilia are required for cerebellar development and Shh-dependent expansion of progenitor pool**. *Dev Biol* 2008, **317**:246-259.

309. Haldipur P, Bharti U, Govindan S, Sarkar C, Iyengar S, Gressens P, Mani S: **Expression of Sonic hedgehog during cell proliferation in the human cerebellum**. *Stem Cells Dev* 2012, **21**:1059-1068.

310. Lewis PM, Gritli-Linde A, Smeyne R, Kottmann A, McMahon AP: **Sonic hedgehog signaling is required for expansion of granule neuron precursors and patterning of the mouse cerebellum**. *Dev Biol* 2004, **270**:393-410.

311. Munoz-Estrada J, Lora-Castellanos A, Meza I, Alarcon Elizalde S, Benitez-King G: **Primary cilia formation is diminished in schizophrenia and bipolar disorder: A possible marker for these psychiatric diseases**. *Schizophr Res* 2018, **195**:412-420.

312. Pruski M, Lang B: **Primary Cilia-An Underexplored Topic in Major Mental Illness**. *Front Psychiatry* 2019, **10**:104.

313. Zaghloul NA, Katsanis N: **Zebrafish assays of ciliopathies**. *Methods Cell Biol* 2011, **105**:257-272.

314. Aviolat H, Nomine Y, Gioria S, Bonhoure A, Hoffmann D, Ruhlmann C, Nierengarten H, Ruffenach F, Villa P, Trottier Y, et al.: **SynAggreg: A Multifunctional High-Throughput Technology for Precision Study of Amyloid Aggregation and Systematic Discovery of Synergistic Inhibitor Compounds**. *J Mol Biol* 2018, **430**:5257-5279.

315. Kimmel CB, Ballard WW, Kimmel SR, Ullmann B, Schilling TF: **Stages of embryonic development of the zebrafish**. *Dev Dyn* 1995, **203**:253-310.

316. Howe K, Clark MD, Torroja CF, Torrance J, Berthelot C, Muffato M, Collins JE, Humphray S, McLaren K, Matthews L, et al.: **The zebrafish reference genome sequence and its relationship to the human genome**. *Nature* 2013, **496**:498-503.

317. Sanna-Cherchi S, Khan K, Westland R, Krithivasan P, Fievet L, Rasouly HM, Ionita-Laza I, Capone VP, Fasel DA, Kiryluk K, et al.: **Exome-wide Association Study Identifies GREB1L Mutations in Congenital Kidney Malformations**. *Am J Hum Genet* 2017, **101**:789-802.

318. Almeida AD, Boije H, Chow RW, He J, Tham J, Suzuki SC, Harris WA: **Spectrum of Fates: a new approach to the study of the developing zebrafish retina**. *Development* 2014, **141**:1971-1980.

319. Livak KJ, Schmittgen TD: **Analysis of relative gene expression data using real-time quantitative PCR and the 2(-Delta Delta C(T)) Method**. *Methods* 2001, **25**:402-408.

320. Thisse C, Thisse B: **High-resolution in situ hybridization to whole-mount zebrafish embryos**. *Nat Protoc* 2008, **3**:59-69.

321. Spataro R, Kousi M, Farhan SMK, Willer JR, Ross JP, Dion PA, Rouleau GA, Daly MJ, Neale BM, La Bella V, et al.: **Mutations in ATP13A2 (PARK9) are associated with an amyotrophic lateral sclerosis-like phenotype, implicating this locus in further phenotypic expansion**. *Hum Genomics* 2019, **13**:19.

322. Fitzpatrick M: **Measuring cell fluorescence using ImageJ**. Edited by; 2014. vol 2017.]

323. Chen PY, Manninga H, Slanchev K, Chien M, Russo JJ, Ju J, Sheridan R, John B, Marks DS, Gaidatzis D, et al.: **The developmental miRNA profiles of zebrafish as determined by small RNA cloning**. *Genes Dev* 2005, **19**:1288-1293.

324. Olson AJ, Krentz AD, Finta KM, Okorie UC, Haws RM: **Thoraco-Abdominal Abnormalities in Bardet-Biedl Syndrome: Situs Inversus and Heterotaxy**. *J Pediatr* 2019, **204**:31-37.

325. French VM, van de Laar IM, Wessels MW, Rohe C, Roos-Hesselink JW, Wang G, Frohn-Mulder IM, Severijnen LA, de Graaf BM, Schot R, et al.: **NPHP4 variants are associated with pleiotropic heart malformations**. *Circ Res* 2012, **110**:1564-1574.

326. Long S, Ahmad N, Rebagliati M: **The zebrafish nodal-related gene southpaw is required for visceral and diencephalic left-right asymmetry**. *Development* 2003, **130**:2303-2316.

327. Gokey JJ, Ji Y, Tay HG, Litts B, Amack JD: **Kupffer's vesicle size threshold for robust left-right patterning of the zebrafish embryo**. *Dev Dyn* 2016, **245**:22-33.

328. Pintado P, Sampaio P, Tavares B, Montenegro-Johnson TD, Smith DJ, Lopes SS: **Dynamics of cilia length in left-right development**. *R Soc Open Sci* 2017, **4**:161102.

329. Gerdes JM, Liu Y, Zaghloul NA, Leitch CC, Lawson SS, Kato M, Beachy PA, Beales PL, DeMartino GN, Fisher S, et al.: **Disruption of the basal body compromises proteasomal function and perturbs intracellular Wnt response**. *Nat Genet* 2007, **39**:1350-1360.

330. Lewis BP, Burge CB, Bartel DP: **Conserved seed pairing, often flanked by adenosines, indicates that thousands of human genes are microRNA targets**. *Cell* 2005, **120**:15-20.

331. Fan Y, Esmail MA, Ansley SJ, Blacque OE, Boroevich K, Ross AJ, Moore SJ, Badano JL, May-Simera H, Compton DS, et al.: **Mutations in a member of the Ras superfamily of small GTP-binding proteins causes Bardet-Biedl syndrome**. *Nat Genet* 2004, **36**:989-993.

332. Huang da W, Sherman BT, Lempicki RA: **Systematic and integrative analysis of large gene lists using DAVID bioinformatics resources**. *Nat Protoc* 2009, **4**:44-57.

333. Toomer KA, Fulmer D, Guo L, Drohan A, Peterson N, Swanson P, Brooks B, Mukherjee R, Body S, Lipschutz JH, et al.: **A role for primary cilia in aortic valve development and disease**. *Dev Dyn* 2017, **246**:625-634.

334. Hjeij R, Lindstrand A, Francis R, Zariwala MA, Liu X, Li Y, Damerla R, Dougherty GW, Abouhamed M, Olbrich H, et al.: **ARMC4 mutations cause primary ciliary dyskinesia with randomization of left/right body asymmetry**. *Am J Hum Genet* 2013, **93**:357-367.

335. Kim J, Lee JE, Heynen-Genel S, Suyama E, Ono K, Lee K, Ideker T, Aza-Blanc P, Gleeson JG: **Functional genomic screen for modulators of ciliogenesis and cilium length**. *Nature* 2010, **464**:1048-1051.

336. Holden JK, Cunningham CN: **Targeting the Hippo Pathway and Cancer through the TEAD Family of Transcription Factors**. *Cancers (Basel)* 2018, **10**.

337. Nakano K, Kanai-Azuma M, Kanai Y, Moriyama K, Yazaki K, Hayashi Y, Kitamura N: **Cofilin phosphorylation and actin polymerization by NRK/NESK, a member of the germinal center kinase family**. *Exp Cell Res* 2003, **287**:219-227.

338. Walia V, Cuenca A, Vetter M, Insinna C, Perera S, Lu Q, Ritt DA, Semler E, Specht S, Stauffer J, et al.: **Akt Regulates a Rab11-Effector Switch Required for Ciliogenesis**. *Dev Cell* 2019, **50**:229-246 e227.

339. Cohen S, Aizer A, Shav-Tal Y, Yanai A, Motro B: **Nek7 kinase accelerates microtubule dynamic instability**. *Biochim Biophys Acta* 2013, **1833**:1104-1113.

340. Nishiguchi KM, Tearle RG, Liu YP, Oh EC, Miyake N, Benaglio P, Harper S, Koskiniemi-Kuendig H, Venturini G, Sharon D, et al.: **Whole genome sequencing in patients with retinitis pigmentosa reveals pathogenic DNA structural changes and NEK2 as a new disease gene**. *Proc Natl Acad Sci U S A* 2013, **110**:16139-16144.

341. Narita K, Kozuka-Hata H, Nonami Y, Ao-Kondo H, Suzuki T, Nakamura H, Yamakawa K, Oyama M, Inoue T, Takeda S: **Proteomic analysis of multiple primary cilia reveals a novel mode of ciliary development in mammals**. *Biol Open* 2012, **1**:815-825.

342. Agarwal V, Bell GW, Nam JW, Bartel DP: **Predicting effective microRNA target sites in mammalian mRNAs**. *Elife* 2015, **4**.

343. Choksi SP, Babu D, Lau D, Yu X, Roy S: **Systematic discovery of novel ciliary genes through functional genomics in the zebrafish**. *Development* 2014, **141**:3410-3419.

344. Shi Y, Su Y, Lipschutz JH, Lobo GP: **Zebrafish as models to study ciliopathies of the eye and kidney**. *Clin Nephrol Res* 2017, **1**:6-9.

345. Sellier C, Campanari ML, Julie Corbier C, Gaucherot A, Kolb-Cheynel I, Oulad-Abdelghani M, Ruffenach F, Page A, Ciura S, Kabashi E, et al.: **Loss of C9ORF72 impairs autophagy and synergizes with polyQ Ataxin-2 to induce motor neuron dysfunction and cell death**. *EMBO J* 2016, **35**:1276-1297.

346. Bedell VM, Westcot SE, Ekker SC: **Lessons from morpholino-based screening in zebrafish**. *Brief Funct Genomics* 2011, **10**:181-188.

347. Miller VM, Nelson RF, Gouvion CM, Williams A, Rodriguez-Lebron E, Harper SQ, Davidson BL, Rebagliati MR, Paulson HL: **CHIP suppresses polyglutamine aggregation and toxicity in vitro and in vivo**. *J Neurosci* 2005, **25**:9152-9161.

348. Schiffer NW, Broadley SA, Hirschberger T, Tavan P, Kretzschmar HA, Giese A, Haass C, Hartl FU, Schmid B: **Identification of anti-prion compounds as efficient inhibitors of polyglutamine protein aggregation in a zebrafish model**. *J Biol Chem* 2007, **282**:9195-9203.

349. Yang H, Liu S, He WT, Zhao J, Jiang LL, Hu HY: **Aggregation of Polyglutamine-expanded Ataxin 7 Protein Specifically Sequesters Ubiquitin-specific Protease 22 and Deteriorates Its Deubiquitinating Function in the Spt-Ada-Gcn5-Acetyltransferase (SAGA) Complex**. *J Biol Chem* 2015, **290**:21996-22004.

350. Zhao C, Omori Y, Brodowska K, Kovach P, Malicki J: **Kinesin-2 family in vertebrate ciliogenesis**. *Proc Natl Acad Sci U S A* 2012, **109**:2388-2393.

351. Arts HH, Knoers NV: **Current insights into renal ciliopathies: what can genetics teach us?** *Pediatr Nephrol* 2013, **28**:863-874.

352. Hollbach N, Tappeiner C, Jazwinska A, Enzmann V, Tschopp M: **Photopic and scotopic spatiotemporal tuning of adult zebrafish vision**. *Front Syst Neurosci* 2015, **9**:20.

353. Randall J, Warr JR, Hopkins JM, McVittie A: **A Single-Gene Mutation of Chlamydomonas Reinhardii Affecting Motility: A Genetic and Electron Microscope Study**. *Nature* 1964, **203**:912-914.

354. Harris EH: **Chlamydomonas as a Model Organism**. *Annu Rev Plant Physiol Plant Mol Biol* 2001, **52**:363-406.

355. Craige B, Brown JM, Witman GB: **Isolation of Chlamydomonas flagella**. *Curr Protoc Cell Biol* 2013, **Chapter 3**:Unit 3 41 41-49.

356. Miertzschke M, Koerner C, Spoerner M, Wittinghofer A: **Structural insights into the small G-protein Arl13B and implications for Joubert syndrome**. *Biochem J* 2014, **457**:301-311.

357. Garrido-Jimenez S, Roman AC, Carvajal-Gonzalez JM: **Diminished Expression of Fat and Dachsous PCP Proteins Impaired Centriole Planar Polarization in Drosophila**. *Front Genet* 2019, **10**:328.

358. Mouse Genome Sequencing C, Waterston RH, Lindblad-Toh K, Birney E, Rogers J, Abril JF, Agarwal P, Agarwala R, Ainscough R, Alexandersson M, et al.: **Initial sequencing and comparative analysis of the mouse genome**. *Nature* 2002, **420**:520-562.

359. Gehrig J, Pandey G, Westhoff JH: **Zebrafish as a Model for Drug Screening in Genetic Kidney Diseases**. *Front Pediatr* 2018, **6**:183.

360. Fontana BD, Mezzomo NJ, Kalueff AV, Rosemberg DB: **The developing utility of zebrafish models of neurological and neuropsychiatric disorders: A critical review**. *Exp Neurol* 2018, **299**:157-171.

361. Bhattarai P, Thomas AK, Cosacak MI, Papadimitriou C, Mashkaryan V, Zhang Y, Kizil C: **Modeling Amyloid-beta42 Toxicity and Neurodegeneration in Adult Zebrafish Brain**. *J Vis Exp* 2017.

362. Rossi A, Kontarakis Z, Gerri C, Nolte H, Holper S, Kruger M, Stainier DY: **Genetic compensation induced by deleterious mutations but not gene knockdowns**. *Nature* 2015, **524**:230-233.

363. Wagner DE, Weinreb C, Collins ZM, Briggs JA, Megason SG, Klein AM: **Single-cell mapping of gene expression landscapes and lineage in the zebrafish embryo**. *Science* 2018, **360**:981-987.

364. Su JL, Chen PS, Johansson G, Kuo ML: **Function and regulation of let-7 family microRNAs**. *Microrna* 2012, **1**:34-39.

365. Narayanan A, Hill-Teran G, Moro A, Ristori E, Kasper DM, C AR, Lu J, Nicoli S: **In vivo mutagenesis of miRNA gene families using a scalable multiplexed CRISPR/Cas9 nuclease system**. *Sci Rep* 2016, **6**:32386.

366. Jiang S, Yan W, Wang SE, Baltimore D: **Let-7 Suppresses B Cell Activation through Restricting the Availability of Necessary Nutrients**. *Cell Metab* 2018, **27**:393-403 e394.

367. Wang G, Yost HJ, Amack JD: **Analysis of gene function and visualization of cilia-generated fluid flow in Kupffer's vesicle**. *J Vis Exp* 2013.

368. Zeng L, Carter AD, Childs SJ: **miR-145 directs intestinal maturation in zebrafish**. *Proc Natl Acad Sci U S A* 2009, **106**:17793-17798.

369. Lu C, Wu J, Xiong S, Zhang X, Zhang J, Mei J: **MicroRNA-203a regulates fast muscle differentiation by targeting dmrt2a in zebrafish embryos**. *Gene* 2017, **625**:49-54.

370. Jia W, Liang D, Li N, Liu M, Dong Z, Li J, Dong X, Yue Y, Hu P, Yao J, et al.: **Zebrafish microRNA miR-210-5p inhibits primitive myelopoiesis by silencing foxj1b and slc3a2a mRNAs downstream of gata4/5/6 transcription factor genes**. *J Biol Chem* 2019, **294**:2732-2743.

371. Cole DG, Diener DR, Himelblau AL, Beech PL, Fuster JC, Rosenbaum JL: **Chlamydomonas kinesin-II-dependent intraflagellar transport (IFT): IFT particles contain proteins required for ciliary assembly in Caenorhabditis elegans sensory neurons**. *J Cell Biol* 1998, **141**:993-1008.

372. Lu H, Toh MT, Narasimhan V, Thamilselvam SK, Choksi SP, Roy S: **A function for the Joubert syndrome protein Arl13b in ciliary membrane extension and ciliary length regulation**. *Dev Biol* 2015, **397**:225-236.

373. Wiens CJ, Tong Y, Esmail MA, Oh E, Gerdes JM, Wang J, Tempel W, Rattner JB, Katsanis N, Park HW, et al.: **Bardet-Biedl syndrome-associated small GTPase ARL6 (BBS3) functions at or near the ciliary gate and modulates Wnt signaling**. *J Biol Chem* 2010, **285**:16218-16230.

374. Smith LA, Bukanov NO, Husson H, Russo RJ, Barry TC, Taylor AL, Beier DR, Ibraghimov-Beskrovnaya O: **Development of polycystic kidney disease in juvenile cystic kidney mice: insights into pathogenesis, ciliary abnormalities, and common features with human disease**. *J Am Soc Nephrol* 2006, **17**:2821-2831.

375. Gerhardt C, Lier JM, Burmuhl S, Struchtrup A, Deutschmann K, Vetter M, Leu T, Reeg S, Grune T, Ruther U: **The transition zone protein Rpgrip1l regulates proteasomal activity at the primary cilium**. *J Cell Biol* 2015, **210**:115-133.

376. Kehl T, Backes C, Kern F, Fehlmann T, Ludwig N, Meese E, Lenhof HP, Keller A: **About miRNAs, miRNA seeds, target genes and target pathways**. *Oncotarget* 2017, **8**:107167-107175.

377. Jokinen J, Dadu E, Nykvist P, Kapyla J, White DJ, Ivaska J, Vehvilainen P, Reunanen H, Larjava H, Hakkinen L, et al.: **Integrin-mediated cell adhesion to type I collagen fibrils**. *J Biol Chem* 2004, **279**:31956-31963.

378. Hur K, Toiyama Y, Schetter AJ, Okugawa Y, Harris CC, Boland CR, Goel A: **Identification of a metastasis-specific MicroRNA signature in human colorectal cancer**. *J Natl Cancer Inst* 2015, **107**.

379. Thammaiah CK, Jayaram S: **Role of let-7 family microRNA in breast cancer**. *Noncoding RNA Res* 2016, **1**:77-82.

380. Griffiths-Jones S, Hui JH, Marco A, Ronshaugen M: **MicroRNA evolution by arm switching**. *EMBO Rep* 2011, **12**:172-177.

381. Bartel DP: **MicroRNAs: genomics, biogenesis, mechanism, and function**. *Cell* 2004, **116**:281-297.

382. Pillai RS, Bhattacharyya SN, Artus CG, Zoller T, Cougot N, Basyuk E, Bertrand E, Filipowicz W: **Inhibition of translational initiation by Let-7 MicroRNA in human cells**. *Science* 2005, **309**:1573-1576.

383. Ma F, Liu X, Li D, Wang P, Li N, Lu L, Cao X: **MicroRNA-466l upregulates IL-10 expression in TLR-triggered macrophages by antagonizing RNA-binding protein tristetraprolin-mediated IL-10 mRNA degradation**. *J Immunol* 2010, **184**:6053-6059.

384. Murphy AJ, Guyre PM, Pioli PA: **Estradiol suppresses NF-kappa B activation through coordinated regulation of let-7a and miR-125b in primary human macrophages**. *J Immunol* 2010, **184**:5029-5037.

385. Nicoli S, Standley C, Walker P, Hurlstone A, Fogarty KE, Lawson ND: **MicroRNA-mediated integration of haemodynamics and Vegf signalling during angiogenesis**. *Nature* 2010, **464**:1196-1200.

386. van der Velden AW, Thomas AA: **The role of the 5' untranslated region of an mRNA in translation regulation during development**. *Int J Biochem Cell Biol* 1999, **31**:87-106.

387. Gallie DR: **The cap and poly(A) tail function synergistically to regulate mRNA translational efficiency**. *Genes Dev* 1991, **5**:2108-2116.

388. Murray EE, Lotzer J, Eberle M: **Codon usage in plant genes**. *Nucleic Acids Res* 1989, **17**:477-498.

389. Camiolo S, Toome-Heller M, Aime MC, Haridas S, Grigoriev IV, Porceddu A, Mannazzu I: **An analysis of codon bias in six red yeast species**. *Yeast* 2019, **36**:53-64.

390. Bornelov S, Selmi T, Flad S, Dietmann S, Frye M: **Codon usage optimization in pluripotent embryonic stem cells**. *Genome Biol* 2019, **20**:119.

391. Mishima Y, Tomari Y: **Codon Usage and 3' UTR Length Determine Maternal mRNA Stability in Zebrafish**. *Mol Cell* 2016, **61**:874-885.

392. Rogers KW, Blassle A, Schier AF, Muller P: **Measuring protein stability in living zebrafish embryos using fluorescence decay after photoconversion (FDAP)**. *J Vis Exp* 2015:52266.

393. Vandemoortele G, Eyckerman S, Gevaert K: **Pick a Tag and Explore the Functions of Your Pet Protein**. *Trends Biotechnol* 2019.

394. McGown A, Shaw DP, Ramesh T: **ZNStress: a high-throughput drug screening protocol for identification of compounds modulating neuronal stress in the transgenic mutant sod1G93R zebrafish model of amyotrophic lateral sclerosis**. *Mol Neurodegener* 2016, **11**:56.

395. Bai Q, Garver JA, Hukriede NA, Burton EA: **Generation of a transgenic zebrafish model of Tauopathy using a novel promoter element derived from the zebrafish eno2 gene**. *Nucleic Acids Res* 2007, **35**:6501-6516.

396. Gao L, Zhang J: **Why are some human disease-associated mutations fixed in mice?** *Trends Genet* 2003, **19**:678-681.

397. Pouladi MA, Morton AJ, Hayden MR: **Choosing an animal model for the study of Huntington's disease**. *Nat Rev Neurosci* 2013, **14**:708-721.

398. Guo DF, Beyer AM, Yang B, Nishimura DY, Sheffield VC, Rahmouni K: **Inactivation of Bardet-Biedl syndrome genes causes kidney defects**. *Am J Physiol Renal Physiol* 2011, **300**:F574-580.

399. Ichimura K, Kurihara H, Sakai T: **Primary cilia disappear in rat podocytes during glomerular development**. *Cell Tissue Res* 2010, **341**:197-209.

400. Chen JK, Taipale J, Cooper MK, Beachy PA: **Inhibition of Hedgehog signaling by direct binding of cyclopamine to Smoothened**. *Genes Dev* 2002, **16**:2743-2748.

Résumé de la thèse

Introduction

Le cil est une organelle conservée au fil de l'évolution qui se projette de presque toutes les cellules de vertébrés. Les cils sont recouverts par la membrane cytoplasmique et sont composés d'un squelette de microtubules ancré dans la cellule via le corps basal. Ils accomplissent diverses fonctions : ils sont requis pour la transduction de signaux extracellulaires pendant le développement, ils jouent un rôle dans la perception de l'environnement tels que les cils connecteurs dans les photorécepteurs de la rétine, ou peuvent avoir une fonction de motilité pour permettre le flux de liquide tel que dans le canal de l'épendyme. Des mutations dans les gènes codant pour des protéines impliquées dans la structure ou la fonction des cils peuvent causer différentes anomalies développementales ou dégénératives, qui sont collectivement appelées ciliopathies. Ce groupe de syndromes, soulignés par un défaut de la même organelle, donne lieu à un ensemble de caractéristiques cliniques distinctives touchant multiples organes.

Les individus atteints de ciliopathies présentent une importante variabilité inter- et intra-familliale, suggérant la présence de gènes modificateurs de la pénétrance et de l'expression de la maladie. De récentes études génétiques et fonctionnelles indiquent que la charge mutationelle à divers loci associés au cil peut influencer le phénotype d'une ciliopathie. Cependant, la recherche des molécules qui régulent les gènes du cil est sous-explorée.

Les microARNs (miARN) sont de petits ARNs non codant, d'environ 22 nucléotides de long, qui inhibent la traduction d'ARN messagers (ARNm) cibles en se fixant sur des séquences complémentaires dans leur région non traduites en 3' (3'UTR). Leur rôle dans la régulation de l'expression des gènes en fait des candidats plausibles pour être des gènes modificateurs des ciliopathies. Afin d'explorer cette hypothèse, mon laboratoire américain a réalisé un criblage de moyenne échelle utilisant 800 inhibiteurs de miARNs dans des cellules épithéliales pigmentées de rétine (RPE) possédant un rapporteur fluorescent du cil (Smo:eGFP). Cette étude a montré que la famille des miARNs *let-7* pouvait promouvoir la ciliogenèse et augmenter la longueur des cils de façon indépendante de son rôle sur le cycle cellulaire. La famille let-7 fut la deuxième famille de miARNs découverte chez *Caenorhabditis elegans* et a depuis été identifiée dans la plupart des espèces avec un rôle dans la prolifération et différentiation cellulaire. Étant donné que la majorité des cibles connues de *let-7* sont des oncogènes, *let-7* a été principalement étudié dans le contexte du cancer.

De nombreuses études fonctionnelles ont permis d'identifier prêt de 1000 protéines impliquées dans la structure ou fonction du cil et cette liste ne cesse de s'agrandir. Ces protéines peuvent avoir une seule fonction caractérisée liée au cil ou plusieurs fonctions connues dépendantes ou indépendantes de la biologie du cil. Des résultats préliminaires dans mon laboratoire d'accueil français ont montré que la protéine Ataxine-7 (ATXN7), une des protéines du complexe de coactivation de la transcription SAGA, pouvait se localiser à la base du cil connecteur des photorécepteurs de souris sauvages, et que cette localisation était perdue lorsque la protéine était mutée par une expansion de la répétition d'acides aminés glutamine (polyQ) située en N-terminus de la protéine. Cette mutation en particulier cause une maladie autosomale dominante nommée Ataxie SpinoCérébelleuse 7 (SCA7) qui fait partie du groupe de maladies par expansion de polyQ. Cette maladie neurodégénérative à manifestation tardive, est caractérisée par une dégénération progressive des neurones du cervelet et de la rétine conduisant respectivement à l'ataxie et à la cécité. Étant donné les études de plus en plus nombreuses suggérant la contribution d'anomalies développementales à des maladies à manifestation tardives

telles que les maladies d'Huntington (également une maladie à expansion de polyQ), d'Alzheimer, de Parkinson et la schizophrénie ; ainsi que notre récente publication qui suggère un rôle pour l'Atxn7 dans le développement du cerveau et de l'œil du poisson-zèbre, il est raisonnable de postuler que l'ATXN7 ait un rôle dans le développement de ces organes qui soit lié au cil et qui contribue au développement de la maladie de SCA7 lorsque l'ATXN7 est mutée.

Objectifs

I. Le premier objectif de ma thèse est d'étudier le rôle potentiel de *let-7b* comme modulateur de la ciliogenèse, au travers de deux approches : d'une part en inactivant l'expression de *let-7b* dans le modèle poisson-zèbre, et d'autre part en explorant l'hypothèse que les cohortes de patients atteints de ciliopathies ont un enrichissement de mutations dans les 3'UTR des cibles de *let-7b*. Notre étude devrait enrichir notre compréhension non seulement de la biologie du cil, mais également des facteurs pouvant expliquer la variabilité phénotypique observée chez les patients atteints de ciliopathies. Une meilleure appréhension de la génétique des ciliopathies a le potentiel d'améliorer les diagnostiques, les pronostics et donc le bien-être des patients.

II. Le second objectif de ma thèse est d'explorer le lien potentiel entre l'ATXN7 et le cil dans le développement de la maladie SCA7 en utilisant le modèle poisson-zèbre. Un modèle poisson-zèbre de SCA7 permettrait une meilleure compréhension de cette maladie encore incurable et aurait aussi le potentiel d'être utilisé pour des criblages de composés thérapeutiques tels que des molécules à propriété anti-agrégeante identifiées dans mon laboratoire français.

III. Le troisième objectif est mineur et consiste à élargir mon éventail technique en participant à d'autre projets menés dans mes laboratoires hôtes américain et français.

Méthodes

I. Afin de valider le rôle de *let-7b* sur la ciliogenèse, j'ai réalisé deux modèles poisson-zèbre inactivés pour *let-7b* : le premier, généré avec la technologie d'édition de génome CRISPR/Cas9 permet une inactivation permanente ; et le second, généré via l'injection d'oligonucléotide anti-sens morpholino (MO) bloque de façon transitoire la maturation du transcrit de *let-7b*. J'ai caractérisé ces deux modèles en déficience de *let-7b* mature à différent stades du développement en utilisant des techniques de microscopie conventionnelle, d'hybridation *in situ*, d'immunomarquage fluorescent et de RT-qPCR. Pour identifier des transcrits candidats cibles de *let-7b*, j'ai utilisé des données d'ARN-seq de RPE traitées avec un inhibiteur ou imitateur synthétique de *let-7b* (obtenues précédemment dans mon laboratoire américain). J'ai filtré la liste d'ARNs surexprimés en présence de l'inhibiteur de *let-7b* et sous-exprimés en présence de l'imitateur avec 2 listes : 1) une liste de cibles prédites de *let-7b* par l'outil en ligne TargetScan qui scrute les 3'UTR de transcrits, et 2) une liste de gènes codant pour des protéines inhibant la ciliogenèse générée par recherche bibliographique. Les données d'ARN-seq filtrées avec une liste de gènes liés au cil a permis d'établir la liste des loci à séquencer dans une cohorte de patients atteints de ciliopathies tels le syndrome de Meckel-Grüber (MKS) et le syndrome de Bardet-Biedl (BBS). Le séquençage et la pré-analyse des données ont été réalisés par les plateformes de séquençage et bio-informatique de l'Université de Duke. J'ai vérifié l'authenticité de chaque mutation détectée dans le logiciel IGV, réattribué les informations de chaque patient à chaque mutation (sexe, ethnicité, locus pathogène primaire), et ai compté les allèles pour détecter un éventuel enrichissement ou appauvrissement chez les patients.

II. Pour étudier si la mutation de l'ATXN7 pouvait avoir un impact sur les fonctions du cil, j'ai utilisé différentes stratégies afin d'exprimer l'ATXN7 mutante dans le poisson-zèbre au stade

embryonnaire ou adulte. D'abord, j'ai préparé plusieurs vecteurs portant les séquences codantes de l'ATXN7 (sauvage ou mutée, pleine longueur (PL) ou tronquée (Δ), avec ou sans le marqueur fluorescent « green fluorescent protein ») à partir desquels j'ai synthétisé de l'ARNm. J'ai ensuite injecté ces ARNms dans des embryons de poisson-zèbre et utilisé des techniques de microscopie conventionnelle et de cryosections pour caractériser l'expression des ARNms au niveau spatio-temporel, avant une caractérisation phénotypique plus approfondies. Par ailleurs, un modèle poisson-zèbre adulte de SCA7 a été généré par la plateforme AMAGEN qui a introduit la séquence sauvage ou mutée de l'ATXN7 tronquée en aval de la séquence du promoteur UAS. Ces poissons adultes doivent être croisés avec une lignée exprimant GAL4 sous le contrôle du promoteur ENO2 afin de générer une progéniture qui surexprime l'ATXN7 exclusivement dans les neurones matures.

III. Dans mon laboratoire américain, j'ai utilisé les techniques d'immunomarquage sur embryons entiers ou cryosections et de marquage TUNEL dans le cadre de projets indépendants mais impliquant l'étude d'organes typiquement affectés dans le cadre des ciliopathies : le rein et la rétine. J'ai également utilisé divers instruments robotisés tels que le Vertebrate Automated Screening Technology et le DanioVison pour capturer des images/vidéos d'embryons en temps réel. Dans mon laboratoire français, j'ai apporté une aide technique notamment pour des expériences de sauvetage du phénotype à une étudiante en thèse qui s'intéressait aux conséquences de l'inactivation de l'atxn7 sur le développement du poisson-zèbre.

Résultats

I. Étude du rôle potentiel de *let-7b* comme modulateur de la ciliogenèse.

1. Let-7b, un modulateur de la ciliogenèse dans le poisson-zèbre.

Afin d'inactiver *let-7b* par la technique Crispr/Cas9 dans le poisson-zèbre, j'ai conçu deux ARN guides (ARNg) ciblant un site de maturation de *let-7b*. L'efficacité de ces ARNg a été déterminée à 94 et 100%, c'est donc le second qui a été utilisé pour toutes les expériences suivantes. L'inactivation de *let-7b* dans le poisson-zèbre dans la génération F0 a donné lieu à plusieurs phénotypes embryonnaires caractéristiques des modèles poissons de ciliopathies, tels que l'hétérotaxie à 2 jours post-fécondation (jpf) évaluée via l'orientation de la boucle cardiaque, et des défauts de migration cellulaire par convergence-extension au stade de 10 somites. Pour expliquer le phénotype d'hétérotaxie, j'ai réalisé une hybridation *in situ* pour le gène nodale *southpaw*, connu pour être impliqué dans la formation de l'asymétrie gauche-droite de l'embryon de poisson-zèbre et ai observé une expression bilatérale ou contra-latérale de *southpaw* dans plus de 50% des embryons. Parce que l'expression unilatérale des gènes nodaux est causée par le flux généré par les cils motiles présents dans la vésicule de Kupffer (VK), je me suis intéressée à cet organe et ai compté et mesuré le nombre de cils. J'ai observé des cils plus courts dans les embryons injectés avec l'ARNg et l'enzyme Cas9, comparé aux contrôles non-injectés ou injectés avec l'ARNg seul. J'ai maintenu cette lignée de poisson-zèbre mutante jusqu'à la génération F3 mais une trop grande présence d'œdèmes cardiaques dans les trois génotypes (sauvage, hétérozygote ou homozygote), possiblement due à une mutation dans le fond génétique des poissons, a interféré avec l'interprétation des résultats.

Les phénotypes observés dans la génération de mutants F0 ont été répliqués avec une plus grande pénétrance dans des embryons de poisson-zèbre injectés avec le MO contre *let-7b* (morphants). Un sauvetage phénotypique partiel de chaque phénotype a été réalisé en co-injectant le MO avec l'imitateur de *let-7b.* Le chevauchement des phénotypes observés dans les

poissons F0 et les morphants ainsi que le sauvetage phénotypique partiel sont indicateurs de la spécificité des phénotypes observés.

2. Les potentiels gènes cibles de let-7b et acteurs de la ciliogenèse.

L'analyse des transcriptomes (ARN-seq) de cellules RPE traitées avec un inhibiteur ou avec un imitateur de *let-7b* a permis d'identifier une liste de 1221 transcrits potentiellement cibles de *let-7b*. La recherche *in silico* de séquences complémentaires à *let-7b* dans les 3'UTR des 1221 ARNm ainsi que l'intersection avec une liste de gènes impliqués dans l'inhibition de la ciliogenèse a permis de réduire la liste à 499 candidats. 5 d'entre eux ont été identifiés via les 3 méthodes employées à savoir l'ARN-seq, la recherche *in silico* de cibles de *let-7b* et la recherche bibliographique sur les inhibiteurs de la ciliogénèse.

3. let-7b comme gène modificateur des ciliopathies

Nous avons choisi une cohorte de patients atteints de forme sévère (68 patients atteints du MKS) et de forme intermédiaire (117 patients atteints du BBS) de ciliopathie dans le but de pouvoir comparer non seulement des patients *versus* contrôles mais aussi une forme sévère *versus* intermédiaire. Une analyse bioinformatique nous a indiqué que les 40 gènes candidats obtenus précédemment portaient un total de 113 séquences cibles de *let-7b* (en effet, un gène peut coder pour plusieurs ARNm possédant eux-mêmes plusieurs cibles de *let-7b* dans leur 3'UTR). Les 113 loci ont été séquencé chez les patients sélectionnés. Aucun allèle rare n'a été identifié. J'ai comparé le nombre et la nature des polymorphismes mononucléotidiques (PMN) détectés chez les patients avec ceux présents chez les contrôles de la base de données en ligne gnomAD. Après correction par la méthode de Bonferroni, 2 mutations se sont avérées enrichie ou appauvrie chez les patients. Cependant, nous suspectons que cela soit dû à la composition ethnique de notre cohorte. J'ai également évalué la charge mutationelle entre les patients MKS et BBS en comparant le nombre de PMN par patients. Elle ne s'est pas révélée significativement différente. Il est important de noter qu'à ce stade notre cohorte était de petite taille et stratifiée par plusieurs ethnicités ce qui a réduit le pouvoir statistique de l'étude.

II. Fonction et dysfonction de l'Ataxine-7 dans l'Ataxie Spinocérébelleuse 7

1. L'Ataxine-7 et le cil

Des données préliminaires du laboratoire, dont la perte de la localisation de l'ATXN7 à la base du cil chez les souris SCA7, et l'observation de phénotypes de ciliopathies dans des embryons de poisson-zèbre injectés avec de l'ARNm d'ATXN7 mutée, permettent d'anticiper un rôle de l'ATXN7 mutée dans le développement de SCA7 qui serait lié au cil. Toutefois, dans mes expériences, des injections d'ARNm d'ATXN7 sauvage ou mutée à des concentrations croissantes n'ont pas réussi à reproduire les résultats préliminaires observés dans l'embryon de poisson-zèbre pour des raisons qui restent encore inconnues. De plus, l'injection d'ARNm codant pour l'ATXN7-Δ mutée, prédite pour être plus toxique, n'a pas non plus donné lieu à des phénotypes. Afin de comprendre cette absence de phénotype, j'ai exploré les hypothèses que les ARNm injectés étaient incorrectement exprimés ou que les protéines produites aient été instables ou dégradées avant d'avoir des effets toxiques. Pour ce faire, des ARNm codant pour des ATXN7 (PL ou Δ) fusionnées à la GFP ont été injectés chez l'embryon et leur expression a été suivie au cours du temps. Bien qu'il s'avère que l'ATXN7-Δ soit plus exprimée que l'ATXN7-PL, les deux formes montrent un niveau d'expression très faible lorsque comparé aux embryons injectés avec de l'ARNm codant pour la GFP seule. Des expériences de suivi spatial de la GFP dans les tissus ont

révélé un signal principalement nucléaire de la fluorescence avec une faible intensité cytoplasmique. Cependant je n'ai pas observé d'agrégat d'ATXN7, suggérant encore que le niveau d'expression était sous optimal pour générer un phénotype.

2. Le rôle de l'Ataxin-7 dans la dégénérescence rétinienne

Les poissons transgéniques générés par la plateforme AMAGEN devaient nous permettre d'étudier la dégénérescence rétinienne de SCA7 de l'embryon au stade adulte dans le poisson-zèbre qui, contrairement au modèle murin, est diurne et possède donc une composition rétinienne plus proche de celle de l'homme. Cette partie du projet a été abandonnée suite à mon déménagement aux Etats-Unis pour la réalisation de l'autre partie du projet de thèse.

Conclusion

I. En utilisant le poisson-zèbre, j'ai pu valider le rôle du miARN *let-7b* sur la ciliogenèse et mon analyse des données d'ARN-seq ont permis d'identifier de solides candidats, acteurs de la ciliogenèse. Cette découverte permet d'impliquer ce miARN largement étudié dans le monde du cancer dans le contexte différent de la biologie du cil. Bien que nous n'ayons pas pu démontrer notre hypothèse que *let-7b* puisse être un gène modificateur des ciliopathies dans notre cohorte actuelle, il est possible que les effets aient été masqués par la taille et stratification. De plus, il serait pertinent d'étendre l'étude à l'ensemble de la famille *let-7*.

II. Grâce à des suivis spatio-temporels de protéines de fusion ATXN7-GFP, j'ai pu expliquer les difficultés à générer mon modèle poisson-zèbre SCA7. Des expériences supplémentaires sont donc nécessaires pour générer le modèle et pour pouvoir répondre à l'hypothèse de la relation ATXN7-cil.

Université de Strasbourg

Lorraine FIEVET

École Doctorale des Sciences de la Vie et de la Santé STRASBOURG

ARN non-codants et protéines effecteurs de la biologie du cil

Résumé

Le cil est une organelle conservée au fil de l'évolution qui se projette de presque toutes les cellules de vertébrés. Des mutations dans les gènes codant pour des protéines impliquées dans la structure ou la fonction des cils peuvent causer différentes anomalies développementales ou dégénératives, qui sont collectivement appelés ciliopathies. Les individus atteints de ciliopathies présentent une importante variabilité inter- et intra-familliale, suggérant la présence de gènes modificateurs de la pénétrance et de l'expression de la maladie. L'utilisation du poisson-zèbre comme organisme modèle permet de 1) valider le rôle du microARN let-7 comme modulateur de la ciliogenèse et ainsi de le considérer comme potentiel gène modificateurs dans les ciliopathies; et 2) d'explorer le rôle putatif de l'Ataxine-7 dans la biologie du cil et une potentielle contribution développementale à la maladie d'ataxie spinocérebelleuse 7 qui est une maladie dégénérative. Une meilleure compréhension de la biologie du cil et des ciliopathies permettrait de mieux diagnostiquer et prendre en charge les patients.

Mots-clés : cil, microARN, ataxie spinocérebelleuse 7, poisson-zèbre

Résumé en anglais

Cilia are conserved organelles projecting from almost every vertebrate cell. Mutations in genes coding for proteins involved in cilia structure or function can cause different developmental and degenerative anomalies, which are collectively termed ciliopathies. Ciliopathy patients present an important inter- and intra-familial phenotypic variability, suggesting the presence of modifier genes of the penetrance and expressivity of the disease. Using the zebrafish model organism enables to 1) validate the role of the microRNA let-7 as a modulator of ciliogenesis, and thus consider it as a potential modifier gene of ciliopathies; and 2) explore the putative ciliary role of Ataxin-7 and a potential developmental contribution to spinocerebellar ataxia 7, which is a degenerative disease. A better understanding of cilia biology and ciliopathies would allow better diagnostics and care of patients.

Keywords: cilia, microRNA, spinocerebellar ataxia 7, zebrafish